EVALUATING THE EFFICACY OF DNA REPAIR BIOMARKERS TO ASSESS HUMAN CELL RESPONSE TO CHEMOTHERAPY USING IMAGING FLOW CYTOMETRY

Sheba Adam Zahir

Division of Biosciences
School of Health Sciences and Social Care

Declaration

I hereby declare that the research presented in this thesis is my own work, except where otherwise specified, and has not been submitted for any other degree.

Sheba Adam Zahir

ABSTRACT

Chemotherapy and radiotherapy are widely accepted as common forms of treatment for cancers. The majority of cancer patients receive chemotherapy alone or in combination with radiotherapy. Most chemotherapeutic drugs cause DNA damage to the rapidly dividing cancer cells but normal cells are also damaged in the process. Therefore DNA repair levels in tumour and normal cells may determine the success of the treatment.

The aim of this work was to evaluate the use of DNA repair biomarkers for assessing responses to chemotherapeutic drugs. The novel technique of imaging flow cytometry was employed to analyse the induction and resolution of γ-H2AX and RAD51 DNA repair biomarkers in DNA repair normal cell lines MRC5-SV1 and NB1-HTERT, an ATM-deficient cell line AT5BIVA (derived from an Ataxia Telangiectasia patient) and an XPF-deficient cell line GM08437B. Two cell lines were also developed, MRC5-SV1^{R} and NB1-HTERT^{R} which had been made resistant to HN2. A range of chemotherapeutic drugs, Adriamycin, Cisplatin and Nitrogen Mustard which have different modes of action were examined in this work.

We have demonstrated distinct differences in γ-H2AX and RAD51 foci induction and resolution between the two DNA repair normal cell lines following exposure to different chemotherapeutic drugs. Additionally, it was demonstrated that both the resistant and sensitive cell lines have elevated γ-H2AX and RAD51 expression profiles in comparison to the parental cell lines over a 48 hour period post treatment with the cross-linking agent HN2. It is concluded that while both the γ-H2AX and Rad51 biomarkers may be useful for determining chemotherapeutic response, a larger cohort of cell lines and tumour samples is required for further analysis.

Publications

1. Bourton EC, Plowman PN, **Adam Zahir S**, Ulus-Senguloglu G, Serrai H, Bottley G, Parris CN Multispectral imaging flow cytometry reveals distinct frequencies of γ-H2AX foci induction in DNA double strand break repair defective human cell lines., Cytometry Part A, Volume 81A, Issue 2, pg. 130-137, 2012.
2. Bourton EC, Plowman PN, Harvey AH, **Adam Zahir S**, Parris CN. The PARP-1 Inhibitor Olaparib Causes Retention of γ-H2AX Foci in *BRCA1* Heterozygote Cells Following Exposure to Gamma Radiation*, Journal of Cancer Therapy*, (In press, 2013).

ACKNOWLEDGEMENTS

First and foremost, I must extend my deepest gratitude towards Dr Christopher Parris for his guidance and support throughout my PhD. I would also like to thank the other members of my team Dr Bourton, Dr Ulus, Hiba Serrai and Hussein Al-Ali. A special mention must be made to Fariha Sharif, I can't thank you enough for generously donating so much of your time and effort towards my project.

There are numerous colleagues that have played a big part over the last four years. Punam, you have gone through this journey with me from day one. We have experienced every high and low together and I can't imagine what it would have been like without your constant reassurances and support and friendship. I would like to extend a special thank you to Dr Chiranjeevi Sandi for his endless help and advice; especially towards the end of my PhD. A huge thank you to my friends Dr Maryam Ojani, Naj, Julie, Jess, Ane, Becky, Azadeh, Savi, Graham, Hussein, Dr Vahid Ezzatizadeh and Dr Sahar Al-Mahdawi for being amazing colleagues; you certainly made this a more enjoyable experience.

There is an exceptional group of people in my life who have supported and encouraged me from day one. Yash, Amee, Yamanee, Mehery, Ahmed, Mareen, Ahu, Shah and Nahu; words will never be sufficient to express what you all mean to me and how much you have unknowingly driven me through this. Yash, you truly have been very tolerant and patient through all of this. Thank you for bringing the fun into my life at the times that I needed it the most. Shalin, thank you for never failing to make me laugh and cheering me up! Shafraz, your love and support got me through some very difficult times and I will always be grateful for that.

This thesis is dedicated to my parents Adam and Husna. None of this would have ever been possible without your unconditional love and belief in me and I have you to thank for everything that I am and have accomplished in my life.

CONTENTS

List of figures

Chapter 1

Chapter 2

Chapter 3

Chapter 4

Chapter 5

Chapter 6

Chapter 7

List of tables

Chapter 1

Chapter 2

Chapter 4

Chapter 5

Chapter 6

Chapter 7

Abbreviations

5-FU - 5 Fluorouracil

ADR - Adriamycin

AF - Alexa fluor

AP - Apurinic / apyrimidine

A-T - Ataxia Telangiectasia

ATM - Ataxia Telangiectasia Mutated

ATR - Ataxia Telangiectasia and RAD3 related

BASC -BRCA1-associated genome surveillance complex

BER - Base Excision Repair

BF - Brightfield

CH - Channel

CS - Cockayne Syndrome

CPD - Cyclobutane Pyrimidine Dimer

DSB - Double Strand Break

daf - data analysis file

FA – Fanconi Anaemia

FEN-1 -Flap Endonuclease / 5'-3' exonuclease

FdUMP - Fluorodeoxyuridine monophosphate

FdUTP - Fluorodeoxyuridine triphosphate

FUTP - Fluorouridine triphosphate

GG-NER - Global Genome Nucleotide Excision Repair

GSH – Glutathione

Gy – Gray

HR - Homologous Recombination

hr - hour

hrs - hours

HN2 - Nitrogen Mustard

ICL - Interstrand crosslinks

^{125}IdU - iododeoxyuridine

IR - Ionising radiation

MDR1 – Multi drug resistance gene

MMR -Mismatch Repair

MRN - MRE11/RAD50/NBS1

NBS - Nijmegen Breakage Syndrome

NER - Nucleotide Excision Repair

NHEJ - Non Homologous End Joining

PBS - Phosphate Buffered Saline

PCNA - Proliferating Cell Nuclear Antigen

PE – Phycoerythrin

P.E. – plating effciency

PIKKs - Phosphatidylinositol-3 kinase related protein kinase family

Pt - Cisplatin

rif - Raw image file

RNAPII - RNA polymerase II

RPA - Replication Protein A

ROS -Reactive Oxygen Species

RT - room temperature

ssDNA - single stranded DNA

SSB - Single strand break

SV - Simian Virus

TC-NER - Transcription coupled Nucleotide Excision repair

TFIIH - Transcription repair factor IIH

TS – Thymidylate Synthase

TTD – Trichothiodystrophy

UV – Ultraviolet

UVB –Ultraviolet B

XRCC1 - X-ray repair cross complementing protein 1

XP- Xeroderma Pigmentosum

Chapter 1

Introduction

1.1 DNA Damage

Our genome is under continual assault from a vast array of exogenous and endogenous factors which result in the formation of DNA lesions such as

- double and single strand breaks
- formation of DNA adducts such as inter or intra strand cross links
- base damage
- formation of dimers as a result of ultraviolet (UV) exposure

Accurate transfer of genetic information during cell division is a vital process and requires precise replication of DNA. It necessitates accurate DNA repair of spontaneous and induced DNA damage to minimise mutations being passed onto daughter cells. Unrepaired lesions have an effect on numerous cellular processes such as replication or transcription and may ultimately lead to the development of cancer due to accumulation of genetic modifications within the somatic cells and inherited genetic disorders if mutations occur in germ cells (Beckman and Loeb 2005). Laboratory models and human carcinogenesis have shown that the accumulation of six or more genetic mutations lead to the development of tumourigenic cells (Hanahan and Weinberg 2000).

Causes of DNA damage can be broadly categorised into three groups (Hoeijmakers 2001). These are

- Environmental agents e.g. ionising radiation, UV rays, tobacco smoke
- By-products of normal cellular metabolism e.g. hydroxyl radicals
- Spontaneous hydrolysis of chemical bonds in DNA

Errors in cellular processes such as DNA replication, recombination or repair can also lead to the fixation of DNA damage leading to mutations. Table 1.1 below shows an overview of the different types of DNA damage that can occur.

Table 1.1: Overview of different types of DNA damage

Type of damage	Cause	DNA repair pathways
Single strand break, Abasic sites	X-rays, alkylating agents, oxygen radicals	Base Excision Repair
Double strand break	Gamma Radiation	Non-homologous End Joining Homologous Recombination
Cyclobutane pyrimidine dimer (CPD) Bulky adduct	UV Light, polycyclic aromatic hydrocarbons	Nucleotide Excision Repair
Inter/Intra strand crosslink	X-rays, anti-tumour drugs such as Cisplatin	Nucleotide Excision Repair Homologous Recombination
Mismatch of base pairs, insertion or deletion of bases	Errors during replication	Mismatch repair

1.1.1 DNA double strand break

The DNA double strand break (DSB) is one of the most toxic lesions in living cells (Valerie and Povirk 2003). It can become cytotoxic if left unrepaired and may lead to cell death. If it is repaired incorrectly, it can lead to genetic instability through events such as loss of heterozygosity, chromosome rearrangements or loss of genetic information; all of which can have numerous consequences such as cell death or inheritable mutations being formed and may subsequently increase an individual's chances of developing cancer and inherited genetic diseases (Scott and Pandita 2006). Subsequently this could cause inactivation of tumour suppressor genes or the activation of oncogenes which can instigate carcinogenesis in cells

(Jackson 2002). DSBs can be induced directly or indirectly by exogenous agents such as ionising radiation (IR) and chemotherapeutic agents. However there are events where DSBs are crucial in order to facilitate recombination between homologous chromosomes and subsequently are intentionally initiated such as during V(D)J recombination and immunoglobulin class-switch recombination as well as during meiosis.

1.1.2 DNA adduct formation

DNA adducts are chemical modifications of the DNA, generally bulky lesions forming on the DNA. The formation of DNA adducts occurs following exposure to cross-linking agents such as the Nitrogen Mustards (i.e. Mechlorethamine), Platinum based drugs (i.e. Cisplatin (Pt)) and Mitomycin C (Cole 1973; McHugh *et al.* 2001). DNA crosslinking can occur in one of three ways and can result in grossly distorted DNA (refer to Figure 1.1)

- Intrastrand - crosslinking of DNA on the same strand
- Interstrand - crosslinking (ICL) of DNA between two complementary strands
- DNA-protein - crosslinking between DNA base and reactive groups on proteins

Figure 1.1 Different types of adducts formed by crosslinking agents (McHugh *et al.* 2001)

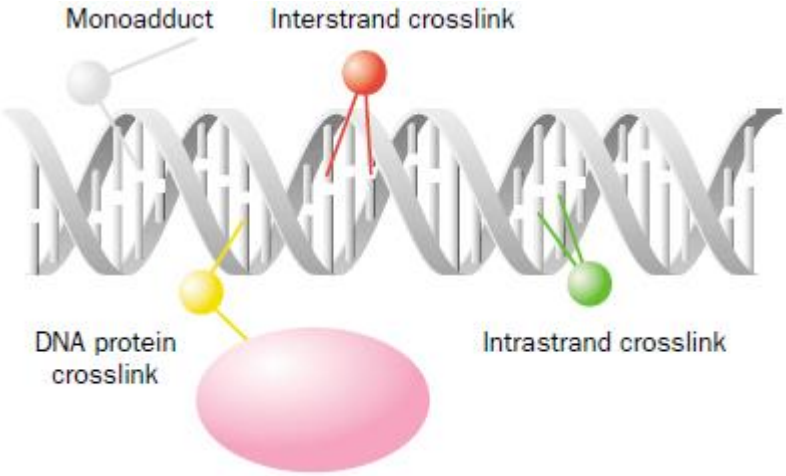

Unless repaired, these adducts can have deleterious effects such as blocking transcription or stalling of replication forks. Additionally the presence of DNA adducts increase the potential for mutagenesis to occur (Dipple 1995). These adducts are very cytotoxic and as such, form the basis of the mechanism of action of many chemotherapeutic agents.

1.1.3 Free Radical Formation

Free radical formation results from intrinsic factors such as the by-product of normal metabolic reactions such as respiration and lipid peroxidation and extrinsic factors such as IR and carcinogenic agents (Dizdaroglu *et al.* 2002). One of the most dangerous compounds formed is the highly reactive hydroxyl radical OH- which is capable of causing oxidative damage to DNA and has been associated with ageing, mutagenesis and carcinogenesis (Dizdaroglu *et al.* 2002). Spontaneous hydrolysis of nucleotide residues or deamination of bases can lead to the formation of abasic sites (Kow 2002).

1.1.4 UV damage

Exposure to ultraviolet B radiation (UVB) results in the formation of DNA damage such as CPDs and (6-4) photoproducts (Ichihashi *et al.* 2003). However it can also lead to other forms of damage such as protein-DNA crosslinks, single strand breaks (SSB) and oxidative base damage (de Gruijl *et al.* 2001).

Figure 1.2: Formation of CPDs and 6-4 photoproducts (taken from (Ichihashi *et al.* 2003)

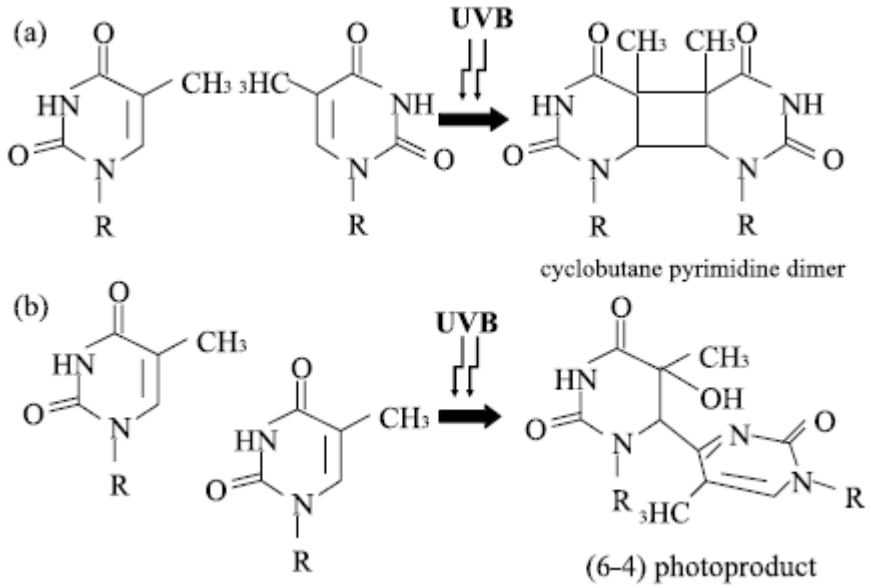

The above shows how adjacent pyrimidine dimmers on the same strand change following exposure to UVB, resulting in the formation of either CPDs (1.2 (a)) or (6-4) photoproducts (1.2(b)).

If left unresolved, this damage can induce mutations in epidermal cells which can lead to the development of skin cancers such as basal cell carcinomas, squamous cell carcinomas and cutaneous melanomas (de Gruijl *et al.* 2001).

1.2 DNA Repair pathways

Due to the possible adverse consequences that may arise from unrepaired DNA damage such as cell death, accumulation of mutations and development of cancer, it is crucial for the cell to repair any lesions prior to cell division to prevent the mutation being passed onto daughter cells (Malumbres and Barbacid 2009) and maintain genomic integrity (Wang *et al.* 2000). DNA repair pathways are an integral part of the cell cycle and these are stringently regulated by a series of cell cycle checkpoints at every phase of the cell cycle (Hoeijmakers 2001). DNA repair pathways in humans include the following

- Excision Repair Pathways
    - Nucleotide Excision Repair (NER)
    - Base Excision Repair (BER)
    - Mismatch Repair (MMR)
- Strand break repair
    - Non Homologous End Joining (NHEJ)
    - Homologous Recombination Repair (HR)
    - Single strand annealing
- Direct Reversal

The following sections will review the DNA repair pathways primarily associated with the repair of DNA damage induced by chemotherapeutic agents.

1.2.1 The DNA Damage Response

Although the exact mechanisms for how the DNA repair pathways that become activated after DNA damage has occurred have yet to be elucidated, sufficient progress has been made to allow for a general organisation of the DNA damage response pathway. It has emerged as a regulatory pathway which has numerous targets but overall its goal is to sense and facilitate the repair of damaged DNA.

There are two central protein kinases at the heart of this pathway, Ataxia Telangiectasia Mutated (ATM) and Ataxia Telangiectasia and RAD3 related (ATR). They appear to work in similar pathways; a consensus which stems from findings that they both phosphorylate p53 on Ser15 (Shiloh 2001). The deleterious effects of a non-functional ATM gene is characterised by the disorder Ataxia Telangiectasia (A-T) which renders individuals sensitive to IR and susceptible to the development of cancers. There are no known diseases which present with impaired ATR function (Harper and Elledge 2007), making it difficult to fully characterise the functionality of this protein.

The MRE11/RAD50/NBS1 (MRN) complex sense the formation of DSBs and recruits ATM to the damaged DNA which results in its autophosphorylation on Serine 1981 (Harper and Elledge 2007). ATM plays a pivotal role in the response to damage induced by IR and controls phosphorylation of downstream targets such as p53, Mdm2, BRCA1 and Chk2 in response to DNA damage (Shiloh 2001).

ATR is thought to be recruited when a replication block such as a stalled replication fork is encountered (Harper and Elledge 2007). When DNA polymerases stall, the replication helicases pursue unwinding of DNA ahead of the replication

fork, producing single strand DNA (ssDNA). The ssDNA then binds to a single strand binding protein, replication protein A (RPA), forming the ssDNA-RPA complex. This complex then recruits ATR via a regulatory subunit known as ATRIP and enables co-localization with the PCNA-related 911 complex. This initiates phosphorylation of the two proteins and down-stream signalling ensues (Harper and Elledge 2007).

1.2.2 Base Excision Repair

BER protects the cellular genome against damage arising as a result of DNA interaction with reactive oxygen species (ROS) such as methylation, deamination and hydroxylation (Seeberg *et al.* 1995) which results in the formation of lesions such as 8-oxo-guanine (Refer to Figure 1.3). It is also thought to be essential in protecting the cell against damage caused by exogenous agents such as IR (Seeberg *et al.* 1995).

Figure 1.3: Oxidative conversion of Guanine into 8-Oxo-Guanine (Niles *et al.* 2006)

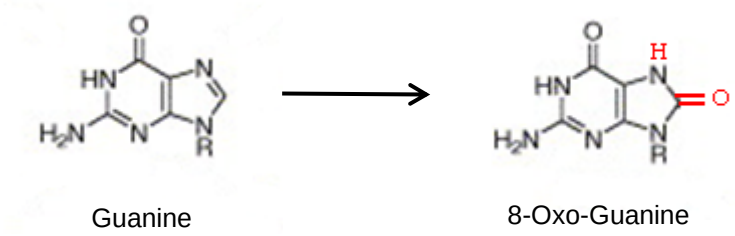

The repair pathway is initiated by DNA glycosylases which cleave the N-glycosylic bond between the damaged base and the deoxyribose backbone at the 5' end of the abasic site (Gary *et al.* 1999). This creates an apurinic or apyrimidine (AP) site which are cytotoxic and must be repaired (Krokan *et al.* 1997). There are two routes that can be taken to process and correct the abasic site after this initial

excision is made. These are the short patch pathway which is the dominant pathway in mammalian cells and the long patch pathway which is dependent on Flap endonuclease/ 5'-3' exonuclease (FEN-1) and Proliferating Cellular Nuclear Antigen (PCNA), a protein found in abundance in the nucleus (Klungland and Lindahl 1997). The short patch pathway involves the removal of a single nucleotide; the gap is then filled by DNA Polymerase β and the strand is sealed by DNA Ligase/XRCC1 (X-ray Repair Cross Complementing protein 1) (Gary *et al.* 1999). The long patch pathway is thought to be activated for altered DNA bases which are not susceptible for removal by DNA Polymerase β (Gary *et al.* 1999). These are usually sites with altered bases or sugars which requires FEN-1 to remove the 5' deoxyribose sugar along with at least one other nucleotide although this has been shown to be extended up to 8 nucleotides being removed in total by Klungland and Lindahl, (1997). An overview of the two distinct branches of this pathway is shown in Figure 1.4.

Figure 1.4: Overview of BER pathway (image taken from (Klungland and Lindahl 1997))

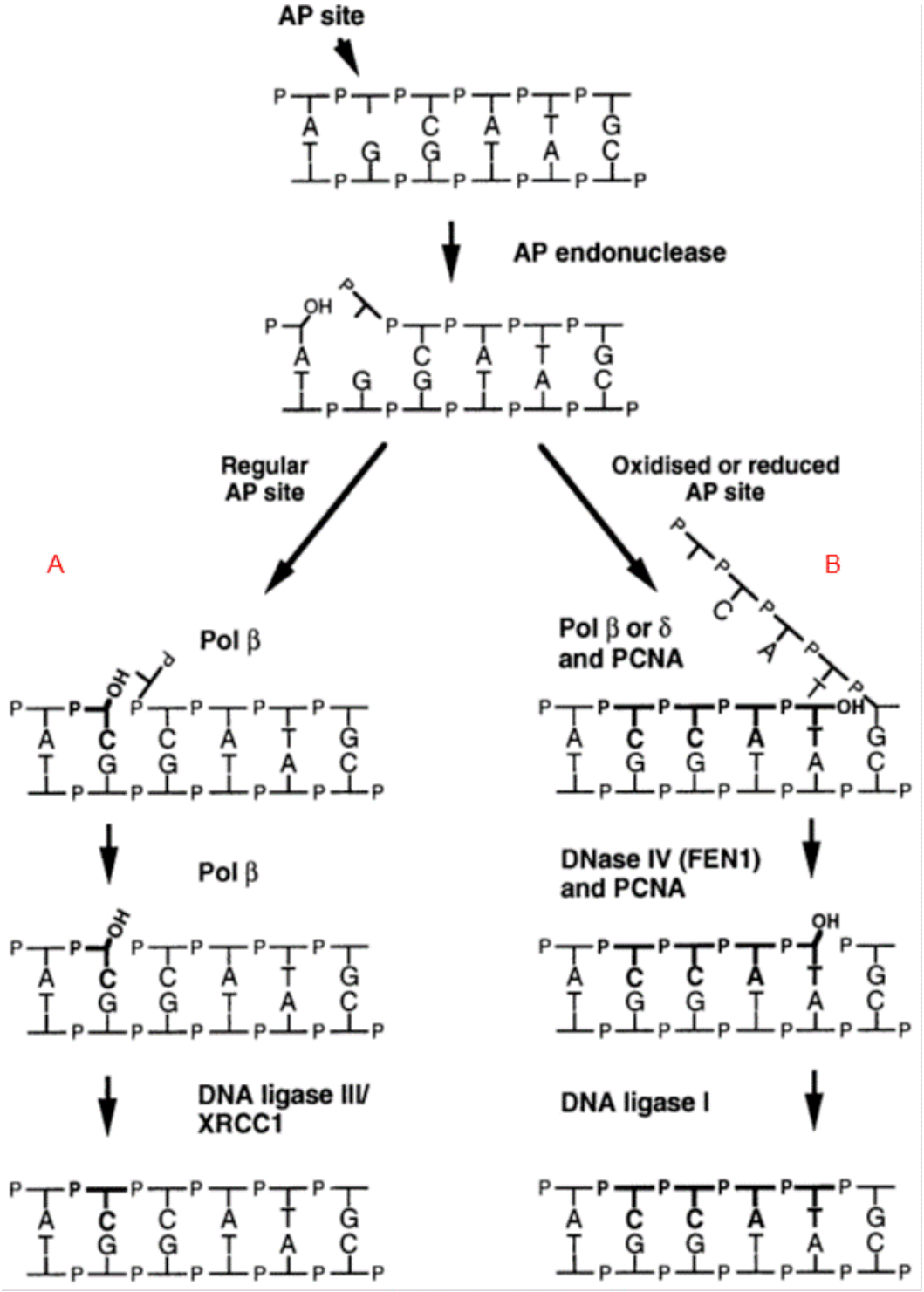

The above figure depicts the two branches of the BER pathway. Figure 1.3A depicts the short patch pathway where a single nucleotide is replaced and this is the usual route of repair for AP site formation. Figure 1.3B indicates the long patch pathway where a stretch of nucleotides are replaced; usually seen during the repair of oxidised or reduced bases which cannot be repaired by the short patch pathway.

1.2.3 Homologous Recombination

HR and NHEJ pathways are the main route taken in the repair of direct DNA DSBs in vertebrate cells (Takata *et al.* 1998). The point at which the cell is progressing through the cell cycle plays a role in determining the pathway that will become activated to repair the DSB (Lees-Miller and Meek 2003). It is generally agreed that in the G1/G0 phase of the cell cycle, DSBs are repaired by NHEJ while HR is more prominent during the late S/G2 phase (Valerie and Povirk 2003). HR is suppressed in G0/G1 and M phases of the cell cycle as supported by findings that Rad51 foci only appear in S and G2 phases (Graeser *et al.* 2010). Takata *et al*, (1998) demonstrated that HR and NHEJ are complementary in repairing the DSBs and concluded that both play a significant role in maintaining the integrity of chromosomes.

HR is essential in both mitosis and meiosis; promoting gene diversity in offspring through the combination of genetic information from both maternal and paternal alleles in the latter process (San Filippo *et al.* 2008). The presence of an intact sister chromatid is required for this repair pathway (Davies *et al.* 2001) which may serve as an explanation as to why this repair pathway is not the most common one used even though it results in the precise repair of the DNA lesion. An overview of this pathway is shown in Figure 1.5.

Figure 1.5: Homologous Recombination (diagram adapted from (San Filippo *et al.* 2008))

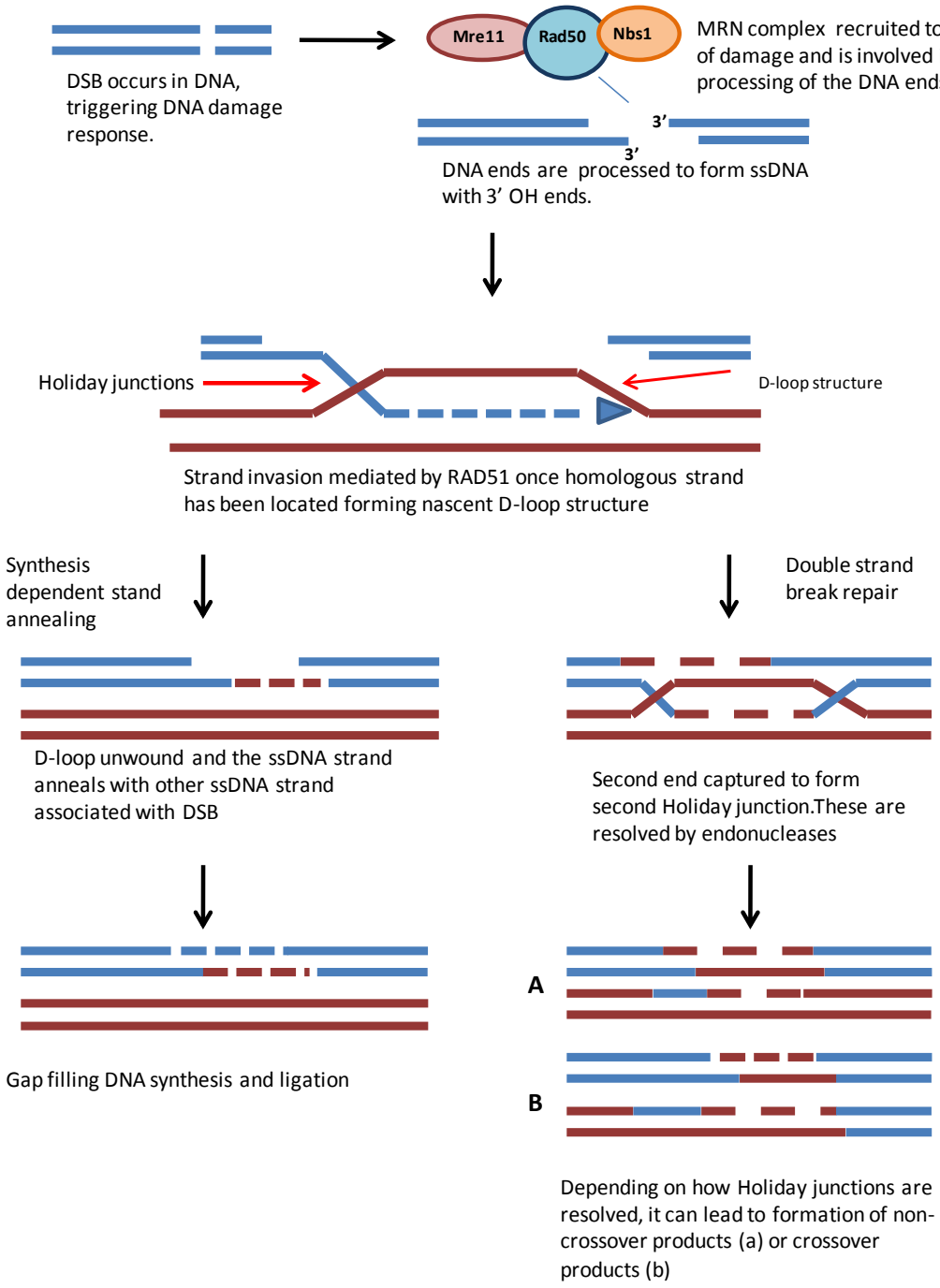

HR can be split into three main stages (Li and Heyer 2008)

- Presynapis – Processing of DNA ends
- Synapsis – Strand invasion
- Post synapsis

The repair pathway (refer to Figure 1.5) is initiated through the formation of a DSB. The MRN complex processes the two strands; producing a ssDNA tail with 3' OH ends. RAD51 binds to ssDNA; a process mediated by BRCA2 (Davies *et al.* 2001), to form the presynaptic filament.

This filament searches for the homologous sequence by capturing a duplex DNA molecule and while the exact procedure that takes place has not yet been established in eukaryotes, the RAD51 homolog in E. *coli* has been shown to locate the homologous sequence through random collisions between the presynaptic filament and the duplex DNA (San Filippo *et al.* 2008).

Once the homologous sequence has been located, the processed 3' end of the DNA molecule invades the duplex DNA, forming a nascent D-loop structure. DNA synthesis then takes place.

The second DNA DSB end is captured by annealing to the extended D-loop which forms Holliday junctions. The process is completed through the resolution of these Holliday junctions by the action of resolvases (Osborn *et al.* 2002). The end products will either be crossover or non-crossover. Cross-over products result from the exchange of an arm of the two participating chromosomes.

Both BRCA1 and BRCA2, which are tumour suppressor genes, play a role in HR. BRCA1 is a component of the BRCA1-associated genome-surveillance complex (BASC) which comprises tumour suppressors, DNA damage sensors and signal transductors (Wang *et al.* 2000). It has been proposed that the BASC complex can influence the repair pathway taken based on the type of DNA lesion inflicted (Turner *et al.* 2005).

In contrast to BRCA1, BRCA2 plays a major role in the progression of HR by regulating RAD51 strand invasion (Carreira *et al.* 2009). It has been demonstrated that BRCA2 promotes HR by directly associating with Rad51 through the 8 conserved RAD51 binding regions (Davies *et al.* 2001). Jensen *et al*, (2010) showed that BRCA2 stabilises Rad51 bound to ssDNa through down regulation of its ATPase activity.

Following processing of the DNA strand break ends by the MRN complex, thought to be regulated by BRCA1 (Turner *et al.* 2005), BRCA2 relocates to the site of damage. BRCA2 works at the crossing point between the processed single strand to aid RAD51 mediated strand invasion by displacing RPA from the overhang (Turner *et al.* 2005).

1.2.4 Non Homologous End Joining (NHEJ)

NHEJ is a quick albeit error-prone method of repairing DNA. It is the main pathway for the repair of induced DSBs as well as programmed DSBs that occur during V(D)J recombination. The basic principle behind this mechanism is simple; detect the broken ends and rejoin them by breaking off incompatible bases. Initially the broken ends of the DNA molecule are detected by the Ku heterodimer which comprises Ku70 and Ku80 subunits. Walker *et al*, (2001) demonstrated that the Ku heterodimer is a symmetrical molecule with a preformed protein ring in the centre which can accommodate duplex DNA. The ring allows the two broken ends to be harnessed together. The Ku heterodimer restricts the DNA molecule movement along the helical structure and also forms a barrier to prevent binding of the broken DNA ends prior to repair taking place (Walker *et al.* 2001).

DNA-PK_{cs}, a member of the phosphatidylinositol-3 Kinase related protein kinase family (PIKKs) (Lees-Miller and Meek 2003) is then recruited by the Ku 70/80 complex to the site of the break. Upon binding to the Ku-DNA complex, DNA-PK_{cs} becomes autophosphorylated and the two ends are brought within close proximity of each other. This process is precise when rejoining compatible blunt ends of DNA but more often than not, end processing is required to produce ligatable ends (Weterings and Chen 2008). The DNA ends are then ligated by the XRCC4/DNA Ligase IV complex which is also thought to play a role in the end processing step (Lees-Miller and Meek 2003). Figure 1.6 represents a general overview of this pathway.

Figure 1.6: Schematic representation of the NHEJ pathway adapted from (Lees-Miller and Meek 2003) and (Hefferin and Tomkinson 2005)

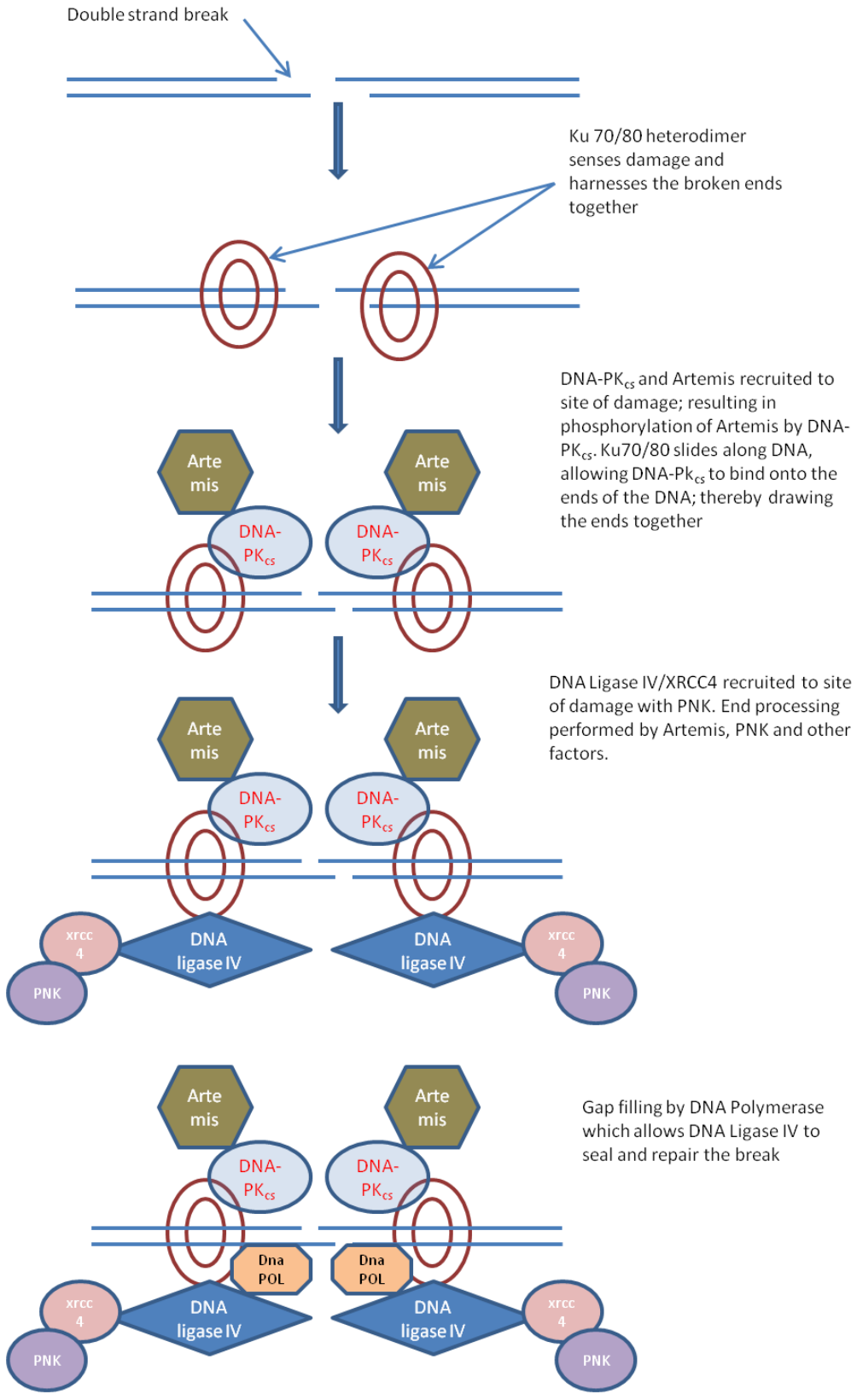

1.2.5 Nucleotide Excision Repair (NER)

NER is a complex repair pathway involving numerous proteins which is responsible for the removal of helix distorting DNA lesions such as UV-light induced lesions i.e. CPDs, DNA adducts formed by chemical agents such as AflatoxinB1 (Fousteri and Mullenders 2008) and ICLs formed by exposure to chemotherapeutic agents such as Pt. NER-deficient individuals present with rare autosomal diseases such as Xeroderma Pigmentosum (XP), Cockayne Syndrome (CS) and Trichothiodystrophy (TTD) ; all of which are associated with a hypersensitivity to sunlight, effectively demonstrating the significant role that NER plays in maintaining genomic stability and integrity (Fousteri and Mullenders 2008).

Two sub pathways exist within this repair pathway; Global Genome NER (GG-NER) and Transcription Coupled NER (TC-NER). GG-NER repairs lesions in untranscribed strands of active genes throughout the entire genome; however the efficiency of its repair varies which is thought to be linked to chromatins surrounding the lesion as NER requires a sister strand to complete its repair (Fousteri and Mullenders 2008). Conversely TC-NER is activated in the repair of DNA lesions encountered in transcribed strands of active genes only (Furuta *et al.* 2002). The other fundamental difference between these two sub pathways lies in the detection of the DNA lesion. UV-DDB and XPC-RAD23B activate the GG-NER pathway when a DNA lesion is sensed whereas TC-NER is activated through the stalling of RNA Polymerase II (RNAPII) complex during transcription.

When RNAPII stalls, two transcription-coupled repair specific factors CSA and CSB are recruited to the site of the damage. CSA encodes 7 WD-40 motifs which are associated with diverse aspects of cellular metabolism and are generally

viewed as having regulatory functions (Henning *et al.* 1995). CSB is able to bind to DNA; thought to be mediated by binding to core histone proteins within the nucleosome (Henning *et al.* 1995). CSA and CSB colocalise with RNAPII to mediate formation of the repair machinery; each has its own role in this process. CSB is required for the recruitment of NER proteins to the stalled RNAPII and CSA in concert with CSB recruit nucleosomal binding proteins HMGN1, XAB2 and TFIIS. Mutations in CSA and CSB lead to the development of CS; which is discussed elsewhere. TC-NER has been implicated as the main repair pathway for the repair of ICLs induced by Cisplatin (Furuta *et al.* 2002). Using cells that were deficient in XP-A, XP-D, CSA AND CSB, Furuta *et al*, (2002) were able to demonstrate hypersensitivity to Pt, despite the fact that these cells still had a functional GG-NER pathway. Their findings were further validated by demonstrating normal resistance in an XP-C cell line which has functional TC-NER but limited GG-NER capacity.

The two sub-pathways share a requirement for activation of the same factors once the lesions has been sensed in order to repair the damage. In both instances, specific factors and NER proteins are recruited to the site of damage. Components of Transcription repair factor IIH (TFIIH), which are coded by XPB and XPD genes, unwind the DNA double helix around the section of the lesion, creating a stretch of ssDNA. The DNA strand is cut at 3' and 5' ends by XPG and ERCC1-XPF respectively. DNA repair then takes place, using the sister strand as a template.

ERCC1-XPF is a structure specific endonuclease involved in the excision process in NER. Deficiencies in ERCC1-XPF lead to increased sensitivity to UV light, characterised in patients suffering from Xeroderma Pigmentosum (Complementation Group F). It incises the damaged strand at the 5' position,

enabling the 3’ end to be used as a template to replaced damaged nucleotides by the DNA repair machinery. However there have been findings to suggest that the functions of this nuclease may not be limited to NER alone (Al-Minawi *et al.* 2009). Al-Minawi *et al*, (2009) indicated that ERCC1-XPF plays a role in the repair of ICLs via the HR pathway which is in line with findings by Niedernhofer *et al,* (2004) who demonstrated that ERCC1-XPF is not required to form DSBs after ICL damage but are crucial in resolving this damage.

Figure 1.7: Overview of the two branches of the NER pathway (taken from (Fousteri and Mullenders 2008))

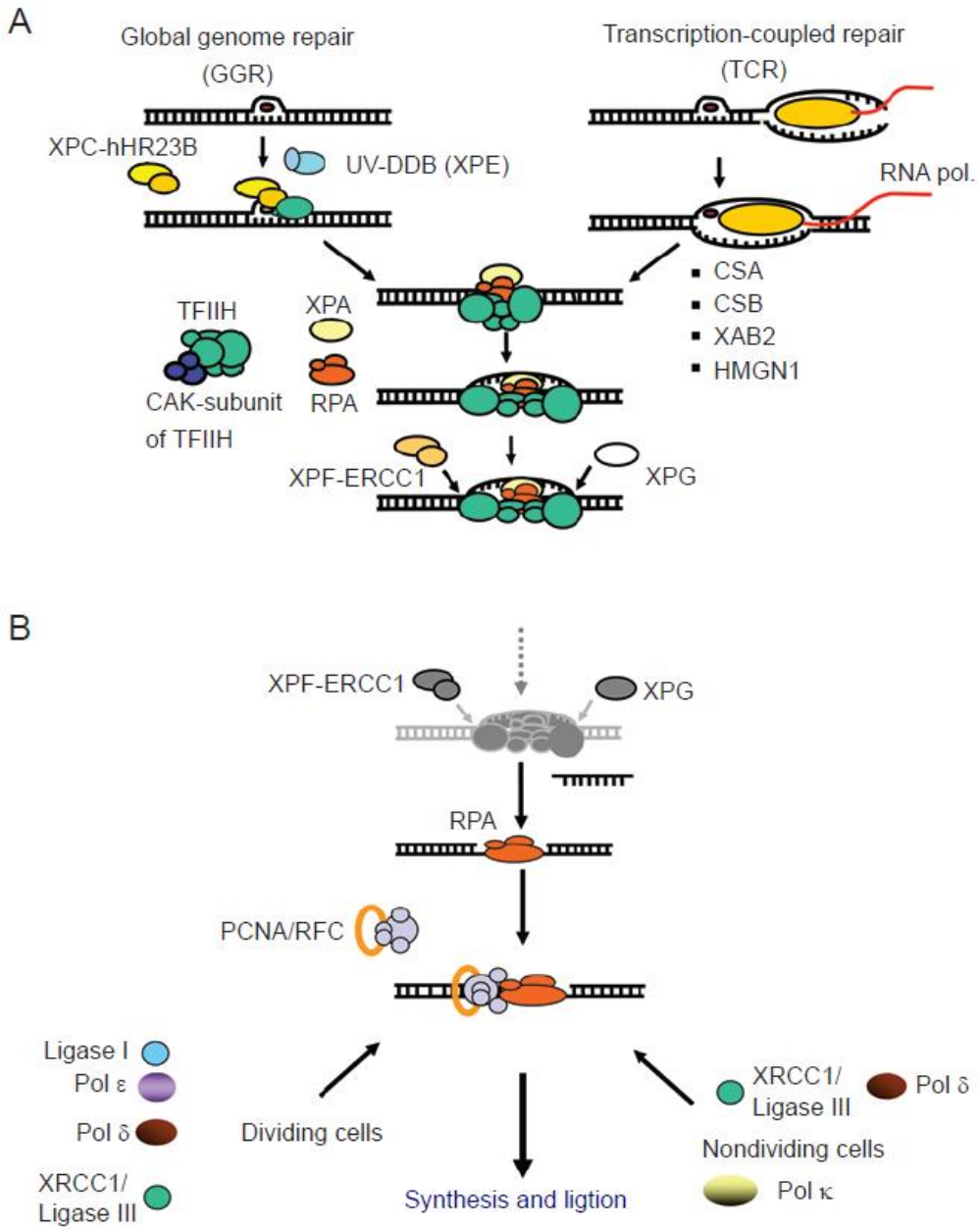

The above shows an overview of the two distinct branches of the NER pathway. Figure 1.7 (A) shows the different mechanisms of damage recognition and Figure 1.7 (B) shows where the two branches overlap to complete repair

1.3 DNA Repair defective disorders

The significance of having fully-functional DNA repair pathways is highlighted in diseases where DNA repair is impaired. The importance of the DNA damage response can be seen in the deleterious consequences experienced by patients with Ataxia Telangiectasia (A-T), Nijmegen breakage syndrome (NBS), Blooms syndrome and Fanconi Anaemia (FA) (Scott and Pandita 2006). These have all been classed as chromosomal instability disorders where patients have a predisposition to the development of cancer and a decline in the efficacy of their immune system (Digweed 2003). There is another group of disorders which are deficient in the NER pathway which render individuals sensitive to UV rays such as XP, CS and TTD. An overview of some of the different disorders affected by defective DNA damage and repair responses is shown in Table 1.2. The clinical manifestations of these disorders emphasize the colossal roles the various DNA repair pathways play in protecting our genome and the importance of recognising and dealing with DNA damage efficiently.

Table 1.2: Overview of disorders affected by defective DNA damage and repair responses (adapted from (Lehmann 2003))

Disorder	Defect	Consequences
Xeroderma Pigmentosum (XP)	XP complementation genes (*XP A-G* & *XP-V*)	Hyper sensitive to UV light
Cockayne Syndrome (CS)	*CS A* or *CSB*	Unable to resume RNA synthesis post UV exposure
Trichothiodystrophy (TTD)	*XPB* or *XPD* helicases or *TTDA*	Dysfuctional transcription
Ataxia Telangiectasia (A-T)	*ATM* gene	Radiosensitivity
Ataxia Telangiectasia Like Disorder (ATLD)	*MRE11* gene	Impaired DSB repair
Nijmegen Breakage Syndrome (NBS)	*NBS1* gene	Impaired DSB repair
Fanconi Anaemia (FA)	Fanconi Anaemia genes	Defective repair of interstrand crosslinks
Bloom's Syndrome	*BLM* gene	Increased sister chromatid exchange
Werner's Syndrome	*WRN* gene	Impaired DNA repair
Rothmund-Thompson Syndrome	*RECQL4* gene	Impaired DNA repair
Severe Combined immunodeficiency (SCID)	*SCIDX1* gene	Defective immune system
Seckel Syndrome	*ATR* gene	Impaired DNA damage response
LIG4 Syndrome	DNA Ligase IV gene	Defective V(D)J recombination
Li-Fraumeni Syndrome	*p53* gene	Unable to effectively induce cell cycle arrest
DNA PK_{CS} deficiency	DNA PK_{cs}	Impaired DSB repair

1.3.1 Ataxia Telangiectasia

A-T is a neurodegenerative condition which usually presents in early childhood (McKinnon 2004). The underlying cause of this syndrome is a mutated ATM gene which usually renders the patient susceptible to the development of cancers such as lymphoma and leukaemia in addition to presenting with immunodeficiencies (McKinnon 2004). The ATM gene is at the core of the signalling cascade that responds to DSBs by coordination of the cellular response to this lesion (Friesner *et al.* 2005). As it is also involved in the response to DSBs caused during V(D)J recombination and meiosis, A-T patients are also known to suffer from sterility due to the defective meiosis recombination that arises as a result of the mutated ATM gene.

Friesner *et al*, (2005) showed that ATM is required for the formation of γ-H2AX foci which is thought to be one of the first cellular responses to DSBs that arise from exposure to ionising radiation which may provide some explanation for the radiosensitivity of these patients. This line of evidence was further backed by Bourton *et al*, (2011) who demonstrated that the AT5BIVA cell line, derived from a patient with classical A-T showed an increased sensitivity to IR in comparison to the normal patients.

1.3.2 Nijmegen Breakage Syndrome

NBS is a rare autosomal disease with a defect in the NBS1 gene where patients are susceptible to the development of B cell lymphomas. Patients present with numerous symptoms such as growth retardation, receding foreheads and mental retardation which worsens with age.

The NBS1 protein plays a pivotal role in the damage response pathway. It directly binds to H2AX and recruits MRE11 and RAD50 to the site of damage. NBS1 associates with MRE11 and RAD50 in response to form the MRN complex. The MRN complex then mediates the repair of DSBs, primarily through HR (Komatsu *et al.* 2007). Their findings led to the conclusion that NBS1 is a key regulator of HR.

1.3.3 Blooms Syndrome

Bloom's syndrome is caused by a loss of function in the *BLM* gene which leads to patients experiencing striking increases in chromosome aberrations, sister chromatid exchange and mutations ((Wang and Heddle 2004)). The *BLM* gene encodes a RecQ helicase which is involved in unwinding of DNA; a necessary step during cellular processes such as replication and repair.

Patients exhibit facial erythema which is sensitive to sunlight and they are also immunocompromised. As with the other chromosomal instability diseases, they show an increased susceptibility to the development of cancers such as leukaemia and lymphoma.

1.3.4 UV-Sensitive Disorders

There are three distinct disorders, CS, XP and TTD which are all associated with hypersensitivity to the effects of UV rays due to defects in various components of the NER pathway but present with differing physical characteristics.

CS patients usually present with physical manifestations such as growth retardation, skeletal and retinal abnormalities, neurological defects, increased sensitivity to sunlight and mental retardation. CS patients have defects in either the *CSA* gene or *CSB* gene which form part of the RNAPII complex to recruit various NER

proteins to the site of damage. These defects lead to the inability for CS patients to resume RNA synthesis post exposure to UV light and there is a deficiency in TC-NER brought about by a deficiency in either CSA or CSB (Lehmann 2003).

XP patients suffer from hyper-pigmentation post exposure to sunlight, very dry scaly skin, loss of elasticity, skin lesions and an increased vulnerability (>1000 fold increase) to the development of various skin cancers (Lehmann 2003). XP patients can be categorised into 8 different complementation groups; XP A-G, which are known as classical XP and XP-V, also known as XP-variant. *XPC* and *XPE* patients present with defects in the GG-NER pathway but a functional TC-NER, providing some form of explanation for the generally milder symptoms exhibited by patients in these two groups in comparison to the others (Diderich *et al.* 2011). The other XP groups present with varying levels of defective TC-NER and GG-NER with *XPA* patients having a completely non-functional NER pathway.

TTD patients suffer from a myriad of symptoms such as **P**hotosensitivity, **I**chthyosis (scaly skin), **B**rittle hair and nails, **I**mpaired intelligence, **D**ecreased fertility and **S**hort stature (PIBIDS). It is generally considered a development disorder with no increased susceptibility to the development of skin cancer even though the *XPB* and *XPD* helicases are affected (Diderich *et al.* 2011). The hallmark of this disease is brittle hair which displays a distinct “tiger tail” banding when examined under polarising microscopy (Faghri *et al.* 2008). TTD patients are primarily affected by dysfunctional transcription as the XPB and XPD helicases have been found to form part of the basal transcription factor TFIIH.

1.4 DNA repair biomarkers

Due to the fact that the major emphasis of this thesis is to evaluate DNA repair biomarkers for their ability to detect patient sensitivity or resistance to chemotherapy, the two principle biomarkers being utilised are reviewed below.

1.4.1 H2AX

The histones are a group of proteins responsible for compacting DNA into the nucleus. They are found as an octomer that consists of 2 molecules of H2A, H2B, H3 and H4; (refer to Figure 1.8). They are positively charged, allowing them to bind to negatively charged DNA very tightly; resulting in the formation of 100kDa protein complex (Fernandez-Capetillo *et al.* 2004). The DNA becomes further condensed by the linker Histone H1 which compresses the nucleosomes into chromatin fibres (Fernandez-Capetillo *et al.* 2004).

Figure 1.8: Structure of histones adapted from (Bohm and Crane-Robinson 1984)

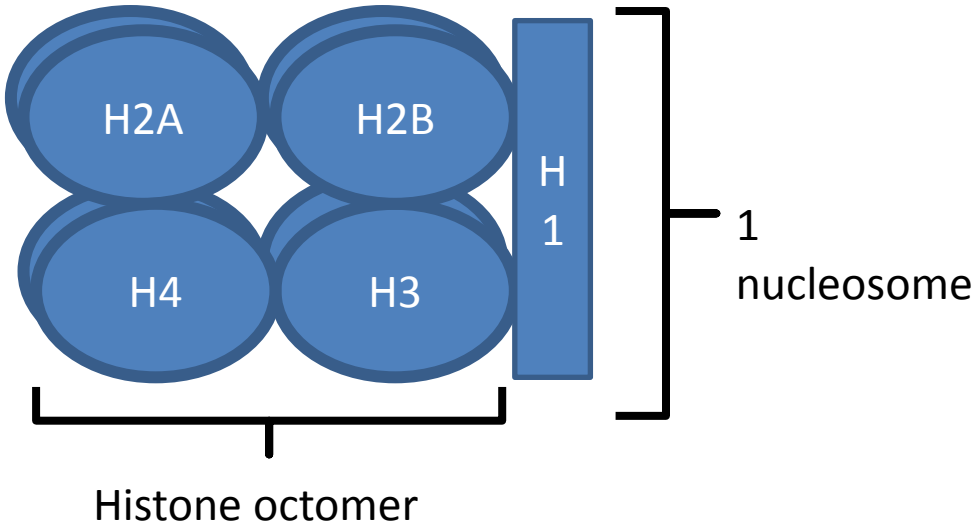

H2AX is one of the isoforms of the Histone H2A protein; distinguished from other isoforms by the presence of a short COOH terminal tail. Rogakou *et al*, (1998) first identified a unique phosphorylation event on the Serine 139 residue located within the COOH tail. In response to exposure to IR and subsequent formation of DSBs, H2AX becomes phosporylated on Serine 139, forming γ-H2AX (Refer to Figure 1.9). The phosphorylated γ-H2AX accumulated around the break in a 2Mb region. Sedelnikova *et al*, (2002) identified that γ-H2AX foci form in a 1:1 ratio with DSBs in the SF-268 human astrocytoma cell line and HT-1080 human fibrosarcoma cell lines. Iododeoxyuridine (^{125}IdU) is known to produce 1 DSB per decay in bacteriophage DNA (Sedelnikova et al, 2002). By measuring the radioactivity of ^{125}IdU as well as calculating the number of γ-H2AX foci in each cell, Sedelnikova *et al*, (2002) were able to show a direct correlation between DSBs and formation of γ-H2AX foci.

Figure 1.9: Example image of γ-H2AX foci obtained from imaging flow cytometry

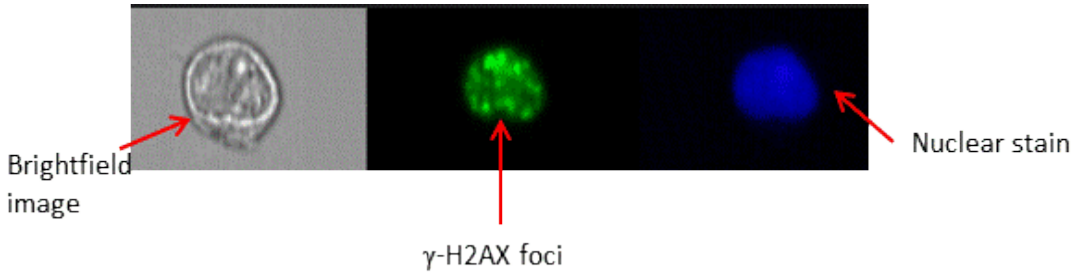

The above figure is shown in Brightfield which allows visualisation of cell morphology, AF488 stained γ- H2AX foci and the cell nucleus which has been stained with Draq-5

H2AX phosphorylation is an integral part of the DNA damage signalling network (Olive and Banath 2009). Repair of DSBs caused by IR then takes place either through NHEJ or HR. The position of the cell in the cell cycle governs which repair pathway will be activated as HR can only take place once cells have

progressed through the S phase due to the necessity of a sister strand's presence. Once DNA repair has taken place, H2AX becomes dephosphorylated and reverts back to its inactive form.

γ-H2AX has been demonstrated to be an effective target in identifying cell sensitivity to a variety of DNA damaging agents which cause direct DNA double strand breaks such as gamma radiation and doxorubicin (Olive and Banath 2009). Bourton *et al*, (2011) have demonstrated that studying γ-H2AX formation could potentially be used to predict patient response to radiotherapy. The study was carried out on a small cohort of patients who had experienced varying levels of normal tissue toxicity in response to radiotherapy. They were able to distinguish differences in the patterns of γ-H2AX formation and dephosphorylation post exposure to IR between patients who had experienced severe normal tissue toxicity compared to patients who had experienced little side effects.

Based on these studies, it could be possible to predict patient response to a range of chemotherapeutic drugs. However, although there is a significant body of work that has defined the formation of γ-H2AX is formed in response to direct DSBs such as those caused by IR, there have been diverse conclusions from studies that have used this biomarker to predict damage and repair responses to agents that do not form direct DSBs. Clingen *et al,* (2008) investigated the use of γ-H2AX as a biomarker of DNA damage in response to treatment with cross-linking agents HN2 and Pt; concluding that γ-H2AX was a highly sensitive marker of DNA damage. They also stated that further work could lead to the use of this marker as a determinant of cellular sensitivity or resistance to chemotherapeutic agents. Conversely Olive and Banath, (2009) investigated the use of the γ-H2AX biomarker as an indicator of

DNA damage post treatment with Pt with the final conclusions being that this may not be the best marker for determining sensitivity to chemotherapeutics. They found that one of the main limitations of this biomarker was that the cells had to transit S phase of the cell cycle in order to form H2AX foci which forms an obstacle when applying this biomarker to non-cycling tumour cells.

1.4.2 Rad-51

Due to the potential limitations that may be encountered in utilising γ-H2AX in identifying indirect double strand breaks, Rad51 may be a useful marker to predict patient outcome to chemotherapy. HR is thought to be responsible for resolving ICLs (Al-Minawi *et al.* 2009) therefore a more specific marker of chemotherapy induced DNA repair may be constructive in this investigation.

Rad51 is one of the key proteins utilised in HR and is responsible for initiating and driving strand invasion in this pathway. The Rad51 gene is located on chromosome 15q15.1; a region implicated in many cancers such as lung, breast and colorectal as having loss of heterozygosity. Rad51 was found to be able to bind to both ssDNA and dsDNa but Jensen *et al*, (2010) showed that the binding of Rad51 to dsDNA was actually counter-productive and inhibited DNA strand exchange.

Haaf *et al,* (1995) showed a dramatic increase in Rad51 foci formation was seen post irradiation in normal human fibroblast cell lines. Figure 1.10 shows an example of RAD51 foci. More information regarding RAD51 foci formation was further elucidated by Raderschall *et al*, (1999) when they showed Rad51 foci formation was occurring at sites of ssDNA; possible indicating the sites where HR was taking place.

Figure 1.10: Example images of RAD51 foci obtained from imaging flow cytometry

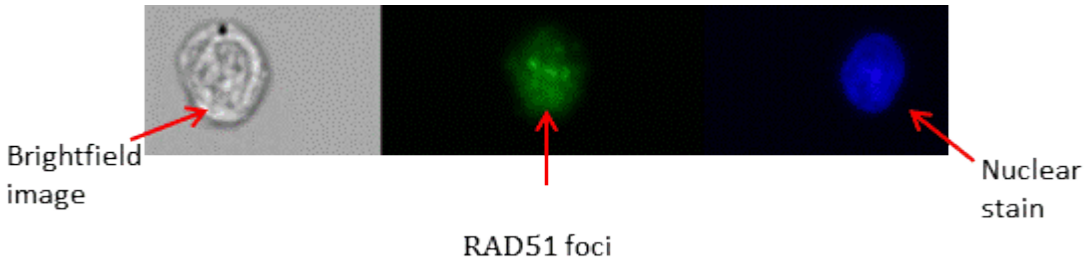

The above image has been depicted in Brightfield to visualise cell morphology, AF488 stained RAD-51 foci and the nucleus which has been stained with Draq5.

Yuan *et al*, (2003) also had similar findings to Raderschall *et al,* (1999) and were also able to demonstrate that Rad51 foci formation was cell cycle dependent. Graeser *et al*, (2010) explored the use of Rad51 as a marker for measuring the response of primary breast cancer tumours to neoadjuvant chemotherapy. The basis for their study was that tumours arising from germline mutations of BRCA1/2 would be defective in HR and therefore would be highly sensitive to chemotherapeutic agents which require HR for the resolution of damage incurred.

1.5 Overview of cancer

Cancer is now the leading cause of death in both men and women in the UK according to statistics published by Cancer Research UK. Nearly 300 000 new cases are diagnosed each year. Despite more than 200 types of cancer existing, there are four types that are predominant in the UK and account for more than half of all new cases; these are breast, lung, colorectal and prostate cancers.

The onset of cancer is considered to be a multi-step process involving three main stages; initiation, promotion and progression (Tysnes and Bjerkvig 2007). There are three notable classes of genes which are involved in tumour initiation; proto-oncogenes, tumour suppressor genes and genes involved with DNA repair mechanisms. Alterations in these genes may lead to disruptions in the control of normal cell growth and differentiation; leading to the transformation of normal cells into neoplastic cells (Tysnes and Bjerkvig 2007). In 1976, Peter Nowell hypothesised that most neoplasms are derived from a single cell; indicating that tumour progression was the result of genetic variability through neoplastic proliferation of the original transformed cell. However it has since emerged that the accumulation of genetic alterations is not the only factor in driving tumour progression (Mueller and Fusenig 2004). Tumours have the ability to manipulate the surrounding supportive tissue (tumour stroma) through interactive signalling to form a more accommodating environment for tumour progression (Mueller and Fusenig 2004).

Chemotherapy, radiotherapy and surgery are the common means of treating cancer although there are other treatments such as hormone and biological therapies also available. Chemotherapy can involve treatment with a

single drug, a combination of drugs or in conjunction with surgery or radiotherapy. Treatment can differ from patient to patient and is dependent on numerous factors such as the type of cancer, the location of the tumour, the stage at which the tumour is at and the age of the patient amongst others.

Chemotherapeutic drugs exert their effect by damaging the DNA of cancer cells thereby causing cell death. However it is not selective in killing cancer cells and the destruction of normal cells leads to the manifestation of side effects.

Side effects are a fundamental limitation of chemotherapy. The extent of normal cell damage governs the level of side effects experienced by the patient. Side effects can include but are not limited to the following (Conklin 2000)

- alopecia
- weight loss
- loss of appetite
- destruction of immune system
- mucositis of the gastrointestinal tract leading to nausea, vomiting and diarrhoea

1.6 Chemotherapeutic Agents

There are diverse classes of chemotherapeutic agents which exert their effects through different mechanisms of action. Table 1.3 below gives an overview of the main categories.

Table 1.3: Different classes of chemotherapeutic agents

Category	Mechanism	Example	Treatment	Side Effects
Anti metabolites	Inhibition of cell division.	5-Fluorouracil Methotrexate	Colorectal, Breast	Fatigue, Nausea, Alopecia
Alkylating Agents	Formation of ICLs	Busulfan Darcarbazine	Hodgkins and Non Hodgkins Lymphoma	Secondary skin cancer
Antimicrotubule agents	Destabilise microtubules	Paclitaxel Vincristine	Ovarian, Breast	Diminished Immune System
Anthracycline Antibiotics	DNA intercalator, inhibits Topoisomerases	Adriamycin	Broad range of cancers	Cardiac Toxicity
Topoisomerase inhibitors	Inhibition of Topoisomerase I and II	Vincristine Etoposide	Stomach, Lung	Neutropenia
Platinum Based Drugs	Inter and Intra strand cross links	Cisplatin Carboplatin	Testicular Bladder	Nephrotoxicity

1.6.1 Anti-metabolites

Anti-metabolite drugs are structurally similar to purine and pyrimidine bases. They exert their effects through the following mechanisms

1. Inhibiting vital biosynthetic processes e.g. competing with metabolites to bind to key enzymes
2. Incorporating themselves into DNA or RNA and inhibiting their normal functions

They are phase specific and work only in the S phase of the cell cycle. Most anti-metabolite drugs have a minimum threshold concentration below which no cytotoxic effects are seen regardless of the duration of exposure (Alison 2002).

5-fluorouracil (5-FU) is a fluoropyrimidine used in the treatment of breast, head and neck cancers amongst others. It was introduced over forty years ago as a treatment for both advanced and early stage colorectal cancer. Although not highly effective as a sole agent, combining it with pro-drugs such as Leucovorin and Methotrexate increases its cytotoxicity through greater inhibition of key enzymes and minimises tumour resistance arising (Alison 2002). Therefore it remains one of the most used treatments of colorectal cancer (Van Cutsem *et al.* 2000).

Figure 1.11: Chemical structure of Uracil and 5-FU (adapted from (Van Cutsem *et al.* 2000))

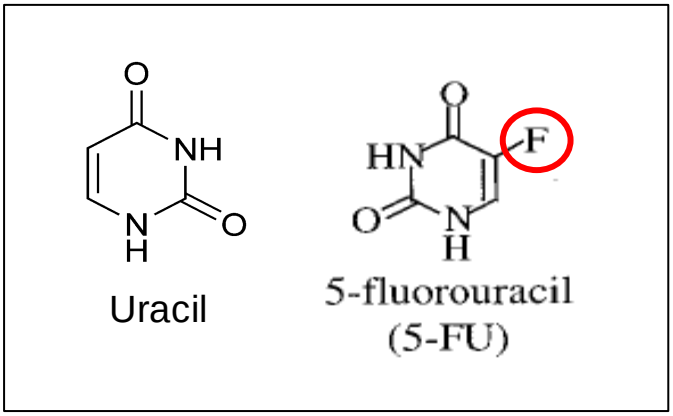

5-FU is an analogue of Uracil; a fluorine atom present in place of Hydrogen at C-5 (Refer to Figure 1.11). The compound incorporates both mechanisms of action through the integration of fluronucleotides into RNA and DNA as well as inhibiting the nucleotide synthetic enzyme thymidylate synthase (TS) (Longley *et al.* 2003).

It enters the cell using facilitated transport mechanism and is then converted into active metabolites (Longley *et al.* 2003)

- Fluorodeoxyuridine monophosphate (FdUMP)
- Fluorodeoxyuridine triphosphate (FdUTP)
- Fluorouridine triphosphate (FUTP)

These metabolites interfere with RNA synthesis, an integral component of DNA replication as well as limiting the actions of TS. TS is a vital enzyme in DNA synthesis, catalysing the conversion of deoxyuridylate (dUMP) to Thymidylate (dTMP) (Giudice *et al.* 2007). Limiting its function will lead to a decrease in the production of dTMP and an accumulation of dUMP in the cell thereby leading to the inhibition of DNA synthesis and repair.

1.6.2 Alkylating Agents

Nitrogen mustard (HN2) based compounds have been appraised for anti-cancer properties since the 1940s. All alkylating agents work by forming covalent bonds with macromolecules that possess nucleophillic centres. This group of compounds can be broadly categorised into two different groups; monofunctional and bifunctional.

Bifunctional agents form covalent bonds on two different bases either located interstrand or intrastrand; creating a crosslink. Monofunctional agents only have one alkylating group and are unable to form crosslinks. They normally interact with DNA through the N7 position of Guanine. Interaction of these agents with DNA results in the formation of DNA adducts which inhibits DNA replication and can subsequently effect or inhibit RNA and protein production.

Mechlorethamine was the first nitrogen mustard based compound to be used in the treatment of cancer (Giuliani *et al.* 1997). One of the limitations of nitrogen mustard is the rapid activation rate of the compound which could potentially lead to the development of very severe side effects such as secondary skin cancer (Giuliani *et al.* 1997). This led to the development of structurally modified nitrogen mustards such as Cyclophosphamide.

1.6.3 Platinum Based Drugs

Pt is a highly effective anticancer agent frequently used in the treatment of many cancers (Pabla *et al.* 2008); with a notably high success rate in the treatment of testicular cancer (Masters and Koberle 2003). It is administered intravenously and is taken up into the cell either through passive diffusion or facilitated uptake although a clear understanding of this mechanism is yet to be clarified. Once inside the cell, Pt has to undergo multiple hydrolysis reactions, resulting in a structural change which allows it to bind to and interact with DNA (Siddick et al, 2003).

Pt exerts its toxicity through the formation of intra and inter strand crosslinks. It can form intrastrand crosslinks between adjacent guanine bases or between adenine and guanine bases which represents approximately 90% of adduct

formation (Crul *et al.* 2003). ICLs are also formed between guanine bases on opposite strands as well as DNA-protein crosslinks. Pt targets proliferating cells and the formation of these lesions prevent core cellular processes such as transcription and replication (Al-Minawi *et al.* 2009). Although a number of DNA adducts are produced by cross-linking agents, the efficacy of these drugs are usually determined by their ability to form ICLs (Welsh *et al.* 2004).

However the use of Pt is limited due to increasing resistance to the drug itself and also due to the severe toxic effects on normal tissue (Olive and Banath 2009). The short term side effects of this agent are typically seen with most chemotherapeutic agents such as nausea, weight loss and hair loss. However the long term side effects, predominantly linked with high dose treatment regimens, are far more dangerous and can leave the patient severely disabled. Some examples of these side effects include

- Loss of hearing with the potential to develop clinical deafness
- Nephro-toxicity
- Cerebral herniation and coma
- Cisplatin neuropathy which manifests as tingling sensations and numbness with the possibility of spinal ataxia development leaving the patient disabled (Harmers *et al.* 1991)

Due to the debilitating side effects associated with Pt, variants of platinum bases drugs were produced such as Carboplatin and Oxaliplatin (Vilmar and Sorensen 2009).

1.6.4 Anthracycline Antibiotics

Anthracycline antiobiotic are regarded as an integral part of chemotherapy and possess great therapeutic potential due to their anti-tumour activity (Rabbani *et al.* 2005). This class of antibiotics all share a common four ring chromophore and contain quinine and hydroquinone groups.

Figure 1.12: The four ring structure seen in all anthracycline antibiotics

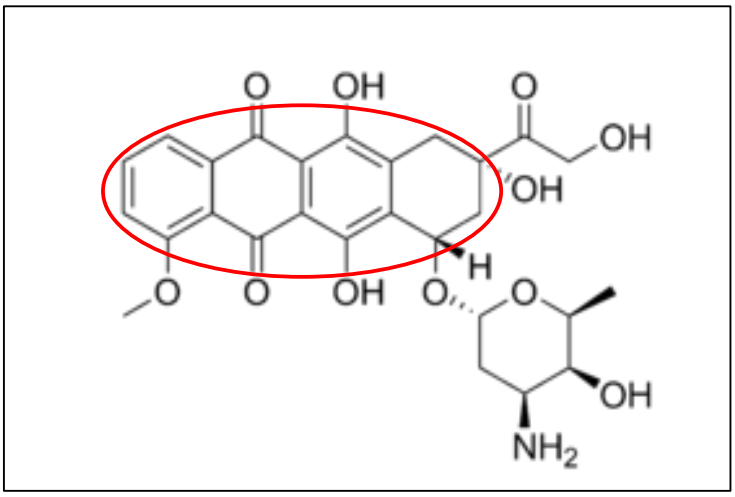

Their mechanism of action is a topic of much controversy. Several different mechanisms of action have been proposed (Gewirtz 1999) such as

- DNA intercalator
- Free radical formation
- DNA binding and alkylation
- DNA cross-linking
- Inhibition of Topoisomerase II

Adriamycin (ADR, also known as Doxorubicin) is regarded as one of the most powerful anticancer agents and is used in the treatment regimen of a broad range of cancers with particular success in solid tumour treatment such as breast, bile

ducts, osteosarcomas and Non-Hodgkins lymphoma (Satoh *et al.* 1988). However a similar predicament to Pt is encountered with this drug in that the highly potent side effects associated with this drug often diminish its clinical use. One of the most limiting side effects associated with Adr is the induction of cardiomyopathy which can lead to congestive heart failure (Tokarska-Schlattner *et al.* 2006). This complication proves a serious obstacle to prolonged use and also limits the dosage that can be administered in one treatment as it has been shown that increased doses of Adr has been linked to an increased incidence of cardiotoxicity (Takemura and Fujiwara 2007).

1.7 Developing resistance to chemotherapy

Development of resistance to chemotherapeutic drugs poses a serious limitation to the effectiveness of this form of treatment (Boehm *et al.* 1997; Carvalho *et al.* 2010) This was highlighted by Agarwal and Kaye, (2003) and Coley, (2008) who both noted that acquiring resistance to treatment regimens accouted for up to 90% of breast and ovarian cancer patients. Resistance can develop in many ways. To some extent, genetic instability and increased mutational rates of tumour cells attributes to this (Boehm *et al.* 1997). However there are numerous other mechanisms that have been proposed that lead to the development of drug resistance such as

- Increased drug efflux
- Upregulated DNA repair
- Inactivation of drug
- Increased tolerance to DNA damage

Increased drug efflux in tumour cells prevents intracellular accumulation of chemotherapeutic agents. P-glycoprotein (P-gp) is a membrane transporter protein encoded by the multi drug resistance (MDR1) gene and has been found to be responsible for preventing drug accumulation in the cytoplasm by transporting the drug across the plasma membrane (Thiebaut *et al.* 1987).

Cellular mechanisms such as increased drug inactivation by cellular metabolites such as Glutathione (GSH), increased levels of DNA repair or evasion of apoptosis may also lead to the development of acquired resistance (Banath and Olive 2003; Siddik 2003). This inherent resistance can then be transferred to daughter cells during mitosis (Goldie and Coldman 1983). Increased expression of

ERCC1 and ERCC2 were found to be associated with Pt resistance in human ovarian cancer patients (Dabholkar *et al.* 1992). ERCC1 is associated with both the NER pathway which is thought be responsible for resolving intrastrand crosslinks and the HR pathway which repairs ICLs (Dronkert and Kanaar 2001). The A2780/C-series of cell lines was established from a human ovarian cancer cell line A2780 and made resistant to Pt through repeated exposure to incrementally increasing concentrations of Pt (Ferry *et al.* 2000). They exhibit a number of resistant mechanisms such as elevated GSH levels, enhanced repair of adduct formation (Johnson *et al.* 1994) and an enhanced ability to tolerate Pt-induced DNA damage (Johnson *et al.* 1997).

A major problem in the development of resistance is that often tumours develop cross-resistance not only to drugs with similar mechanisms of action but also to functionally and structurally unrelated drugs (Ferry *et al.* 2000). It is important to identify patients who do not have the desired responses to treatment regimens as hypersensitive patients will suffer from debilitating and adverse side effects which could even lead to death in some cases. Similarly patients who are resistant to particular chemotherapeutic agents need to be readily recognised in order to avoid them undergoing needless treatments which will not help to slow down disease progression and instead be able to initiate alternative forms of treatment.

1.8 Aims

The aims of this project were as follows

1) To validate the use of the Imagestream which employs the novel imaging flow cytometry technique for DNA damage assays

2) To determine the response of repair normal immortalised cell lines to classical anti-cancer drugs such as HN2, Pt and Adr

3) To validate the efficacy of the DNA repair biomarkers γ-H2AX in assessing the rate of DNA repair in normal cells

4) To validate the efficacy of the DNA repair biomarker RAD51 in measuring the rate of DNA repair in normal cells

5) To determine whether resistance is associated with increased DNA repair as measured by γ-H2AX and Rad51. DNA repair normal cell lines were compared with resistant cell lines and a XPF-deficient cell line to evaluate this.

Chapter 2

Materials and Methods

2.1 General Cell Maintenance

2.1.1 Cell Culture

Cells were routinely cultured in Dulbecco's Modified Eagle Medium (DMEM) (PAA Laboratories Ltd., Yeovil, Somerset, UK) which was supplemented with 10% foetal calf serum (PAA Laboratories Ltd.), 2mM L-glutamine and 100 units/mL penicillin and streptomycin (PAA). Cells were grown in 100mm Petri dishes (Sarstedt Ltd, Leicester, UK) as monolayers at 37^{o}C in a humidified atmosphere of 5% CO_2 in air. All cell culture was carried out in a temperature controlled laboratory. Cell culturing was conducted in a Heraeus Class ii Laminar Flow hood.

2.1.2 Cell Lines

Secondary immortalised fibroblast cell lines were used throughout the different experiments conducted for this thesis. Cell lines with a range of DNA repair capacity were selected for this study. Details of cell lines are shown below in Table 2.1.

Table 2.1: Details of cell lines used

Cell line	DNA repair capacity	Details
MRC5-SV1 (Arlett *et al.* 2006)	DNA repair normal	Derived from fibroblast foetal lung cells and immortalised through expression of the SV 40 Large T antigen
NB1-HTERT (Ulus-Senguloglu *et al.* 2012)	DNA Repair normal	Derived from normal individual and immortalised through transfection of the HTERT gene
MRC5-SV1^{R}	Resistant to HN2	Developed through continual exposure to gradually incremented doses of HN2. Resistant to 5.3µg/mL HN2
NB1-HTERT^{R}	Resistant to HN2	Developed through continual exposure of parental cell line NB1-HTERT to gradually incremented doses of HN2. Resistant to 3.5µg/mL HN2
AT5BIVA (Murnane *et al.* 1985)	DSB repair defective	Derived from classical A-T patient and immortalised through expression of Simian Virus Large T antigen. A-T patients have defective ATM gene involved in cell signalling post formation of DSBs and exhibit increased sensitivity to IR
XP14BRNeo17 (Abbaszadeh *et al.* 2010)	DSB repair defective	Derived from XP patient with additional defective DNA-PK$_{cs}$ gene and immortalised through transfection of the pSV3neo immortaling vector. Patient exhibits sensitivity to both UV light and IR
GM08437B (Coriell Institute, New Jersey, USA)	Impaired GG-NER function	Deficient in XPF which forms part of the endonuclease complex with ERCC1. Exhibits sensitivity to cross-linking agents such as Pt and HN2

2.1.3 Trypsinisation of cells

Cells were left to reach about 95% confluency before sub-culturing them. When sub- culturing cells, medium was first aspirated off using a glass Pasteur pipette and cells were rinsed with 10 mL of Versene (Phosphate Buffered Saline (PBS) + 0.2% EDTA) to remove any traces of medium. Approximately 1 mL of 0.25% Trpysin-EDTA (Fisher Scientific, Loughborough, Leicester, UK) was added to the plate and the cells were kept at 37^{o}C for 10 minutes to allow cells to detach from the dish. Cells were then recovered from the plate in 10 mL of medium and seeded into plates at an approximate density of $1x10^{5}$ cells per plate.

2.1.4 Cell Counting

Cell counting was performed using either a glass haemocytometer or the Countess (Invitrogen, Life Technologies, Paisley, UK). Cell counts were primarily performed using the Countess. However the Countess is limited by its measurement range ($1x10^{4}$ - $1x10^{7}$ cells/mL). Therefore if cell concentrations were below this, then accurate cell counts could not be obtained. In these circumstances, a traditional Neubauer glass haemocytometer was used instead.

When counting cells using the haemocytometer, cells were detached from petri dishes using 1 mL of Trypsin (Fischer-Scientific). Once cells had detached, they were recovered in 10 mL of complete medium. 10 µL of the cell suspension was added to 10 µL of Trypan Blue to allow for exclusion of dead cells from the cell count. 10 µL of the cell suspension mixed with the Trypan blue was loaded onto a glass haemocytometer and cell counts were performed at 20x magnification using an Olympus CK2 microscope.

2.1.5 Cell Freezing

Cell freezing was deemed necessary to conserve stocks of the cell lines being used. They were frozen in freezing medium which was comprised of 20% FCS, 10% DiMethyl Sulfoxide (Sigma-Aldrich) and 80% DMEM medium containing penicillin/streptomycin and L-glutamine.

Cells were grown in 10mm Petri dishes until they were 95% confluent. Medium was aspirated off the cells and the cells were then rinsed with 10mL of PBS. Cells were then detached from the dish using 1 mL of 0.25% Trpysin-EDTA. After recovering the cells in 10 mL of medium, they were transferred into a 15 mL tube (Sarstedt) and centrifuged for 5 minutes at 1500rpm. The supernatant was then discarded and the cell pellet was resuspended in 1 mL of freezing medium.

The cell suspension was transferred to cryo-vials (Sarstedt) and placed in cell freezing containers (Nalgene, Sigma-Aldrich). These containers have a foam insert soaked in isopropanol which allows for a gradual freezing rate of 1^{o}C/minute. Cells were kept in these containers at -80^{o}C for twenty-four hrs to ensure they had reached the correct temperatures before being relocated to liquid nitrogen dewers for long term storage.

2.2 Imaging flow cytometry protocol for the γ-H2AX radiation assay

2.2.1 Cell lines

The cell lines used for this study were

- XP14BRneo17 (Abbaszadeh *et al.* 2010)
- AT5BIVA (Murnane *et al.* 1985)
- MRC5-SV1 (Arlett *et al.* 2006)

2.2.2 Cell fixation

Untreated control cells and cells exposed to 2 Gy of gamma radiation were fixed at 30 min, 3, 5 and 24 hours (hrs) post irradiation. Cells were detached using 1 mL of 0.25% Trypsin-EDTA and washed twice in ice-cold PBS). They then were fixed in 50:50 (V:V) methanol:acetone at 4^{o}C. Cells were stored no longer than 72 hrs prior to γ-H2AX antibody staining.

2.2.3 Gamma Radiation Dose Response Curve

To determine the level of fluorescence induced by different doses of gamma radiation and thus the level of γ-H2AX induction and DNA damage, each of the three cell lines were irradiated as proliferating monolayers with 0,2,4,6,8 Gy gamma irradiation from a ^{60}Cobalt source (Puridec Irradiation Technologies Ltd, Oxon, UK) at a distance of 25cm from the gamma source. This provided a dose rate of 1.3 – 1.4 Gy/min. They were fixed 30 minutes post irradiation and total nuclear fluorescence was determined through Imagestream^{x} analysis (as described in Section 3.28). On the basis of the dose response curves generated for each cell line, all future experiments were conducted following a dose of 2 Gy gamma irradiation.

2.2.4 Antibodies and Immunocytochemistry

Fixed cells were rehydrated with three washes in PBS and then permeabilised in PBS containing 0.25% Triton X-100 (Sigma-Aldrich, Dorset, UK) for 5 minutes at room temperature (RT). After blocking the cells in blocking buffer comprised of PBS containing 0.1% Triton X-100 and 0.5% nonfat milk protein (Premier International Food Ltd. UK, Spalding, Lincolnshire, UK), cells were incubated at 4^{o}C overnight in mouse monoclonal anti-serine^{139} γ-H2AX antibody (Clone JBW 301, Millipore UK Ltd., Hampshire, UK) at 1:10000 dilution.

Following three washes in wash buffer made up of PBS containing 0.1% Triton X-100, cells were incubated for 1hr at RT in anti-mouse IgG (whole molecule) R-phycoerythrin (PE) conjugated antibody diluted in block buffer to 1:50. Cells were washed again in wash buffer three times and once in PBS. Samples were then resuspended in 100 μL of Accumax flow cytometry buffer with 5 μM Draq5 (Biostatus Ltd., Leicestershire, UK). Two samples for fluorescence compensation were prepared with either the secondary antibody (R-phycoerythrin conjugate) or Draq5 being omitted from the process. These were fixed at 30 minutes post irradiation.

2.2.5 *In Situ* Detection of γ-H2AX foci

The number of γ-H2AX foci detected using *in situ* fluorescence microscopy was compared with the results generated from the Imagestream^{X}.

The three cell lines were grown to approximately 70% confluence on 13 mm glass cover slips and exposed to 2 Gy gamma radiation as previously described above. Cell fixation and antibody staining was also carried out as described above.

γ-H2AX foci were counted in the nuclei of at least 100 cells for each cell line in untreated cells as well as treated cells fixed at 30 min, 3, 5 and 24 hrs post irradiation. Microscopy carried out using an Axioscope 2 fluorescence microscope with a 100-fold magnification objective (Zeiss, Goettingen, Germany).

2.2.6 Imaging Flow Cytometry

The Imagestream (Amnis Inc., Seattle, Washington) enables images of individual cells in flow to be captured using up to six different optical channels (Refer to Table 2.2). Using the Inspire ™ data acquisition software, 20 000 images were captured using Channel (Ch) 01 for brightfield (BF), Ch03 for PE representing the γ-H2AX foci and Ch05 for Draq5 to represent the nuclear staining of each cell. The lasers used were

- 800nm to capture BF images
- 488nm to capture PE and Draq5 fluorescence
- 765nm to capture side scatter images

Cell classifiers were applied to BF in order to only capture objects between 50 and 300 units on an arbitrary scale. This range of values was previously established empirically from preliminary experiments to primarily show single cell images. Using a 488nm laser set at 75mW power, images were captured at 40X magnification at an approximate rate of 150 images per second, creating a raw image file (rif).

Table 2.2: Imagestream^X Fluorochrome Chart

Ch	Band (nm)		488	561	592	658	785
1	430 -505	**DAPI, Hoechst**, PacBlue, CascadeBlue, AF405,eFluor405,DyLight405, CFP, LIVE/DEAD Violet					
2	480-560	PacOrange, CascadeYellow, AF430, QD525	**AF488, FITC, GFP**, YFP, DYlIGHT488, PKH67, Syto 13, Spectrum Green, Lyso TrackerGreen, Mito TrackerGreen, QD525				
3	560-595	QD564, QD585	**PE**, PKH26, Cy3, AF555, DSRed	**PE, Cy3, AF546, AF55**, DyLight549, PKH26,DSRed, SpectrumOrange, Milto TrackerOrange			
4	595-660	QD625, eFluor650	**PE-TexRed, ECD,** PE-AF610, 7AAD, PI, RFP, QD625, eFluor625	**AF568**, AF594, AF610, DyLight594, PE-TexRed, ECD,TexRed, PE-Af610, RFP,mCherry, 7AAD, PI	**TexRed, AF594,** AF568, AF610, DyLight594, PE-TexRed, ECD, TexRed, PE-AF610, RFP, mCherry, 7AAd, PI		
5	660-745	QD705, eFluor650	**PE-Cy5, PE-AF647,** PerCP, PerCP-Cy5.5, DRAQ5, QD705,eFluor650	**PE-Cy5, PE-AF647,** DRAQ5	**AF647, AF660,** AF680, APC, Cy5, DyLight649, PE-AF647, PE-Cy5, DRAQ5	**DRAQ5, AF647, AF660, AF680,** APC, Cy5, DyLight649, DyLight680, PE-AF647, PE-Cy5, PerCP, PerCP-Cy5.5	
6	745-800	QD800	**PE-Cy7, PE-AF750,** QD800	**PE-Cy7, PE-AF750**	APC-Cy7, APC-AF750, APC-eFluor750	APC-Cy7, APC-AF750, APC-eFluor750, Cy7, AF750, DyLight750, eFluor750, PE-Cy7, PE-AF750	SSC

This table shows the broad range of fluorescents ligands that can be used with the Imagestream. The fluorochromes used for studies carried out in this thesis are highlighted in red.

2.2.7 Image Compensation

Compensation was performed using the samples that had been stained with either PE or Draq5 only. Images for these samples were captured without the BF illumination or scatter as it was important to detect intensity of fluorescence in these samples with only a single source of illumination, the 488nm laser set at 75mW. A compensation matrix was generated using the Ideas^{TM} software using control files created for the PE and Draq5 samples. This is a table of coefficients whereby detected light from each image is placed into the proper channel (Ch03 for PE and Ch05 for Draq5) on a pixel by pixel basis. The coefficients are normalised to 1 and each coefficient represents the leakage of either fluorochrome into juxtaposed channels.

Figure 2.1: Image compensation

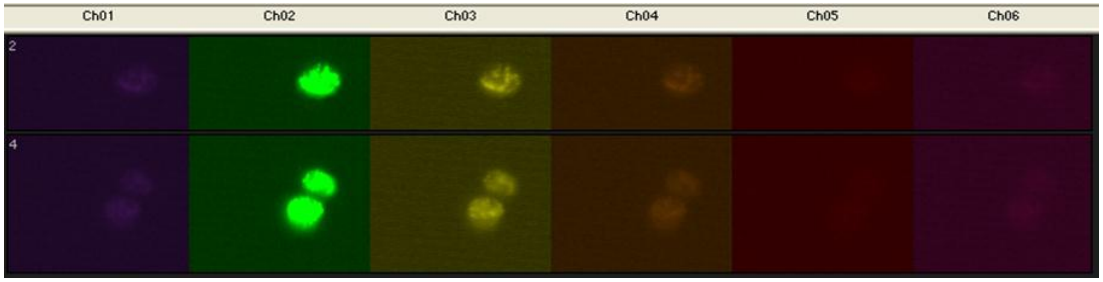

The above figure shows an example of uncompensated images obtained using a Imagestream^{X}. It can be seen to which extent the fluorochrome (AF488, normally depicted in Ch02 only) leaks into nearby channels. The compensation tool with the IDEAS software allows for the correction of this leakage.

Compensation is performed to eliminate any crosstalk that may occur where the fluorochrome leaks into other channels. This allows for accurate and true representation of fluorescence for each cell image. Table 2.3 shown below is an example of a typical compensation matrix table. Calculated compensation values were then applied to each sample file during analysis.

Table 2.3: Typical compensation matrix created in Ideas™ software

	Ch01	Ch02	Ch03	Ch04	Ch05	Ch06
Ch01	1	0	0.061	0	0.036	0
Ch02	0	1	0.277	0	0.125	0
Ch03	0	0	1	0	0.100	0
Ch04	0	0	0.518	1	0.143	0
Ch05	0	0	0.208	0	1	0
Ch06	0.02	0	0.087	0	0.352	1

The values in this table represent coefficients of leakage into juxtaposing channels. It can be seen that as you move away from the principal channel (indicated as having a value of 1), the coefficient of leakage is decreasing. We use values that have a margin of error that is less than 0.001

2.2.8 Analysis using Ideas™ software and calculation of foci numbers

The sample fixed 30 minutes post irradiation with 2Gy gamma radiation was used to create a template file with which all other samples in the investigation would be analysed with. This file was chosen due to it being likely to be the highest induction of γ-H2AX foci and therefore the brightest intensity of PE. Templates were created for each individual cell line.

The rif file created by the Inspire™ software was loaded into the Ideas™ software. Cell images were examined in BF, PE (γ-H2AX foci) and Draq5 (nuclear morphology) channels. The image gallery properties were adjusted to optimise the displayed fluorescent images.

The analysis process comprises a multistep process and initially uses a series of predefined “building blocks” provided within the software. These tools generate a series of scatter and histogram plots which allow for the identification of single

and focussed cells, stained for both Draq5 and PE. Identification of single cells is determined by the creation of a scatter plot of the population defined by cell area and cell aspect ratio from the BF images whereby each dot within the scatter represents a single cell. The single cell region was defined by visually validating the BF images and gated using the polygon region tool (refer to Figure 2.2 below.)

Figure 2.2: Gating for single cells

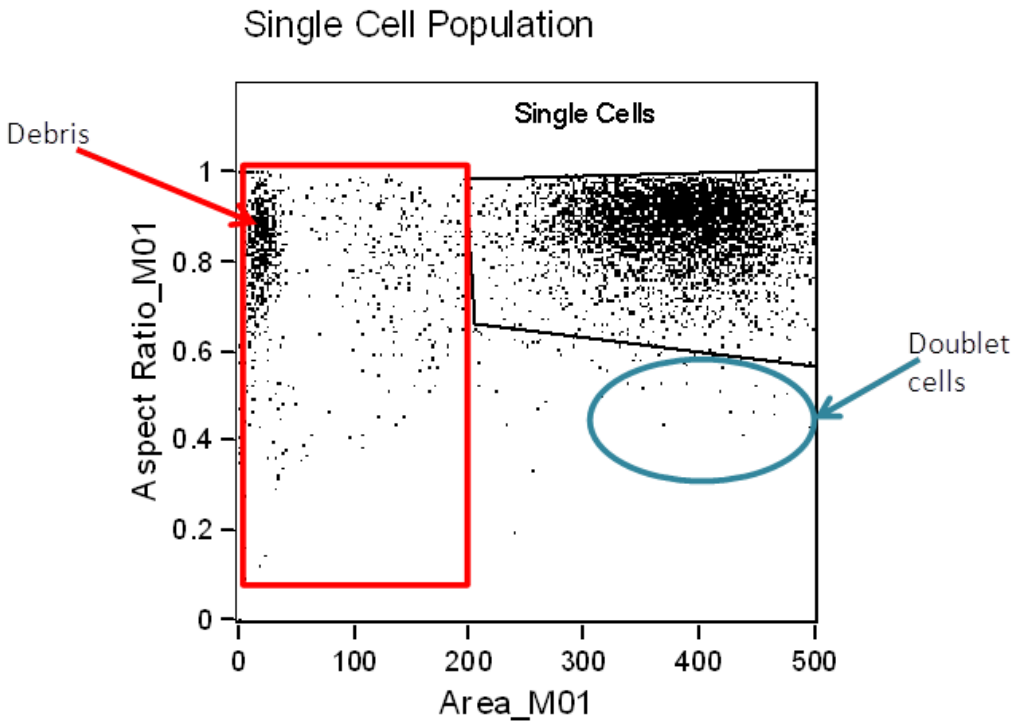

Identification of single cells within the population based upon cell area and aspect ratio. Single cells are gated using the polygon tool. The area marked in red indicates either debris or beads that have been collected during the run and the area indicated in blue represents doublet cells. These are all excluded from the single cell population that has been gated.

Using the "In Focus" tool, a histogram of the single cell population gated above was produced. The cells were distributed into "bins" based on the calculated focus of the BF images. Clicking on individual bins enables visualisation of all images within that particular bin in the image gallery. Single cells in focus were defined using the line region tool as shown in Figure 2.3.

Figure 2.3: Gating for cells in focus

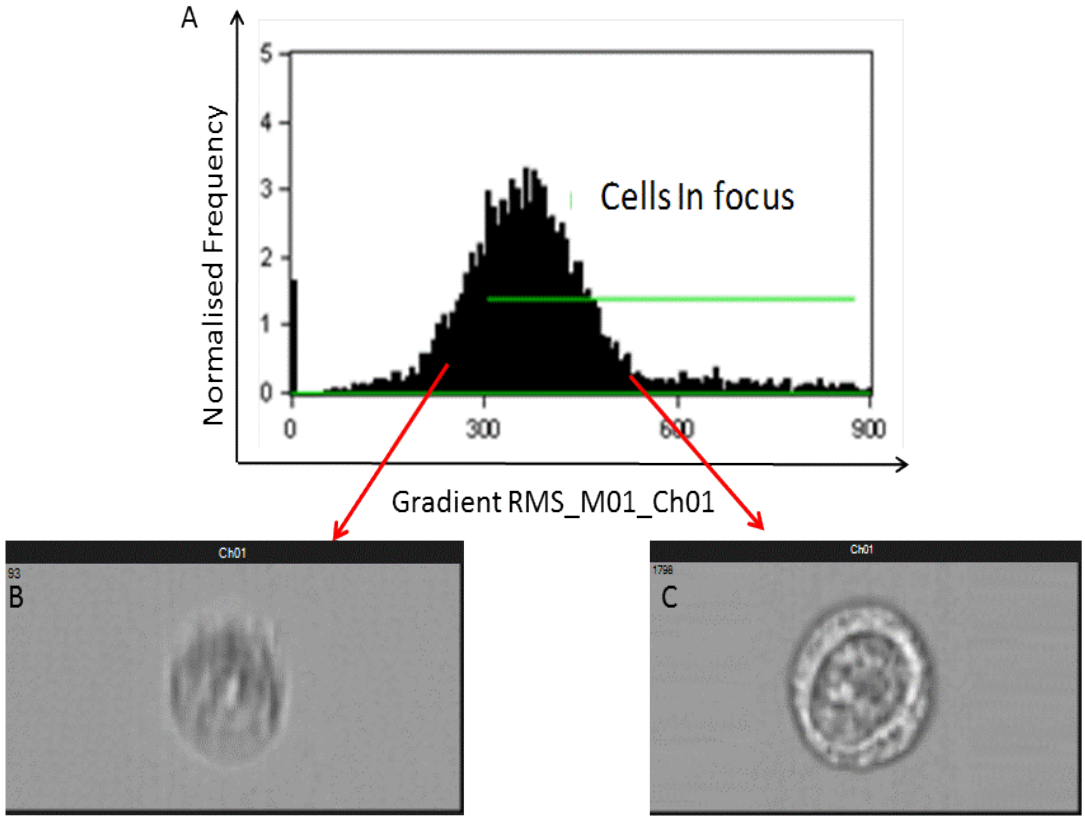

Identification of cells within the population that are in focus. (A) A histogram is produced of the single cell population and cells are distributed according to focal plane. Cells are gated using the Line region tool (shown in green). (B) Image of cell out of focus and (C) Image of cell in focus

Using the fluorescence positive two colour tool, a scatter plot was then generated of the single cells in focus that stained for both PE and Draq5. The polygon tool was utilised to gate the cells that satisfied these parameters (Refer to Figure 2.4 below).

Figure 2.4: Gating for cells stained positive for PE and DRAQ5

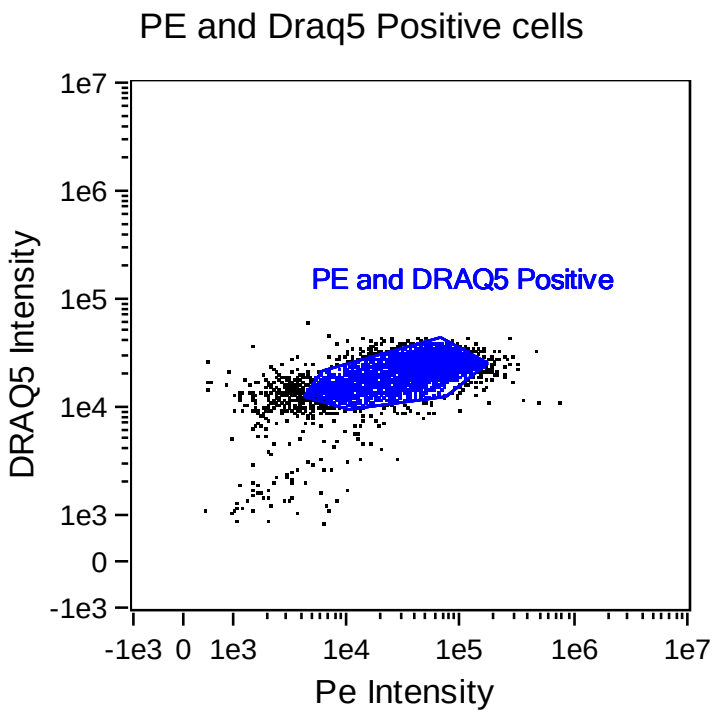

A histogram representing the population of single cells in focus. Using the polygon region tool, the portion of cells that were positive for both PE and Draq5.

2.2.9 Masking strategy to determine the Number of γ-H2AX foci in each nucleus

To determine the number of γ-H2AX foci within the nucleus of each cell, a series of masks were created which identified the region of interest. To ensure that γ-H2AX foci within each cell were identified correctly, a "truth population" of cells with known numbers of γ-H2AX foci ranging from 0 - 30 or more was created. Using this population of cells, a spot mask was created using the spot function of the Mask Manager. Using the spot to background ratio, foci were masked that were at least two-fold brighter than the background with a minimum diameter of 2 pixels. A nuclear morphology mask was then created using the Draq5 (Ch05, nuclear staining) image of each cell. To determine the number of γ-H2AX foci within the nuclear region of each cell, these two masks were combined using Boolean logic. This process has been shown below in Figure 2.5. Images are shown in BF (Ch01), PE

for γ-H2AX staining (Ch03) and Draq5 for nuclear staining (Ch05). Cells are first shown unmasked, then with the application of a morphology mask and spot mask; finally showing localisation of γ-H2AX foci within the nuclear region of the cell.

Figure 2.5: Masking strategy workflow to determine γ-H2AX Foci

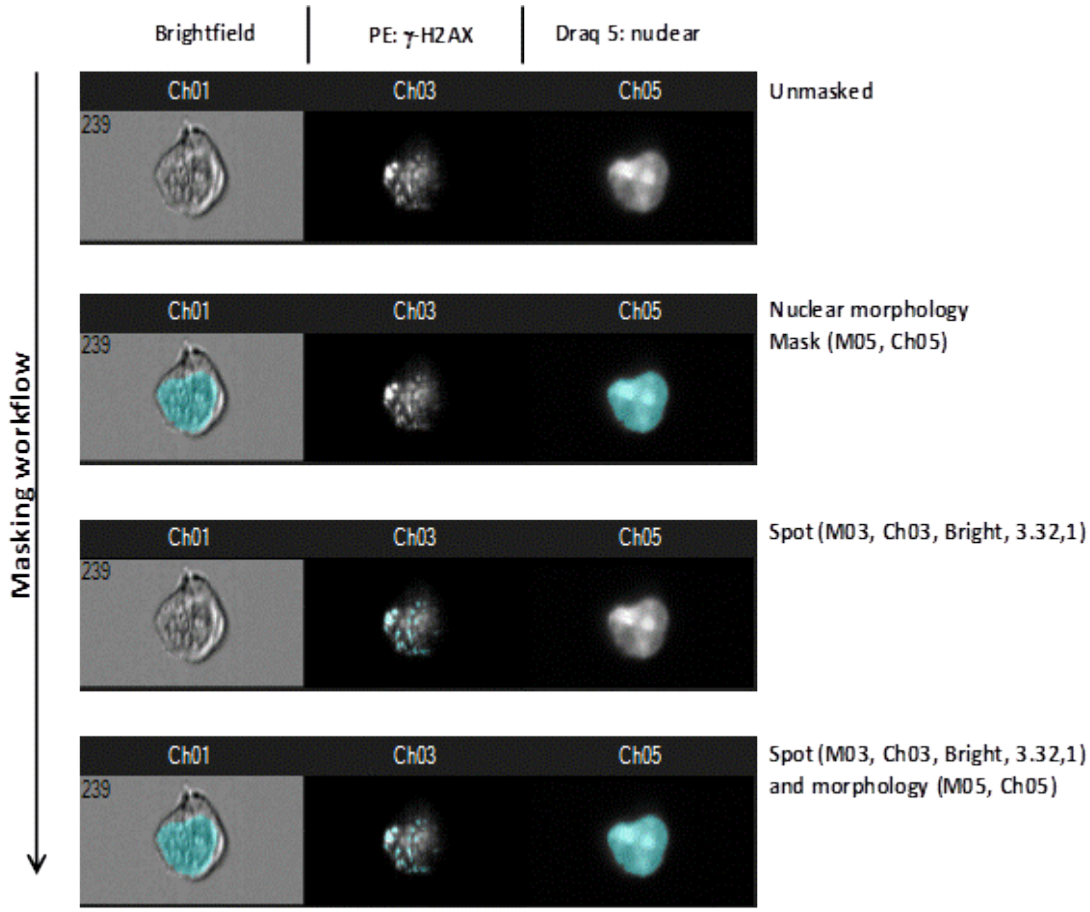

Masking workflow whereby γ-H2AX foci were identified, masked and enumerated. This first row of images depicts an example cell in BF, PE (Ch03) and Draq5 (Ch05). Then a nuclear morphology mask is created using the Draq5 stained images from Ch05 as its reference. Next a spot mask is applied to the images seen in Ch03 (γ-H2AX foci). Finally these two masks are combined to allow for foci calculation within the nucleus only. The associated name path for foci calculation from the Ideas software is shown to the right of each row of images.

The final mask that was created was converted using the Features tool in the software to allow enumeration of foci and creates a histogram of normalized frequency of foci against foci number. An example of this is shown below in Figure

2.6. The Morphology mask was also used to create an Intensity feature set to measure intensity on Ch03 which allows for the calculation of total nuclear intensity within each cell.

Figure 2.6: Typical foci distribution seen 30 minutes post irradiation

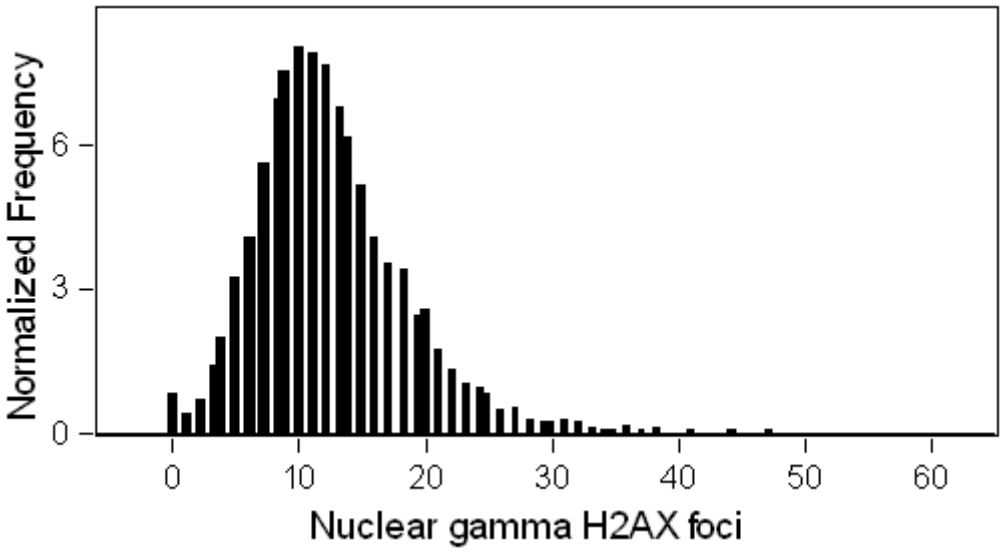

The above shows a typical distribution plot of γ-H2AX foci for a sample fixed 30 minutes post exposure to 2 Gy of gamma radiation.

Once the analysis was completed for the 30 minute time point, the data analysis file (daf) that was created was saved as a template file. This allows you to apply the same Spot masks and Intensity masks across all the time points that were collected for each cell line. A separate template file was created for each of the different cell lines used in this study.

2.3 Clonogenic Assays

2.3.1 Cell lines and Chemotherapeutic Agents

The immortalised cell lines used in this investigation were the

- NB1 - HTERT (Ulus-Senguloglu *et al.* 2012)
- AT5BIVA (Murnane *et al.* 1985)
- MRC5-SV1 (Arlett *et al.* 2006)

During the preliminary experiments performed, it was observed that the three cell lines formed colonies at different rates. Therefore the cell numbers that were plated for each of the cell lines after drug exposure were adjusted according to rate of growth. The details of this can be seen below in Table 2.4.

Table 2.4: Cell numbers plated for each cell line.

Dose	AT5BIVA	MRC5-SV1	NB1-HTERT
Control	500	250	250
Dose 1	750	250	500
Dose 2	1000	500	750
Dose 3	1000	500	750
Dose 4	2000	750	1000
Dose 5	2000	750	1000

The four chemotherapeutic agents that were used were Adr, Pt, HN2 and 5-FU. Each drug was seen to exert different levels of toxicity on the cells and the concentration ranges used for each drug were optimized in a series of preliminary experiments. Table 2.5 shows the final concentration ranges used for each agent.

Table 2.5: Dose ranges used for each chemotherapeutic agent

Dose	HN2 (µg/mL)	Pt (µg/mL)	Adr (ng/mL)	5-FU (µg/mL)
1	0.5	15	50	50
2	1	20	75	100
3	1.5	25	100	150
4	2	30	125	200
5	2.5	35	150	250

All dilutions were carried out in serum-free medium. HN2 was obtained in powder form and was initially dissolved into serum free medium. Pt was also obtained in powder form but initially dissolved in DMSO due to poor solubility in serum-free medium. Adr was obtained in aqeous form and diluted in serum-free medium.

$2x10^5$ cells were plated into 6 cell culture plates (60mm, Sarstedt). They were left to grow over a 48 hour period to reach approximately 70 – 80% confluence before drug treatment commenced. The plates were then incubated with increasing doses of each drug for 1 hr at 37^{o}C. After the 1 hr treatment; cells were rinsed with 5mL of Versene and then harvested with 1ml of Trypsin for 10 minutes. Cells were then recovered into 15 ml tubes in 10 ml of DMEM medium.

10 µL of the cell suspension was mixed with 10 µL of Trypan blue (Sigma Aldrich) to exclude dead cells from the total count. The cells were then loaded onto glass haemocytometers and counted under a microscope at 10 X magnification.

Cells were then diluted to the appropriate counts as shown in Table 1 and plated out into 3 cell culture plates (100mm, Sarstedt) for each dose of the drug. These cells were then left to form colonies over a 14 – 21 day period.

When plates were deemed ready to fix, the medium was decanted and they were rinsed with water. Cells were fixed over a 20 minutes period using 100% Industrial Methylated Spirit. This was then rinsed off and the cells were stained using Methylene Blue (BDH Laboratory Supplies, Poole UK) for 1 hr. After this time, the stain was decanted and the plates were rinsed with water.

2.4 Imaging flow cytometry protocol for the γ-H2AX chemotherapy assay

2.4.1 Cell lines

The cell lines employed in this study were the same ones previously described in Section 2.3.1.

2.4.2 Chemotherapeutic Agents

Table 2.6 shows the drug doses used for each of the cell lines. These doses were established as being the IC_{50} values for each individual cell line as determined by clonogenic assays performed (described in detail in Section 2.3). The IC_{50} value was defined as being the dose seen to kill approximately 50% of the cell population post 1 hr exposure to each chemotherapeutic agent.

Table 2.6: Drug doses used for each cell line in the in the γ-H2AX assay

Cell line	HN2	Pt	Adr
MRC5-SV1	0.5 μg/mL	12 μg/mL	56 ng/mL
NB1-HTERT	0.3 μg/mL	6 μg/mL	93 ng/mL
AT5BIVA	0.2 μg/mL	7 μg/mL	84 ng/mL

To determine the level of γ-H2AX- associated fluorescence induced by the different chemotherapeutic agents, each of the three cell lines were treated with their individual IC_{50} dose of each drug derived from clonogenic assays (Refer to Table 2.6). All cell lines were treated as proliferating monolayers and were at approximately 80% confluency when treated.

2.4.3 HN2 Dose Response

All three cell lines were exposed to a range of HN2 concentrations - 0.5, 1.5 and 2.5 μg/mL for 1 hr. This was done to examine whether fluorescence levels increased in an exponential manner as the dose of HN2 was increased. All cells were fixed at 24 hrs post treatment as detailed in Section 2.2.2

2.4.4 Cell Fixation

Cells were fixed as described in Section 2.2.2 at 3, 5, 24, 30 and 48 hrs post treatment for HN2. However following preliminary experiments for Adr and Pt, these fixation points were altered following to 6, 12, 24, 30, 48 and 72 hrs post treatment with these drugs as it was seen that DNA repair had not completed in the 48 hr period.

2.4.5 Immunocytochemistry

A similar protocol was followed for immunocytochemistry of these cells as described in section 2.2.4 with two alterations.

The first decision was to switch one of the constituents of the blocking buffer from 0.5% nonfat milk to 10% rabbit serum. This showed an improvement in the level of background seen. Secondly, the secondary antibody was switched from PE to Alexa Fluor (AF) 488 rabbit anti-mouse IgG (Life Technologies, Paisley, UK). The reason for this was two-fold, firstly it was seen to produce brighter, more distinct staining at much lower concentrations (1:1000 compared to 1:40 required for PE). There was also less leakage to juxtaposed channels during imaging, making

flow cytometry compensation more robust and reliable between the fluorescence emitted by AF488 and the nuclear stain Draq5.

Two samples for fluorescence compensation were prepared with either the secondary antibody (AF488) or Draq5 being omitted from the process. These were fixed at 24 hrs post treatment with all drugs.

2.4.6 Imagestream data acquisition and image compensation

The protocol undertaken to acquire images and compensate for fluorescence was as previously described in Section 2.2.6 and Section 2.2.7.

2.4.7 Analysis using Ideas^{TM} software and calculation of foci numbers using the Spot Wizard

The concept of the Imagestream is a novel technique; having only recently emerged in the last five years. Subsequently the Ideas^{TM} software is constantly being upgraded with new features being added to aid swift and competent analysis of data. Therefore the procedure used for analysis of data was adapted to accommodate these new features and differs slightly from the method that has been described in section 2.2.8. The new feature was an automated Spot wizard which selects the best mask for foci enumeration and represents a more reliable and enhanced method for analysis of DNA damage foci in cells.

The sample fixed 24 hrs post treatment with all drugs was used to create a template file with which all other samples collected during the experiment would be analysed with. This file was chosen due to it being likely to show the highest induction of γ-H2AX foci and therefore the brightest intensity of AF488. Two

principal methods were utilised for the quantification of γ-H2AX foci. Enumeration of individual γ-H2AX foci was calculated as well as determining the overall intensity emitted by the AF488 probe within the nuclei of the cells. Templates were created for each individual cell line.

The Spot Wizard initially directs the gating of the sample for the single and in focus cells according to the parameters described in section 2.2.8 (refer to Figure 2.2 and Figure 2.3). The wizard then requires the definition of two distinct populations; one population of cells that have low numbers of foci (usually 0 or 1) and another population of cells which represent high numbers of foci (Refer to Figure 2.7).

Figure 2.7: Truth populations identified by the Spot Wizard

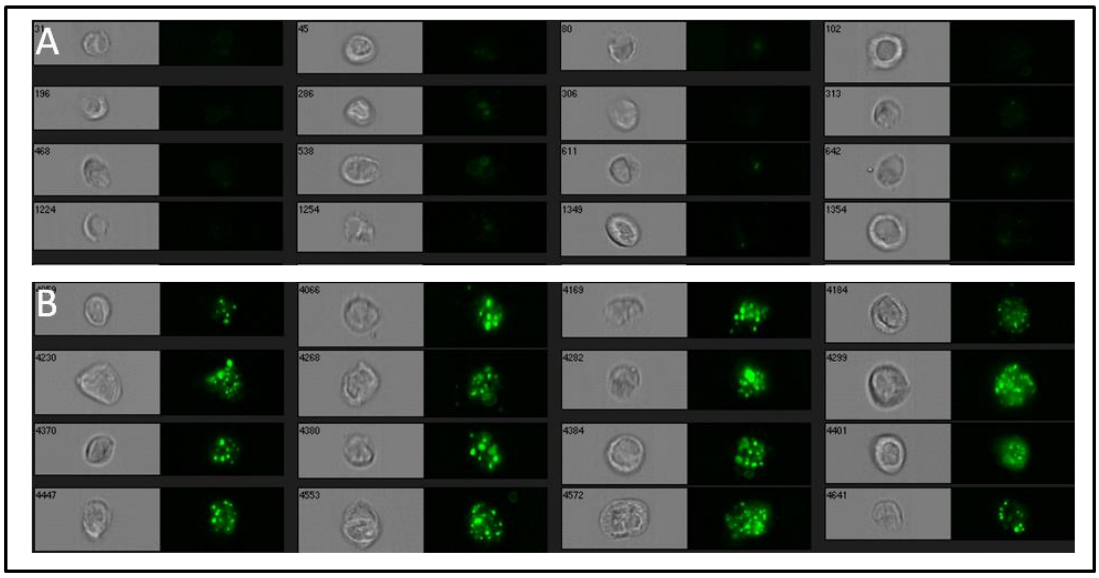

Figure 2.7(A) shows a population of cells with no foci and Figure 2.7(B) depicts a population of cells with high numbers of foci. Images above are shown in Ch01 (representing BF images) and Ch02 (representing AF488 staining of γ-H2AX foci)

50 cells were identified for each population by using the "Tagging tool". The population of cells which identified the high number of foci accounted for different

types of staining patterns seen such as foci shape and size, intensity of the staining and the level of background. The identification of these two diverse populations directs the software to choose a mask and feature most suitable to account for all the factors and generates a histogram representing the γ-H2AX foci distribution for that sample.

However a manual modification then needs to made to the auto-generated mask as this wizard does not distinguish whether the spots being counted are solely in the nucleus. Therefore a Morphology Mask is created using the Mask manager (as described in Section 2.2.9). Utilising Boolean logic, the mask generated by the software is combined with the Morphology Mask and a new histogram is generated showing the distribution of γ-H2AX foci within the nuclei of the cells in the population of cells that has been gated for the parameters described earlier (Refer to Figure 2.8 below).

Figure 2.8: Histogram representing distribution of γ-H2AX foci within nuclear region of cells

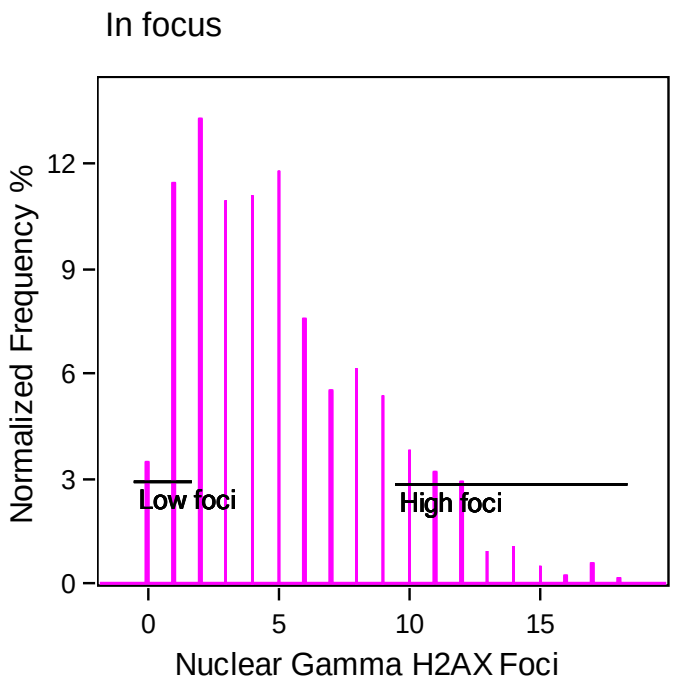

The Morphology Mask was also used to create an Intensity feature which calculates the intensity of AF488 within the nucleus of these cells (Refer to Figure 2.9 below).

Figure 2.9: Histogram showing the nuclear intensity of a sample

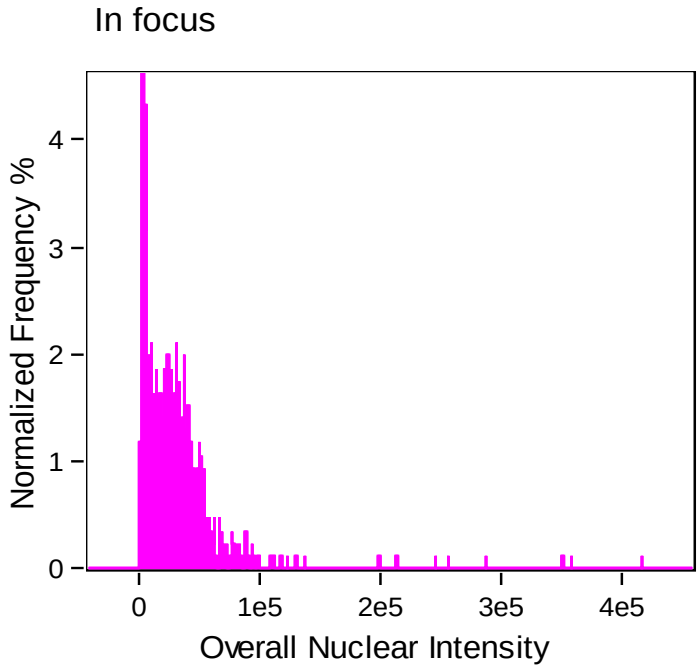

Once these masks and features were created for the template file, it was then applied to all other time points collected for each cell line for each drug. A new template was created for each cell line for the repeats of these experiments as the staining patterns such as background and intensity can vary considerably from experiment to experiment.

The following figure (refer to Figure 2.10) depicts examples of cells with differing numbers of foci which the Spot Mask feature was able to differentiate between. The same image is also shown in greyscale (refer to Figure 2.11) to show clearer visualisation of the mask over the γ-H2AX foci in these cells.

Figure 2.10: Multispectral images with increasing numbers of foci masked by the Spot Wizard

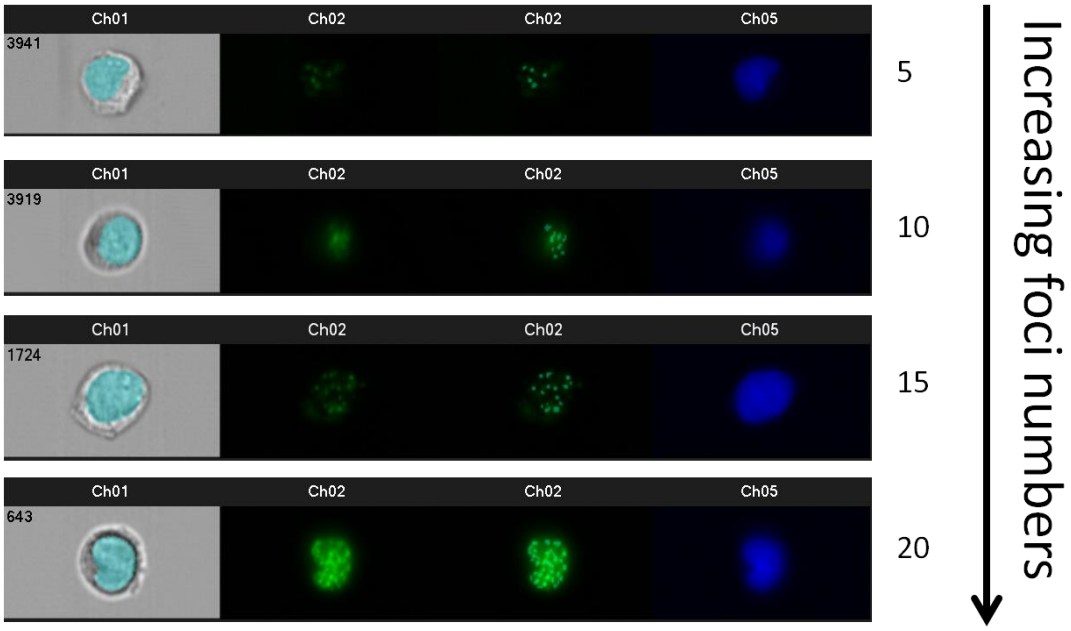

The above figure shows example images of cells with increasing numbers of foci. Ch01 shown in the first column depicts the BF image of these cells with the morphology mask shown in blue which highlights the nuclei of the cells. Ch02 shown in the second column (representing AF488 staining) depicts the unmasked cells whilst the third column depicts the same images masked with the γ-H2AX foci mask. Ch05 shows the morphology of the nucleus of these cells.

Figure 2.11: Multispectral images with increasing numbers of foci shown in greyscale

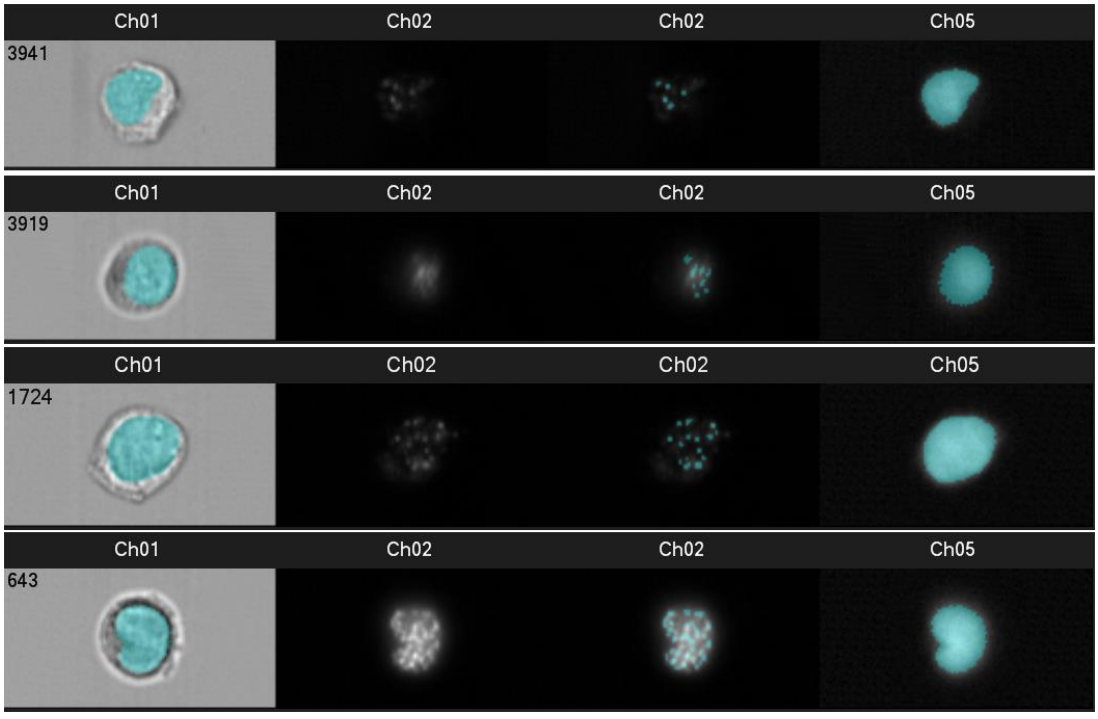

The validity of the auto-generated mask was verified by comparing its accuracy to the masks that were being created manually earlier. This was done by utilising an aspect of the Ideas software called “Find the best feature”. This tool analyses and evaluates all the possible features that could be used to extract the information required from the data and generates a RD value derived using Fischer’s Discriminate Ratio for all suitable features. Table 2.7 below gives an example of the data that can be generated using this tool.

Table 2.7: Example table of Fischers Discriminate Ratio values generated in IDEAS™

Population	High
Spot Count_Peak(M02, Channel 2, Bright, 3.5), low, Mean RD	4.234
NUCLEAR GAMMA H2AX FOCI (PEAK), low, Mean RD	4.165
NUCLEAR GAMMA H2AX FOCI (SPOT), low, Mean RD	3.109
Bright Detail Intensity R3_Morphology(M05, Ch05)_Ch02, low, Mean RD	2.866
Std Dev_Morphology(M05, Ch05)_Ch02, low, Mean RD	2.826
Modulation_M02_Ch02, low, Mean RD	2.738
Bright Detail Intensity R7_Morphology(M05, Ch05)_Ch02, low, Mean RD	2.737
Bright Detail Intensity R3_MC_Ch02, low, Mean RD	2.697
Modulation_Morphology(M05, Ch05)_Ch02, low, Mean RD	2.298
Gradient Max_Morphology(M05, Ch05)_Ch02, low, Mean RD	1.23
Bright Detail Intensity R3_MC_Ch03, low, Mean RD	1.083
Bright Detail Intensity R3_MC_Ch01, low, Mean RD	0.9567
Bright Detail Intensity R3_MC_Ch05, low, Mean RD	0.9009
Gradient RMS_Morphology(M05, Ch05)_Ch02, low, Mean RD	0.8409
Bright Detail Intensity R3_MC_Ch06, low, Mean RD	0.7807
Bright Detail Intensity R3_MC_Ch04, low, Mean RD	0.7599
Contrast_Morphology(M05, Ch05)_Ch02, low, Mean RD	0.6983
Contrast_M02_Ch02, low, Mean RD	0.6105
H Entropy Std_Morphology(M05, Ch05)_Ch02_5, low, Mean RD	0.5995
Contrast_M01_Ch01, low, Mean RD	0.5549
H Contrast Std_Morphology(M05, Ch05)_Ch02_5, low, Mean RD	0.5517
H Homogeneity Std_Morphology(M05, Ch05)_Ch02_5, low, Mean RD	0.4757
H Energy Std_Morphology(M05, Ch05)_Ch02_5, low, Mean RD	0.4388
Gradient RMS_M05_Ch05, low, Mean RD	0.4218
H Variance Std_Morphology(M05, Ch05)_Ch02_5, low, Mean RD	0.4146
Gradient RMS_M02_Ch02, low, Mean RD	0.3535
H Energy Mean_Morphology(M05, Ch05)_Ch02_5, low, Mean RD	0.3145
Gradient RMS_M04_Ch04, low, Mean RD	0.2888
Modulation_M04_Ch04, low, Mean RD	0.2888
Gradient RMS_M01_Ch01, low, Mean RD	0.2887
Contrast_M04_Ch04, low, Mean RD	0.2869

The above values were generated using the "Find the best feature" tool in the Ideas™ software. The values represents RD values derived using the Fischers Discriminate ratio. In this table, the RD value indicates the ability of that particular feature to distinguish individual foci and the higher the value, the better the feature is. The feature highlighted in red (at top of table) was created using the Spot wizard. The two features highlighted in blue (second and third row of table) were created manually. These values show that the auto-generated feature provides better statistical separation of foci not only in comparison to the manually created features but all available features in the software.

2.5 Analysis of DNA repair in chemosensitive and chemoresistant cell lines using γ-H2AX

2.5.1 Developing Resistant Cell lines

Two parental repair normal cell lines MRC5-SV1 and NB1-HTERT were taken to develop resistant cell lines. This was achieved by exposing them to gradual increasing doses of HN2. This was made up in complete medium containing HN2 concentrations starting from 0.5 μg/mL. Cells were then left to grow until they became confluent before increasing the concentration by 1.5 fold of the previous dose. Please refer to Table 2.8 for the range of doses used. The NB1-HTERT^{R} cell line was maintained at 3.5 μg/mL HN2 as this was approximately 10 fold higher than the IC50 of the parental cell line. Similarly the MRC5-SV1^{R} cell line was maintained at 5.3 μg/mL HN2. Cells were cultured in drug-treated medium at the relevant concentration every third passage to maintain resistance. Cells were cultured in drug-free medium for a minimum of seven days prior to any experiments being carried out on them.

Table 2.8: Dose ranges used to induce resistance in parental cell lines

Dose	Concentation (μg/mL)
1	0.5
2	0.75
3	1
4	1.5
5	2.3
6	3.5
7	5.3

Cells took approximately 3 – 4 weeks to grow through each dose of drug and become confluent.

2.5.2 Clonogenic Assays

Clonogenic assays were carried out as described in section 2.3. These were performed on the resistant cell lines to establish that they exhibited higher levels of resistance to HN2 in comparison to the parental cell lines. These were also carried out on the XPF-deficient cell line to highlight the sensitivity of this cell line to cross-linking agents.

The chemotherapeutic agents utilised in this study were HN2 and Pt. The dose ranges used in these experiments were as detailed in Table 2.9 below.

Table 2.9: Dose ranges used for clonogenic assays

Dose	HN2 (µg/mL) for resistant cell lines	HN2 (µg/mL) for GM08437B	Pt (µg/mL) for resistant cell lines	Pt (µg/mL) for GM08437B
1	0.5	0.1	15	4
2	1	0.2	20	8
3	1.5	0.3	25	12
4	2	0.4	30	16
5	N/A	0.5	35	20

The above table details the dose ranges used in the clonogenic assays. Lower concentration ranges had to be used for the GM08437B cell line due to their sensitivity to these agents.

2.5.3 γ-H2AX Assay with HN2

The IC_{50} values of HN2 derived for the parental cell lines were used on the resistant cell lines, this was to allow for comparable results with the repair normal cell lines as described in Section 2.4. The GM08347B cell line was subjected to the same dose of HN2 that the NB1-HTERT parental cell line had been exposed to. This was to account for the sensitivity of this cell line to cross-linking agents as the concentrations derived for the NB1-HTERT parental cell line were lower than those derived for the MRC5-SV1 parental cell line. Refer to Table 2.10 for details of the concentrations used. All cell lines were treated as proliferating monolayers and were at approximately 80% confluency when treated. Cells were fixed in 50:50 methanol:acetone (V:V) at 3, 5, 24, 30 and 48 hrs post treatment. They were stored at 4^{o}C prior to undergoing the immunocytochemistry protocol as detailed in Section 2.4.5.

Table 2.10: Concentrations of HN2 used in the γ-H2AX assay

Cell line	HN2
MRC5-SV1	0.5 μg/mL
MRC5-SV1^{R}	0.5 μg/mL
NB1-HTERT	0.3 μg/mL
NB1-HTERT^{R}	0.3 μg/mL
GM08437B	0.3 μg/mL

These values represent the IC_{50} values derived for the parental cell lines in response to treatment with HN2

2.5.4 ERCC1 expression levels post treatment with HN2

Cell lines were exposed to the relevant IC_{50} dose as detailed above in **Error! eference source not found.** for 1 hr and fixed at 24 hrs and 48 hrs post treatment. Compensation samples were fixed at 24 hrs post treatment. All samples were fixed in 50:50 methanol:acetone and stored at 4 ^{o}C.

2.5.5 Immunocytochemistry

Cells were stained as described in Section 2.4.5. ERCC1 expression levels were detected using a mouse monoclonal anti-ERCC1 primary antibody (Abcam) at a 1:200 dilution.

2.5.6 Imagestream data acquisition and image compensation

The protocol undertaken to acquire images and compensate for fluorescence was as previously described in Section 2.2.6 and Section 2.2.7.

2.5.7 Imagestream data analysis using Ideas^{TM} software and calculation of foci numbers

Foci counts and overall nuclear intensity was determined for each of the cell lines. Data analysis was carried out as described in Section 2.4.7

2.6 Analysis of DNA repair in chemosensitive and chemoresistant cell lines using RAD51

All cell lines described in Section 2.5 were employed in this study.

2.6.1 Chemotherapeutic Agents

Table 2.11: HN2 doses used for each cell line in the Rad51 assay

Cell Line	IC_{50} for HN2
MRC5-SV1 Parental and MRC5-SV1^{R}	**0.5 µg/mL**
NB1-HTERT Parental, NB1-HTERT^{R}, GM08437B	**0.3 µg/mL**

To determine the level of RAD51 foci formation induced by HN2 treatment, the cell lines were treated with their respective concentration of HN2 detailed in Table 2.11. IC_{50} doses derived for the parental cell lines (as detailed in Chapter 4) were utilised for this study. The XPF cell line was treated with the IC_{50} dose obtained for the NB1-HTERT cell line as the concentrations derived for the NB1-HTERT parental cell line were lower than those derived for the MRC5-SV1 parental cell line. This was to account for the sensitivity of this cell line to cross-linking agents. All cell lines were treated as proliferating monolayers and were at approximately 80% confluency when treated.

2.6.2 Cell fixation and Permeabilisation

Cells were fixed at 6, 12, 24, 30 and 48 hrs post treatment with their respective doses of HN2. These time points were selected to encompass a 2 day period to allow for evaluation of DNA repair kinetics. Cells were detached using

1 mL of 0.25% Trypsin-EDTA and washed twice in PBS. They were then fixed and permeabilised in 100% methanol at -20^{o}C.

2.6.3 Immunocytochemistry

Cells were rehydrated with three washes in PBS and then blocked in blocking buffer comprised of PBS containing 20% rabbit serum (PAA) and 0.1% Triton-X 100. Cells were incubated at 4^{o}C overnight in mouse monoclonal anti-RAD51 antibody (Clone 14B4, Abcam) at 1:200 dilution.

Following three washes in wash buffer made up of PBS containing 0.1% Tritox X-100, cells were incubated for 1 hr at RT in AF488 antibody diluted in block buffer to 1:1000. Cells were washed again in wash buffer three times and once in PBS. Samples were then resuspended in 100 μL of Accumax flow cytometry buffer with 5 μM Draq5 (Biostatus Ltd., Leicestershire, UK). Two samples for fluorescence compensation were prepared with either the secondary antibody (AF488) or Draq5 being omitted from the process. These were fixed at 24 hrs post treatment for all cell lines.

2.6.4 Imagestream data acquisition and image compensation

The protocol undertaken to acquire images and compensate for fluorescence was as previously described in Section 2.2.6 and Section 2.2.7.

2.6.5 Imagestream data analysis using Ideas™ software and calculation of foci numbers

Foci counts and overall nuclear intensity was determined for each of the cell lines. Data analysis was carried out as described in Section 2.4.7

Chapter 3

Validation of imaging flow cytometry for the identification of DSBs in human cells following gamma radiation exposure

3.1 Introduction

DSBs are potentially lethal lesions that must be rapidly repaired in order to ensure cell survival and maintain genomic integrity (Hoeijmakers 2001). They can occur for many reasons such as exposure to IR during clinical radiotherapy (Bourton *et al.* 2011), exposure to anticancer chemotherapeutic drugs (Clingen *et al.* 2008) and through interaction with endogenously derived ROS formed through normal cellular metabolism (Conklin 2000).

A critical event in the signalling and subsequent repair of DSBs is the phosphorylation of H2AX by ATM and ATR to form the γ-H2AX protein. The number of foci seen is thought to correlate on a 1:1 basis with the number of DSBs formed (Sedelnikova *et al.* 2002). The accumulation of γ-H2AX molecules seen at the site of these DSBs leads to the formation of nuclear foci (Rogakou *et al.* 1998). The repair of these DSBs are normally carried out through two pathways; HR and NHEJ (Scott and Pandita 2006). HR and NHEJ pathways are the main route taken in the repair of DNA DSBs in vertebrate cells (Takata *et al.* 1998). The point at which the cell is progressing through the cell cycle plays a role in determining the pathway that will become activated to repair the DSB (Lees-Miller and Meek 2003). It is generally agreed that in the G1/G0 phase of the cell cycle, DSBs are repaired by NHEJ while HR is more prominent during the late S/G2 phase (Valerie and Povirk 2003). Takata *et al*, (1998) demonstrated that HR and NHEJ are complementary in repairing the DSBs and concluded that both play a big role in maintaining the integrity of chromosomes.

In repair normal mammalian cells, the induction of γ-H2AX foci occurs rapidly following the formation of DSBs. Within 1 - 3 hrs, the majority of these DSBS

have been repaired and subsequently leads to the dephosphorylation and loss of the γ-H2AX foci within the nucleus (Rogakou *et al.* 1998). In cells which exhibit signs of defective DNA repair mechanisms, there is a persistence of γ-H2AX foci seen which is due to failure to resolve these DNA DSBs (Bourton *et al.* 2011). This has been shown in a variety of cells derived from patients with different DNA repair disorders such as A-T or FA. The ATM gene is mutated in this disorder which is thought to inactivate the induction of DSB repair resulting in the persistence of γ-H2AX foci within the nucleus (Friesner *et al.* 2005). Furthermore, Abbaszadeh *et al*, (2010) demonstrated that the prolonged appearance of γ-H2AX foci in the nuclei of irradiated cells was due to a defect in the DNA-PK_{cs} gene, a vital component of the NHEJ pathway. The persistence of γ-H2AX foci in cells hypersensitive to DNA damaging agents has prompted extensive research into the application of γ-H2AX as a biomarker to predict tumour response and the level of side effects experienced in patients receiving clinical radiotherapy and/or chemotherapy (Bourton *et al.* 2011).

In this study, the novel technique of imaging flow cytometry was employed to estimate the number of foci induced in normal and repair defective immortalized human fibroblasts exposed to 2 Gray (Gy) gamma radiation. The counting and imaging of more than 20000 cells demonstrated a persistence of γ-H2AX foci in the nuclei of two DSB repair defective cell lines (XP14BRNeo17 and AT5BIVA) for up to 24 hrs post irradiation. However in a repair normal cell line (MRC5-SV1), rapid induction of foci was followed by DNA repair and disappearance of foci within 3 hrs post irradiation. Significantly higher numbers of foci were induced in the DSB repair normal cell line compared with the two repair defective cell strains. These findings

indicate that application of imaging flow cytometry provides an accurate assessment of the levels of DNA damage in cells and adds to the growing number of high throughput methods for the analysis of DNA damage in cells.

3.2 Results

3.2.1 Gamma Radiation Dose Response Curve

The induction of fluorescence in the three cell lines was determined by counting 20 000 cells with the Imagestream^{x} following exposure to 0,2,4,6,8 Gy gamma radiation. A nuclear morphology mask was created using the Mask Manager in Ideas^{TM} and was used to derive the intensity of PE staining (γ-H2AX) in the nucleus. A dose response curve was produced (Refer to Figure 3.1) using the mean level of intensity seen in each of the samples exposed to an increasing level of gamma radiation.

Figure 3.1: Dose response curve post irradiation with increasing doses of gamma radiation

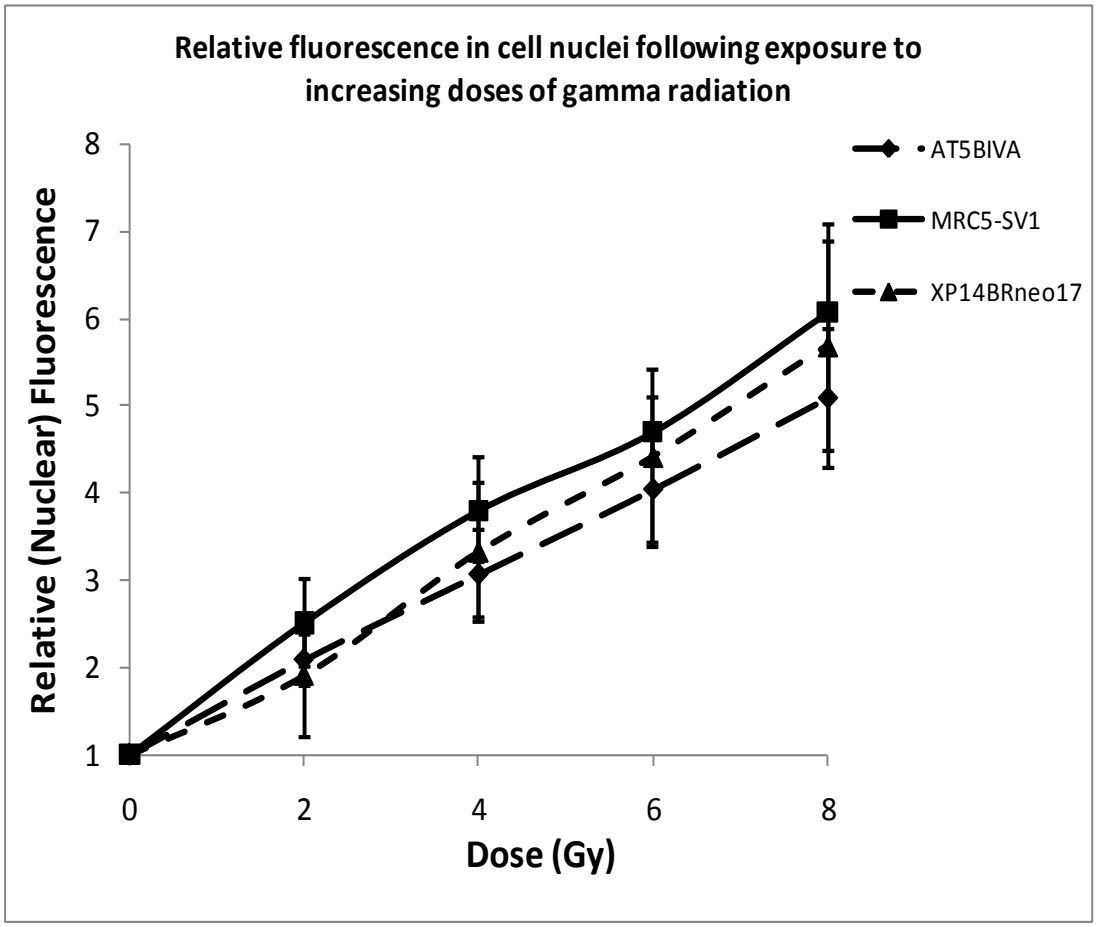

AT5BIVA, MRC5-SV1 and XP14BRneo17 cell lines were exposed to 0, 2, 4, 6, 8 Gy gamma radiation. The fluorescence is indicative of γ-H2AX foci which were labelled with PE. In all three cell lines, an increasing level of fluorescence is seen as the dose of gamma radiation is increased.

It was observed that as the dose of gamma radiation was incremented, there was a 1 - 1.5 fold increase in the level of nuclear fluorescence. For all subsequent experiments in this study, a dose of 2 Gy gamma radiation was used to induce γ-H2AX foci. The 2 Gy dose was seen to fall within the linear phase of the dose response curves generated for each of the cell lines and it relates to the clinical doses used for treatment which are generally a series of 2 Gy fractionated doses.

3.2.2 γ-H2AX Foci Quantification Using the Imagestream^X

The average number of foci per cell in each of the three cell lines was analysed and quantified using the Imagestream^X. The data was derived from three independent experiments and is shown in Figure 3.2. γ-H2AX foci were enumerated by applying a Morphology and Spot mask to each of the cell images produced for each time point as shown in Figure 2.5. In unirradiated cells, the mean number of foci per nucleus is 1.13 for the repair normal MRC5-SV1 fibroblasts and 0.76 for the repair defective AT5BIVA cells while a mean number of 2.21 foci were seen in the repair defective XP14BRNeo17 cell line. Following exposure to 2 Gy gamma radiation at a dose rate of 1.3 - 1.4 Gy per minute, there was a significant increase in the number of foci in all cell lines at 30 minutes post irradiation. This is consistent with the induction of DNA DSB repair as a consequence of exposure to gamma radiation. The MRC5-SV1 cells exhibit 14.04 foci per cell whilst the AT5BIVA cells show an average of 17.17 foci and the XP14BRNeo17 cells have a mean number of 12.26 foci per cell. During the ensuing 24 hr period, the three cell lines were examined at three different time points, 3, 5 and 24 hrs post exposure to 2 Gy gamma radiation. There was a distinct variance in the behaviour of the three cell

lines during this time period in terms of resolving the DNA DSBs that had occurred during the treatment. The repair normal cells, MRC5-SV1 cells show that the majority of the γ-H2AX foci have disappeared with the average foci count dropping to 1.58, indicating that most of the DNA DSBs have been repaired. The AT5BIVA cells are known to have defective DNA repair mechanisms and the results show that even at 24 hrs post irradiation, there is an average of 18.72 foci per cell. The XP14BRNeo 17 cells show an intermediate response in comparison to the MRC5-SV1 and AT5BIVA cells with an average of 8.10 foci per cell after 24 hrs.

The application of a Student's unpaired *t*-test reveals that differences in the persistence of γ-H2AX foci within the three cell lines are statistically significant with 95% confidence levels. The AT5BIVA cells retain a significant number of foci after 24 hrs in comparison to the repair normal cell line, MRC5-SV1 ($P < 0.008$) as do the XP14BRNeo17 cells ($P < 0.001$). The AT5BIVA cells also retain significantly more foci than the XP14BRNeo17 cells at 24 hrs ($P < 0.05$).

Figure 3.2: Average number of H2AX foci seen post irradiation with 2 Gy gamma irradiation over 24 hrs

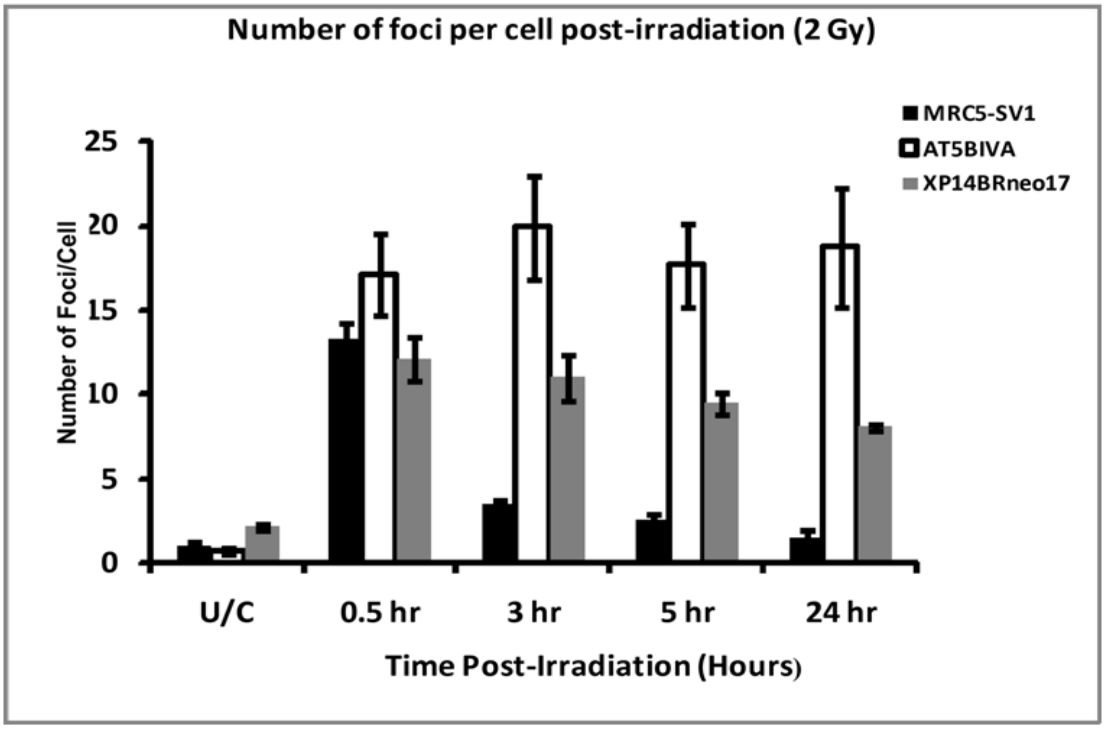

The mean number of γ-H2AX foci seen in MRC5-SV1, AT5BIVA and XP14BRNeo17 cell lines over a 24 hr period post exposure to 2Gy gamma radiation. Error bars represent the standard error of the mean derived from three independent experiments in which 20 000 cells were analysed at each time point for each cell line.

Figure 3.3: Foci Distribution in the three cell lines over the ensuing 24 hour period post exposure to 2 Gy gamma radiation

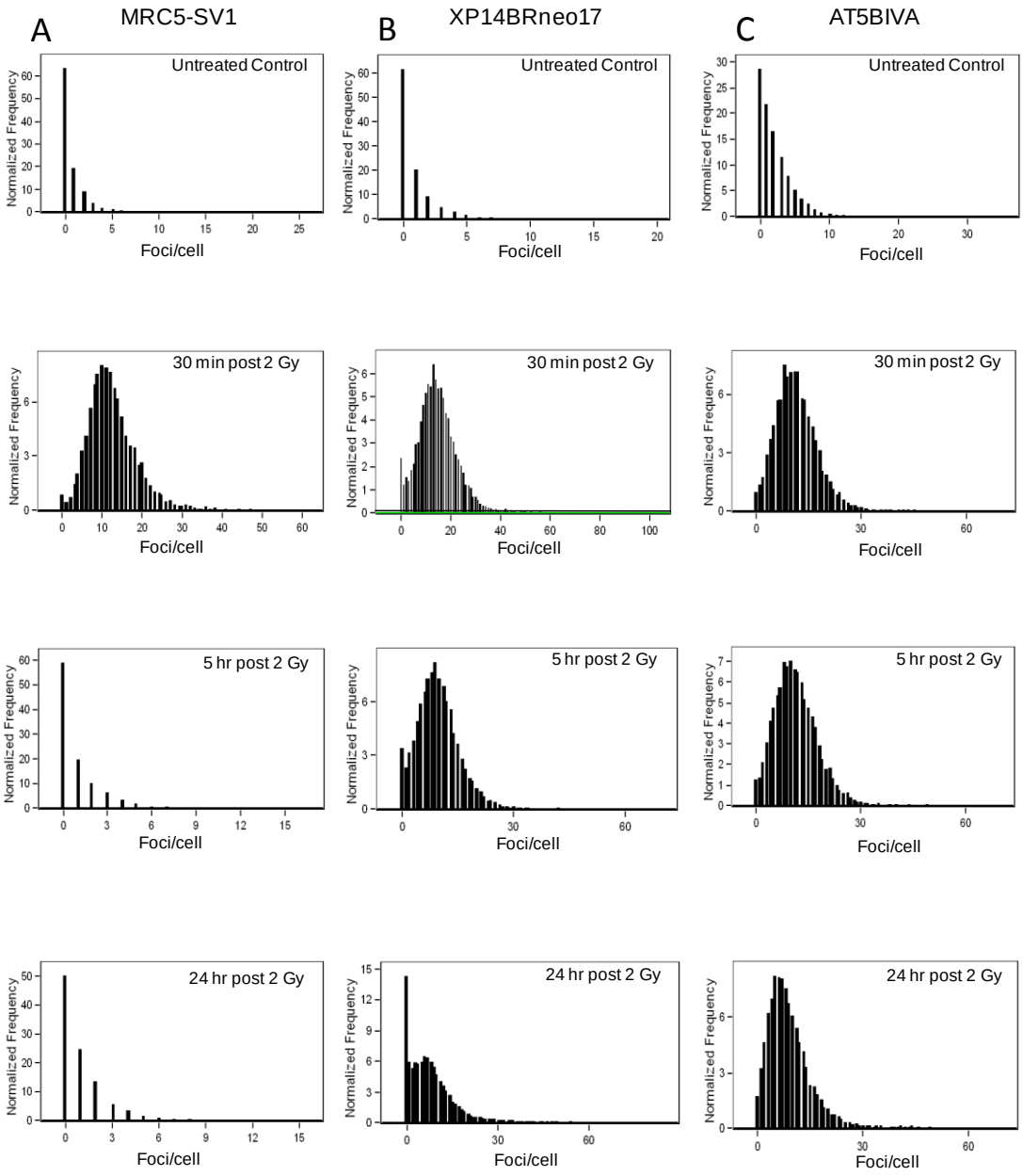

The above figure shows the foci distribution seen in (A) MRC5-SV1, (B) XP14BRNeo17 and (C) AT5BIVA. A dramatic induction in γ-H2AX foci induction was seen in all three cell lines at 30 minutes post exposure to 2 Gy gamma radiation. At 24 hrs post irradiation, the MRC5-SV1 foci distribution is similar to its untreated control whereas the AT5BIVA cell lines still retained the majority of the γ-H2AX foci. The XP14BRNeo17 cell line shows an intermediate response with some retention of γ-H2AX foci.

3.2.3 *In Situ* Quantification of γ-H2AX Foci

To validate the γ-H2AX foci counts derived from the Imagestream^X analysis, the induction of foci within the three cells lines was also determined using *in situ* immunofluorescence. Cells were examined using a fluorescence microscope with x100 magnification objective and it can be seen that the mean number of foci observed in the cell lines following 2 Gy gamma radiation exposure is higher than the numbers derived from the Imagestream^X. However there is still a similar relationship observed in the differences in the number of foci retained at the end of the 24 hr period. The results for this experiment are shown in Figure 3.4.

Figure 3.4: Average number of γ-H2AX foci calculated post irradiation with 2 Gy gamma irradiation using *in situ* immunofluorescence

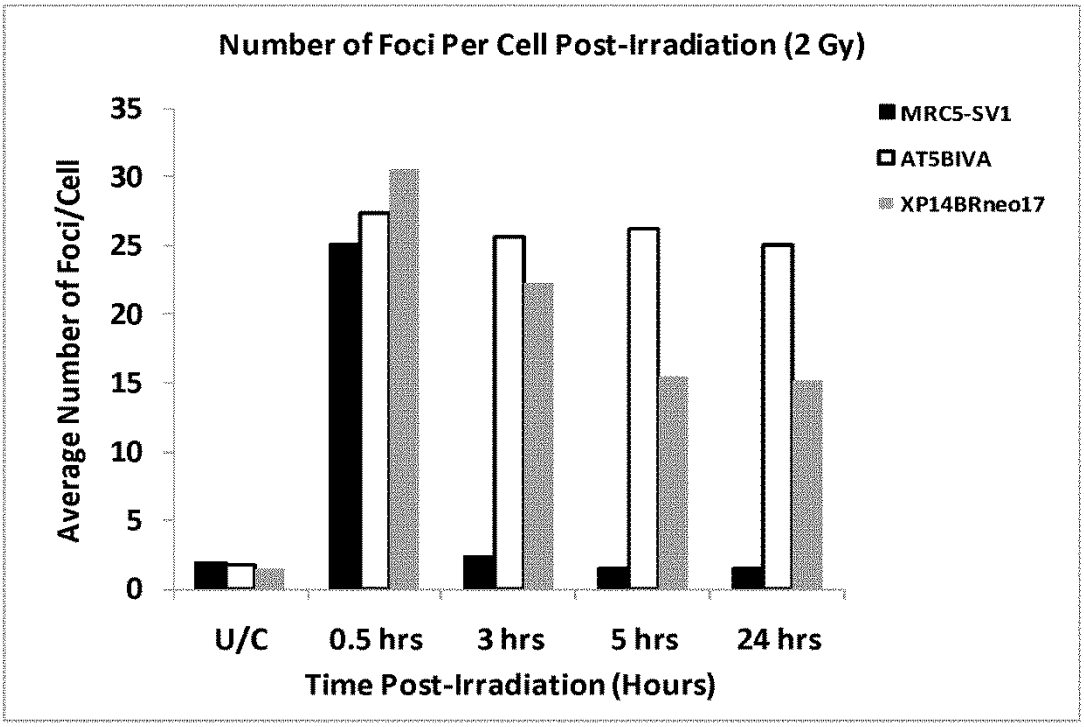

The mean number of γ-H2AX foci seen in MRC5-SV1, AT5BIVA and XP14BRNeo17 cell lines over a 24 hr period post exposure to 2 Gy gamma radiation measured using *in situ* immunofluorescence. Error bars represent the standard error of the mean derived from three independent experiments in which 100 cells were analysed at each time point for each cell line.

3.2.4 Comparison of Total and Nuclear Fluorescence

The relative nuclear fluorescence exhibited by the γ-H2AX foci induction (seen in Ch03) can be readily compared with the total cellular fluorescence (also seen on Ch03 but measured without the application of the Morphology Mask which would direct the analysis software to exclude any staining that fell outside the nucleus). The total cellular fluorescence data is similar to data that would be derived from using classical flow cytometry which has zero resolution. Subsequently this enables a comparison between imaging and classical flow cytometry. Figure 3.5 compares the total cellular fluorescence in comparison to the nuclear cellular fluorescence in the three cell lines post exposure to 2 Gy gamma radiation.

Figure 3.5: Comparison of total and nuclear fluorescence levels

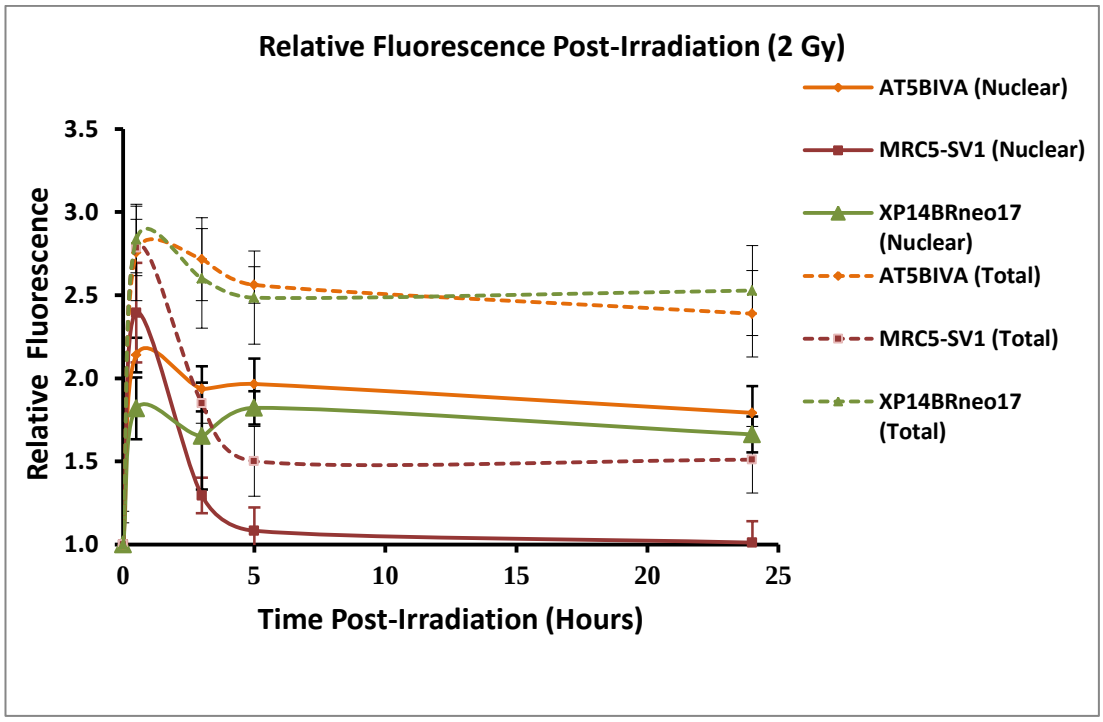

The relative levels of nuclear and total fluorescence exhibited in the three cell lines. Closed symbols indicate the nuclear fluorescence whilst the open symbols indicate total cellular fluorescence. Relative fluorescence was calculated by diving actual fluorescence levels seen at each time point by the fluorescence exhibited in the control cells for each cell line. The dramatic increase in fluorescence indicates the presence of γ-H2AX foci in the nuclei of the cells. A rapid drop in fluorescence is seen in the MRC5-SV1 repair normal cells after 3 hrs whilst the AT5BIVA and XP14BRNeo17 cells show to retain high levels of fluorescence even after 24 hrs. Error bars represent the standard error of the mean where approximately 20000 cells were collected from three independent experiments.

In all cell lines, the level of fluorescence induction appears to mimic similar patterns to foci induction and repair seen; be it total or cellular fluorescence. In the repair normal MRC5-SV1, there is approximately a 2.5 fold increase in the level of nuclear fluorescence 30 minutes post exposure to 2 Gy gamma radiation. These levels are seen to drop considerably by 3 hrs postirradiation which is consistent with the repair of DNA DSBs induced by the exposure to gamma radiation and by 24 hrs, the level of nuclear fluorescence has returned to similar levels to that of the control cells. In the AT5BIVA cells, nuclear fluorescence levels are retained even

after 24 hrs, thought to be seen due to the lack of DNA DSB repair taking place and are in line with the level of foci retention exhibited at 24 hrs.

The XP14BRNeo17 cell line also exhibits defective DNA repair where one of the vital components of the NHEJ pathway, the DNA-PK_{cs} gene has lost its functionality, rendering the cells hypersensitive to the effects of ionising radiation. It can be seen that the levels of nuclear fluorescence in the AT5BIVA cells and the XP14BRNeo17 cells are quite similar at 24 hrs despite the AT5BIVA showing higher levels of foci retention. This could be due to differences in the size of foci seen and subsequently the intensity of foci staining in the different cell line nuclei.

When comparing the total cellular fluorescence with the nuclear cellular fluorescence, it can be seen that the total cellular fluorescence is higher for each cell line. This could be due to non-specific staining within the cytoplasm of the cells. However, the total cellular fluorescence retention patterns are similar for each of the cell lines when compared to the nuclear cellular fluorescence levels. For example, the total cellular fluorescence for the MRC5-SV1 repair normal cells increase by approximately 2.7 fold in comparison at 30 minutes post exposure to 2 Gy gamma radiation in comparison to the untreated cells. However at 3 hrs, these levels drop down to approximately 1.5 fold of the control cells as DNA DSB repair has begun in these cells and by 24 hrs, fluorescence levels are similar to those exhibited by the control cells.

3.3 Discussion

This investigation was a quantitative study of radiation-induced γ-H2AX foci induction in the repair normal MRC5-SV1 cell line and two DNA repair defective cell lines, XP14BRNeo17 and AT5BIVA. The novel technique of imaging flow cytometry was employed to conduct this study using the Imagestream^{x}. Using the Imagestream^{x} allowed for images of every individual cells to be captured in flow on a maximum of 6 optical channels. There were three main channels used for these series of experiments which were Ch0 1 (BF), Ch03 (PE for γ-H2AX staining) and CH05 (Draq5 for nuclear staining), enabling the measurement of the intensity and number of nuclear γ-H2AX foci localised to the nucleus of each cell. It also enabled the collection and analysis of over 20000 cells which was never considered a practical approach when using fluorescence microscopy. Similarly, analysing samples using flow cytometry allowed for the collection of higher numbers of cells but it was not possible to analyse the number of foci seen in each cell.

Using imaging flow cytometry, it has been possible to detect differences in the induction and repair of DNA DSBs (measured by quantifying the number of γ-H2AX foci) in the three different cell lines. The MRC5-SV1 cells exhibit a repair profile typical of many other repair competent cell lines (Abbaszadeh *et al.* 2010).

The AT5BIVA cell line derived from an AT patient exhibits a similar induction of DNA DSBs, indicated by the increase in the number of γ-H2AX foci seen at 30 minutes postirradiation. However at 24 hrs, high levels of foci are still seen which is thought to be due to the defective *ATM* gene which renders the DNA repair mechanisms inept to resolve DNA DSBs.

The XP14BRNeo17 cell line also shows a similar increase in the number of γ-H2AX foci seen 30 minutes after 2 Gy gamma irradiation. However at 24 hrs, there is only a partial retention of γ-H2AX foci seen. Earlier investigations with this cell line revealed a splicing defect in the DNA-PK_{cs} gene which is integral in the NHEJ pathway (Abbaszadeh *et al.* 2010). This defect resulted in a heterozygous phenotype whereby both the normal and a defective splice variant of the gene were produced in the patient; ultimately leaving the cells hypersensitive to clinical radiation. It is likely that the intermediate retention of foci after 24 hrs could be due to the haploinsufficiency of the DNA-PK_{cs} gene which resulted in only partial repair of the DNA DSBs taking place.

In this study, the results obtained from imaging flow cytometry were compared with those derived from *in situ* microscopy. While similar profiles of γ-H2AX foci induction were seen within the three cell types, there was a noticeable increase in the number of foci scored using the *in situ* methods (Figure 3.4 and Figure 3.5). The most likely reason for this may be due to the difference in magnification used for the in situ microscopy (x100 objective) in comparison to the Imagestream^X (x40 objective). However the relative differences in foci induction profiles remained the same; regardless of the method used to quantify them.

It was also possible to compare nuclear fluorescence with total fluorescence, thereby enabling comparison of imaging flow cytometry and classical flow cytometry. Both approaches showed differences in the DNA repair capacity of the three cell lines employed in this study; however the increases in total cellular fluorescence were higher than the total nuclear fluorescence. As this was seen in all

cell lines, it is likely that these differences were due to non-specific staining of the cytoplasm.

Overall, imaging flow cytometry has provided a novel technique for quantification of γ-H2AX foci in cells. Comparisons with classic methods such as *in situ* immunofluorescence and conventional flow cytometry have shown the data derived from the Imagestream^X yields similar patterns of foci induction in the different cell lines employed in this investigation. The ability to image cells in flow has allowed for a quick and accurate method for detecting differences in DNA repair profiles of different cell lines. Allowing for this analysis to be carried out on large numbers of cells (approximately 20 0000) provides robust data and the technically simple and rapid method permits for high throughput and prompt data analysis. The volume of data that can be captured in a relatively short time compensates for the lower resolution images that are produced by the Imagestream^X in comparison to other microscopy image capture methods.

Chapter 4

Determining cellular sensitivity to a range of cytotoxic chemotherapeutic drugs using clonogenic assays

4.1 Introduction

The γ-H2AX assay described in the previous chapter was designed to assess the validity of the Imagestream^{x} to measure γ-H2AX expression levels in cell lines with different defects in DNa DSB after exposure to 2 Gy gamma radiation. The study successfully identified differences in DNA repair levels between the repair normal MRC5-SV1 cell line and the two DNA repair defective cell lines AT5BIVA and XPBR14neo17.

Chemotherapy is one of the other main forms of treatment for cancer patients either in conjunction with radiotherapy and surgery or as a treatment regimen on its own (Clingen *et al.* 2008). Chemotherapy primarily works by damaging DNA of dividing cells. However its toxicity is not limited to tumour cells and healthy cells are also targeted which may lead to the manifestations of debilitating side effects such as alopecia, weight loss and destruction of the immune system. Subsequently there is an increasing need emerging for a predictive assay which could map response to this type of treatment to identify hypersensitive patients.

There is an array of chemotherapeutic agents currently in clinical use which exhibit different modes of action which would presumably have an effect on the level of toxicity they exert. This therefore would be reflected in the concentration of each drug required to inflict a level of DNA damage on patient cells without causing irreversible effects to cell function and viability. The drugs that were selected for this study are Pt (Sigma Aldrich), HN2 (Sigma-Aldrich) ADR (Duchefa Biochemie, 2003 RV Haarlem, The Netherlands) and 5-FU (Duchefa Biochemie) (Refer to Table 4.1 for more details).

Table 4.1: Overview of chemotherapeutic agents used and their mechanism of action

Chemotherapeutic Agent	Mechanism of Action	Treatment
Cisplatin (Pt)	Formation of interstrand crosslinks	Broad range of cancers such as breast cancer
Nitrogen Mustard (HN2)	Formation of interstrand crosslinks	Non Hodgkin's Lymphoma
5-Fluorouracil (5-FU)	Inhibition of thymidylate synthase and incorporation of metabolites into RNA and DNA	Colorectal Cancer
Adriamycin (ADR)	Inhibition of Topoisomerase II, DNA intercalator, DSB formation	Broad range of solid tumours

These agents were chosen as they are commonly used chemotherapeutics in the treatment of various cancers such as breast cancer, colon cancer, prostate cancer and lymphomas (Harmers *et al.* 1991; Longley *et al.* 2003) and differ in their mechanisms of action.

HN2 and Pt cause inter or intra strand DNA cross links which can lead to the inhibition of DNA synthesis (Smith *et al.* 1995). 5-FU is an anti-metabolite capable of incorporating itself into the DNA subsequently inhibiting normal functions as well as inhibiting vital biosynthetic processes (Longley *et al.* 2003). The full extent of the damage that Adriamycin is able to exert has not been completely elucidated as yet but it is thought to have multiple mechanisms of actions such as inducing free radical formation, inhibiting Topoisomerase II activity, DNA intercalator and causing DNA cross links.

Following the method of developing the γ-H2AX assay for radiation, it was deemed necessary to determine the toxicity of each drug on each cell line prior to designing a predictive assay for chemotherapy. The clonogenic assay was selected as the assay of choice for evaluating cellular response to each drug.

Clonogenic assays were first established by Puck and Marcus in 1956 and were considered the "gold standard assay" in radiobiology by the early 1970s (Hoffman 1991). It is the only viability assay capable of measuring a cell's ability to form a colony after treatment, thereby providing an assessment of reproductive cell survival (Katz *et al.* 2008). It is also able to detect the cytotoxic effects of any drug as long as the agent interferes with cell reproducibility (Katz *et al.* 2008).

There are drawbacks to this technique such as the lengthy period taken for the formation of colonies. However it is still considered a reliable method of determining cellular responses to chemotherapy although it has been argued that there are quicker and more effective methods such as the tetrazolium salt, 3-4,5 dimethylthiazol-2,5 diphenyl tetrazolium bromide (MTT) assay or the Lactate Dehydrogenase (LDH) release assay (Hoffman 1991).

The MTT assay involves quantifying the rate of conversion of MTT into purple coloured formazan by oxidative activity of living cells. A decline in the level of MTT conversion, measured by a spectrophotometer is thought to indicate cell damage (Abe and Matsuki 2000). The Lactate Dehydrogenase Assay has similar principles where the release of the intracellular enzyme LDH is measured upon damage of the plasma membrane. It is agreed that there are disadvantages to using clonogenic assays such as the lengthy time involved to elicit results which ranges from 10 to 21 days in comparison to the MTT assay which can yield results in 72 hrs.

However there are other advantages such as the simplicity of performing this experiment and obtaining survival data, low costs of performing these types of experiments and most importantly, it is able to distinguish between cytotoxic and cytostatic cells which the MTT assay is not able to (Hoffman 1991).

The purpose of this study was to determine the half maximal inhibitory concentration of the chemotherapeutic agents, also known as the IC_{50}. This concentration kills 50% of the target cell population. By visually counting the number of colonies that form after the cells have been exposed to a range of different concentrations of each drug and making a comparison against the number of colonies that have formed on the control plates, the IC_{50} can be determined.

4.2 Results

4.2.1 Colony counting

Colony counting was performed using the rule that a minimum of 50 cells will be considered to be a colony (Franken *et al.* 2006). Individual colonies were counted by eye with the aid of a microscope to verify the number of cells in smaller colonies. There was a decrease in the number of colonies seen as the drug concentration was increased as shown in Figure 4.1 below.

Figure 4.1: Typical colony formation seen 10 - 21 days post exposure to drugs

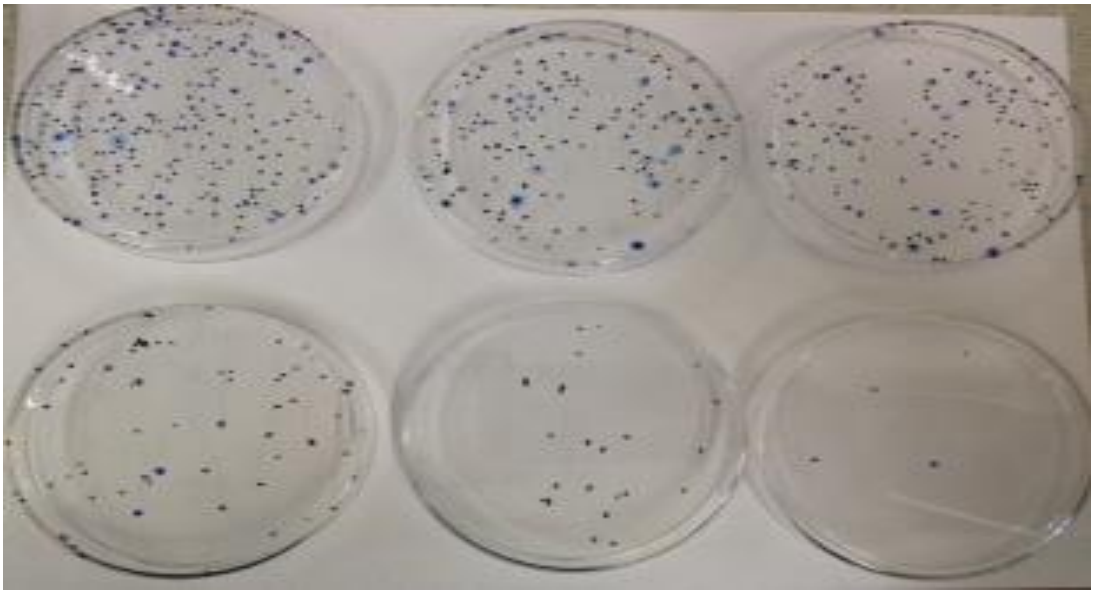

The above figure shows example plates from a typical clonogenic assay; depicting the reduction of colony formation as the dose of the drug is increased

4.2.2 Calculating survival rates

Plating efficiency (P.E.) was first determined by analyzing colony growth on the control plates using the following formula which provides the percentage of colonies that will form from the total number of cells initially plated.

Number of colonies formed/Number of cells initially plated x 100

Survival rates in the treated plates was then determined in two steps using the following formulas. First the number of colonies that would theoretically have formed had the plates not been treated with drug was determined using the following formula

P.E. x number of cells plated at that dose

Then the survival rate was determined by the following formula

Number of colonies formed/ number of colonies that should have formed x 100

This was then plotted to determine IC_{50} values of each drug for each individual cell line.

4.2.3 Determining IC_{50} values of HN2

All cell lines were exposed to a range of concentrations of HN2 from 0.5 μg/mL to 2.5 μg/mL. Figure 4.2 shows the survival rates of the cells at each concentration. It was observed that the survival rates of all cell lines decreased as the concentration of HN2 was increased. There was not much change in survival rates between 2 μg/mL and 2.5 μg/mL, resulting in the formation of a plateau of survival at the top end of the dose range for the NB1-HTert and MRC5-SV1 cell lines. The IC_{50} was graphically determined to be 0.45 μg/mL for the MRC5-SV1 cell line, 0.3 μg/mL for the NB1-HTERT cell lines and 0.2 μg/mL for the AT5BIVA cell line.

Figure 4.2: Cell survival for all cell lines post exposure to HN2

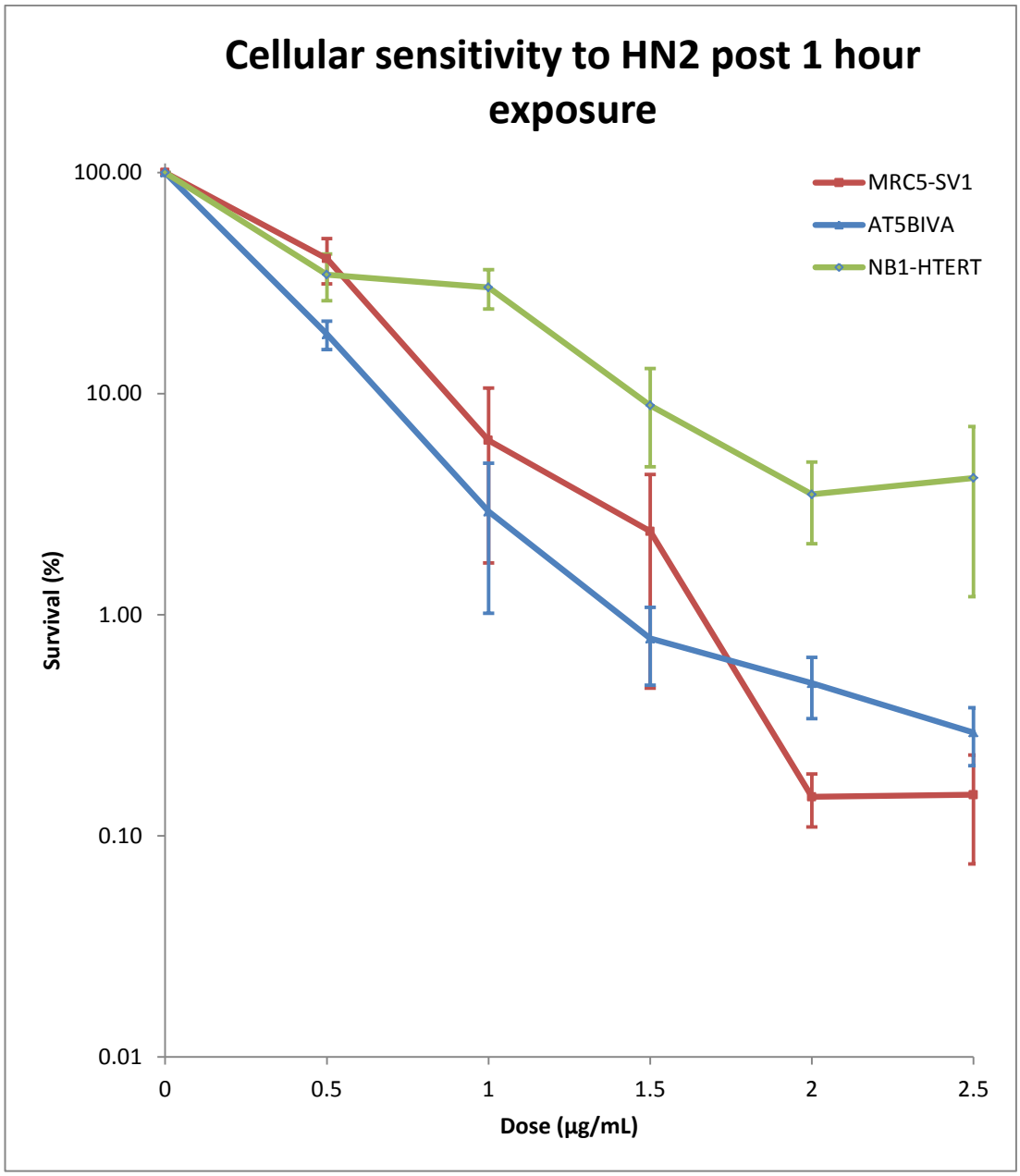

The effect of HN2 on the three cell lines, AT5BIVA, MRC5-SV1 and NB1-HTERT. Data was derived from 3 independent experiments and error bars represent standard error of the mean. All cell lines were treated with HN2 concentrations ranging between 0.5 and 2.5 µg/mL. There was a decrease in survival seen as the concentration of HN2 was increased in all cell lines. IC_{50} values were graphically determined as being 0.5 µg/mL for MRC5-SV1, 0.3 µg/mL for NB1-hTERT and 0.2 µg/mL for AT5BIVA.

4.2.4 Determining IC_{50} values of Pt

All cell lines were exposed to a range of concentrations of Pt from 15 μg/mL to 35 μg/mL. Figure 4.3 shows the effect of this drug on all three cell lines. Cell kill was seen over 2 decades with MRC5-SV1 and NB1-HTERT survival levels forming a plateau again when survival rates at the 2 highest doses were analysed. The IC_{50} values for the MRC5-SV1 cell line was 12 μg/mL, 6 μg/mL for the NB1-HTERT cell line and 7 μg/mL for the AT5BIVA cell line.

Figure 4.3: Cell survival for all cell lines post exposure to Pt

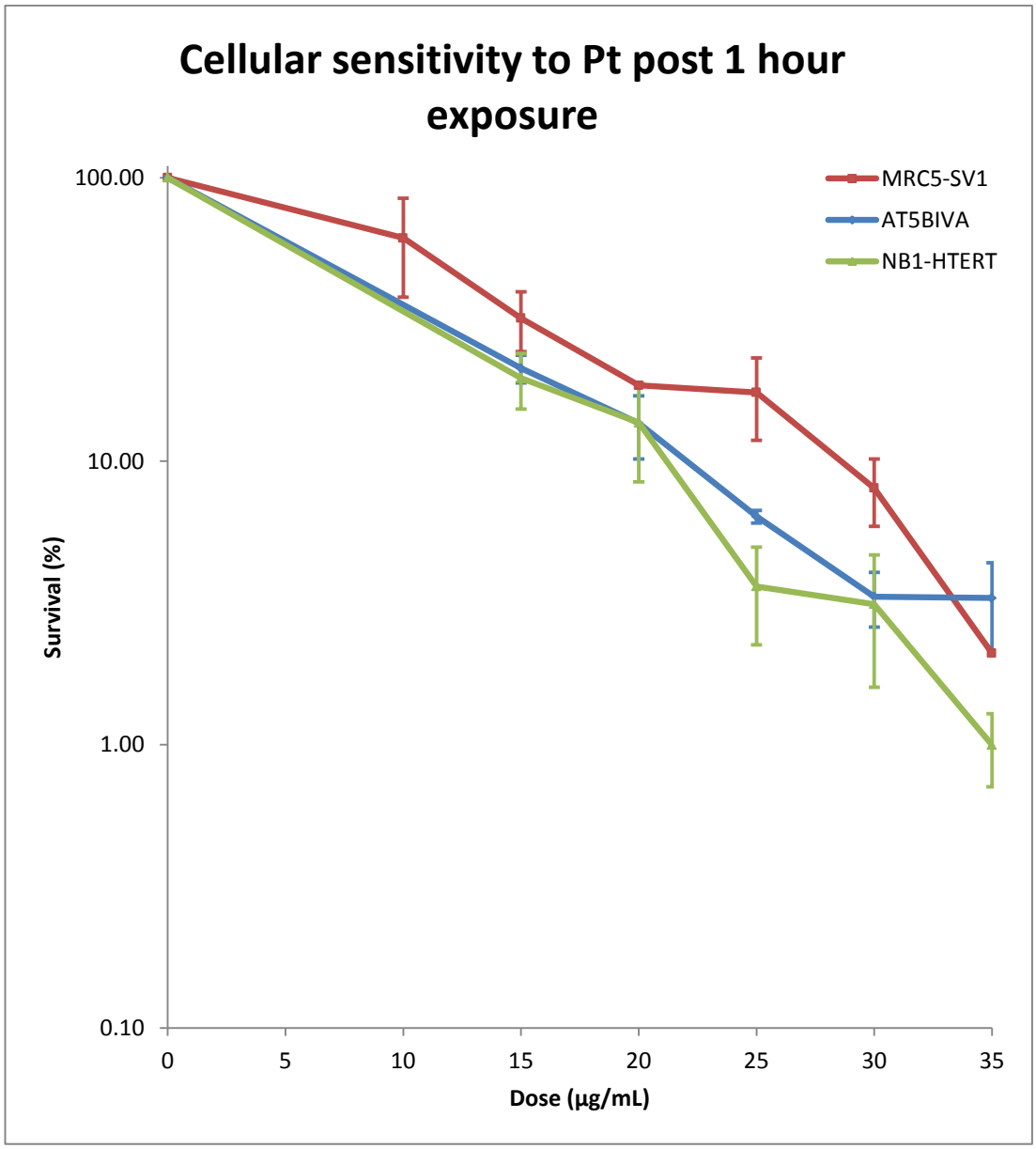

The effect of Pt on the three cell lines, AT5BIVA, MRC5-SV1 and NB1-hTERT. All cell lines were treated with Pt concentrations ranging between 15 and 35 µg/mL. There was a decrease in survival seen as the concentration of Pt was increased in all cell lines. IC_{50} values were graphically determined as being 12 µg/mL for MRC5-SV1, 6 µg/mL for NB1-hTERT and 7 µg/mL for AT5BIVA. Data was derived from 3 independent experiments and error bars represent standard error of the mean.

4.2.5 Determining IC_{50} values of Adr

All cell lines were exposed to a range of concentrations of ADR from 50 ng/mL to 150 ng/mL. Figure 4.4 depicts the survival levels of all 3 cell lines after a 1 hour exposure to Adriamycin. As seen with the other drugs, the level of survival decreased proportionately as the concentration of drug was increased. The IC_{50} was graphically determined to be 56 ng/mL for the MRC5-SV1 cell line, 93 ng/mL for the NB1-HTERT cell line and 84 ng/mL for the AT5BIVA cell line.

Figure 4.4: Cell survival for all cell lines post exposure to Adr

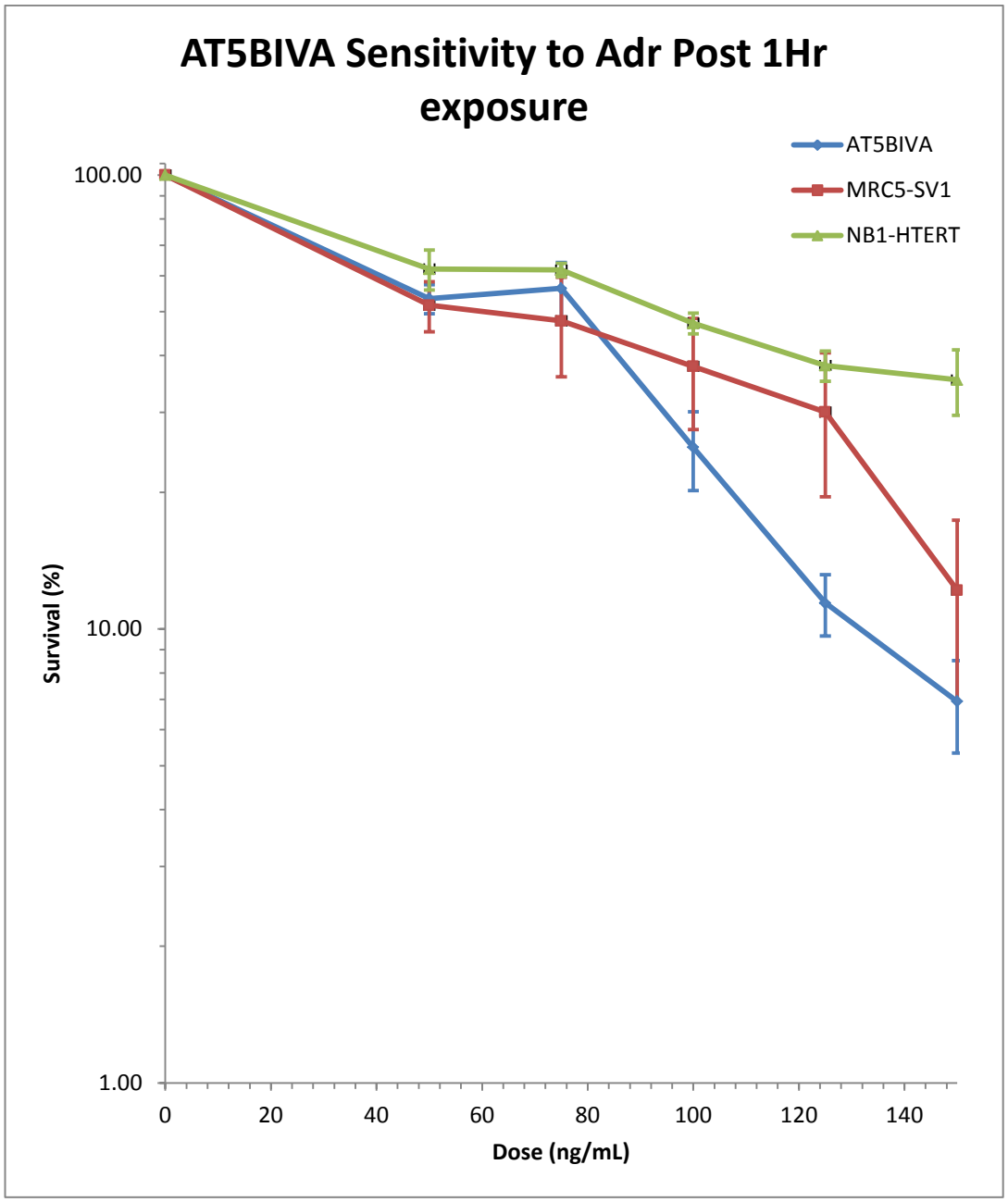

The effect of ADR on the three cell lines, AT5BIVA, MRC5-SV1 and NB1-HTERT. All cell lines were treated with Pt concentrations ranging between 50 and 150 ng/mL. There was a decrease in survival seen as the concentration of Pt was increased in all cell lines. IC_{50} values were graphically determined as being 56 ng/mL for MRC5-SV1, 93 ng/mL for NB1-HTERT and 84 ng/mL for AT5BIVA. Data was derived from 3 independent experiments and error bars represent standard error of the mean.

4.2.6 Determining IC_{50} values of 5-FU

All cell lines were exposed to a range of concentrations of 5-FU from 50 μg/mL to 200 μg/mL. Figure 4.5 represents the survival levels of all 3 cell lines after a 1 hour exposure to 5-Fluorouracil. Survival rates steadily declined between cells treated at 50 μg/mL to the cells treated at 100 μg/mL after which point a sharp decline in survival was seen between the two highest doses The IC_{50} was graphically determined to be 190 μg/mL for the MRC5-SV1 cell line, 161 μg/mL for the NB1-HTERT cell line and 132 μg/mL for the AT5BIVA cell line.

Figure 4.5: Cell survival for all cell lines post exposure to 5-FU

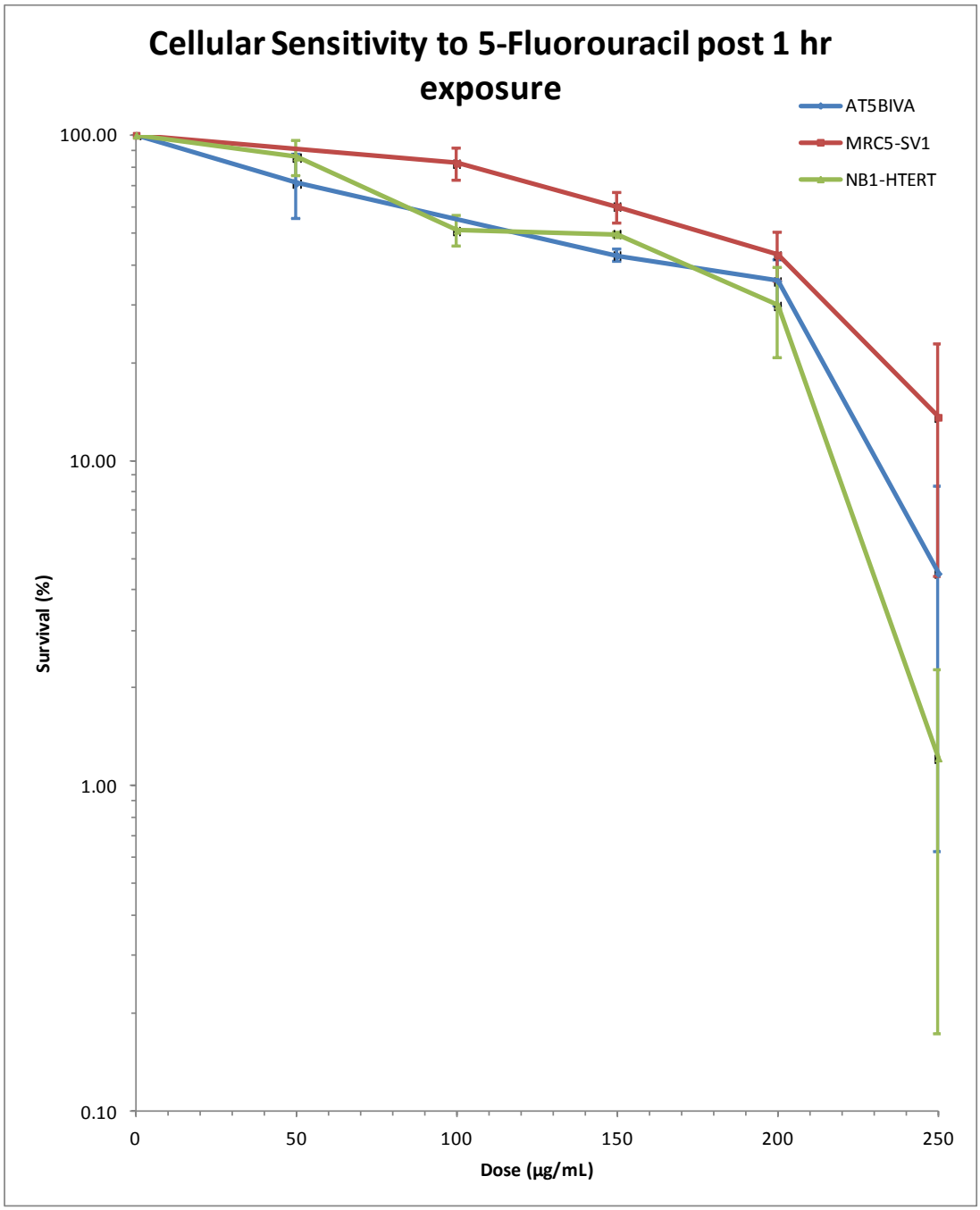

The effect of 5-FU on the three cell lines, AT5BIVA, MRC5-SV1 and NB1-HTERT. All cell lines were treated with 5-FU concentrations ranging between 50 and 250 µg/mL. There was a decrease in survival seen as the concentration of Pt was increased in all cell lines. IC_{50} values were graphically determined as being 190 µg/mL for MRC5-SV1, 161 µg/mL for NB1-HTERT and 132 µg/mL for AT5BIVA. Data was derived from 3 independent experiments and error bars represent standard error of the mean.

Table 4.2: IC_{50} values derived for all cell lines

Cell line	HN2	Pt	Adr	5-FU
MRC5-SV1	0.5 μg/mL	12 μg/mL	56 ng/mL	190 μg/mL
NB1-HTERT	0.3 μg/mL	7 μg/mL	93 ng/mL	161 μg/mL
AT5BIVA	0.2 μg/mL	6 μg/Ml	84 ng/mL	132 μg/mL

The above table summarises the IC_{50} values derived for each cell line with each of the four chemotherapeutic agents. The MRC5-SV1 cell line was observed as being the most resistant cell line to all chemotherapeutic agents with the exception of Adr. However the AT5BIVA cell line demonstrated unexpected resistance to the cross-linking agents with similar IC_{50} values derived in comparison to the repair normal NB1-HTERT cell line. However when the second repair normal cell line, MRC5-SV1, is considered, AT5BIVA cell line exhibited a 50% decrease in resistance. This may be an indication of previously undetected sensitivity to cross-linking agents in the NB1-HTERT cell line.

4.3 Discussion

The IC_{50} values that were obtained from the colony forming assays provides a dose of the drug that will inflict damage onto cells without killing off the entire population (i.e. killing approximately 50% of the cell population). It is crucial to have accurate data regarding these values as they form the basis of the drug concentrations that will be used in the γ-H2AX assay being designed to predict patient response to chemotherapeutic agents.

The results of these clonogenic assays support the theory that all drugs have different levels of toxicity as demonstrated by the differing ranges of concentrations used for each drug and it also shows it is possible for the toxicity of the drug to vary between individuals as indicated by the differing IC_{50} values obtained for each cell line treated with the same drug.

The MRC5-SV1 repair normal cell line was seen to be the most resistant to the effects of the cross-linking agents, HN2 and Pt with its IC_{50} values being nearly double the values obtained for the other two cell lines (Refer to Table 4.2). It was hypothesized that AT5BIVA, a cell line derived from an individual with the DNA repair defective Ataxia Telangiectasia disorder, would exhibit an increased sensitivity to these drugs and require a much lower concentration of each drug to achieve a cell kill of 50% due to having an impaired *ATM* gene, rendering the cells DNA repair defective (Hickson *et al.* 2004). However it was seen that this cell line had very similar IC_{50} values for all drugs to the NB1-HTERT cell line which was derived from a repair normal individual. This suggests that the DNA DSB repair pathways are not required for the repair of lesions caused by these drugs. However when compared to the other DNA repair normal cell line, MRC5-SV1, a 2-fold

increase in colony forming ability was seen in the MRC5-SV1 cell line. The contradicting results between the two DNA repair normal cell lines indicates a need for a larger number of cell lines to be included in this study such as more DNA repair normal individuals as well as cell lines with known repair deficiencies in other DNA repair pathways.

Interestingly it was observed that the results derived from the ADR clonogenic assay showed MRC5-SV1 as being the most sensitive cell line to this drug with the NB1-HTERT cell line having an IC_{50} value nearly double that of MRC5-SV1. ADR has a different mode of action to the two cross-linking agents, Pt and HN2 and this may have had an impact on the sensitivity exhibited by the MRC5-SV1 cell line to this drug.

The IC_{50} values derived for the cell lines from the other clonogenic assays will now be utilised in designing a chemotherapy γ-H2AX assay for each drug; the results of which are detailed in Chapter 5. Although survival data was obtained for all cell lines in response to treatment with 5-FU, this was a very challenging process and it was very difficult to obtain consistent data for the cell lines. Therefore the decision was taken to exclude this drug from the remainder of the project. It is thought that the cell line exhibiting higher resistance to each chemotherapeutic drug will show increased expression of γ-H2AX levels. γ-H2AX expression in response to chemotherapeutic drugs which do not induce direct DSB are thought to be indicative of incisions being made at the site of lesion formation (i.e. ICL formation in response to Pt treatment). Therefore increased γ-H2AX expression would likely indicate an upregulated rate of DNA repair through increased incisions of the DNA damage being formed.

Chapter 5

Evaluation of γ-H2AX as a biomarker for chemotherapeutic drug response in human cells

5.1 Introduction

The role of γ-H2AX in response to IR has been well established since its unique phosphorylation events in response to the formation of DSBs were first identified nearly 15 years ago by William Bonner and co-workers (Rogakou *et al.* 1998). The induction of direct DSBs through exposure to agents such as X-rays or IR leads to rapid formation of γ-H2AX foci. Cytotoxic agents such as DNA synthesis inhibitors, alkylating agents and Topoisomerase I and II inhibitors can also induce γ-H2AX foci formation in response to DNA strand breaks arising during the repair process of non-DSB lesions (Dickey *et al.* 2009). Investigations such as the retrospective study by Bourton *et al*, (2011) which employed γ-H2AX as a marker of DNA damage successfully identified patients who were hyper-sensitive to IR thus revealing the potential application of this biomarker as a predictive diagnostics tool for identifying over-reactions to standard clinical radiotherapy. This was determined by the persistence of γ-H2AX foci seen 24 hrs after exposure to 2 Gy of gamma radiation in peripheral blood lymphocytes derived from cancer patients. Bourton *et al* (2012) explored the viability of using the Imagestream to assess DSB formation in response to IR and we were able to demonstrate the differences in repair levels between three cell lines known to exhibit different repair kinetics in response to IR (Refer to Chapter 3). γ-H2AX foci detection has been shown to be a much more sensitive indication of DNA damage in comparison with other techniques such as pulsed field gel electrophoresis or comet assays (Sedelnikova *et al.* 2002). γ-H2AX expression levels can be quantified through immunofluorescence, flow cytometry or western blotting and persistence of foci after the initial induction of damage implies unrepaired DNA damage (Dickey *et al.* 2009). The central role

that γ-H2AX plays in the detection of DNA damage and/or repair has been exploited to improve treatment efficacy. These areas include

- measuring levels of X-ray induced DSBs in angiography patients (Kuefner *et al.* 2009)
- toxicity studies on novel chemotherapeutic agents (Banath and Olive 2003)
- measuring tumour response to anti-cancer agents (Garcia-Villa *et al.* 2012).

Kuefer *et al* (2009) employed γ-H2AX to monitor the effects of radiation by measuring X-ray induced DNA DSBs and this revealed that analysing H2AX formation elicited additional information regarding cardiac toxicity in patients post treatment.

Cytotoxic chemotherapy is used extensively as a common means of treating cancer either in combination with surgery and radiotherapy or as a single treatment (Clingen *et al.* 2008). Most chemotherapeutic drugs target DNA of cancer cells; causing irreversible damage and ultimately leading to cell death. However chemotherapeutic cytotoxic drugs are not normally selective in killing cancer cells and the destruction of normal cells leads to the manifestation of side effects. Serious and unpleasant side effects are a fundamental limitation of chemotherapy and can vary dramatically between individuals. Subsequently, the utilisation of DNA damage and repair proteins is being increasingly being investigated in order to gauge the ability to predict possible outcomes of patient chemotherapy (Clingen *et al.* 2008). The efficacy of DNA repair in individuals may govern the level of side effects experienced by the patient.

Whereas the appearance of γ-H2AX foci post-irradiation is indicative of DNA damage, γ-H2AX foci appearing post treatment with chemotherapy, particularly in

the case of agents that do not induce direct DSBs, may be reflective of both chemotherapy induced DNA damage or repair processes taking place (Huang *et al.* 2004). There have been several studies examining the potential of γ-H2AX as a potential marker of cell sensitivity to chemotherapeutic agents such as Huang *et al,* (2004) who determined that the elevated expression of γ-H2AX post treatment seen in HL-60 (human promyelocytic leukaemic cells) with chemotherapeutic agents such as Pt could be arising due to collapsed replication forks. Replication forks refer to the region where daughter strands are synthesised during the replication process. It requires the unwinding of DNA parental double helix by specific DNA helicases in order to synthesise the complementary strand and this process can be halted by the presence of an ICL (i.e. such as those induced by Pt) which would prevent the unwinding of the parental DNA strands. There is no direct evidence supporting the formation of DSBs as an initial form of damage post treatment with the ICL-inducing agent Pt (Olive and Banath 2009). Similarly Clingen *et al*, (2008) determined that DSBs were initiated in both Chinese hamster and human ovarian cancer calls in response to the formation of ICLs to mediate repair of these lesions which caused a concomitant increase in γ-H2AX foci.

This study investigated the cytotoxicity of three chemotherapeutic drugs, Pt, HN2 and Adr by measuring γ-H2AX foci induction. HN2 is a bifunctional alkylating agent which is capable of forming both intrastrand and interstand crosslinks (Rink and Hopkins 1995). Pt is a platinum based compound whose main form of cytotoxicity is exerted by covalently linking the two DNA strands; forming an interstrand crosslink (Siddik 2003). Adr is known to exert its toxicity through multiple mechanisms such as inhibition of Topoisomerase II and intercalation with

DNA (Hawtin *et al.* 2010). These agents also may induce other forms of DNA damage such as oxidative stress; however any such damage is considered secondary to the main mechanisms mentioned above. The three cell lines utilised in this study; MRC5-SV1, AT5BIVA and NB1-HTERT, were all seen to exhibit a different γ-H2AX induction and repair profile in response to each drug. These findings show that even in two cell lines with no known DNA repair defects, MRC5-SV1 and NB1-HTERT, the level of resistance varied greatly in response to treatment with the same drug. These findings further emphasizes the need for development of individualised therapies based on personal responses to treatment regimens (Schwaiger and Peschel 2006).

5.2 Results

5.2.1 HN2 Dose Response

Induction of γ-H2AX associated fluorescence was measured in each of the cell lines post treatment with 0.5, 1.5 and 2.5 μg/mL HN2 for 1 hr. A nuclear morphology mask applied to the cells to determine the intensity of AF488 (indicative of γ-H2AX) in the nucleus. The resulting dose response curve seen in Figure 5.1 shows that the level of relative fluorescence increases in all three cell lines as the dose of HN2 is increased.

Figure 5.1: Relative fluorescence levels of cells post exposure to increasing doses of HN2

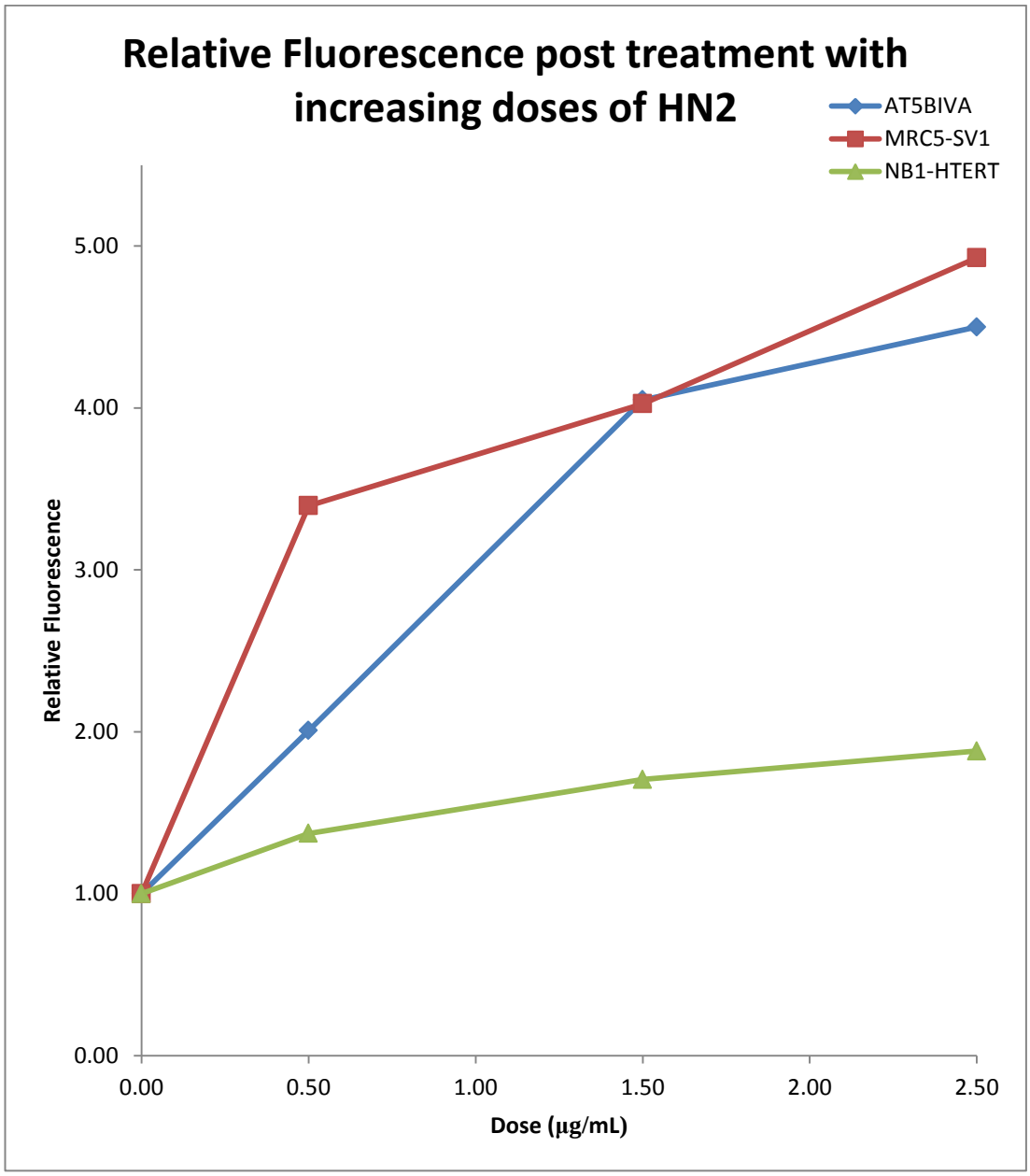

The relative levels of nuclear fluorescence exhibited in the three cell lines post treatment with increasing doses of HN2 ranging from 0.5 - 2.5 µg/mL. Relative fluorescence was calculated by dividing actual fluorescence levels seen at each time point by the fluorescence exhibited in the control cells for each cell line. All cells were fixed 24 hrs post treatment and it can be seen that there is an increase in relative florescence as the dose of HN was increased.

5.2.2 γ-H2AX Foci quantification post treatment with HN2

The average number of foci per cell in each of the three cell lines post 1 hour treatment with HN2 was analysed and quantified using the Imagestream^X. γ-H2AX foci were enumerated by applying a Morphology (nuclear region of cell) and Peak (AF488 staining representing γ-H2AX foci) mask to each of the cell images produced for each time point as described elsewhere in Section 2.4.7. The results are shown in Figure 5.2. The total nuclear fluorescence was also determined for each of the cell lines and is shown in Figure 5.3.

In untreated cells, the mean number of foci per nucleus is 2.24 for the MRC5-SV1 fibroblasts and 5 for the NB1-HTERT cells while a mean number of 3.58 foci were seen in the AT5BIVA cell line. Following a 1 hr treatment with HN2, the induction of γ-H2AX was observed at 5 different times over a 48 hour period. There was a variance in the behaviour of these cell lines with each cell line showing a different time scale for the peak of γ-H2AX foci induction. By 5 hrs post treatment with 0.2 μg/mL HN2, the AT5BIVA cell line exhibited the peak of γ-H2AX foci formation with a mean number of 4.17 foci per cell. The NB1-HTERT cell line showed a peak of γ-H2AX foci formation at 24 hrs after treatment with 0.3 μg/mL HN2; exhibiting an average of 7.55 foci per cell. The most dramatic increase in γ-H2AX foci induction was seen in the MRC5-SV1 cell line with an average of 13.51 foci noted at 30 hrs post treatment with 0.5 μg/mL HN2. However by 48 hrs, all cell lines showed that the majority of these γ-H2AX foci have disappeared; exhibiting similar levels to their respective control samples. This was presumed to be indicative that the damage exerted by HN2 has now been repaired.

The total nuclear fluorescence was also determined for each of the cell lines. It was seen the patterns of fluorescence appear to closely correlate to the number of γ-H2AX foci calculated in each cell line; i.e. a dramatic increase in foci seen at 24 hrs (calculated as approximately 6 times higher than the control sample) in the MRC5-SV1 cell line was mimicked by a 7 fold increase in the level of fluorescence seen at the same time point.

Analysis of variance (ANOVA) was used to determine whether there was a significant difference in the distribution of foci over the 48 hour time period. Comparison of the three cell lines showed that the behaviour of each cell line was significantly different ($p<0.001$), refer to Table 5.1 below.

Table 5.1: ANOVA Statistical Analysis of foci distribution in cell lines treated with HN2

Cell line	F	P-value
AT5BIVA v NB1-HTERT	1970.942	<0.001
AT5BIVA v MRC5-SV1	5005.1	<0.001
NB1-HTERT v MRC5-SV1	5415.05	<0.001

The F value is obtained by dividng the variance of the group means by the mean of within group variances. It allows for testing of the hypthoesis that variance due to treatment is significantly larger than the variance due to experimental error.

The relative fold increases in γ-H2AX foci induction were also calculated and are shown in Figure 5.4. The AT5BIVA and NB1-HTERT showed modest fold changes at 24 hrs in comparison to the MRC5-SV1 cell line which indicated a 6 fold increase when compared to the untreated control sample. At 48 hrs, majority of foci induction seen in all cell lines at 24 hrs has disappeared.

Figure 5.2: Average foci numbers over a 48 hour period post treatment with HN2

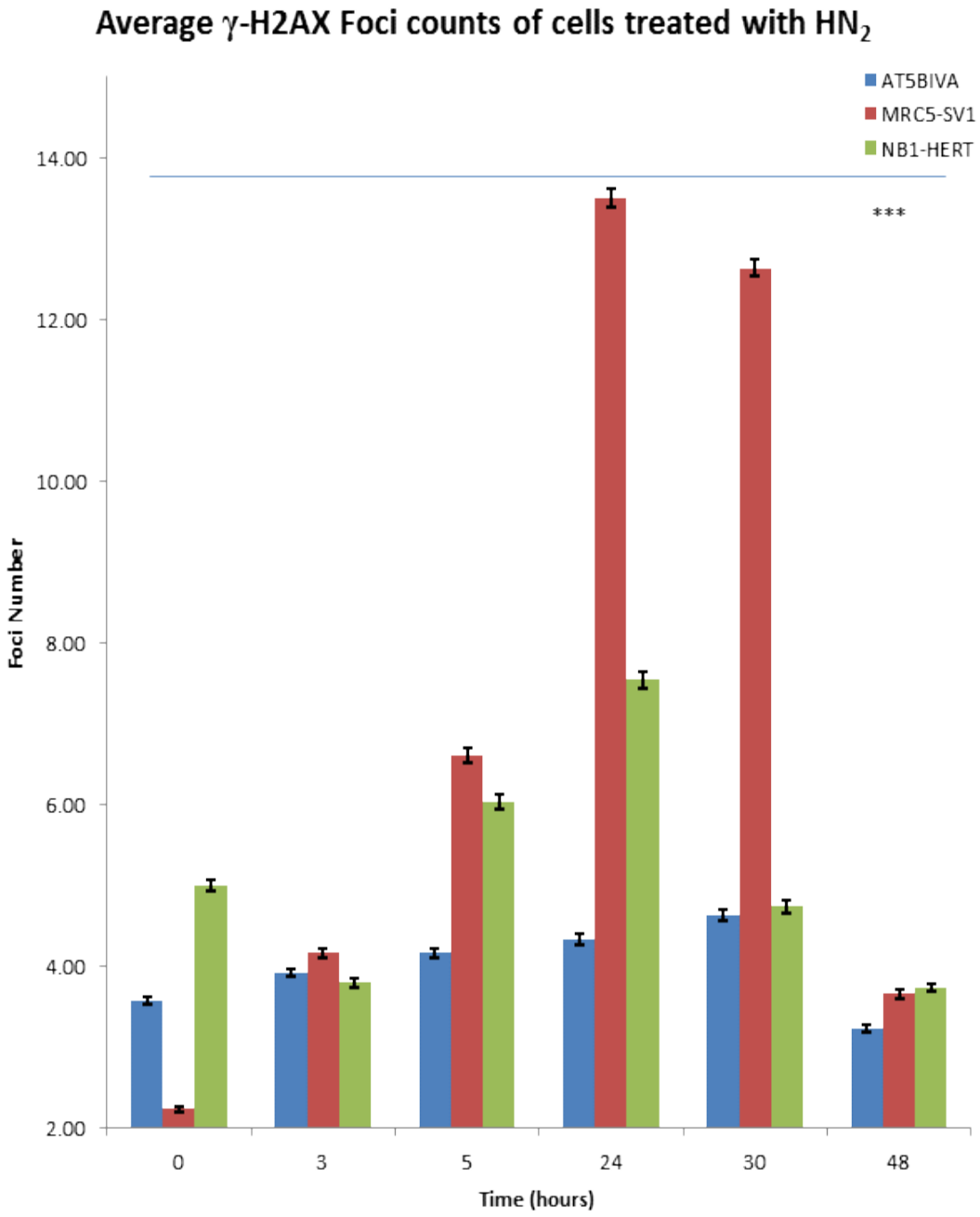

The mean number of γ-H2AX foci seen in MRC5-SV1, NB1-HTERT and AT5BIVA cell lines over a 48 hour period post treatment with 0.5, 0.3 and 0.2 µg/mL to HN2. Error bars represent the standard error of the mean derived from three independent experiments. Standard error was calculated by dividing the standard deviation of the mean by the square root of the number of cells counted for each sample. There is a vast increase in the number of γ-H2AX foci at 24 hrs and 30 hrs for the MRC5-SV1 cell line. Although not as dramatic, there is an increase in the number of γ-H2AX foci seen at 24 hrs for the NB1-HTERT cell line in comparison to the control. The AT5BIVA cell line showed a modest increase in γ-H2AX foci across the 48 hour period. The number of γ-H2AX foci seen at 48 hrs in all cell lines has returned to similar levels to that seen in the control samples of these cell lines. * ANOVA analysis of the foci distribution indicates a significant difference between the three cell lines (p value = <0.001)**

Figure 5.3: Relative fluorescence levels of cells post 1 hour treatment with HN2

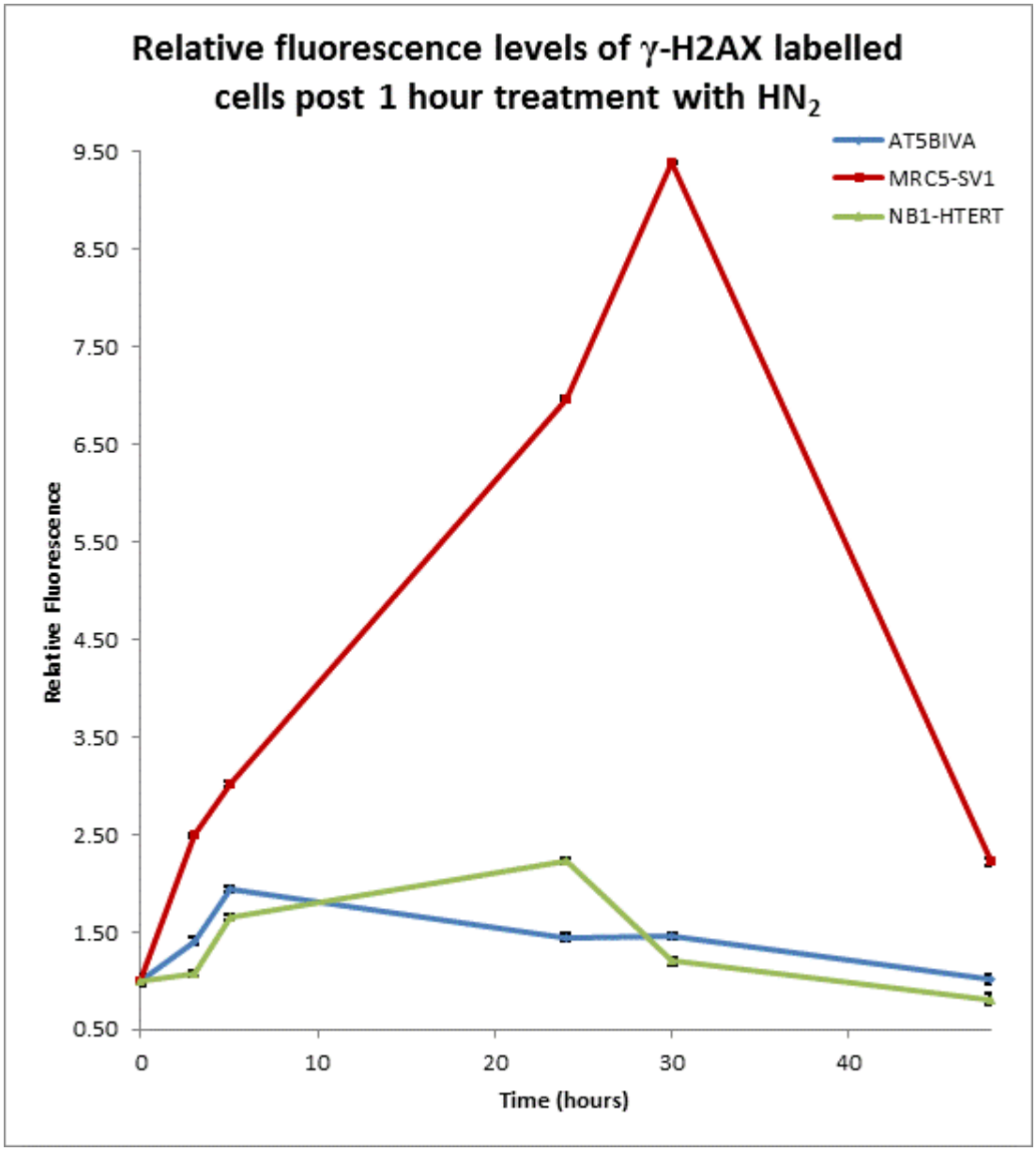

The relative levels of nuclear fluorescence exhibited in the cell lines post treatment HN2 treatment. Relative fluorescence was calculated by dividing actual fluorescence levels seen at each time point by the fluorescence exhibited in the control cells for each cell line. A dramatic increase in fluorescence was exhibited by the MRC5-SV1 cell line at 30 hrs post treatment with 0.5 µg/mL HN2, indicating the presence of γ-H2AX foci in the cell nuclei. AT5BIVA cells showed the peak of fluorescence at 5 hrs post treatment with 0.2 µg/mL HN2 whilst this was seen at 24 hrs post treatment with 0.3 µg/mL HN2 in NB1-HTERT cells. At 48 hrs post treatment, relative fluorescence levels of NB1-HTERT cells and AT5BIVA cells have returned to similar levels exhibited by the control samples while the MRC5-SV1 cell line still displayed fluorescence levels at approximately 2.4 fold of the control sample. Error bars represent the standard error of the mean where approximately 10000 cells were collected from three independent experiments. Standard error was calculated by dividing the standard deviation of the mean by the square root of the number of cells counted for each sample

Figure 5.4: Relative fold changes in cell lines post treatment with HN2

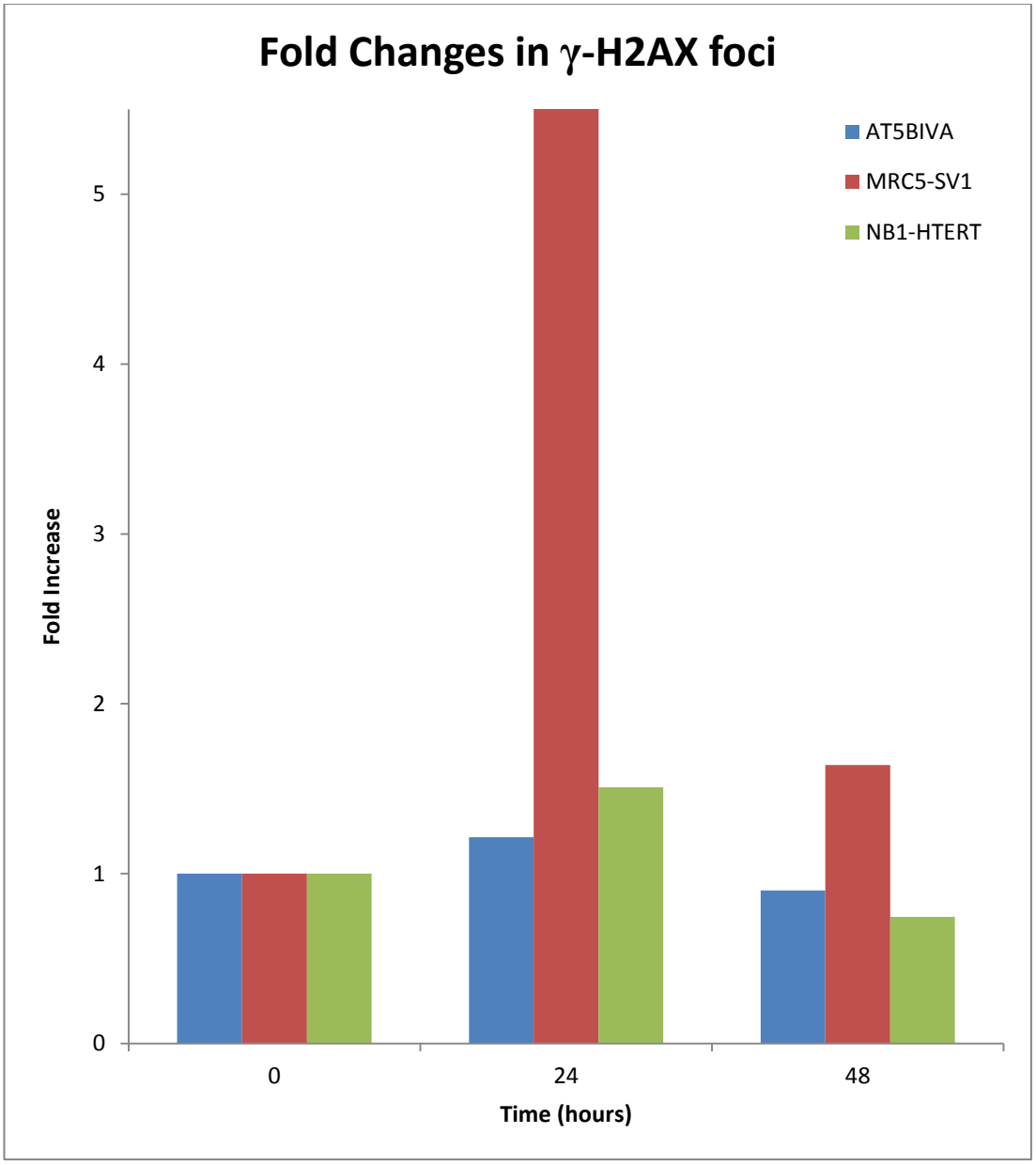

The fold increase in foci numbers were calculated for each of the cell lines by dividing the foci counts seen at 24 hrs and 48 hrs by the foci counts calculated for each of the control samples. The foci counts of the control samples were normalised to 1. The AT5BIVA cell line shows a 1.2 fold increase at 24 hrs while the MRC5-SV1 cell line shows a 6 fold increase at the same time point. The NB1-HTERT cell line shows a 1.5 fold increase at 24 hrs and this has decreased to -0.5 fold of the control at 48 hrs. The AT5BIVA cell line also shows a decrease below the control at 48 hrs. However the MRC5-SV1 cell line shows a 1.6 fold increase in comparison to the untreated control at 48 hrs.

5.2.3 γ-H2AX Foci quantification post treatment with Pt

The average number of foci per cell in each of the three cell lines post 1 hr treatment with Pt was analysed and quantified using the Imagestream^X as depicted in Figure 5.5. γ-H2AX foci were enumerated as described in section 2.4.7.

In untreated cells, the mean number of foci per nucleus is 3.59 for the MRC5-SV1 fibroblasts and 3.93 for the NB1-HTERT cells while a mean number of 2.88 foci were seen in the AT5BIVA cell line. The three cell lines exhibited different DNA repair profiles in response to the Pt treatment. The MRC5-SV1 cell line showed a peak of γ-H2AX foci induction at 48 hrs post treatment with 12 μg/mL Pt. In contrast, the NB1-HTERT cell line indicated that the peak of γ-H2AX foci induction was at 24 hrs post treatment with 6 μg/mL Pt and most of the γ-H2AX foci have disappeared at 48 hrs. The AT5BIVA cell line also showed peak of γ-H2AX foci at 24 hrs post treatment with 7 μg/mL Pt.

The fold increases in foci induction are higher for the AT5BIVA cell line at 6 hrs and 24 hrs in comparison to the NB1-HTERT cell line, which is shown in Figure 5.7. However at 48 hrs and 72 hrs, both cell lines show similar fold changes which is corroborated by similar relative nuclear fluorescence seen at these times points, seen in Figure 5.6.

By 72 hrs, both the AT5BIVA cell line and NB1-HTERT cell lines show γ-H2AX foci have returned to levels similar to that exhibited by their control samples whilst the MRC5-SV1 cell line still exhibits foci levels at a 1.6 fold increase in comparison to the untreated control. Relative fluorescence levels measured for the cell lines showed similar increments in relation to the foci counts and is shown in Figure 5.5.

ANOVA statistical analysis showed a significant difference in the distribution of foci over the 72 hour time period in all cell lines (Refer to Table 5.2).

Table 5.2: ANOVA Statistical Analysis of foci distribution in cell lines treated with Pt

Cell line	F	P-value
AT5BIVA v NB1-HTERT	1424.84	<0.001
AT5BIVA v MRC5-SV1	1876.061	<0.001
NB1-HTERT v MRC5-SV1	1673.32	<0.001

Figure 5.5: Average foci numbers over a 72 hour period post treatment with Pt

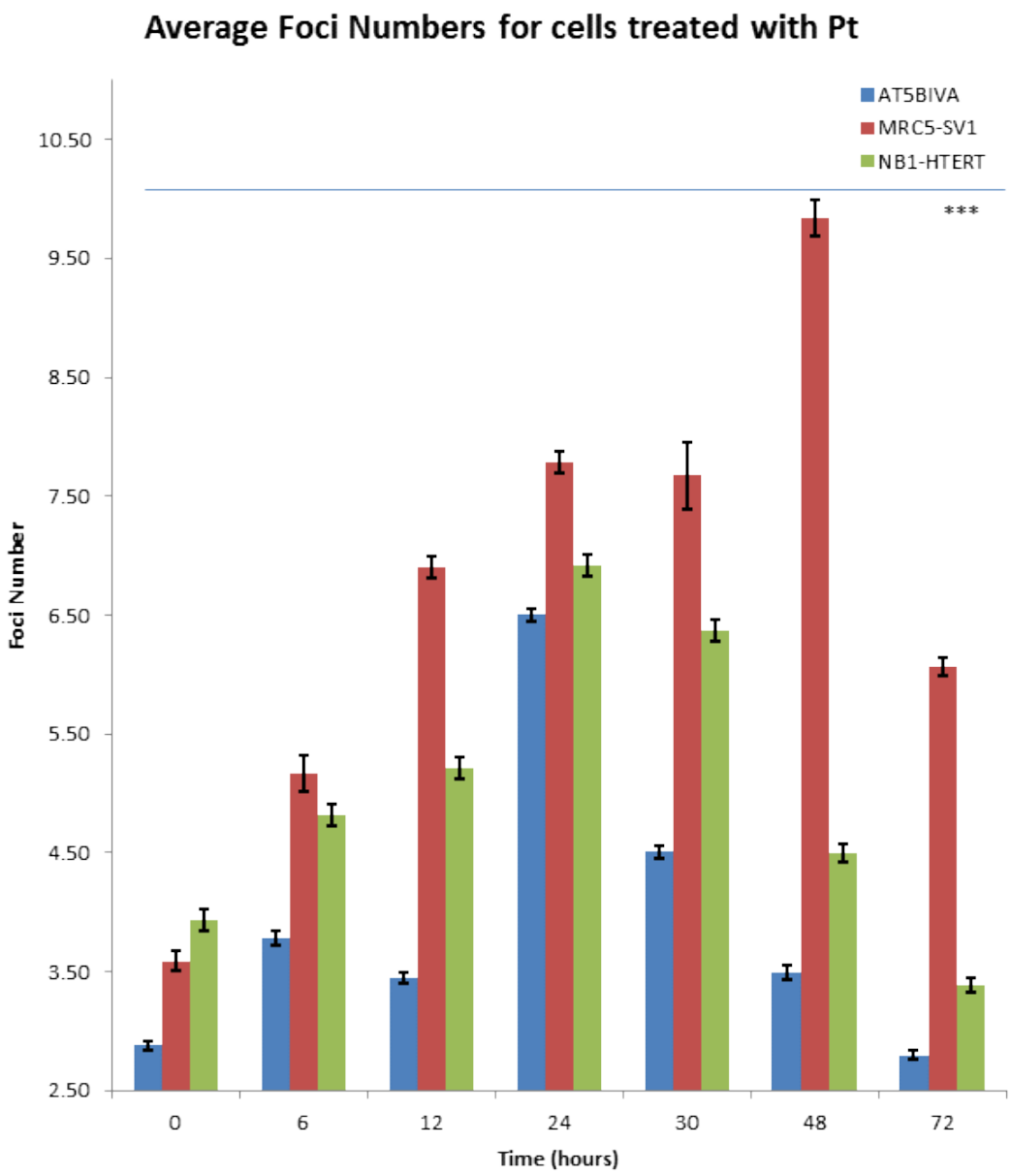

The average foci numbers seen in the three cell lines over a 72 hr period. A similar pattern of repair is seen in the AT5BIVA and NB1-HTERT cell lines with a peak of foci induction seen at 24 hrs post treatment with 7 and 6 µg/mL Pt respectively and complete repair being seen at 72 hrs. The MRC5-SV1 cell line shows a peak of foci induction at 48 hrs post treatment with 12 µg/mL Pt and still shows foci retention at 72 hrs with a 2 fold increase seen in comparison to its control sample. Error bars represent the standard error of the mean where approximately 10000 cells were collected from three independent experiments. Standard error was calculated by dividing the standard deviation of the mean by the square root of the number of cells counted for each sample. * ANOVA analysis showed significant differences between each of the three cell line (p value = <0.001)**

Figure 5.6: Relative fluorescence levels of cells post 1 hour treatment with Pt

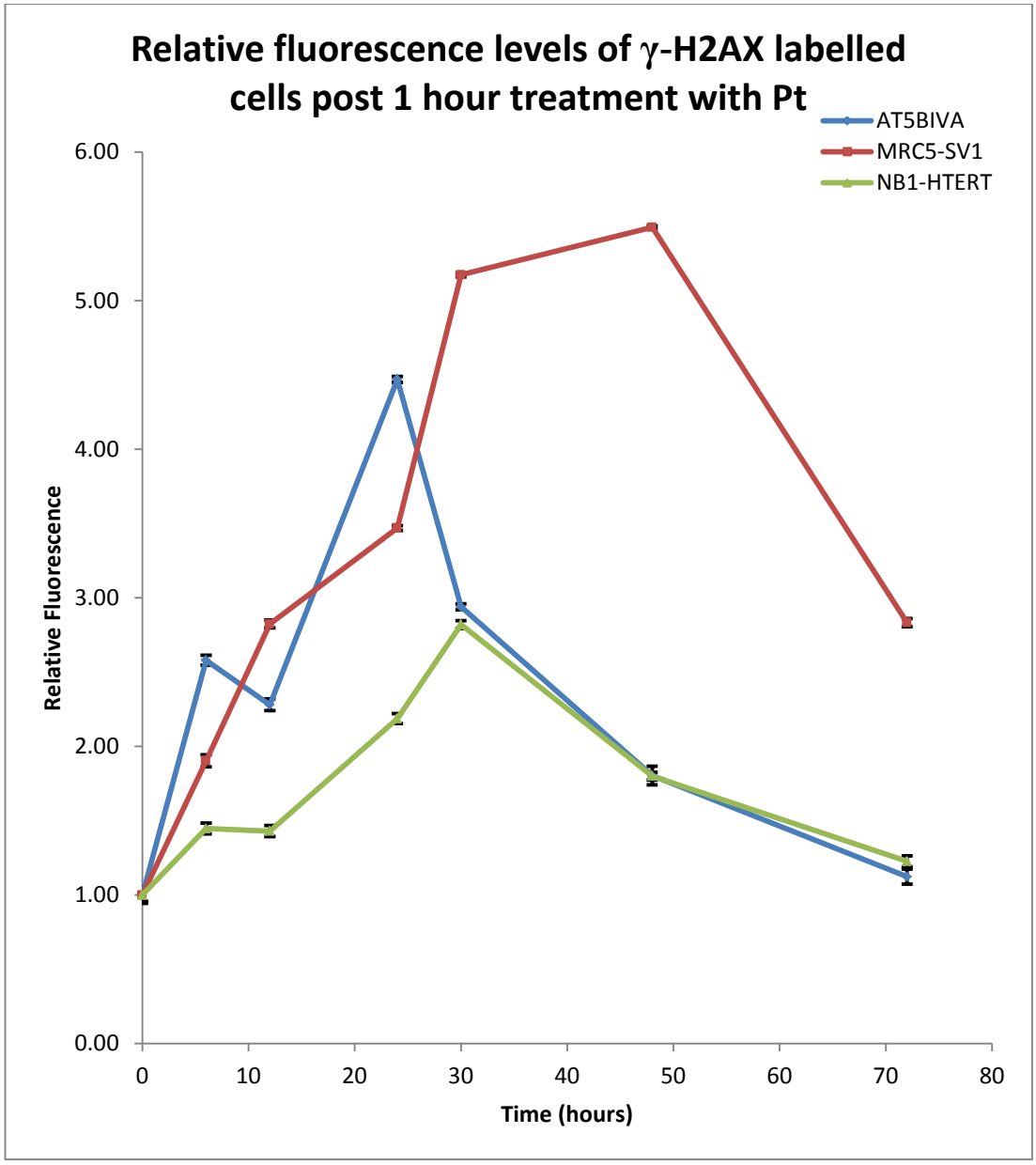

The relative levels of nuclear fluorescence exhibited in the three cell lines. Relative fluorescence was calculated by dividing actual fluorescence levels seen at each time point by the fluorescence exhibited in the control cells for each cell line. The NB1-HTERT cell line shows a peak of fluorescence at 24 hrs while the AT5BIVA cell line peaks at 30 hrs. The MRC5-SV1 samples show a peak of fluorescence being achieved at 48 hrs. At 48 hrs post treatment, the NB1-HTERT cells and AT5BIVA cells show a drop in fluorescence and at 72 hrs, levels of fluorescence have returned to similar levels exhibited by the control samples while the MRC5-SV1 cell line still showed fluorescence levels at over 2.5 fold of the control sample. Error bars represent the standard error of the mean where approximately 10000 cells were collected from three independent experiments. Standard error was calculated by dividing the standard deviation by the square root of the number of cells counted for each sample

Figure 5.7: Relative fold changes of γ-H2AX foci in cell lines post treatment with Pt

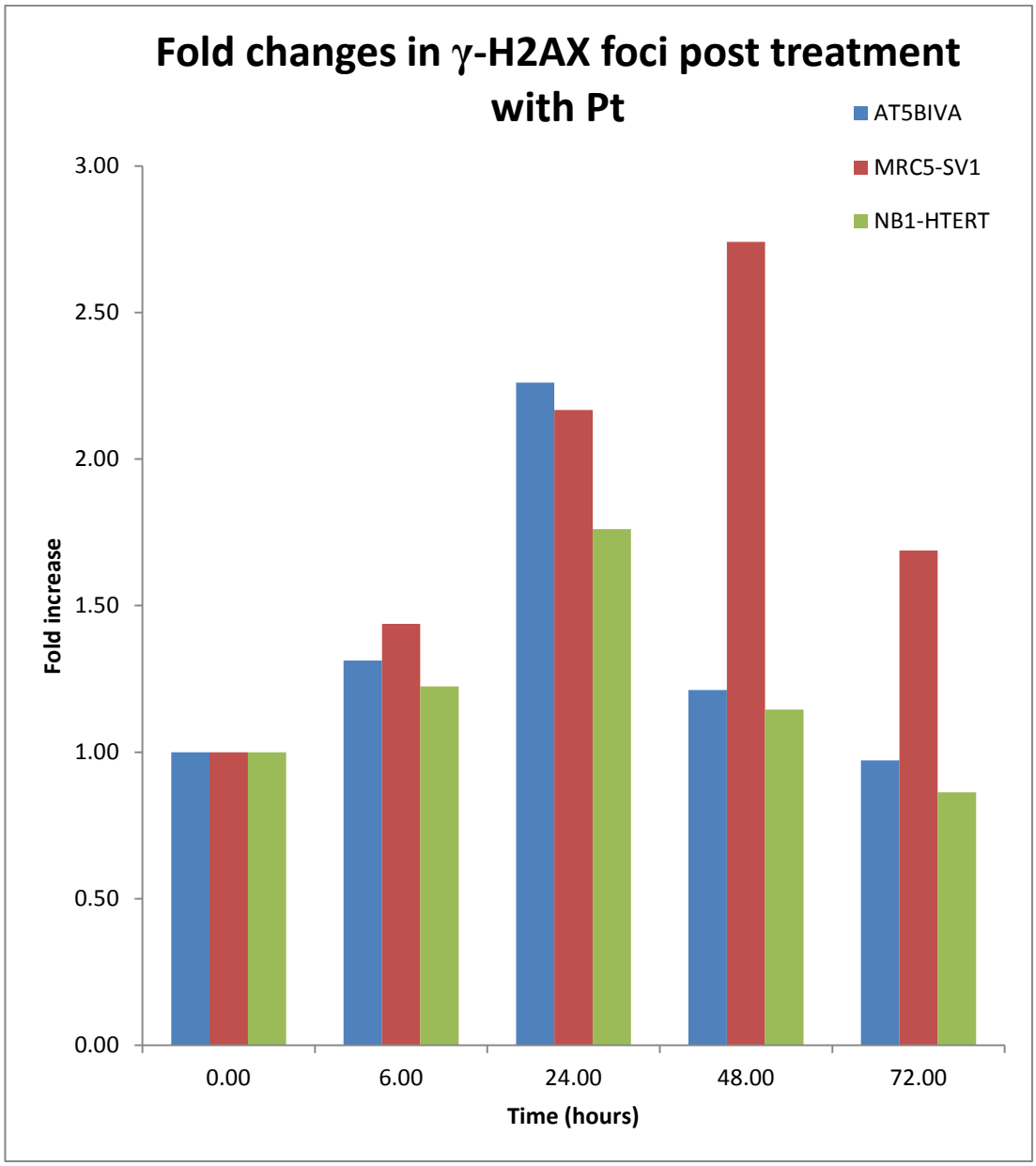

The fold increase in foci numbers were calculated for each of the cell lines by dividing the foci counts seen at 6, 24, 48 and 72 hrs by the foci counts derived for each of the control samples. The foci counts of the untreated controls were normalised to 1. At 6 hrs and 24 hrs, the cell lines all showed a similar pattern of an increase in foci induction although actual fold increases in foci differed between the three cell lines. However it can be seen that at 48 hrs, the AT5BIVA and NB1-HTERT both started to show a reduction in foci numbers while the MRC5-SV1 cell line foci induction increased in comparison to the 24 hour time point. By 72 hrs, AT5BIVA and NB1-HTERT indicate that foci counts had dropped below levels observed in their untreated controls. The MRC5-SV1 cell line also showed a decrease in foci induction at this time point although it was still at a 1.6 fold increase in comparison to the untreated control.

5.2.4 γ-H2AX Foci quantification post treatment with Adr

The average number of foci per cell in each of the three cell lines post 1 hr treatment with Adr was analysed and quantified using the Imagestream^X as depicted in Figure 5.8. γ-H2AX foci were enumerated by the masking strategy described in Section 2.4.7.

In response to treatment with Adr, all cell lines exhibited peaks of γ-H2AX foci at 24 hrs. In the NB1-HTERT and MRC5-SV1 cell line, levels of γ-H2AX foci then proceeded to decline at the subsequent times points examined after 24 hrs. However the AT5BIVA cell line which averaged 9.42 foci at 24 hrs showed a decreased foci count at 30 hrs but showed an increased foci count of 9.09 at 48 hrs. Nevertheless, all cell lines had decreased to levels similar or below their untreated controls at 72 hrs. Relative nuclear fluorescence was also calculated for these cell lines (Refer to Figure 5.9) and appeared to correlate with the pattern of foci induction seen in the AT5BIVA cell line. However with respect to the NB1-HTERT cell line, the peak of fluorescence was seen at 12 hrs post treatment with 1.6 fold increase. At 24 hrs, the fluorescence levels have decreased to a 1.38 fold increase in comparison to the untreated control. Similarly the MRC5-SV1 cell line exhibited a peak of foci induction at 24 hrs but the peak of relative fluorescence was observed at 30 hrs.

Increases in foci induction were also calculated as fold changes at the following time points; 6 hr, 24 hr, 48 hr and 72 hr and expressed in relation to the individual control samples for each cell line (Refer to Figure 5.10). The AT5BIVA cell appeared to show the highest induction of γ-H2AX foci with a 1.7 fold increase seen at the 24 hr time point. At 24 hrs, the MRC5-SV1 cell line showed a 1.3 fold increase

in γ-H2AX foci induction and by 48 hrs, results indicated DNA repair is already complete with foci induction below the level seen in the untreated control. This was further correlated by the relative nuclear fluorescence data which showed a steep drop from the 30 hr time point to the 48 hour time point. The NB1-HTERT cell also showed a 1.3 fold increase in γ-H2AX foci at 24 hrs and at 72 hrs, foci induction has dropped below the level observed in the untreated control. Application of the ANOVA statistics revealed significant differences in foci distribution between each of the cell lines ($p = <0.001$).

Table 5.3 ANOVA Statistical Analysis of foci distribution in cell lines treated with Adr

Cell line	F	P-value
AT5BIVA v NB1-HTERT	439.49	<0.001
AT5BIVA v MRC5-SV1	361.87	<0.001
NB1-HTERT v MRC5-SV1	320.63	<0.001

Figure 5.8: Average foci numbers over a 72 hour period post treatment with Adr

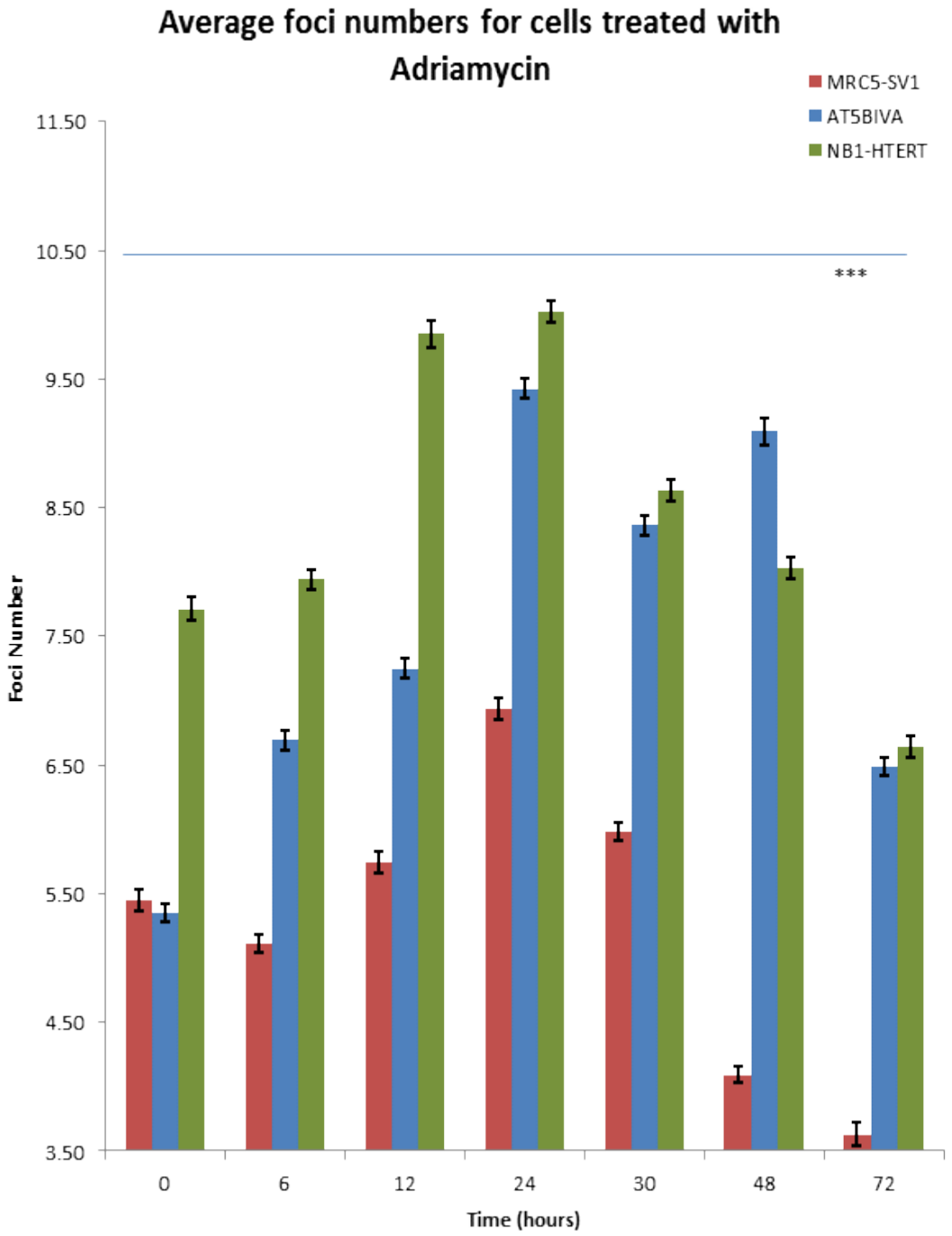

The average foci numbers seen in the three cell lines over a 72 hour period post 1 hour treatment with Adr. All three cell lines show the peak of foci induction at 24 hrs post treatment, NB1-HTERT being treated with 93 ng/mL Adr, AT5BIVA with 84 ng/mL Adr and MRC5-SV1 with 56 ng/mL. By 48 hrs, the MRC5-SV1 cell line has dropped to levels below that of its untreated control and the NB1-HTERT exhibits a similar characteristic at 72 hrs. The AT5BIVA cell line shows some foci retention at 72 hrs with a 1.2 fold increase seen in comparison to its control sample. Error bars represent the standard error of the mean where approximately 10000 cells were collected from three independent experiments. Standard error was calculated by dividing the standard deviation by the square root of the number of cells counted for each sample. * ANOVA analysis showed significant differences between each of the three cell line (p value = <0.001)**

Figure 5.9: Relative fluorescence levels of cells post 1 hour treatment with Adr

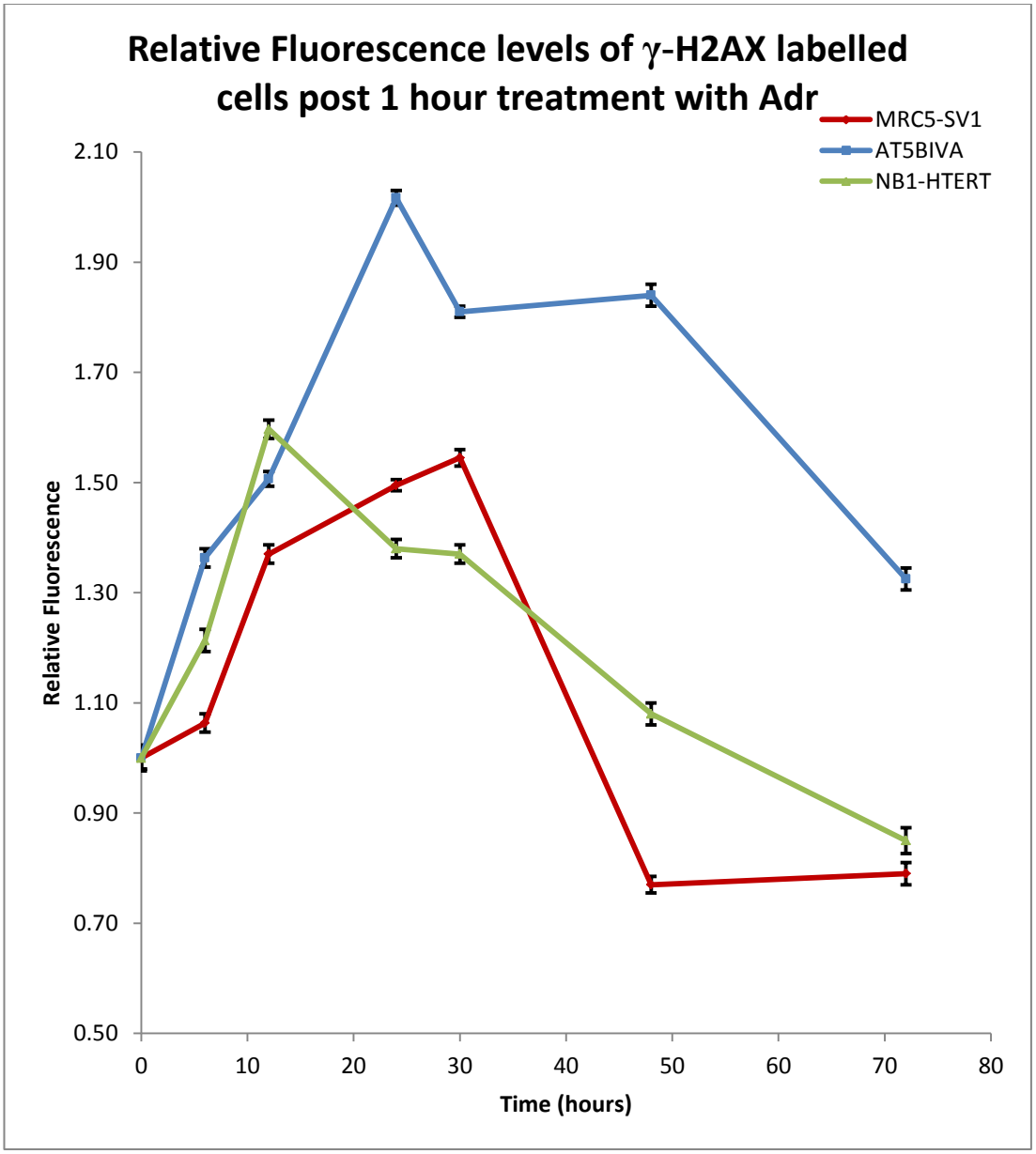

The above shows relative fluorescence levels of cell lines post 1 hour treatment with their relative IC_{50} doses (93ng/mL NB1-HTERT, 84ng/mL AT5BIVA, 56 ng/mL MRC5-SV1). It was seen that the AT5BIVA cell line showed the highest induction of fluorescence with a 2 fold increase seen at the peak of foci formation at 24 hrs. In the MRC5-SV1 cell line, it can be seen that the peak of fluorescence is seen at 30 hrs and there is a steep decline in fluorescence in the next sample collected at 48 hrs. Standard error was calculated by dividing the standard deviation by the square root of the number of cells counted for each sample

Figure 5.10: Relative fold changes of γ-H2AX foci in cell lines post treatment with Adr

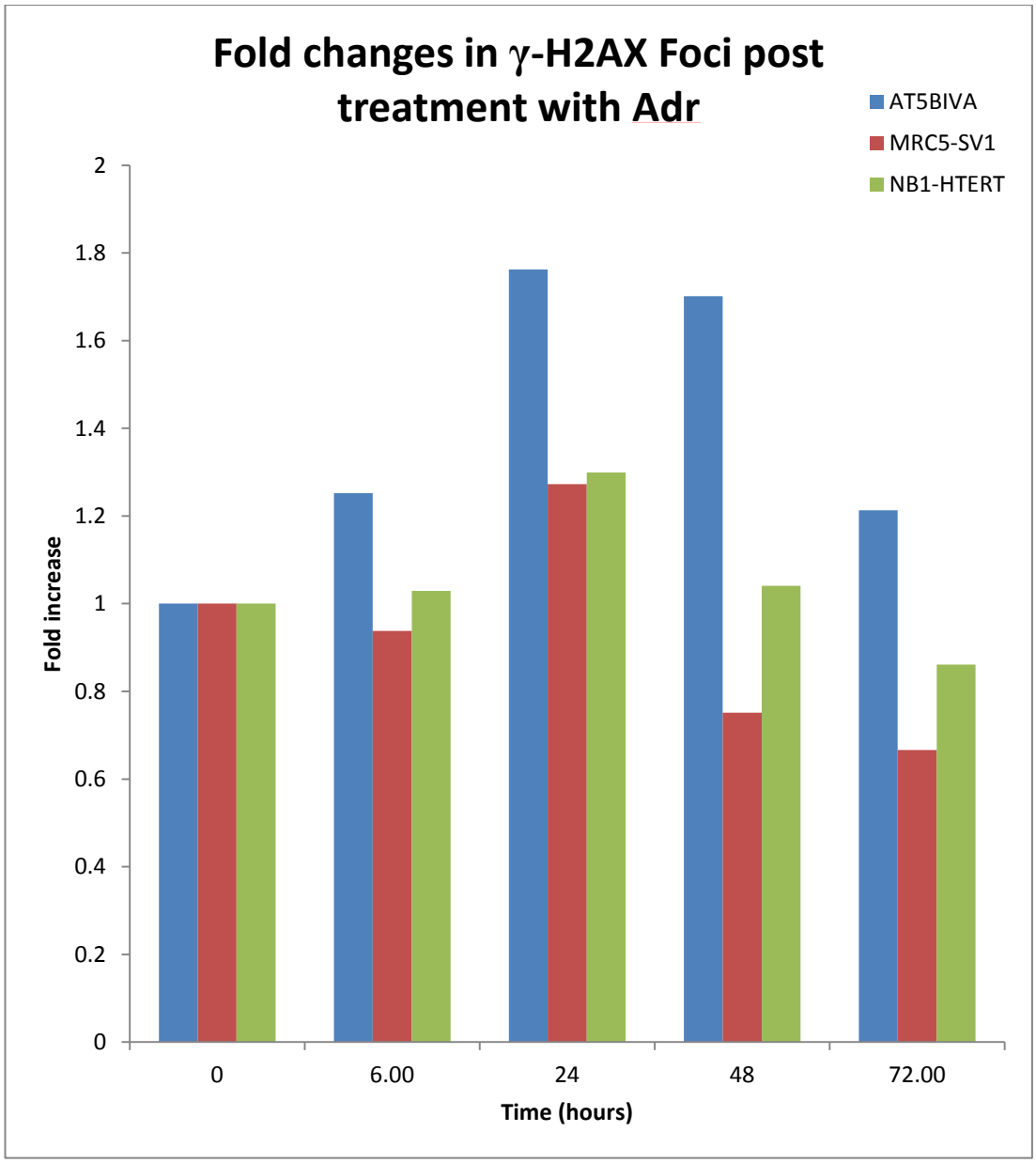

The fold increase in foci numbers were calculated for each of the cell lines by dividing the foci counts seen at 24 hrs and 48 hrs by the foci counts calculated for each of the control samples. The foci counts of the control samples were normalised to 1. The AT5BIVA cell line shows approximately 1.8 fold increase at 24 hrs while the MRC5-SV1 and NB1-HTERT cell lines show a 1.3 fold increase at the same time point. At 48 hrs, the AT5BIVA cell line still shows a similar increase while the NB1-HTERT cell shows a 1.2 fold increase. The MRC5-SV1 cell line has decreased to levels below that observed in its untreated control. At 72 hrs, the AT5BIVA cell line still indicates some foci retention with a fold increase of approximately 1.2 in comparison to its untreated control while the other two cell lines exhibit foci levels below their untreated controls.

Figure 5.11: Typical distributions of γ-H2AX foci in cell nuclei post 1 hour treatment with HN2

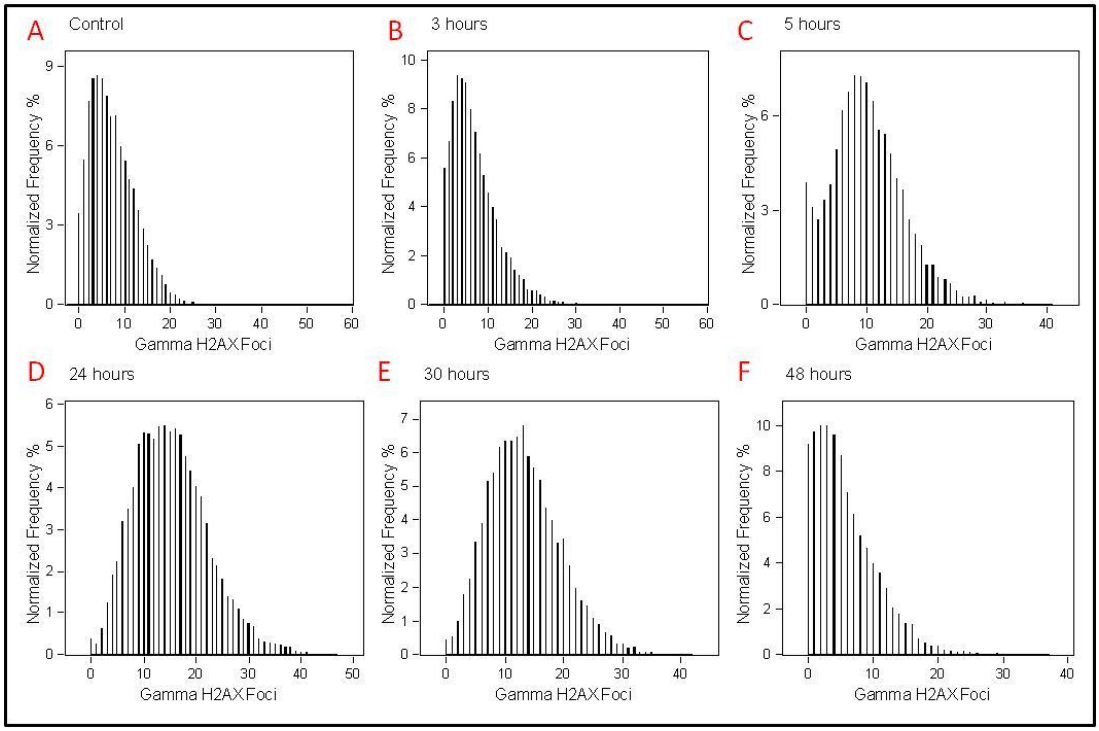

The above shows typical distributions of γ-H2AX foci in MRC5-SV1 cells post 1 hour treatment with HN2. Figure 5.11A depicts the distribution seen in the control cells and as expected, the peak of the histogram is seen closer to the left of the graph, representing that a higher proportion of the cells had 0 -10 foci and no cells had more than 25 foci. The peak gradually shifts over the next 24 hrs, (5.11B and 5.11C) and at 24 hrs represented in 5.11D, the peak of the histogram is seen to have shifted towards the centre of the graph, an indication that a higher proportion of the cells now had between 10 and 25 foci and the maximum number of foci had increased to 40 foci. By 48 hrs (5.11F), the distribution of γ-H2AX foci had returned to similar levels seen in the control sample; thereby indicating that damage induced by the HN2 treatment had now been repaired.

Figure 5.11 above depicts an example of the histograms that were generated with the IDEAS^{TM} software when the Spot Mask (described in Section 5.26) was applied to the images collected by the Inspire software. These histograms depict the distribution of γ-H2AX foci for the samples collected at different time points. It was noted that the distribution gradually started shifting to the right in the samples collected at 3 and 5 hrs with a more symmetrical appearance seen at 24 and 30 hrs. At 48 hrs, the distribution of foci looks similar to the untreated control.

Figure 5.12: Comparison of foci numbers seen in the MRC5-SV1 cell line post treatment with chemotherapeutic drugs

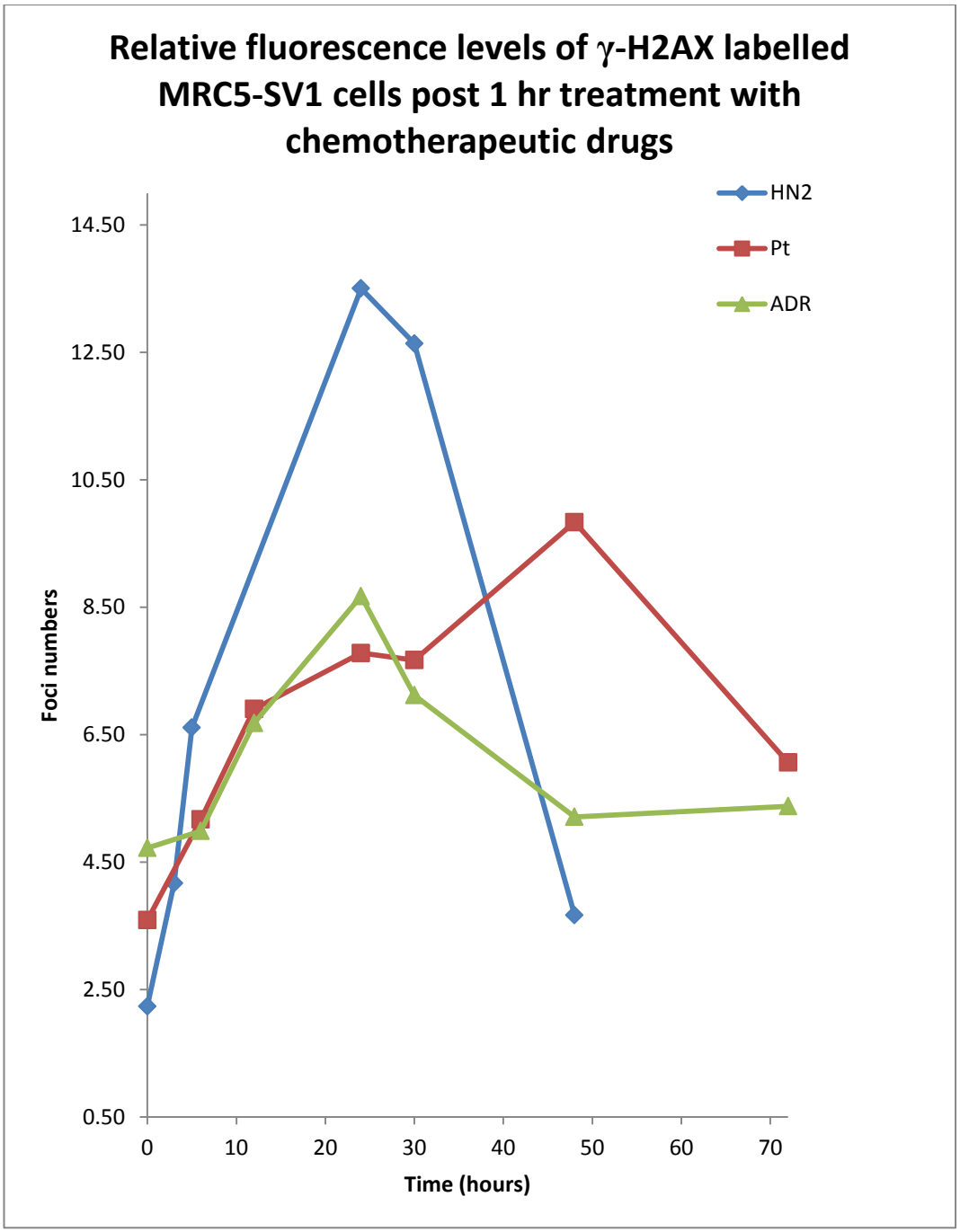

The average foci numbers seen in the MRC5-SV1 cell lines over a 72hr period post 1 hour treatment with different chemotherapeutic drugs. It was seen that the highest induction of foci was seen post treatment with 0.5 µg/mL HN2 at 24 hrs. By 48hrs, γ-H2AX foci levels had returned to similar levels to the untreated control. Interestingly, treatment with 12 µg/mL Pt led to the peak of γ-H2AX foci formation at 48hrs. However by 72 hrs, it can be seen that γ-H2AX foci levels have returned to similar levels as the untreated control. Post treatment with 56 ng/mL ADR, the peak of γ-H2AX foci formation was seen at 24 hours but foci induction was not as high as seen post treatment with HN2.

Figure 5.13: Comparison of foci numbers seen in the NB1-HTERT cell line post treatment with chemotherapeutic drugs

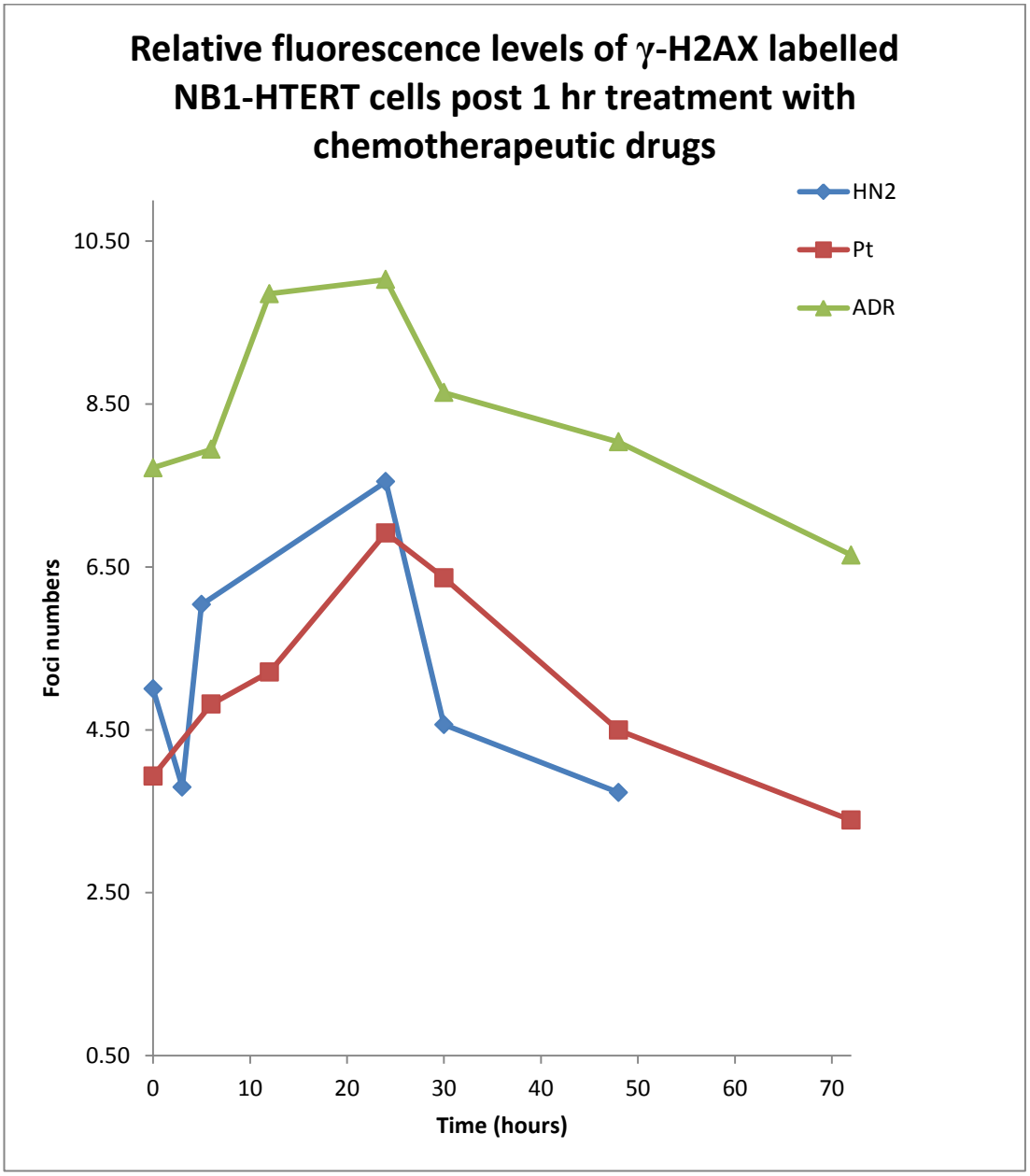

The average foci numbers seen in the NB1-HTERT cell lines over a 72hr period post 1 hr treatment with different chemotherapeutic drugs. It was seen that the highest induction of foci was seen post treatment with 93 ng/mL ADR at 24 hrs. A similar level of induction of γ-H2AX foci was seen in response to treatment with both cross-linking agents, HN2 (treated with 0.3 µg/mL) and Pt (treated with 6 µg/mL).

Figure 5.14: Comparison of foci numbers seen in the AT5BIVA cell line post treatment with chemotherapeutic drugs

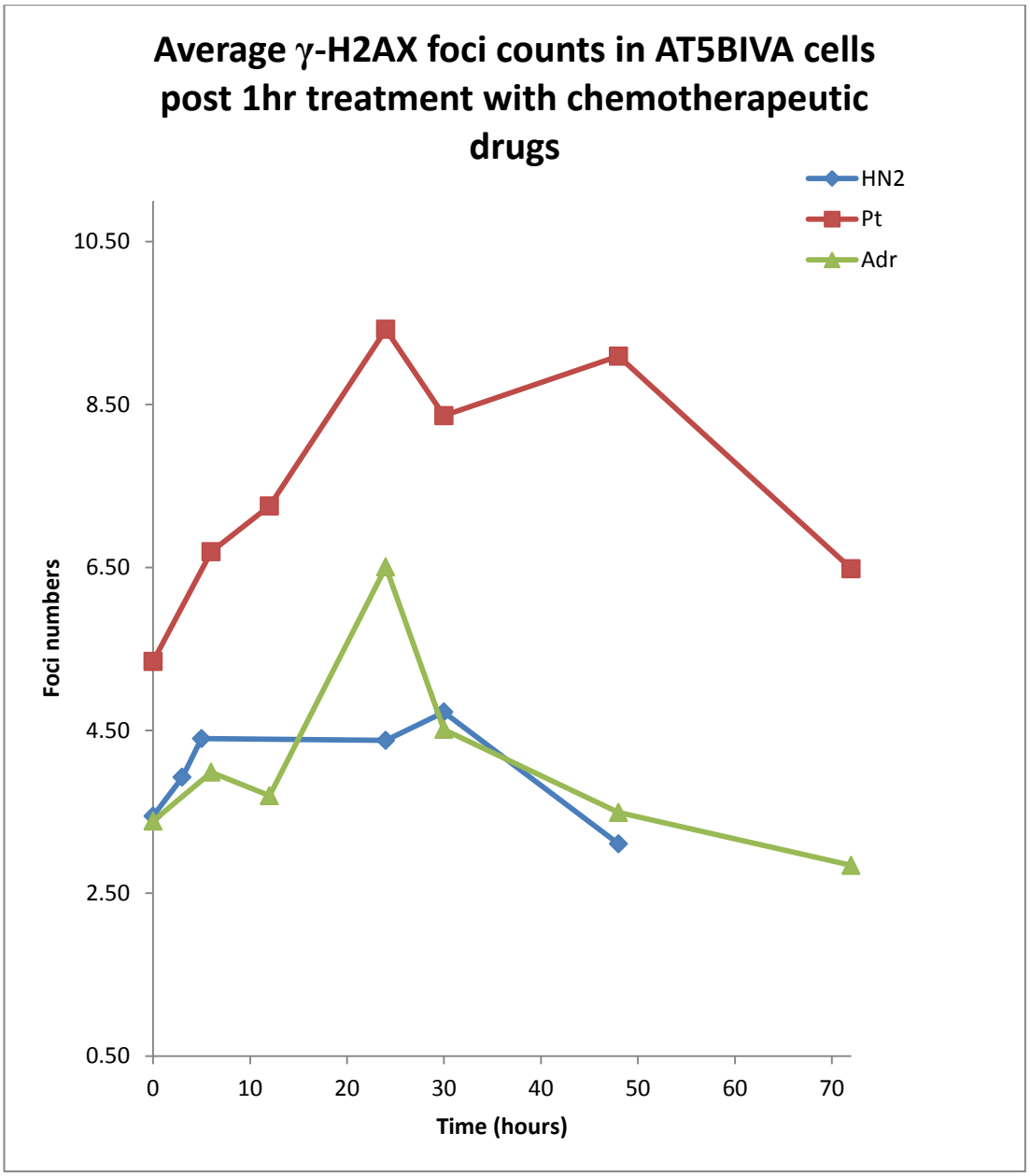

The average foci numbers seen in the AT5BIVA cell lines over a 72hr period post 1 hr treatment with different chemotherapeutic drugs. Little change was seen across the 48 hr period post treatment with HN2. Post treatment with 7 µg/mL Pt and 84 ng/mL Adr, there was a clear peak of γ-H2AX foci formation seen at 24 hrs. With all drugs, γ-H2AX levels returned to similar levels to the untreated control by the end of the 2 or 3 day period.

5.3 Discussion

This study looked at the response of three cell lines to three different chemotherapeutic agents; Pt, HN2 and Adr by analysing γ-H2AX foci induction. Two of the cell lines, MRC5-SV1 and NB1-HTERT are repair normal cell lines with no known DNA repair defects. The AT5BIVA cell line which was derived from an Ataxia Telangiectasia patient is known to have a defect in the ATM gene which is involved in the initial stages of repairing DSBs (Friesner *et al.* 2005) and exhibits sensitivity to IR (Bourton *et al.* 2012). However the results obtained for this cell line did not seem to exhibit an increased sensitivity to the chemotherapeutic agents used. ATM is known to be involved in the signalling cascade for DSBs but it is known that ATR rather than ATM becomes phosphorylated in response to other types of DNA damage such as the formation of cross-links to initiate repair (Harper and Elledge 2007). Furthermore it has been shown that inhibition of ATR in a human cancer cell line, DLD-ATR-Seckel was seen to enhance the effects of a range of anti-cancer agents such as 5-FU, Pt and Adriamycin (Wilsker and Bunz 2007). Therefore it may be likely that that the DNA repair mechanisms and responses of ATM-deficient cells such as the AT5BIVA cell line may not be sensitive to agents that do not form double strand breaks as their primary mechanism of exerting cytotoxicity. There is limited literature regarding chemosensitivity in A-T patients but a case study carried out by Tamminga *et al* (2002) on a 14 year old A-T patient revealed limited sensitivity to the anticancer agents, Vincristine, Predisnone and Adriamycin. However this was only seen after doses was adjusted to a third of normal dosage levels found. This again emphasises the need for a bigger cohort of cell lines in

order to fully understand the DNA repair mechanisms involved in the repair of chemotherapy-induced damage.

With all drugs, the peak of γ-H2AX foci induction was seen 24 to 48 hrs after the 1 hr treatment in both the MRC5-SV1 and NB1-HTERT cell line. This was also seen in the AT5BIVA cell line post treatment with Pt and Adr. However post treatment with HN2 in the AT5BIVA cell line, the peak of H2AX foci formation was seen at 5 hrs with modest changes seen in the ensuing period. These findings are in line with other studies which suggest γ-H2AX foci induction in response to chemotherapeutic agents which do not form direct DSBS; primarily cross-linking agents such as Pt, is indicative of DSBs being formed during the course of DNA repair (Clingen *et al.* 2008),(Olive and Banath 2009). Based on this assumption, it was observed that 48 hrs after treatment with HN2, complete DNA repair was observed in the AT5BIVA and NB1-HTERT cell line due to the disappearance of the majority of the γ-H2AX foci. The MRC5-SV1 cell line still indicated foci retention but as the induction of H2AX foci at 24 hrs was so dramatic, it was assumed that DNA repair was nearing completion at 48 hrs as there was an approximately 70% decrease in foci in comparison to the foci count observed at 24 hrs. HR is required for the repair of the lesions formed and this repair pathway functions during the S/G2 phase of the cell cycle. This may provide an explanation for the peak of γ-H2AX foci being seen at either 24 or 48 hrs after treatment and further supports the theory that γ-H2AX foci is indicative of DNA repair taking place.

When treated with Pt, it was observed that the repair process took 72 hrs to complete in the MRC5-SV1 cell line but only 48 hrs in the other two cell lines. As the other two cell lines exhibited increased sensitivity to Pt as seen from the results of

the clonogenic assays; these results may be indicative that the Pt administered during treatment was becoming inactivated through cellular defence mechanisms (Godwin *et al.* 1992). Pt is a highly reactive compound once it undergoes hydrolysis (Siddik 2003) but this also makes it vulnerable to endogenous nucleophiles such as glutathione and metallathionein. Cellular levels of glutathione have been shown to be increased in the presence of DNA damaging agents and attempts to protect the DNA are made by binding to the drug and thereby reducing its rate of reaction (Godwin *et al.* 1992). In response to Adr, peak formation of γ-H2AX foci was also seen at 24 hrs in all cell lines post 1 hour treatments with their relevant IC_{50} doses and repair was completed by the end of the 72 hour time period in the NB1-HTERT and AT5BIVA cell lines. However in the MRC5-SV1 cell line, repair had completed by the end of the 48 hour time period.

Each of these cell lines were treated with the individual IC_{50} doses derived from the clonogenic assays. This allowed for a comparable assay where each drug exerted the same level of cytotoxicity on all the cell lines. Significantly different DNA repair profiles were identified for each of the cell lines examined. There is a trend that has emerged from this data in that the cell line exhibiting the highest level of resistance to each individual drug was also seen to exhibit the highest number of foci at each time point sampled. The MRC5-SV1 cell line exhibited the highest level of resistance to Pt and HN2 as determined by the clonogenic assays (detailed in Chapter 4) and it also showed the highest induction of γ-H2AX foci in response to treatment with both of these cross-linking agents. The NB1-HTERT cell line exhibited the highest resistance to Adr and this also showed the highest induction of γ-H2AX foci in response to treatment with this drug. There are a

number of reasons that this could be occurring; however it is most likely to be indicative of increased rate of DNA repair in these cell lines. Studies such as Clingen et al, (2007) and Niedernhofer et al, (2004) have shown the accumulation of γ-H2AX foci in response to treatment with chemotherapeutic agents such as Pt and Mitomycin C and furthermore Clingen et al, (2008) revealed a persistence of γ-H2AX foci in chemo-sensitive cell lines. It has been established that γ-H2AX foci forms in a 1:1 ratio with DSBs (Sedelnikova *et al.* 2002) and H2AX phosphorylation in response to treatment with agents such as Pt is indicative of strand breaks being formed during the repair process (Dickey *et al.* 2009) . Therefore it could be theorised that a higher number of γ-H2AX foci being seen in response to treatment with chemotherapeutic agents could represent an increased rate of DNA repair.

A smaller cohort of cell lines was initially selected in order to develop this assay in a manageable way and it has revealed some interesting data. However there is a clear need to increase the cohort size in order to elucidate firm trends in γ-H2AX foci expression levels in response to treatment with chemotherapeutic drugs.

To gain further understanding into the induction of γ-H2AX foci in response to anti-cancer agents, resistant cell lines will be developed using two of the parental cell line employed in this chapter; MRC5-SV1 and NB1-HTERT. This is detailed and discussed further in the following chapters.

Chapter 6

Analysis of DNA repair in human cell lines made resistant to the ICL agent HN2

6.1 Introduction

Development of resistance to chemotherapeutic drugs poses a serious limitation to the effectiveness of this form of treatment (Boehm *et al.* 1997; Carvalho *et al.* 2010) This was highlighted by Agarwal and Kaye 2003 (Agarwal and Kaye 2003) who noted that that acquiring resistance to Pt accounted for treatment failure and deaths in up to 90% of patients with ovarian cancer. They found that 70% of patients responded well to initial Pt-based therapies but this figure declined to only 15- 20% survival rates at the end of a 5 year period. Similar statistics were established by Coley, (2008) who reviewed the prognosis of patients with metastatic breast cancer. Initial response rates to chemotherapy were seen in 30 - 70 % of patients but this declined to 20 - 30% of patients with disease progression who entered into a second round of chemotherapy. Ultimately 90% of deaths were accountable to the development of resistance to chemotherapy in metastatic breast cancer patients.

Resistance can develop in many ways. To some extent, genetic instability and increased mutational rates of tumour cells attributes to this (Boehm *et al.* 1997). However there are numerous other mechanisms that have been proposed that lead to the development of drug resistance. Repeated exposures to a single neoplastic agent often can lead to the development of cross-resistance to drugs which have similar mechanisms of action; i.e. it has been seen that patients that acquire resistance to Pt often develop cross-resistance to other cross-linking agents (Siddik 2003). Tumours which exhibit this are known as having a multi-drug resistant phenotype. The development of cross-resistance indicates that similar

pathways may be activated in response to these drugs to protect the cellular DNA from damage and undergoing apoptosis.

Increased drug efflux may serve as another mechanism of drug resistance as this prevents the cell from intracellular accumulation of anticancer agents. P-glycoprotein (P-gp), a membrane transporter protein encoded by the MDR1 gene, normally functions as a barrier to the uptake of xenobiotics but has the capacity to export anticancer agents from cells (Fojo and Coley 2007). The majority of chemotherapeutic agents widely used have compounds which serve as a substrate for P-gp and the overexpression of the MDR1 gene has been found to lead to P-gp preventing the intracellular accumulation of the drug (Lorico *et al.* 1996).

The multi-drug resistant protein 1 (MRP1) belongs to a family of 11 membrane transporters and there is increasing evidence that these transporters can also contribute to the development of drug resistance (Fojo and Coley 2007). Lorico *et al*, (1996) demonstrated that a double knockout of the MRP gene lead to an increased sensitivity to chemotherapeutic agents whilst Rudas *et al*, (2003) established an increase in the level of MRP1 after the administration of chemotherapy. Taken together, these findings very likely mean that over-expression of the MRP gene could lead to the development of drug resistance. This was established by Cui *et al*, (1999) who demonstrated that over-expression of MRP2 lead to the development of resistance towards Pt and Adr amongst other drugs

Cellular mechanisms such as increased drug inactivation by cellular metabolites such as Glutathione, increased levels of DNA repair or evasion of apoptosis may also lead to the development of acquired resistance (Banath and

Olive 2003; Siddik 2003). This inherent resistance can then be transferred to daughter cells during mitosis (Goldie and Coldman 1983).

This study will be focussing on the repair kinetics of resistant, sensitive and normal cell lines in response to treatment with ICL-inducing agents. Table 6.1 below shows different types of ICL inducing agents. ICL formation only accounts for a small proportion of the total number of DNA adducts with intrastrand cross-link formation being the primary form of DNA adduct formed; in the case of Pt, this accounts for approximately 90% of adduct formation (Crul *et al.* 2003). Nevertheless, the formation of ICLs is the main mechanism of cytotoxicity in these drugs due to the impairment of strand separation which in turn inhibits key cellular processes such as transcription and replication (Deans and West 2011).

Table 6.1: Different classes of ICL-inducing agents (adapted from (de Jager *et al.* 2001))

ICL Agent	Primary Target	% of DNA adducts in cell	Distortion of DNA helix
Cisplatin	G - G	5 – 8	Major
Nitrogen Mustard	G - G	1 – 5	Major
Psolaren	T - T	30 - 40	Minor
Mitomycin C	G-G	5 – 13	Minor
Carmustin	G-C	<8	Unknown

The main mode of repair for ICLs is mediated through the association of two different DNA repair pathways, NER and HR. ERCC1-XPF is a structure specific endonuclease involved in the excision process in NER and has been shown to be the

only two NER proteins to have key roles in the repair of ICLs. This has been determined by numerous studies such as De Silva *et al*, (2002) and Clingen *et al,* (2008). ERCC1-XPF plays a role in the repair of ICLs via the HR pathway. It is thought that the ERCC1-XPF complex is recruited to the site of damage by XPA (Al-Minawi *et al.* 2009). It incises one side 5' of the DNA lesion and the other side is incised by XPG, thereby creating a DSB (Al-Minawi *et al.* 2009). This is supported by findings by Niedernhofer *et al*, (2004) who demonstrated that in mouse embryonic fibroblasts, ERCC1-XPF is not required to form DSBs after ICL damage but are crucial in resolving this damage.

A study by Clingen *et al*, (2008) examined the mechanisms of action involved in γ-H2AX expression after exposure to ICL agents. They found γ-H2AX foci were retained in DNA repair defective Chinese hamster cells in comparison to wild type. Furthermore they also showed a persistence of foci in chemo-sensitive human ovarian cancer cells in comparison to chemo-resistant cells. Therefore it highlighted the potential use of γ-H2AX as a marker of DNA damage induced by chemotherapeutic agents and concluded that the ability of cells to repair DNA ICLS could determine the level of sensitivity to anti-cancer agents such as Pt. The formation of DSBs can be detected by quantifying nuclear γ-H2AX foci and has been demonstrated to identify radiosensitivity in individuals (Bourton *et al.* 2011).

Understanding the mechanisms of actions that lead to resistance may provide useful knowledge in the development of new therapies with alternate mechanisms of action. As indicated above, there are diverse factors that could attribute towards the development of resistance. Furthermore the development of drug resistance accounts for a vast proportion of treatment failure and it can lead

to patients experiencing all the deleterious side effects of chemotherapy with no improvement in prognosis of the disease. This study focused on the use of multi-spectral imaging flow cytometry to identify the expression of γ-H2AX in response to cross-linking agents such as HN2 and how this may differ between normal, resistant and sensitive patients. The development of biomarkers to monitor patient response to chemotherapy could lead to marked improvements in overall survival rates and help to isolate mechanisms of resistance in individual patients.

6.2 Results

6.2.1 Clonogenic Assays

Colony counting and calculation of survival rates was carried out as detailed in Chapter 4 (refer to section 4.2.1 and 4.2.2).

6.2.1.1 Determining IC_{50} values of HN2

The parental and resistant cell lines were exposed to a range of concentrations of HN2 from 0.5 μg/mL to 2.5 μg/mL. The GM08437B cell line (deficient in XPF) was exposed to a range of concentrations of HN2 from 0.1 μg/mL to 0.5 μg/mL. Figure 6.1 depicts the survival rates of all cell lines at their respective concentration ranges.

It was observed that the MRC5-SV1^{R} cell line showed a 3 fold increase in resistance to HN2 in comparison to the parental cell line. Similarly the NB1-HTERT^{R} cell line showed a 2.7 fold increase in resistance to HN2 in comparison to the parental cell line. As expected, the GM08437B cell line showed an increased sensitivity to the drug in comparison to all other cell lines observed with survival levels dropping below 5% at 0.5 μg/mL. The IC_{50} was graphically determined for each of the cell lines and shown below in Table 6.2. The fold increase in resistance is shown in Table 6.3.

Table 6.2: IC_{50} values for all cell lines post treatment with HN2

Cell Line	IC_{50} Value
MRC5-SV1 Parental	0.5 μg/mL
MRC5-SV1^{R}	1.4 μg/mL
NB1-HTERT Parental	0.3 μg/mL
NB1-HTERT^{R}	0.82 μg/mL
GM08437B	0.2 μg/mL

Figure 6.1: Comparing resistance of cell lines post 1 hour treatment with HN2

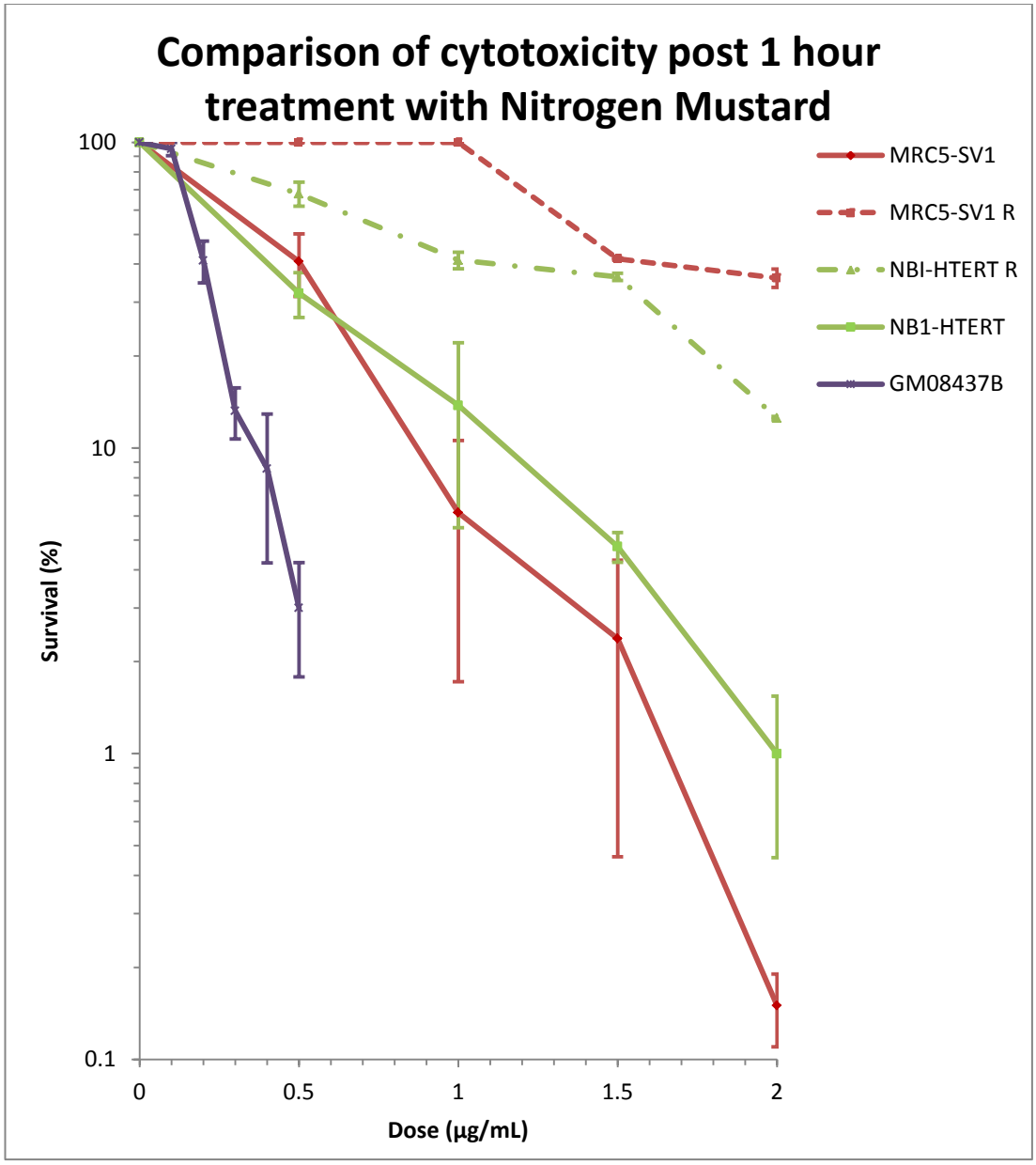

The above shows the survival rates of all cell lines post treatment with HN2. It can be seen that the two resistant cell lines (indicated by the dotted lines) have an increased level of resistance to HN2 at all doses of the drug. The XPF deficient cell line (shown in purple) shows an increased sensitivity to the drug with a steep decline in survival seen as the dose of HN2 is increased. Standard error was calculated by dividing the standard deviation of the mean by the square root of the number of repeats.

Table 6.3: Fold increase in resistance in resistant cell lines to HN2 in comparison to parental cell lines

Cell line	Fold increase in resistance
MRC5-SV1^{R}	2.8
NB1-HTERT^{R}	2.7

6.3.1.1 Determining IC_{50} values of Pt

The parental and resistant cell lines were exposed to a range of concentrations of Pt from 15 μg/mL to 35 μg/mL. The GM08437B cell line (deficient in XPF) was exposed to a range of concentrations of Pt from 4 μg/mL to 20 μg/mL. Figure 6.2 depicts the survival rates of all cell lines at their respective concentration ranges.

It was observed that the MRC5-SV1^{R} cell line showed a 1.9 fold increase in resistance to HN2 in comparison to the parental cell line. The NB1-HTERT^{R} cell line showed a 3.2 fold increase in resistance to HN2 in comparison to the parental cell line. The GM08437B cell line showed an increased sensitivity to Pt in comparison to the MRC5-SV1 parental cell line but showed that its resistance was higher to Pt than the NB1-HTERT parental cell line. The IC_{50} was graphically determined for each of the cell lines and shown below in Table 6.4. The fold increase in resistance is shown in Table 6.5.

Table 6.4: IC_{50} values for all cell lines post treatment with Pt

Cell line	IC50 for Pt
MRC5-SV1 Parental	12 μg/mL
MRC5-SV1^{R}	23 μg/mL
NB1-HTERT Parental	6 μg/mL
NB1-HTERT^{R}	19 μg/mL
GM08437B	7.8 μg/mL

Figure 6.2: Comparison of resistance in cell lines post 1 hour treatment with Pt

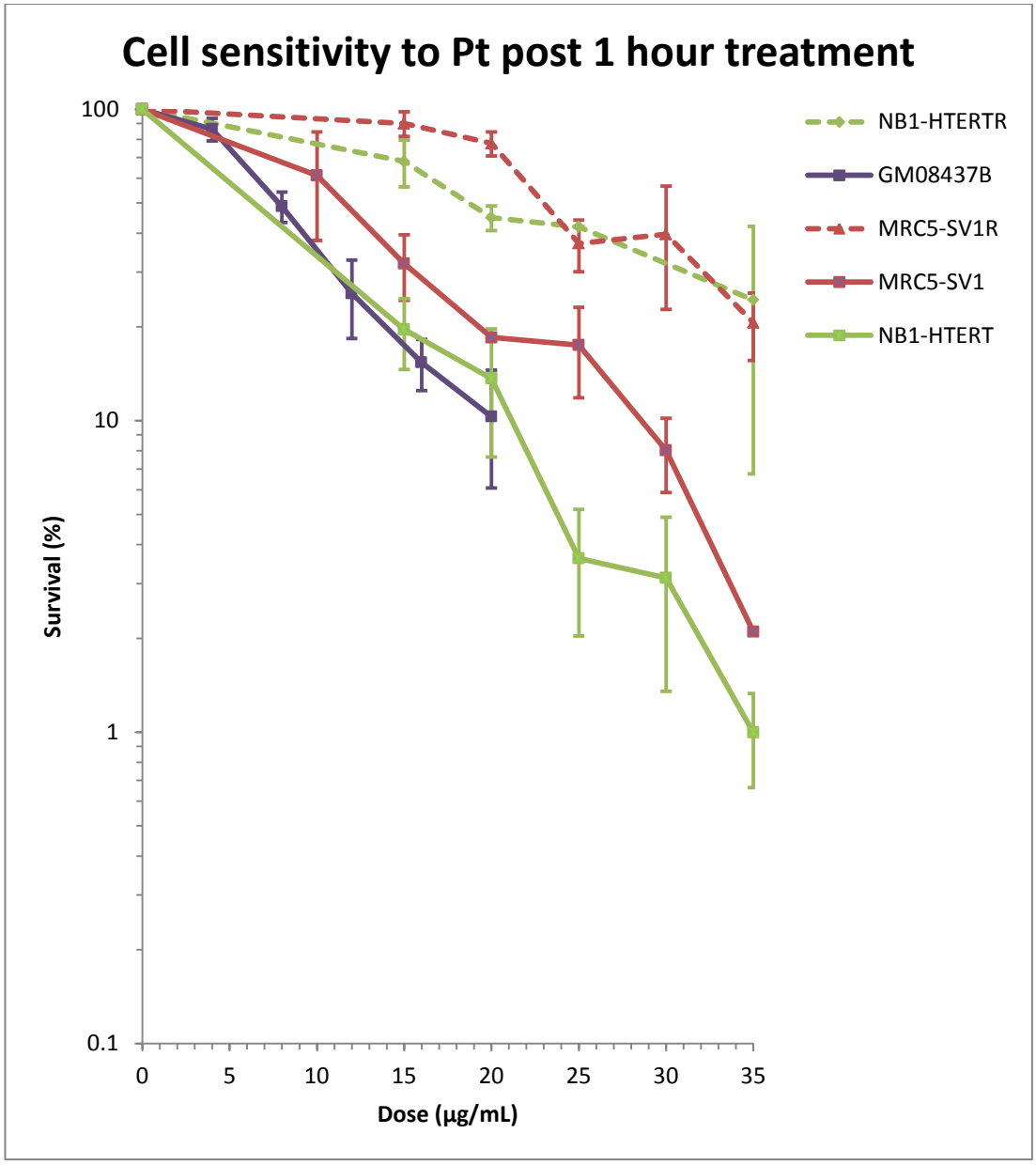

The above shows the survival rates of all cell lines post treatment with Pt. It can be seen that the two resistant cell lines (represented by the dotted lines) have an increased level of resistance to Pt at all doses of the drug. The Gm08437B cell line shows an increased sensitivity to this cell line in comparison to one of the repair normal cell line MRC5-SV1 but not the other repair normal cell line NB1-HTERT. Standard error was calculated by dividing the standard deviation of the mean by the square root of the number of repeats.

Table 6.5: Fold increase in resistance in resistant cell lines to Pt in comparison to parental cell lines

Cell line	Fold increase in resistance
MRC5-SV1^{R}	1.9
NB1-HTERT^{R}	3.2

6.3.1 γ-H2AX Foci quantification post treatment with HN2 in the NB1-HTERT, NB1-HTERT^{R} and GM08437B cell lines

The average number of foci per cell in each of the cell lines post 1 hr treatment with 0.3μg/mL HN2 was analysed and quantified using the Imagestream^{X}. γ-H2AX foci were enumerated by applying a Morphology and Peak mask as previously described. The results for the average foci numbers calculated for the NB1-HTERT, NB1-HTERT^{R} and GM08437B cell lines are shown in Figure 6.3. The total nuclear fluorescence was also determined for each of the cell lines and is shown in Figure 6.4.

The NB1-HTERT parental cell line showed a lower number of γ-H2AX foci across the whole time period that was sampled in comparison to the NB1-HTERT^{R} cell line. In the parental cell line, there is a sharp increase in foci number from 3 hrs to 5 hrs with an approximate 2 fold increase seen. In contrast, the resistant cell line shows little differences at the same time points.

In comparison to the untreated control, the NB1-HTERT parental cell line shows a 1.5 fold increase in foci induction at 24 hrs whilst the NB1-HTERT resistant cell line only shows a 1.1 fold increase in foci induction (Refer to Figure 6.5). At 48 hrs, foci numbers in the parental cell line have decreased well below levels seen in the untreated control. However in the resistant cell line, foci numbers stay at a 1.2 fold increase of the untreated control.

The GM08437B cell line exhibits the most dramatic induction of foci, showing a 2.4 fold increase in comparison to its untreated control. At 48 hrs, this is still 1.5 fold higher than the untreated control.

Analysis of the total nuclear fluorescence for these three cell lines (Refer to Figure 6.4) showed that the repair normal NB1-HTERT and repair defective GM08437B cell lines resembled similar patterns of a peak of fluorescence at 24 hrs and by 48 hrs, this was seen to be declining. However the NB1-HTERT^{R} cell line did not form any type of obvious peak when examined at the different time points and appeared to still be increasing at 48 hrs.

Analysis of variance (ANOVA) was used to determine whether there was a significant difference in the distribution of foci over the 48 hour time period. Comparison of the three cell lines showed that the distribution of γ-H2AX foci between the three cell lines were significantly different ($p<0.001$), refer to Table 6.6 below.

Table 6.6: ANOVA Statistics for foci distribution in the NB1-HTERT, NB1-HTERT^{R} and GM08437B cell lines

	F	P-value	F criteria
NB1-HTERT parental v resistant	1277.009	<0.001	2.214845
Interaction	2.442791	0.03203	2.214845
NB1-HTERT parental v GM08437B	408.4305	<0.001	2.214845
Interaction	304.5921	<0.001	2.214845
NB1-HTERT^{R} V GM08437B	214.4096	<0.001	2.214845
Interaction	93.4434	<0.001	2.214845

Figure 6.3: Average foci numbers over a 48 hour period in NB1-HTERT parental, resistant and GM0837B (XPF deficient) cell lines post treatment with HN2

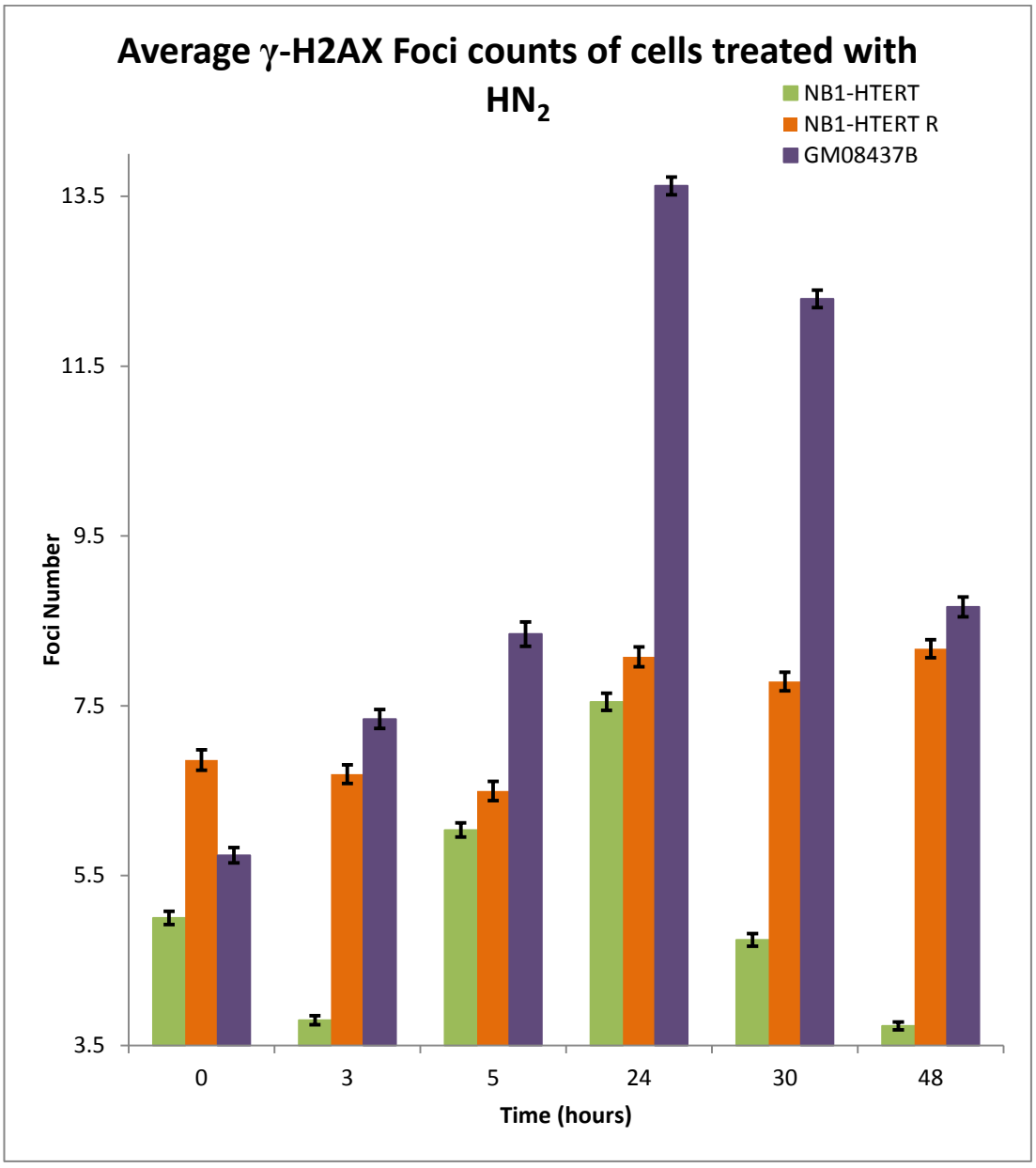

The mean number of γ-H2AX foci seen in NB1-HTERT, NB1-HTERT^{R} and GM08437B cell lines over a 48 hr period post exposure to 0.3μg/mL HN2. Error bars represent the standard error of the mean derived from three independent experiments in which approximately 10000 cells were analysed at each time point for each cell line. Standard error was calculated by dividing the standard deviation of the mean by the square root of the number of cells counted for each sample There is a vast increase in the number of γ-H2AX foci at 24 hrs seen in the GM08437B cell line. Foci numbers for the NB1-HTERTR remain relatively similar over the 48 hr period while the NB1-HTERT parental cell line shows a clear pattern of induction and disappearance of γ-H2AX foci over the same time period. At 48 hrs, there is still a clear retention of foci seen in the GM08437B cell line. Standard error was calculated by dividing the standard deviation by the square root of the number of cells counted for each sample

Figure 6.4: Relative fluorescence levels of NB1-HTERT parental, resistant and GM0837B (XPF deficient) cell lines post 1 hour treatment with HN2

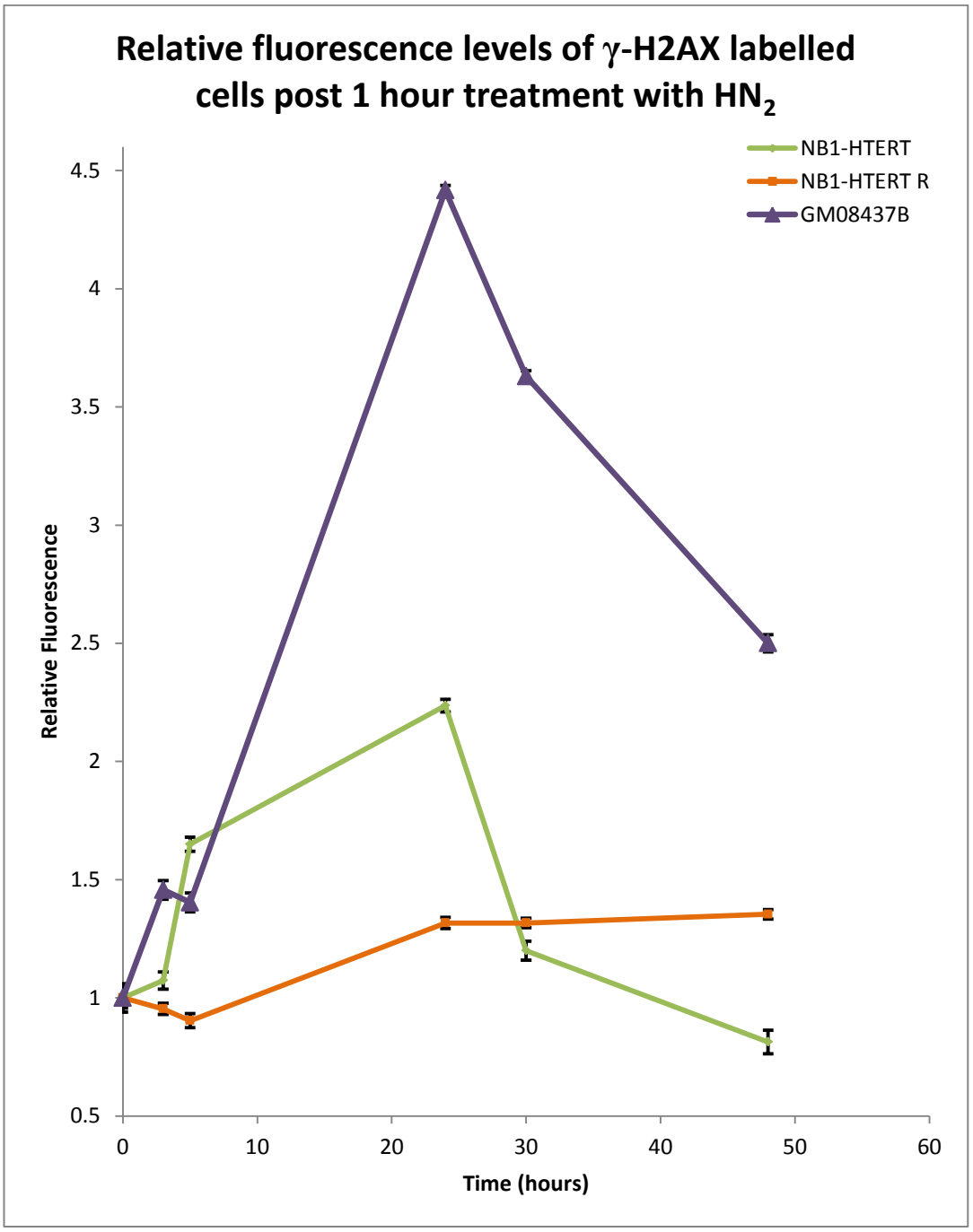

The relative levels of nuclear fluorescence exhibited in NB1-HTERT, NB1-HTERT^R and GM08437B cell lines post treatment with 0.3µg/mL HN2 treatment. Relative fluorescence was calculated by dividing actual fluorescence levels seen at each time point by the fluorescence exhibited in the control cells for each cell line. A dramatic increase in fluorescence was exhibited by the GM08437B cell line at 24 hrs post treatment. The NB1-HTERT parental and resistant cell line also peaked at 24 hrs post treatment but at much lower levels. At 48 hrs post treatment, relative fluorescence levels of NB1-HTERT parental and resistant cell lines had returned to similar levels exhibited by the control samples. However the GM08437B cell line still showed a 2.5 fold increase in comparison to its control. Standard error was calculated by dividing the standard deviation by the square root of the number of cells counted for each sample.

Figure 6.5: Comparison of fold increases in NB1-HTERT parental, resistant and GM0837B (XPF deficient) cell lines cell lines at 24 hrs and 48 hrs

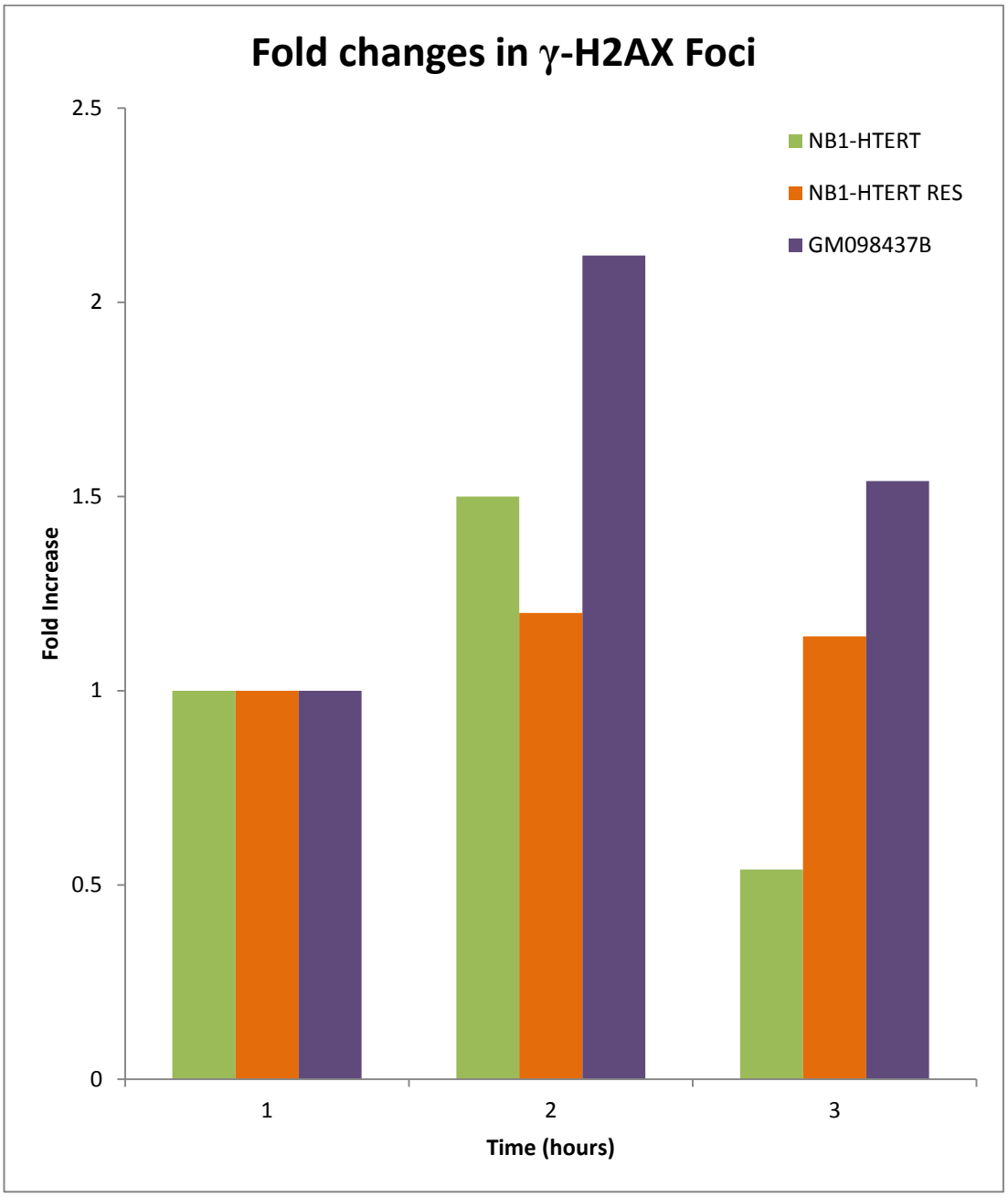

The fold increase in foci numbers were calculated for each of the cell lines by dividing the foci counts seen at 24 hrs and 48 hrs by the foci counts calculated for each of the control samples. The foci counts of the control samples were normalised to 1. The NB1-HTERT parental cell line shows a 1.5 fold increase at 24 hrs and this has decreased to -0.5 fold of the control at 48 hrs. The NB1-HTERT^{R} cell line shows a modest induction of foci at 24 hrs and at 48 hrs, this remains at 1.2 fold compared to the control. In contrast, the GM08437B cell line shows a more substantial fold change at 24 hrs with the foci count more than doubled the count seen in its control sample and at 48 hrs, this still remains at 1.54 fold increase in comparison to the control sample.

6.3.2 γ-H2AX Foci quantification post treatment with HN2 in the MRC5-SV1 and MRC5-SV1^R cell lines

The average number of foci per cell in the MRC5-SV1 parental and resistant cell lines post 1 hr treatment with 0.5μg/mL HN2 was analysed and quantified using the Imagestream^X. γ-H2AX foci were enumerated by applying a Morphology and Peak mask as previously described. The average foci numbers are shown in Figure 6.6. The total nuclear fluorescence was also determined for each of the cell lines and is shown in Figure 6.7.

The MRC5-SV1 parental cell line showed less than half the number of γ-H2AX foci exhibited in the resistant cell line at the untreated control, 3 hrs, 5 hrs and 48 hrs. At 24 hrs, there is a clear increase in foci induction in the parental cell line and this is slightly higher than the resistant cell line. However the MRC5-SV1 foci induction does not appear to exhibit any dramatic increases or decreases over the same time period. Analysis of relative fold changes over the 48 hour period indicated minor to little changes in the MRC5-SV1^R cell line in comparison to the parental cell line (Refer to Figure 6.8)

Analysis of the total nuclear fluorescence showed that there was a large induction in fluorescence at 30 hrs post treatment in the MRC5-SV1 parental cell line and a sharp decrease between 30 hrs and 48 hrs. In comparison, the MRC5-SV1^R cell line depicted a largely straight line with a much smaller incline at the peak of fluorescence. These results exhibit a similar trend to that seen with the NB1-HTERT^R cell line.

Analysis of variance (ANOVA) was used to determine whether there was a significant difference in the distribution of foci over the 48 hour time period. The

results showed that the behaviour of the two cell lines were significantly different ($p<0.001$), refer to Table 6.7 below.

Table 6.7: ANOVA Statistics of foci distribution on the MRC5-SV1 and MRC5-SV1^{R} cell lines

	F	P-value	F criteria
MRC5-SV1 parental v resistant	200.0467	<0.001	2.214846
Interaction	72.10537	<0.001	2.214846

Figure 6.6: Average foci numbers in the MRC5-SV1 parental and resistant cell lines over a 48 hour period post 1 hour treatment with HN2

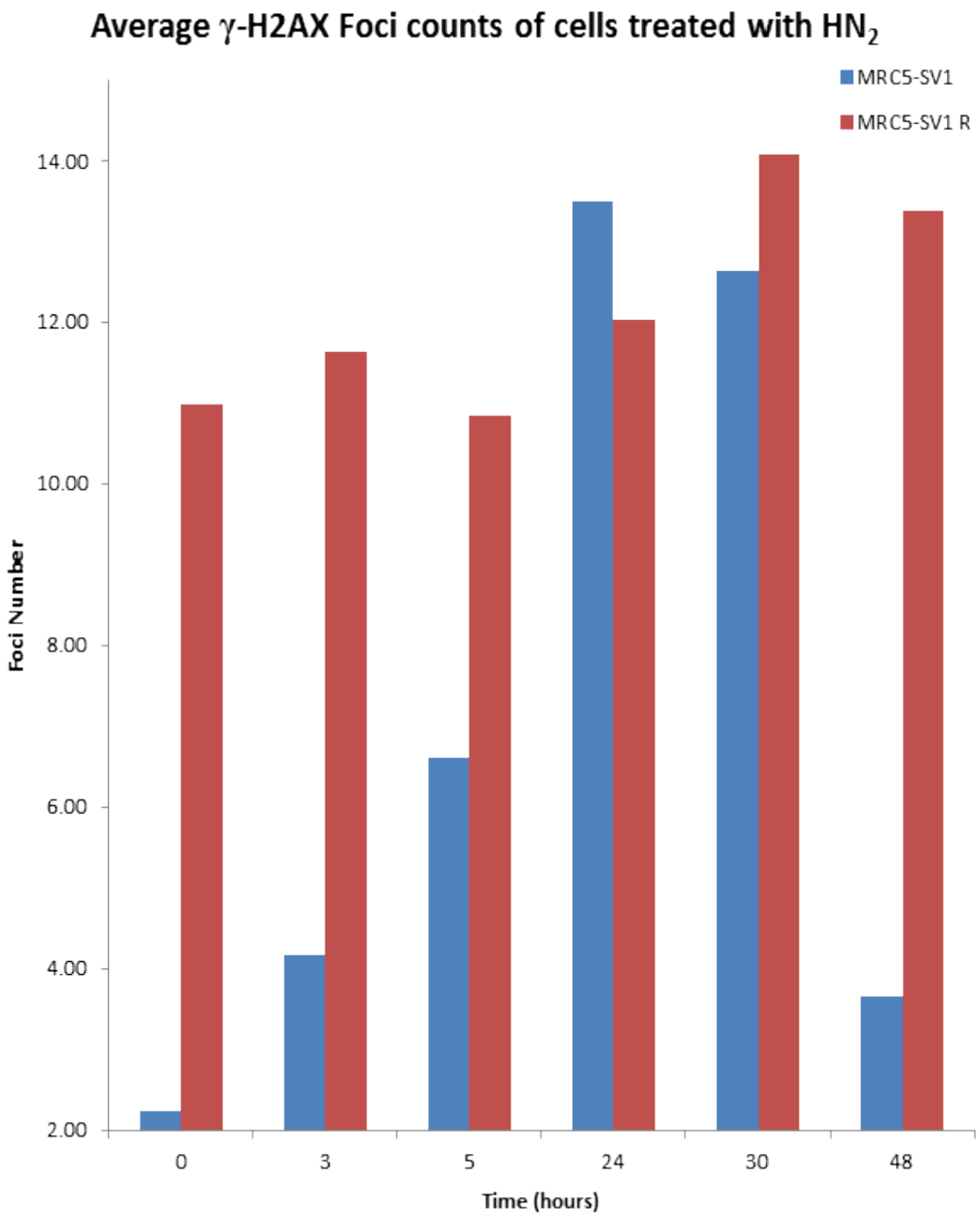

The mean number of γ-H2AX foci seen in MRC5-SV1 parental and resistant cell lines over a 48 hour period post exposure to 0.5 μg/mL HN2. In the MRC5-SV1 cell line, there is a clear peak of H2AX foci formation at 24 hrs which has largely disappeared by 48 hrs. However the MRC5-SV1^{R} does not exhibit a clear trend with foci numbers fluctuating across the time period examined. Error bars represent the standard error of the mean derived from three independent experiments in which approximately 10000 cells were analysed at each time point for each cell line. Standard error was calculated by dividing the standard deviation of the mean by the square root of the number of cells counted for each sample.

Figure 6.7: Relative fluorescence levels of the MRC5-SV1 parental and resistant cells post 1 hour treatment with HN2

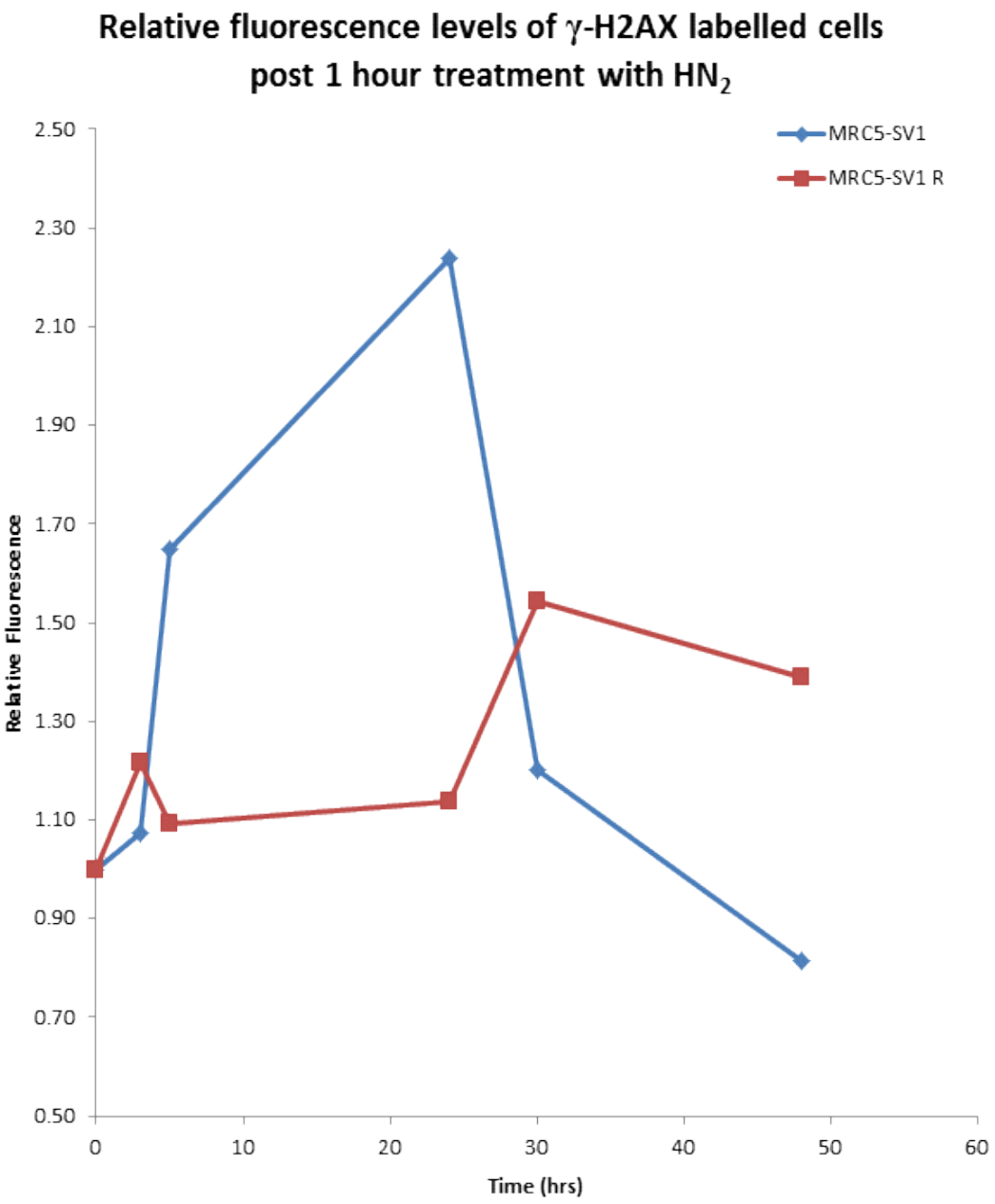

The relative levels of nuclear fluorescence exhibited in the MRC5-SV1 parental and resistant cell lines over a 48 hour period post exposure to 0.5 µg/mL HN2. Relative fluorescence was calculated by dividing actual fluorescence levels seen at each time point by the fluorescence exhibited in the control cells for each cell line. A dramatic increase in fluorescence was exhibited by the MRC5-SV1 parental cell line at 30 hrs post treatment. A slight increase in fluorescence was also seen for the MRC5-SV1^R cell line at the same time point. A sharp decline in fluorescence was seen at 48 hrs for the MRC5-SV1 parental cell line. In comparison, the resistance cell line only exhibits a minor decrease in fluorescence. Standard error was calculated by dividing the standard deviation of the mean by the square root of the number of cells counted for each sample.

Figure 6.8: Comparison of fold increases in the MRC5-SV1 parental and resistant cell lines at 24 hrs and 48 hrs

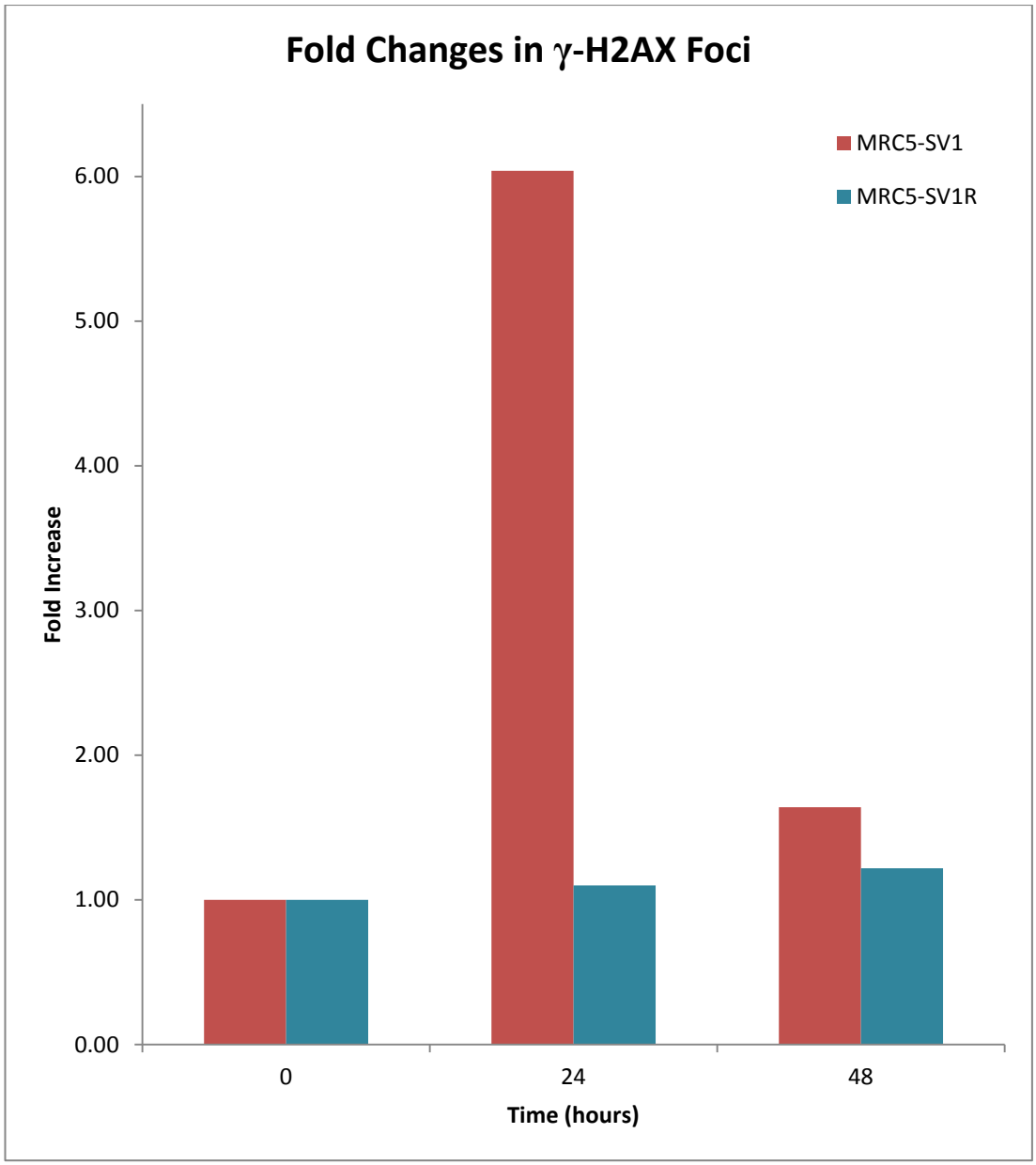

The fold increase in foci numbers were calculated for each of the cell lines by dividing the foci counts seen at 24 hrs and 48 hrs by the foci counts calculated for each of the control samples. The foci counts of the control samples were normalised to 1. The MRC5-SV1 cell line showed a 6-fold increase at 24 hrs and at 48 hrs, this has decreased to a 1.5 fold increase in comparison to the control cell line. The MRC5-SV1^{R} cell line does not show much change in foci induction across the same time period; showing a 1.1 fold increase at 24 hrs and 1.2 fold increase in comparison to the control at 48 hrs.

6.3.3 ERCC1 Foci quantification post treatment with HN2 in the NB1-HTERT, NB1-HTERT^{R} and GM08437B cell lines

ERCC1 expression levels were examined to determine whether changes seen in excision levels detected by γ-H2AX were due to an upregulation of the endonuclease ERCC1-XPF. ERCC1 foci were analysed and quantified using a Spot mask (set to visualise AF488 staining on Ch02) combined with a nuclear morphology mask (Created on Ch05 to visualise nuclear staining) as previously described in Chapter 2.

Figure 6.9: Increasing numbers of ERCC1 Foci with increasing numbers of foci

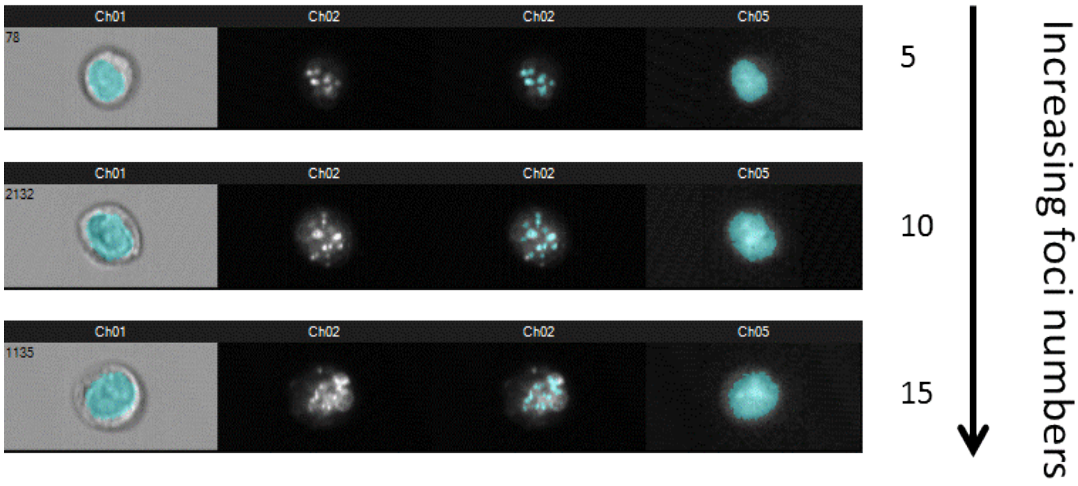

The above figure shows example images of ERCC1 shown in grey scale. Ch01 shown in the first column depicts the BF image of these cells with the morphology mask shown in blue which highlights the nuclei of the cells. Ch02 shown in the second column (representing AF488 staining of the ERCC1 foci) depicts the unmasked cells whilst the third column depicts the same images masked with the ERCC1 foci spot mask. Ch05 shows the morphology of the nucleus of these cells.

ERCC1 foci counts remained unchanged throughout the 48 hr time period in the NB1-HTERT parental cell line. There was an approximate 2 fold increase in ERCC1 foci seen in the untreated control sample of the NB1-HTERT^{R} cell line in comparison to the untreated control of the parental cell line. ERCC1 foci counts

continually decreased in the NB1-HTERT^{R} cell line over the 48 hr time period. The untreated control sample for the GM08437B cell line showed the lowest levels of ERCC1 foci in comparison to the other two cell lines. However at 24 hrs, there is a dramatic increase in ERCC1 foci levels seen in the GM08437B cell line with a 3.5 fold increase seen. These levels are seen to decrease at 48 hrs to levels similar to the untreated control. The overall nuclear fluorescence data shows a similar trend to the foci counts calculated for these cell lines.

Figure 6.10: Average ERCC1 foci counts over a 48 hour period post treatment with HN2

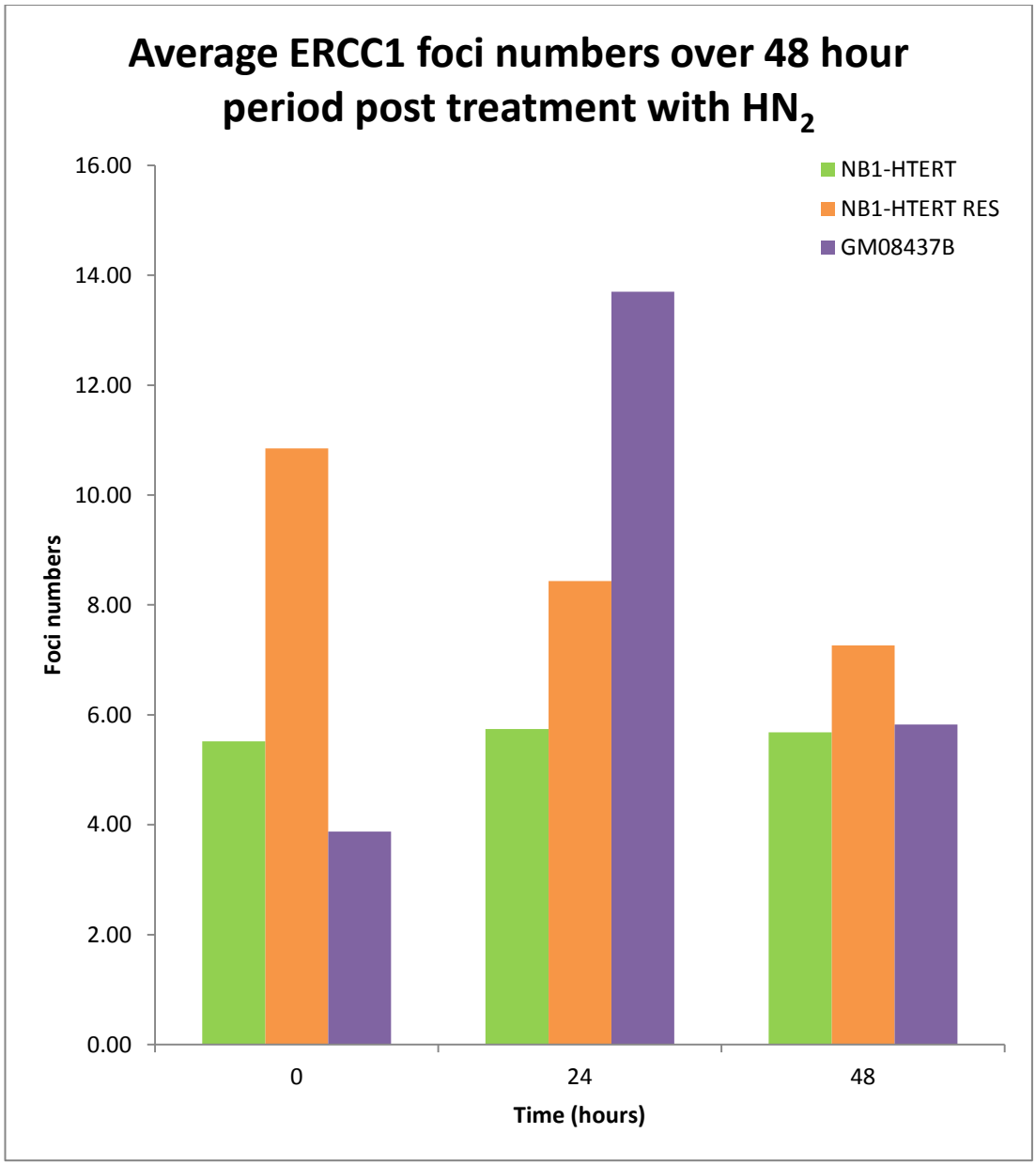

The above shows the average ERRC1 foci numbers in NB1-HTERT, NB1-HTERT^R and GM08437B cell lines post 1 hour treatment with 0.3µg/mL HN2. ERCC1 foci levels are higher in the NB1-HTERT^R control cell line in comparison to the parental and resistant cell lines. Over the 48 hour time period, the foci count is seen to decrease in the resistant cell line. The NB1-HTERT parental cell line shows that ERCC1 expression stays relatively similar over the 48 hour period. In the GM08437B cell line, there is a 3.5 fold increase at 24 hrs in ERCC1 foci levels which is seen to decrease to a 1.5 fold increase of the untreated control at 48 hrs.

Figure 6.11: Relative nuclear intensity of ERCC1 post treatment with HN2

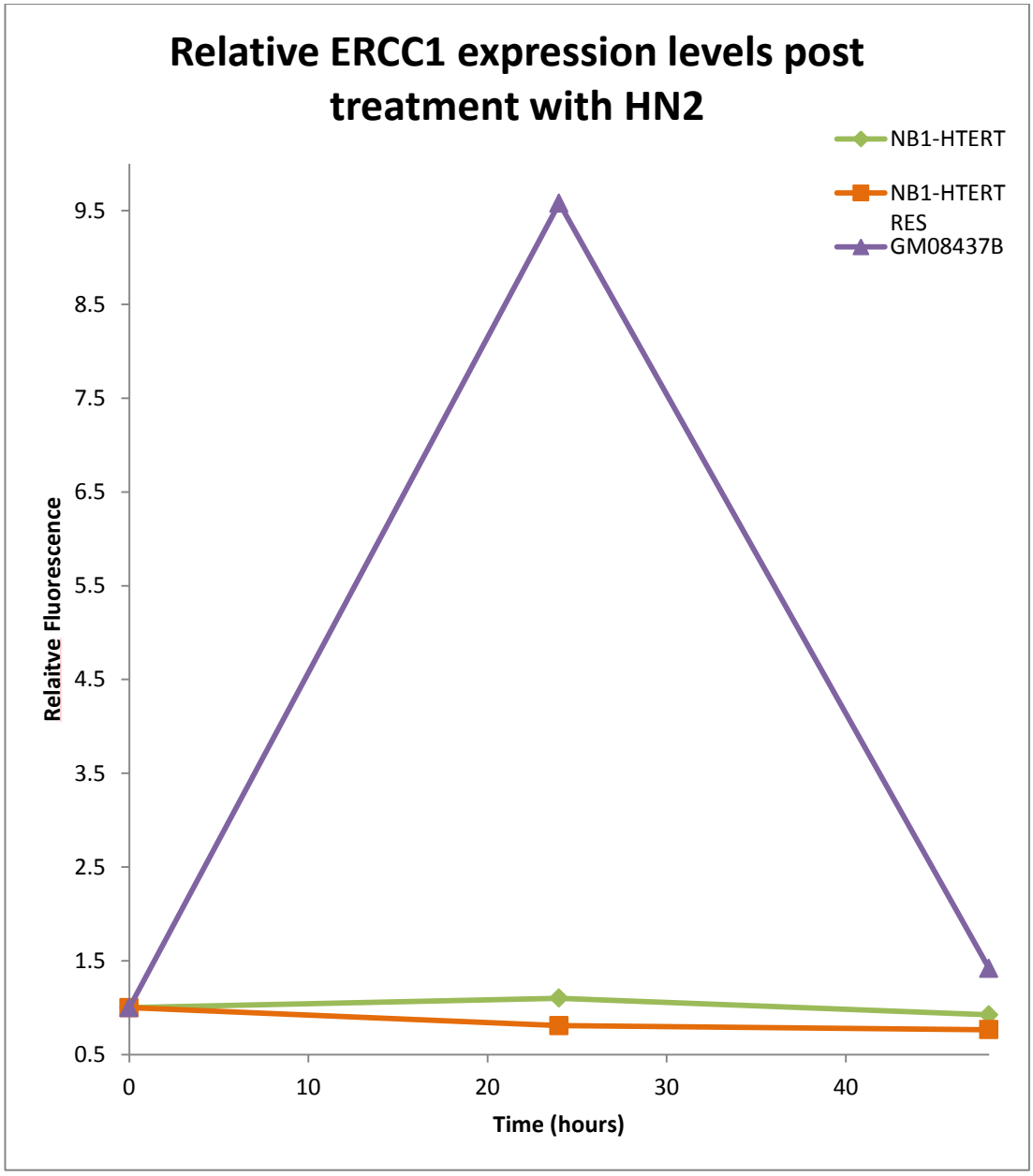

Relative ERCC1 nuclear fluorescence in NB1-HTERT, NB1-HTERT^{R} and GM08437B cell lines post 1 hour treatment with 0.3µg/mL HN2. It was observed that fluorescence levels of the NB1-HTERT and NB1-HTERT^{R} parental cell line did not differ significantly over the 48 hour period. However in the GM08437B cell line, there was a nearly 10-fold increase in florescence observed at 24hrs which then decreased at levels similar to the untreated control at 48 hrs.

6.3.4 ERCC1 Foci quantification post treatment with HN2 in the MRC5-SV1 and MRC5-SV1^{R} cell lines

ERCC1 foci were quantified by creating a Spot Mask using the Spot Wizard as detailed in Chapter 2.

ERCC1 foci counts remained unchanged between the untreated control and 24 hour samples for the MRC5-SV1 parental cell line with a 1.2 fold increment in foci counts seen at the 48 hr time point. The MRC5-SV1^{R} cell line showed a 2 fold increase in ERCC1 foci in its untreated control in comparison to the untreated control of the parental cell line. The level of ERCC1 foci decrease throughout the 48 hour time period in the MRC5-SV1^{R} cell line.

The overall nuclear fluorescence was calculated for these cell lines through the application of an Intensity feature created in the same manner as detailed in Chapter 5 (Section 5.26). The fluorescence data obtained for the MRC5-SV1 cell line showed a continuous increment with a 3.3 fold increase seen at 48 hrs. The converse was seen in the MRC5-SV1^{R} cell line with fluorescence levels dropping well below the untreated control at 48 hrs.

Figure 6.12: Average ERCC1 foci counts over a 48 hour period post treatment with HN2 in MRC5-SV1 and MRC5-SV1^{R} cell lines

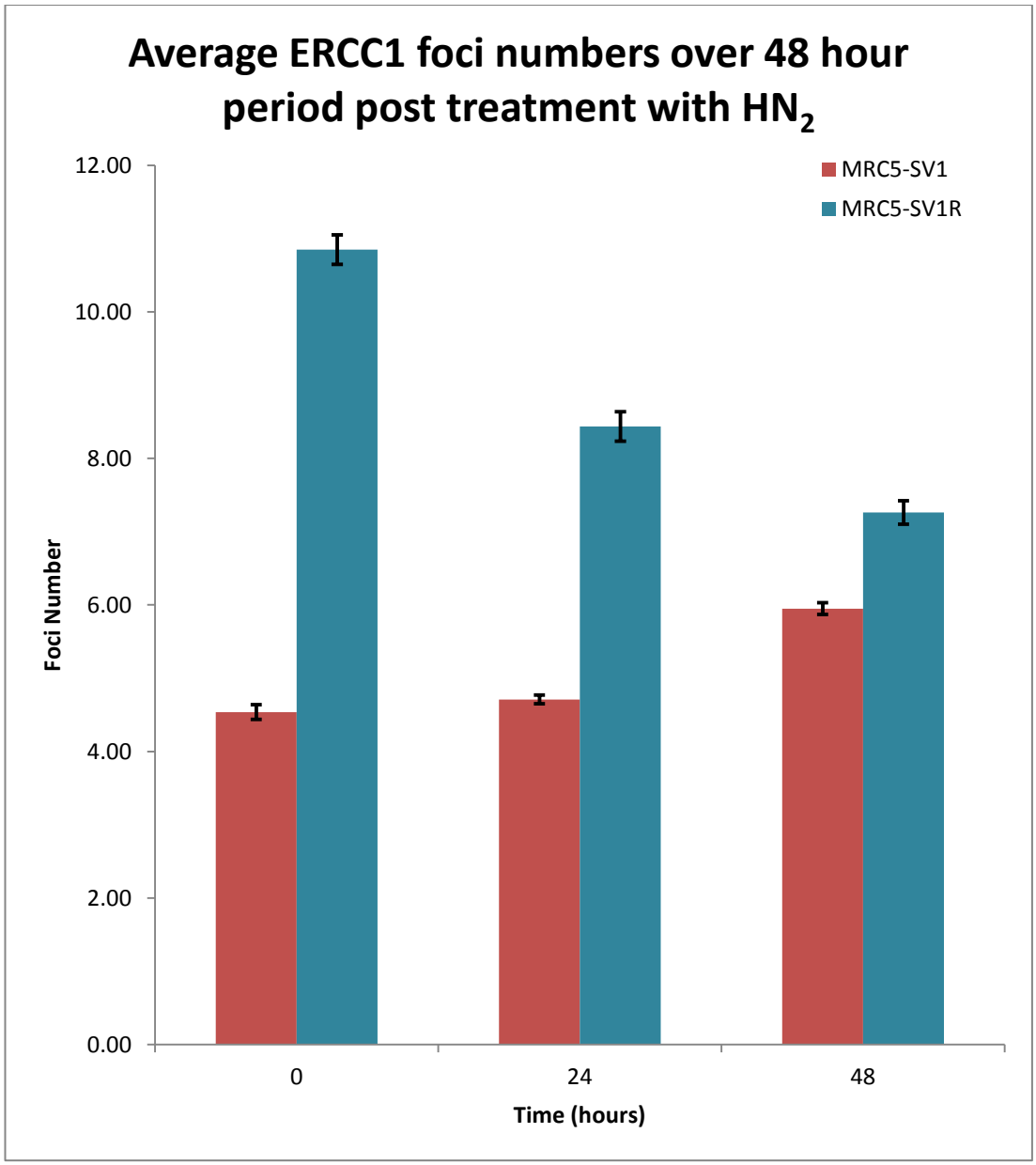

The above shows average ERCC1 foci numbers in the MRC5-SV1 and MRC5-SV1^{R} cell lines post treatment with 0.5µg/mL HN2. ERCC1 foci levels are higher in the MRC5-SV1^{R} control cell line in comparison to the parental cell line. Over the 48 hour time period, the foci count is seen to decrease in the resistant cell line. However the contrary is seen in the MRC5-SV1 parental cell line with foci counts increasing over the 48 hr period. Standard error was calculated by dividing the standard deviation of the mean by the square root of the number of cells counted for each sample

Figure 6.13: Relative nuclear intensity of ERCC1 post treatment with HN2

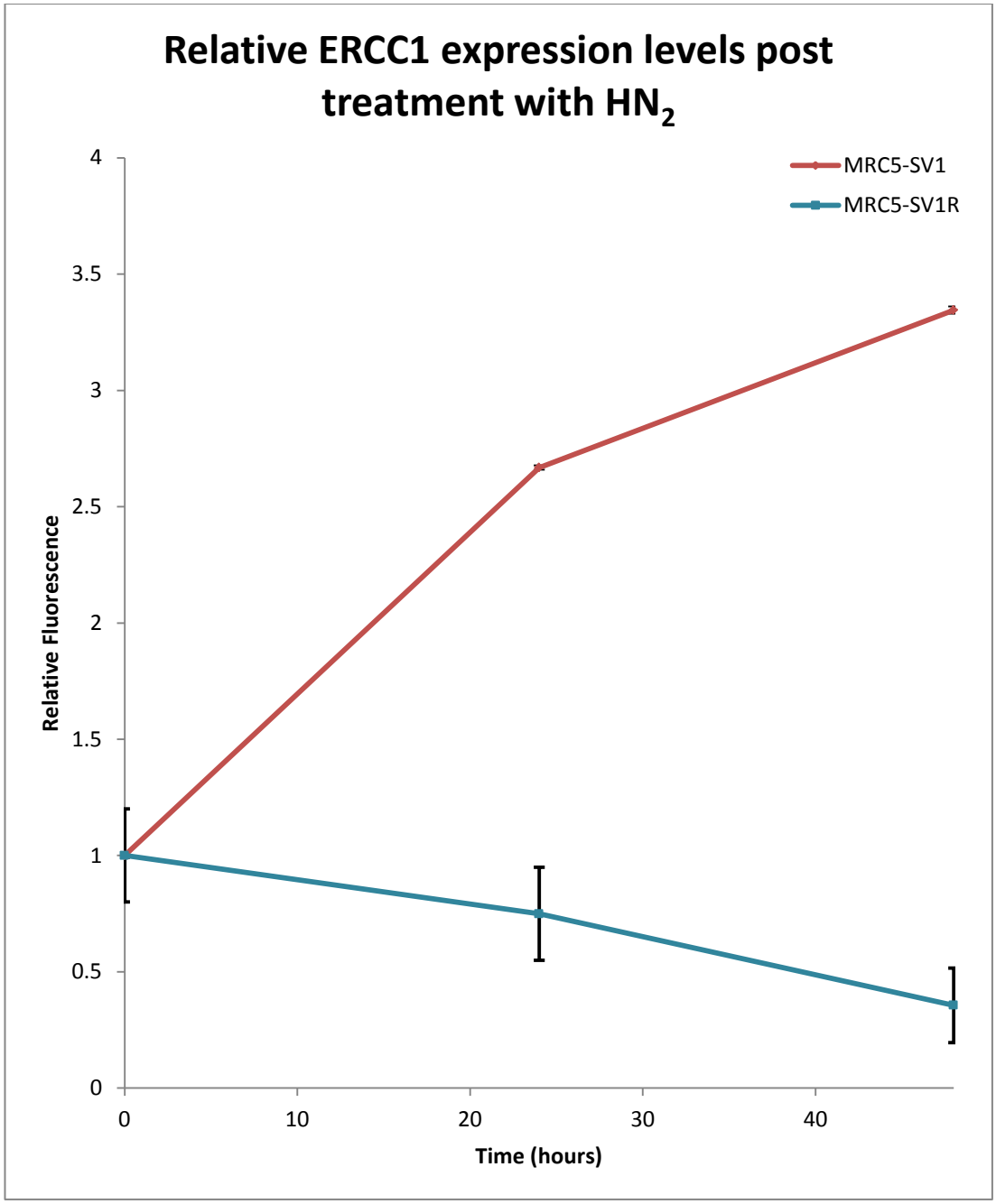

Relative ERCC1 nuclear fluorescence calculated for the MRC5-SV1 parental and MRC5-SV1^R cell lines post 1 hour treatment with 0.5µg/mL HN2. Increases in fluorescence are seen over the 48 hour time period for the MRC5-SV1 parental cell line whilst the fluorescence was seen to decrease in the resistant cell line over the same time period. Standard error was calculated by dividing the standard deviation of the mean by the square root of the number of cells counted for each sample

6.3 Discussion

This study looked at the response of five different cell lines to the cross-linking chemotherapeutic agent; HN2 by analysing γ-H2AX foci induction over a 48 hr period. Two of the cell lines, MRC5-SV1 and NB1-HTERT are repair normal cell lines with no known DNA repair defects. These were used to create resistant cell lines; MRC5-SV1^{R} and NB1-HTERT^{R} through continuous exposure to HN2. Clonogenic assays confirmed that the MRC5-SV1^{R} cell line showed a 3 fold increase in resistance to HN2 in comparison to the MRC5-SV1 parental cell line. Similarly the NB1-HTERT^{R} cell line showed a 2.7 fold increase in resistance to HN2. The fifth cell line, GM08437B has a known defect in the XPF gene and therefore was expected to show increased sensitivity to cross-linking agents.

γ-H2AX induction post treatment with ICL agents can be indicative of DSB formation during the initiation of DNA repair (Kuraoka *et al.* 2000). Studies have shown that tumours often exhibit enhanced DNA repair in response to chemotherapeutic agents (Salles *et al.* 2006). Masuda *et al*, (1988) demonstrated that DNA repair capacity did contribute to the resistant phenotype exhibited by the 2780 human ovarian carcinoma cell line. Although there are multiple other mechanisms by which resistance may arise; Masuda *et al*, (1988) postulated that once the DNA adduct has been formed, this causes irreversible damage to the DNA and one of the primary cellular mechanisms to survive would be through efficient repair of the lesion. Their findings were in line with other numerous other studies such as those conducted by Ferry *et al*, (2000) and Johnson *et al*, (1997). Similarly Koberle et al, (1997) demonstrated that diminished DNA repair of Pt-induced

damage played a role in rendering testis tumour cells hypersensitive to DNA damaging agents.

Comparison of γ-H2AX induction in the NB1-HTERT parental and NB1-HTERT^{R} revealed the resistant cell line had increased foci induction at every time point sampled in comparison to the parental cell line. Therefore it is likely that the NB1-HTERT^{R} cell line could have acquired resistance through upregulation of DNA repair pathways by increasing the rate of incisions of the cross-linked DNA possibly by the ERCC1-XPF endonuclease.

Another route of acquiring resistance could be through increased tolerance of DNA damage as suggested by Lanzi *et al*, (1998). Comparison of the MRC5-SV1 parental and MRC5-SV1^{R} resistant cell lines also showed increased numbers of γ-H2AX induction in the resistant cell line. However unlike the NB1-HTERT parental and resistant cell lines, there were much higher background levels of γ-H2AX seen in the untreated control of the MRC5-SV1^{R} cell line in comparison to the parental cell line. There was a 4.9 fold difference between the untreated controls. This data indicates that the mechanism of resistance for the MRC5-SV1^{R} cell line could be due to an enhanced ability to tolerate DNA DSBs.

Numerous studies have shown that cells deficient in either ERCC1 or XPF render them highly sensitive to ICL agents (Kuraoka *et al.* 2000; De Silva *et al.* 2002; Niedernhofer *et al.* 2004; Clingen *et al.* 2008; Al-Minawi *et al.* 2009). ERCC1-XPF have been shown to "unhook" ICLs by making dual cuts on one strand of the cross-linked DNA (Clingen *et al.* 2008) and Kuraoka et al, (2000) determined that this initiates the repair process of ICLs. However there are other studies which dispute this fact (Bhagwat et al, 2009). Findings by Niedernhofer *et al*, (2004) revealed

ERCC1-deficient cells still induced γ-H2AX formation and determined that ICL-induced DSB formation was independent of the ERCC1-XPF endonuclease. This correlates with findings in this study which showed the GM08437B cell line, deficient in XPF, also induced γ-H2AX formation. Much higher induction of γ-H2AX foci was seen in this cell line in comparison to the NB1-HTERT parental and NB1-HTERT^{R} cell lines and there was also persistence of foci exhibited at 48 hrs. This is in line with findings by Clingen *et al*, (2008) who demonstrated a persistence of foci in ERCC1 deficient cells in comparison to resistance cells post treatment with Pt. Recent developments have been made into the role that the FA pathway plays in the repair of cross-linked DNA (Crossan and Patel, 2012). Bhagwat et al, 2009 indicates that MUS81-EME1, recruited by various FA proteins makes the initial incision at the site of the cross-link; thereby creating a DSB. ERCC1-XPF then makes the second incision, resulting in the "un-hooking" of the cross-link. This theory provides an explanation for the induction of γ-H2AX foci in the XPF-deficient cell line but still does not provide a firm conclusion about the increased induction of γ-H2AX foci seen in this cell line. It could be postulated that the persistence of the γ-H2AX foci is linked to the inability of the cells to complete repair of the cross-linked DNA. However, this study would need to be extended to include FA patient cell lines in order to draw more informed conclusions about the expression levels of γ-H2AX in chemo-sensitive cells.

Findings by Britten *et al (2000)* indicated that analysis of ERCC1 mRNA levels elicited an insight into determining resistance to Pt in human cervival tumour cells. Based on these findings, ERCC1 protein expression levels were also determined for each of the five cell lines in response to a 1 hour treatment with HN2. This was

done to determine whether an increased rate of “unhooking” of the ICLs was attributing to the resistance seen in the two resistant cell lines. There was an increased expression of ERCC1 seen in the two resistant cell lines in comparison to their respective parental cell lines in the control samples. However ERCC1 expression decreased over the 48 hour time period in the resistant cell lines and furthermore the GM08437B cell line showed a vast induction in ERCC1 foci at 24 hrs. Analysis of total nuclear fluorescence mimicked the same trends seen with total foci counts and it was not possible to relate the findings of the ERCC1 experiments to the H2AX data obtained to identify a trend in expression levels. Therefore it was not possible to draw firm conclusions on the rate of “unhooking” of ICLs in these cell lines using the ERCC1 marker.

Recent evidence has implicated genes from the FA pathway in initiating the excisions to remove ICLs (Crossan and Patel 2012). These genes may likely be more sensitive markers of DNA damage and repair capacities post treatment with cross-linking agents and they form the basis of future work I would undertake in further exploring the mechanisms behind resistant and sensitive cellular phenotypes.

Using γ-H2AX to predict chemosensitivity in patients may not be the most robust marker due to the conflicting data obtained for the XPF cell line. However both the resistant cell lines exhibited increases in H2AX foci in comparison with the parental cell lines. This mimics the trend identified in Chapter 5 where the cell line exhibiting the highest resistance to each of the chemotherapeutic agents also showed the highest induction of γ-H2AX foci. Therefore it may be possible to identify chemoresistance in patients using this marker. However, a much larger sample set would be required in order to ascertain the true validity of γ-H2AX as a

diagnostic tool in identifying sensitive and resistant patients. Another important factor to consider is that γ-H2AX is a general marker of DNA damage rather than indicative of a particular repair pathway activation. Additionally the full repair kinetics post exposure to chemotherapeutic agents has yet to be elucidated in order to fully understand the γ-H2AX formation in cell lines such as the XPF deficient cell line GM08437B employed in this study. Most studies confirm that the ERCC1-XPF endonuclease is involved in the "un-hooking" mechanism of the cross linked DNA and produces a suitable substrate for the HR pathway to complete DNA repair (Ferry *et al.* 2000; McHugh *et al.* 2001; Clingen *et al.* 2007). However the ERCC1 deficient embryonic stem cells employed in the study by Niedernhofer *et al* (2004) also showed H2AX formation post treatment with Pt and De Silva *et al* (2002) established that ERCC1 and XPF deficient cell lines were not hypersentive to cross-linking agents due to defective "unhooking" of ICLs.

As the use of γ-H2AX has produced conflicting data, the potential of using a biomarker specific to a DNA repair pathway to identify chemosensitivity in patients was explored in the following chapter.

Chapter 7

Evaluation of the RAD51 protein as a DNA repair biomarker for chemotherapeutic response

7.1 Introduction

HR is one of two DNA repair pathways that are responsible for the repair of DSBs. This pathway is also involved in other functions (Plo *et al.* 2008) such as

- Gene diversification
- Molecular evolution
- Chromosome segregation in meiosis
- Repair of DNA ICLs
- Recovery of stalled replication forks

The formation of ICLs poses a serious threat to the genomic stability due to the inhibition of essential cellular processes such as transcription and DNA synthesis (Wang *et al.* 2011). Due to the complex nature of ICL formation, the repair of ICLs is a significant challenge for cells and requires the coordinated interaction of multiple independent DNA pathways (Al-Minawi *et al.* 2009).

The preferred route taken for repair of ICL induced DNA damage is through the combination of components of the NER pathway and HR (Clingen *et al.* 2008). Kuraoka *et al*, (2000) first demonstrated that the ERCC1-XPF endonuclease is involved in initiating repair of ICLs. There are several possible mechanisms for ERCC1-XPF; one of which involves the "unhooking" of the ICL through dual incisions either side of one arm of the ICL (Kuraoka *et al.* 2000). This then breaks the covalent bond between the two DNA strands (Clingen *et al.* 2008), providing a suitable substrate for the initiation of HR through the initiation of a DSB. RAD51 is involved in searching for an intact homologous duplex and binds to the ssDNA forming a presynaptic filament. RAD51 then mediates strand invasion and exchange of genetic information once the homologous strand has been located.

Studies have been carried out using the RAD51 as a biomarker of DNA damage in response to various DNA damaging agent. Haaf *et al*, (1995) showed an induction of nuclear RAD51 foci in human fibroblast cells in response to treatment with IR, UV irradiation and methyl methanesulfonate. They also demonstrated a role for RAD51 in the repair of DNA damage during meiosis. Findings by Raderschall *et al*, (1999) revealed that nuclear RAD51 foci showed preferential formation at sites of damaged ssDNA and theorised that the foci were indicating sites of filament formation on ssDNA. Hannay *et al*, (2007) demonstrated that RAD51 was being overexpressed in a number of human soft tissue sarcoma cell lines. They further demonstrated that treating the human SKLMS1 leiomyosarcoma cell line with Adr increased the expression of the RAD51 protein in comparison to the untreated control cells which was determined by western blotting. They concluded that the overexpression of RAD51 was leading to the development of chemoresistance and this was further validated by showing that inhibiting Rad51 expression markedly increased cell sensitivity to Adr.

This study investigated the use of RAD51 as a potential biomarker in identifying chemosensitivity or resistance to the ICL-inducing agent, HN2. RAD51 plays an integral role in HR which has been shown to be centrally involved in the repair of ICLS and furthermore having defective components of the HR pathway has been shown to contribute to the development of cancers such as breast and ovarian (Clingen *et al.* 2008; Li and Heyer 2008). Therefore it was hypothesised that analysis of RAD51 expression levels could elucidate information such as whether DNA repair of ICLs is up-regulated in cell lines made resistant to HN2.

7.2 Results

Figure 7.1: Multispectral images of Rad51 foci with increasing numbers of foci

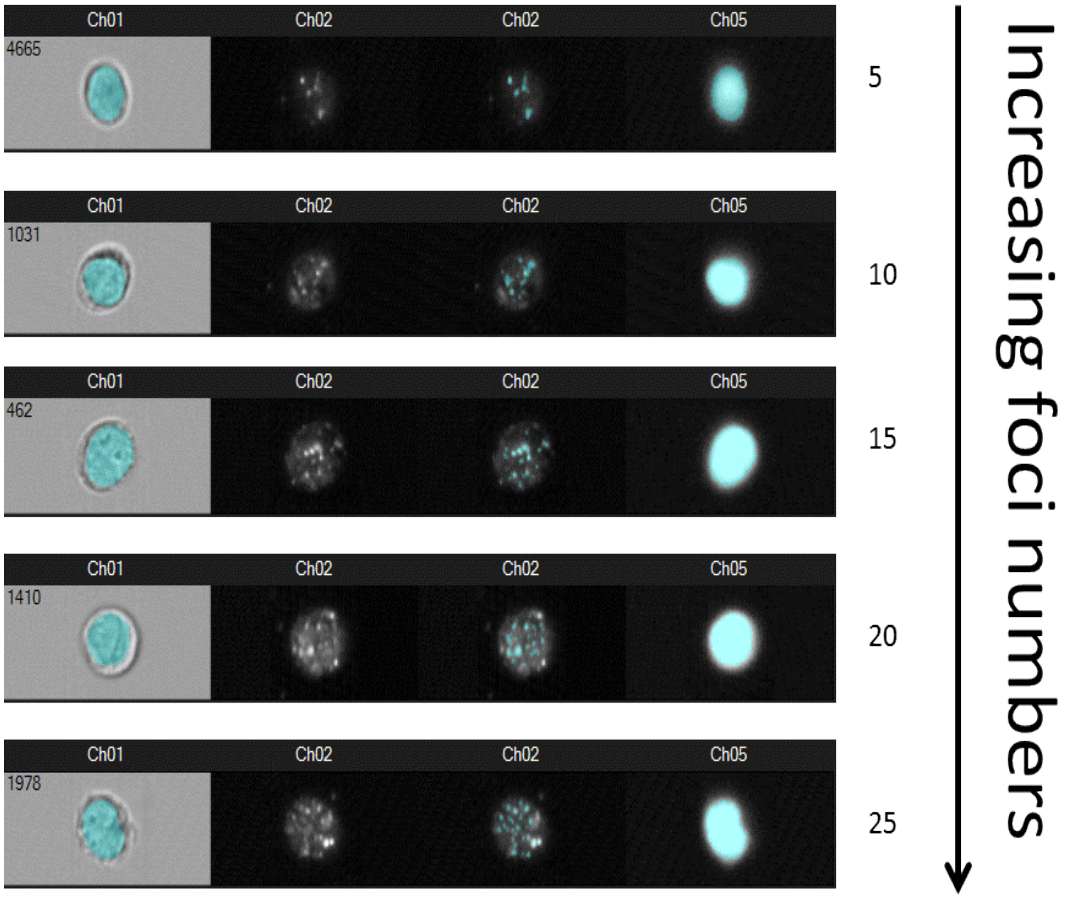

The above figure shows example images of cells with increasing numbers of Rad51 foci. Ch01 shown in the first column depicts the BF image of these cells with the morphology mask shown in blue which highlights the nuclei of the cells. Ch02 shown in the second column (representing AF488 staining) depicts the unmasked cells whilst the third column depicts the same images masked with the RAD51 foci spot mask. Ch05 shows the morphology of the nucleus of these cells.

Figure 7.1 above shows example images of the RAD51 foci visualised in the cell lines post treatment with HN2. A spot mask was created using the Spot Wizard function for each cell line as detailed in Chapter 5. This was then combined with a nuclear morphology mask to enumerate the RAD51 foci present in the nucleus of each cell.

7.2.1 Quantification of RAD51 foci post treatment with HN2 in the MRC5-SV1 and MRC5-SV1^{R} cell lines

The average number of RAD51 foci per cell in the MRC5-SV1 parental and resistant cell lines post 1 hr treatment with 0.5µg/mL HN2 was analysed and quantified using the Imagestream^{X}. RAD51 foci were enumerated by applying a Morphology and Peak mask to each of the cell images produced for each time point as detailed in previous chapters. The average foci numbers are shown in Figure 7.2. The total nuclear fluorescence was also determined for each of the cell lines and is shown in Figure 7.3.

At all time points examined, the MRC5-SV1 parental cell line showed fewer RAD51 foci than the MRC5-SV1^{R} cell line. There was a 3.7 fold difference seen between the untreated controls of the two cell lines. There was little change seen between samples collected at 6 hrs and 24 hrs in the MRC5-SV1 parental cell line. This then increased by 1.2 fold at 30 hrs. A similar fold change was observed between the 6 hour and 24 hour samples for the MRC5-SV1^{R} cell line. Foci counts at 24 hrs and 30 hrs for the resistant cell line were similar. A further increase in RAD51 foci was seen at 48 hrs for the MRC5-SV1^{R} cell line; leaving it at a 1.5 fold increase of the untreated control. In the MRC5-SV1 parental cell line, there was a decrease in foci seen at 48 hrs in comparison to the 30 hour sample. However this remained at a 2 fold increase of the untreated control.

The relative nuclear fluorescence data for the parental cell line showed that at 30 hrs, there was a peak of relative fluorescence and this was shown to decrease at 48 hrs; although it remained at a 1.5 fold increase of the untreated control. In contrast, the nuclear fluorescence exhibited by the MRC5-SV1^{R} cell line continued

to increase over the same hour time period. The relative fluorescence data appears to correlate with the foci counts in these cell lines.

Statistical analysis of the data using ANOVA revealed significant differences (p value <0.001) in the distribution of foci between the MRC5-SV1 parental and resistant cell lines (See Table 7.1 below)

Table 7.1: ANOVA Statistical analysis of foci distribution in the MRC5-SV1 parental and resistant cell lines

	F	*P-value*	*F criteria*
MRC5-SV1 parental v resistant	**33.542**	**<0.001**	**2.374078**
Interaction	**33.823**	**<0.001**	**2.374078**

Figure 7.2: Average RAD51 Foci numbers over a 48 hour period post treatment with HN2

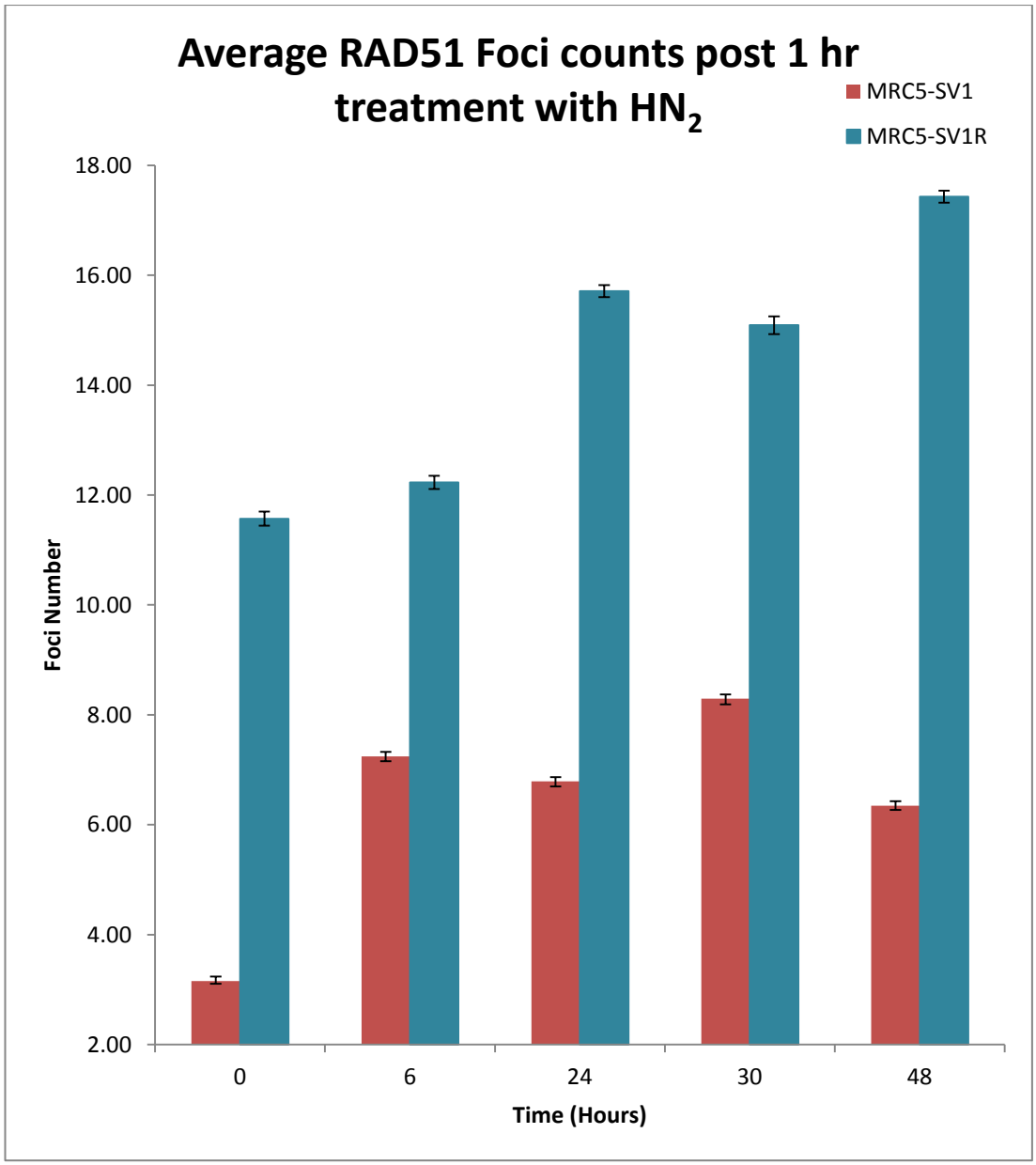

The above shows nuclear RAD51 foci counts for the MRC5-SV1 and MRC5-SV1^R cell lines. There is a 3.7 fold difference between the MRC5-SV1 parental and resistant cell lines in the untreated controls. Although the foci counts are seen to increase in the parental cell line, there is little difference seen between the time points. In contrast, the RAD51 foci counts in the MRC5-SV1^R cell line are seen to continually increase over the 48 hour time period. Standard error was calculated by dividing the standard deviation of the mean by the square root of the number of cells counted for each sample.

Figure 7.3: Relative Fluorescence of cells post 1 hour treatment with HN2

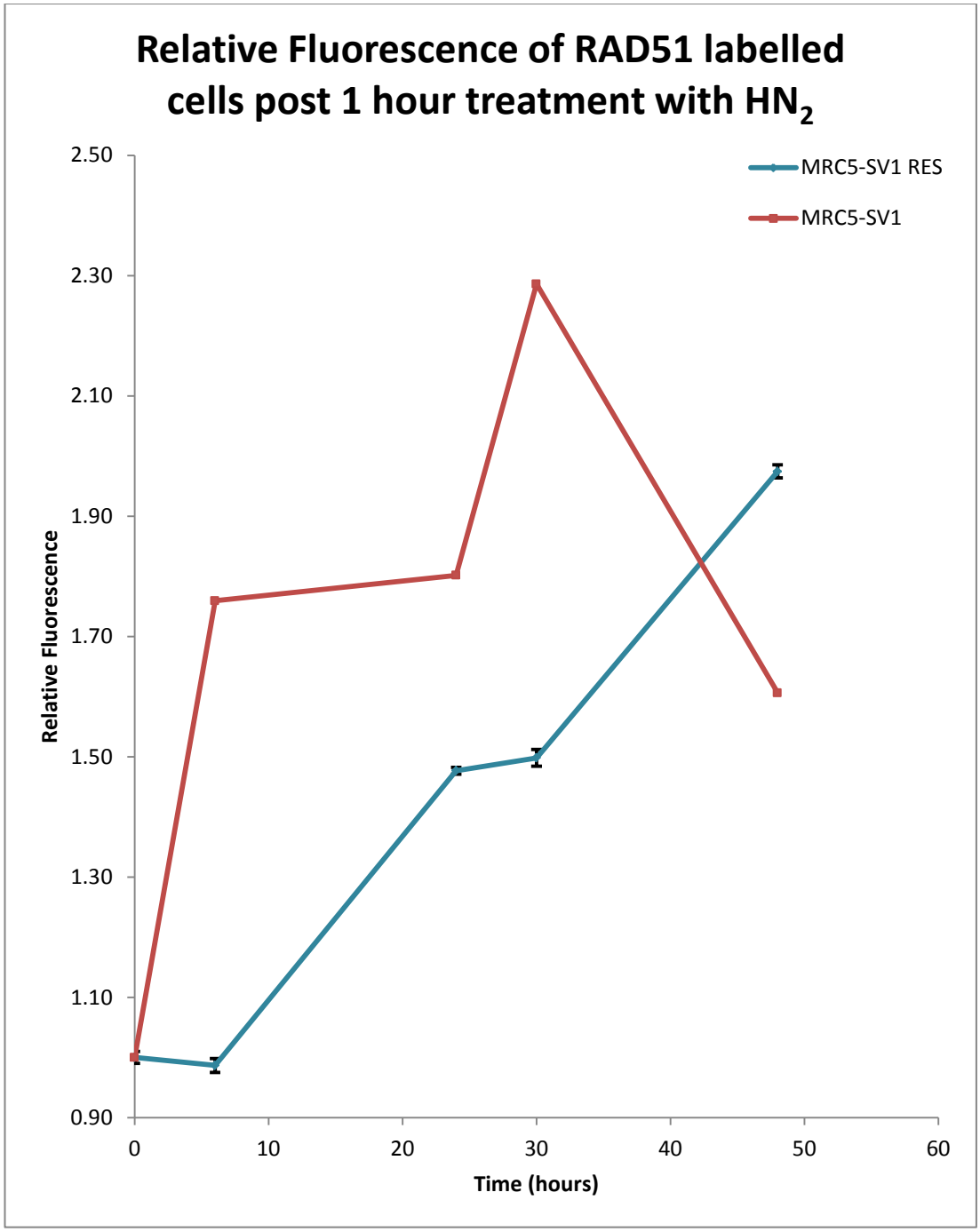

The above shows the relative nuclear fluorescence levels of the MRC5-SV1 parental and MRC5-SV1^R cell lines. There is a 1.8 fold increase in fluorescence seen at 6 hrs in the MRC5-SV1 parental cell line. Fluorescence levels remain unchanged between 6 hrs and 24 hrs and appear to peak at 30 hrs before starting to decline. However in the MRC5-SV1^R cell line, relative fluorescence levels are continually increasing over the 48 hour time period. Standard error was calculated by dividing the standard deviation of the mean by the square root of the number of cells counted for each sample.

7.3.1 Quantification of RAD51 foci post treatment with HN2 in the NB1-HTERT, NB1-HTERT^{R} and GM08437B cell lines

The average number of RAD51 foci per cell in the NB1-HTERT, NB1-HTERT^{R} and GM08437B cell lines was analysed and quantified using the Imagestream^{X} post treatment with 0.3 μg/mL HN2. RAD51 foci were enumerated by applying a Morphology and Peak mask to each of the cell images produced for each time point as previously described. The average foci numbers are shown in Figure 7.4. The total nuclear fluorescence was also determined for each of the cell lines and is shown in Figure 7.5.

The NB1-HTERT^{R} cell line showed little change in RAD51 foci counts over the 48 hour period post treatment with HN2. It also showed lower levels of RAD51 in comparison to both the NB1-HTERT parental cell line and the GM08437B cell line. There was a 1.5 fold increase in RAD51 foci seen between 6 hrs and 24 hrs in the NB1-HTERT parental cell line. The peak of RAD51 formation was seen at 24 hrs which then was seen to slowly decrease at 30 and 48 hrs although it was not a dramatic decrease.

The GM08437B cell line shows an increase in RAD51 across the 48 hour time period with a 1.2 fold increment at each time point. At 48 hrs, RAD51 foci counts remain at a 1.9 fold increase in comparison to the untreated control.

Relative fluorescence data for the cell lines appear to show a similar trend to the foci counts obtained for the NB1-HTERT parental and GM08437B cell lines. However the NB1-HTERT^{R} had much higher levels of fluorescence than the other two cell lines even though the foci counts were much lower in this cell line. Statistical analysis of the data using ANOVA revealed that the three cell lines all

showed significantly different RAD51 foci distributions across the 48 hour time period (Refer to Table 7.2 below).

Table 7.2: ANOVA Statistical analysis of foci distribution in the NB1-HTERT, NB1-HTERT^{R} and GM08437B cell lines

	F	*P-value*	*F criteria*
NB1-HTERT parental v resistant	**369.9995**	**<0.001**	**2.372509**
Interaction	**115.9683**	**<0.001**	**2.372509**
NB1-HTERT parental v GM08437B	**469.9547**	**<0.001**	**2.372509**
Interaction	**403.3087**	**<0.001**	**2.372509**
NB1-HTERT^{R} V GM08437B	**694.5374**	**<0.001**	**2.372509**
Interaction	**271.1347**	**<0.001**	**2.372509**

Figure 7.4: Average RAD51 Foci numbers over a 48 hour period post treatment with HN2

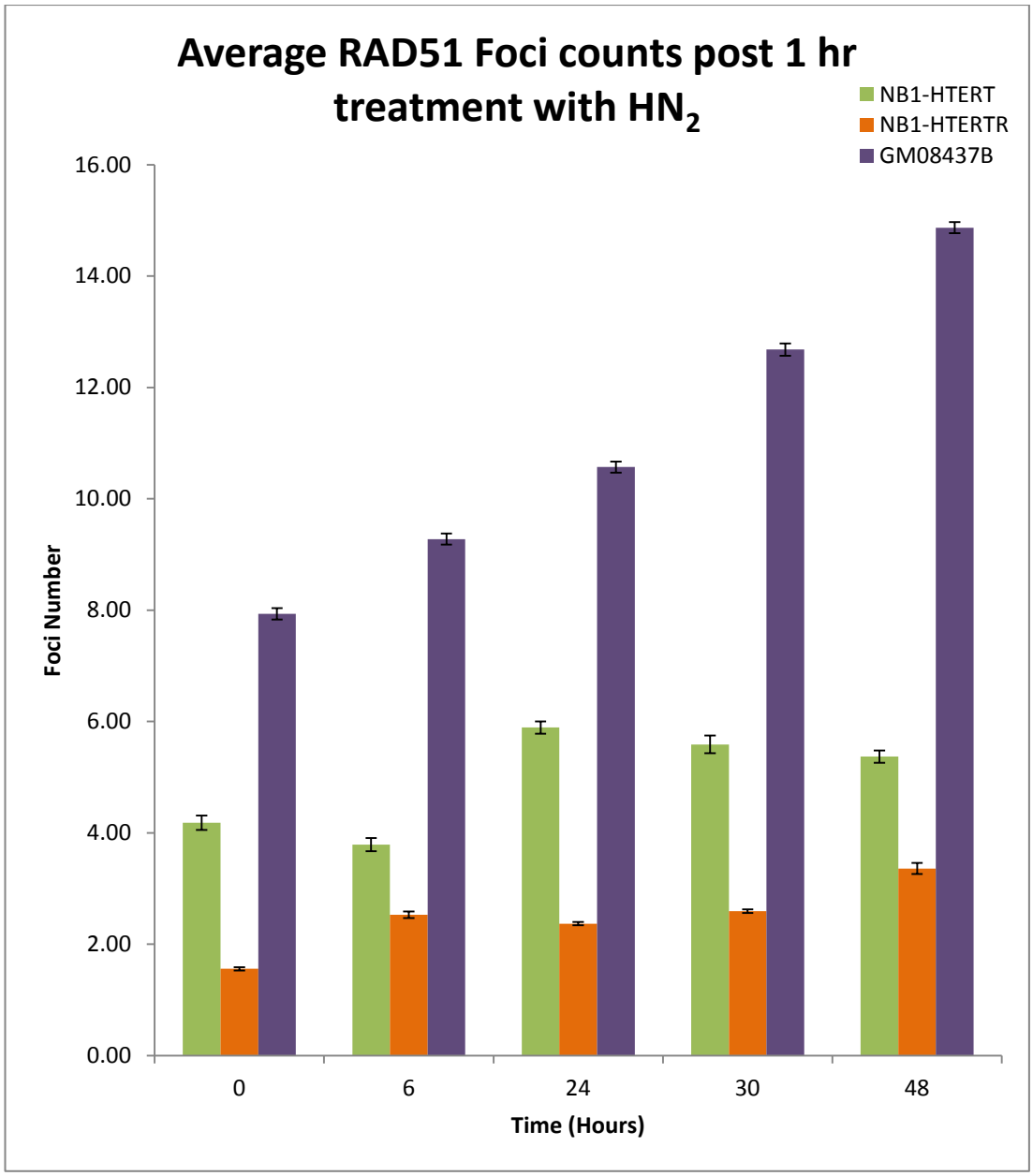

The average RAD51 foci counts for the NB1-HTERT, NB1-HTERT^R and GM08437B cell lines post 1 hour treatment with 0.3µg/mL HN2. The NB1-HTERT^R cell line showed little change in RAD51 foci counts over the 48 hour time period. The NB1-HTERT parental cell line showed an increased expression of RAD51 foci in comparison with the NB1-HTERT^R resistant cell line at all time points examined. The GM08437B cell line showed the highest expression of RAD51 foci of all 3 cell lines examined and this was seen to continually increase over the 48 hour time period. Standard error was calculated by dividing the standard deviation of the mean by the square root of the number of cells counted for each sample.

Figure 7.5: Relative Fluorescence of cells post 1 hour treatment with HN2

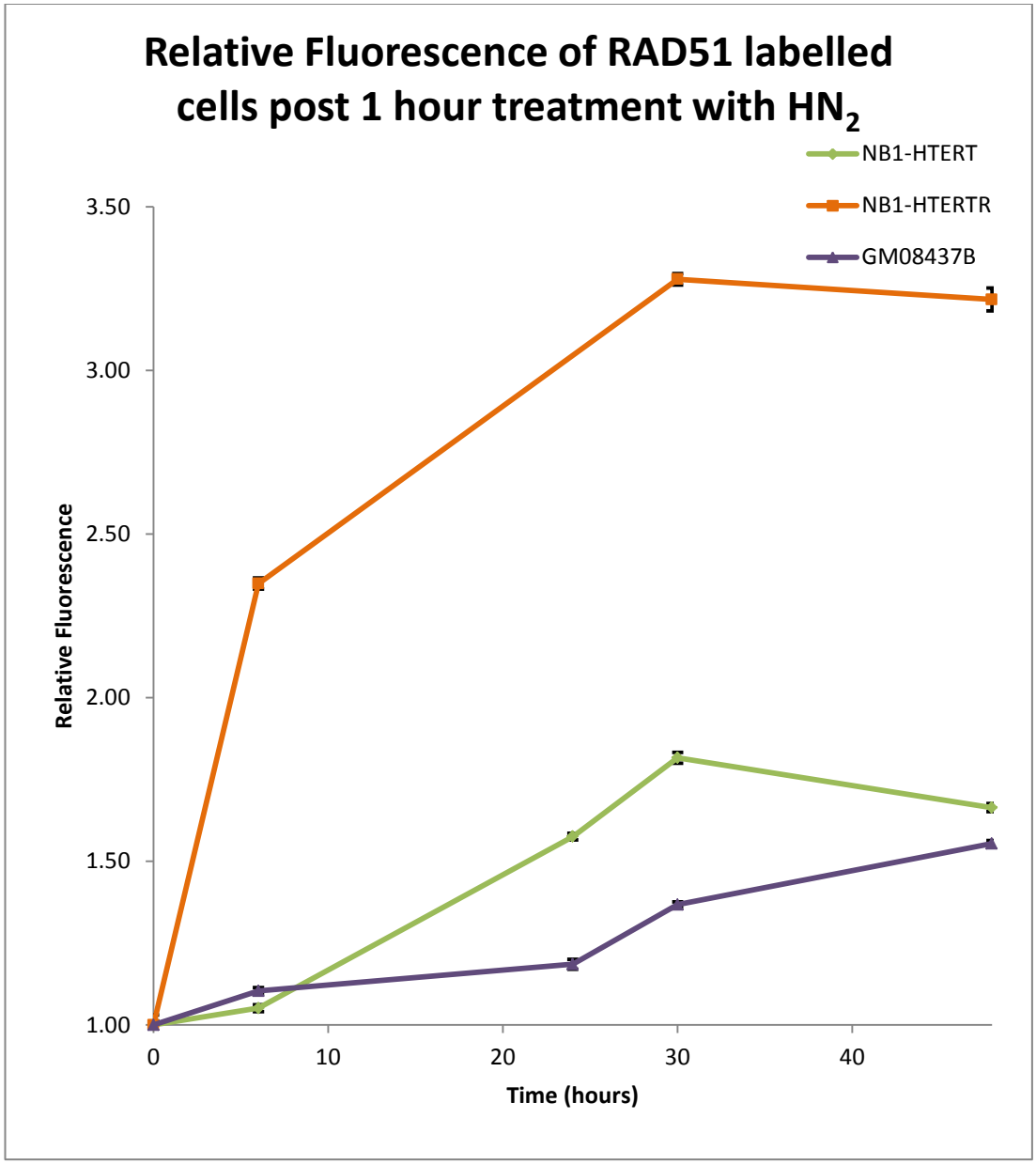

Relative nuclear fluorescence levels for NB1-HTERT parental, NB1-HTERT^R and GM08437B cell lines. The NB1-HTERT parental cell line shows an increase in fluorescence between 6 hrs and 24 hrs and this is seen to peak at 30 hrs before starting to decrease at the 48 hour time point. However it still maintains fluorescence levels at a 1.7 fold increase in comparison to the untreated control. The GM08437B cell line shows a steady increment in fluorescence levels across the 48 hour time period. The NB1-HTERT^R cell line shows a steep increase in fluorescence at 6 hrs and this is seen to continually increase up to 30 hrs with a slight decrease seen at 48 hrs. Standard error was calculated by dividing the standard deviation of the mean by the square root of the number of cells counted for each sample.

7.3 Discussion

This study compared the expression levels of RAD51 in five different cell lines over a 48 hour time period in response to a 1 hour treatment with HN2. MRC5-SV1 and MRC5-SV1^{R} cell lines were treated with a higher dose of HN2 (0.5μg/mL) as the parental cell line exhibited higher resistance to this drug in comparison with the NB1-HTERT cell line (See Chapter 4). Increased levels of RAD51 foci were seen in the MRC5-SV1^{R} cell line across the 48 hour time period examined in comparison to the MRC5-SV1 parental cell line. A comparison of the untreated controls revealed a 3.7 fold increase in RAD51 foci in the MRC5-SV1^{R} cell line. At 48 hrs, there was a 2.7 fold increase in RAD51 foci in the MRC5-SV1^{R} cell line.

This line of evidence suggests that there is an upregulation in the homologous recombination DNA repair pathway in the MRC5-SV1^{R} cell line. This is supported by observations that the level of RAD51 foci increased 1.2 fold between 6 hrs and 24 hrs in the MRC5-SV1^{R} cell line while a similar increase was exhibited by the MRC5-SV1 parental cell line between 24 hrs and 30 hrs; suggesting an earlier onset of HR in the resistant cell line. These findings are in line with that of Al-Minawi et al, (2009) who reported that HR proteins play a crucial role in the repair of ICLs. Thereby it is proposed that the MRC5-SV1^{R} cell line acquired resistance to HN2 by up-regulating HR which would allow it to resolve damage incurred by the formation of ICLs more rapidly than its parental cell line.

However the NB1-HTERT^{R} cell line did not exhibit a similar increase in RAD51 foci in comparison to the parental cell line. Instead it showed lower levels of RAD51 foci across the entire 48 hour time period examined which suggests that there is no up-regulation of HR seen in this cell line. Clonogenic data from Chapter 6 confirmed

that the resistant cell line exhibited a 2.7 fold increase in resistance to HN2. Therefore it is possible that the NB1-HTERT^{R} cell line acquired resistance to HN2 through increased efflux of the drug out of the cell or by increased inactivation of HN2 through interactions with intracellular metabolites such as Glutathione. Alternatively it could have become more tolerant to the induction of DNA DSBs.

The GM08437B cell line exhibited a steady increment in RAD51 foci at every time point observed over the 48 hour time period. Findings by Al-Minawi *et al*, (2009) indicated that ERCC1-XPF is not required for the formation of RAD51 foci which supports the findings in this chapter. Findings from the previous chapter have indicated the presence of DSBs in the GM08437B cell line in response to treatment with HN2. Therefore it is possible that RAD51 is still being recruited to the site of damage but DNA repair is not reaching completion as numerous findings support the theory that the ERCC1-XPF endonuclease is critical in the latter stages of ICL-induced DNA damage repair (De Silva *et al.* 2002; Niedernhofer *et al.* 2004; Clingen *et al.* 2008; Wang *et al.* 2011). In order to determine whether RAD51 is functional, expression levels of HR proteins downstream of RAD51 could be examined.

The increased expression in RAD51 seen in the MRC5-SV1^{R} cell line post treatment with HN2 in comparison to the parental cell line correlates with the findings that expression of γ-H2AX was also increased in this cell line. This provides a firm indication that there was an upregulation in DNA repair capacities of the MRC5-SV1^{R} cell line. However contradictory findings were seen in the NB1-HTERT^{R} cell line as this showed an increase in γ-H2AX expression post treatment with HN2 in comparison to the parental cell line but did not show an increase in RAD51

protein levels. Therefore further work needs to be done with a bigger cohort of DNA repair normal and defective cell lines and also perhaps a wider array of chemotherapeutic drugs.

Chapter 8

General Discussion

This project examined the efficacy of two DNA biomarkers γ-H2AX and RAD51 in predicting patient response to chemotherapy and identifying sensitive and resistant cellular phenotypes. The novel technique of imaging flow cytometry was employed in the detection of these two biomarkers post treatment with different chemotherapeutic agents. Six different cell lines were utilised in this project:

- MRC5-SV1 (derived from DNA repair normal)
- NB1-HTERT (derived from DNA repair normal)
- AT5BIVA (derived from classical A-T patient)
- MRC5-SV1^{R} (HN2 resistant)
- NB1-HTERT^{R} (HN2 resistant)
- GM08437B (derived from an XP-F patient)

γ-H2AX and RAD51 expression levels were first evaluated in DNA repair normal cell lines and compared with resistant and sensitive cell lines to investigate whether distinguishable trends of increased foci formation or foci persistence could be linked to chemo-sensitivity or chemo-resistance.

Side effects are a fundamental limitation of chemotherapy. The extent of normal cell damage governs the level of side effects experienced by the patient and can be extremely variable between individuals. Additionally the development of resistance to chemotherapeutic agents accounts for treatment failure in more than 90% of breast and ovarian cancers (Ferry *et al.* 2000; Agarwal and Kaye 2003). Therefore the development of an assay that could identify these patients prior to undergoing therapy would aid in improving patient outcome and ultimately their quality of life.

As the formation of γ-H2AX foci has been well-established post treatment with IR, the initial study looked at whether it was possible to detect differences in the induction and repair of DNA DSB post exposure to IR in three cell lines with different DNA repair capacities using the Imagestream. The data derived from the Imagestream was compared with classic methods such as *in situ* immunofluorescence and conventional flow cytometry. Similar patterns of foci induction in the different cell lines were seen using all three methods. This then initiated the development of a chemotherapy γ-H2AX assay to examine whether distinct DNA damage and repair profiles could be established in a similar manner to those established in response to IR.

The chemotherapy γ-H2AX assay measured the response of cell lines to different chemotherapeutic agents by analysing γ-H2AX foci induction. In response to treatment with chemotherapeutic agents such as cross-linking agents, γ-H2AX formation is thought to be indicative of incisions being made during DNA repair. A clear trend has emerged from this data in that cell lines exhibiting higher levels of resistance to each individual drug were also seen to exhibit the highest number of foci at each time point sampled. Therefore it is possible that the explanation for the increased foci numbers is due to an increased rate of DNA repair, likely through an increase in the number of incisions being made. This reasoning is supported by studies such as Clingen *et al*, (2007) and Niedernhofer *et al*, (2004) who have shown the accumulation of γ-H2AX foci in response to treatment with chemotherapeutic agents such as Pt and Mitomycin C.

The RAD51 assay revealed increased RAD51 expression levels in one of the resistant cell lines, MRC5-SV1^{R} in comparison with its parental cell line. AS HR is

known to have a critical role in completing repair of ICLs, this increase in RAD51 levels could indicate an upregulation of the HR pathway in this cell line. Interestingly, the NB1-HTERT^{R} cell line did not show increases in RAD51 foci with much lower levels of RAD51 expression seen over the 48 hour time period. This may be indicating that this cell line may have acquired resistance through other mechanisms such as an increased tolerance to the formation of DNA DSBs as the results of the γ-H2AX assay revealed increases in foci formation in the NB1-HTERT^{R} resistant cell line.

The kinetics of γ-H2AX formation in response to chemotherapeutic agents that do not form direct strand breaks has yet to be fully elucidated and it is not fully understood how DSB formation occurs during the course of DNA repair of these lesions. However the γ-H2AX biomarker has been successful in identifying different DNA damage and repair profiles in normal cell lines as well as chemo-resistant cell lines. However, it did not elicit a clear difference in foci formation between chemo-sensitive and chemo-resistant cell lines as both cellular phenotypes revealed increased γ-H2AX foci formation in comparison to the two DNA repair normal cell lines examined in this investigation. However a much larger sample set encompassing more control cell lines as well as cell lines with defects in different DNA repair pathways would be needed to ascertain the true validity of γ-H2AX as a diagnostic tool in identifying sensitive and resistant patients. The RAD51 biomarker has also successfully identified a potential upregulation of the HR pathway in the MRC5-SV1^{R} cell line. The information discerned from the expression levels of this marker may provide more insight into the overall patient response to treatment with ICL agents as it is indicative of a specific DNA repair pathway. However foci

formation seen with the RAD51 marker was not as clear cut and reliable as the formation of γ-H2AX foci.

Overall both markers have high potential in identifying chemo-sensitive and resistant patients but there is a lot of scope for further work in this area. As previously mentioned, a bigger cohort of cell lines encompassing a wider range of DNA repair defects should now be used to further investigate the trends in RAD51 and γ-H2AX foci induction and resolution in response to chemotherapeutic drugs. The cohort should also include more control cell lines as there were some contradictory results seen between the two DNA repair normal cell lines used here. The differences in sensitivity seen between the two cell lines in response to the different chemotherapeutics could be highlighting that responses can vary greatly between individuals but this can only be determined by examining more DNA repair normal cell lines. By examining a bigger cohort, I believe it would enable us to determine if there is a true trend in γ-H2AX and RAD51 foci induction emerging that can readily identify hypersensitivity and resistance in individuals.

Recent studies have revealed that 15 genes belonging to the FA pathway play a vital role in the maintenance of genomic stability (Crossan and Patel 2012) and have a central role in ICL repair. They are involved in the coordination of multiple repair processes; particularly nucleases that are vital for incising the ICLS. Enhancing knowledge of the mechanisms of DNA repair in response to chemotherapy would allow for improved therapies that could circumvent the development of resistance and undoubtedly vastly improve patient response and overall survival rates especially in cancers such as ovarian or breast cancer where treatment failure accounts for nearly 90% of patient deaths.

Therefore it is concluded that both γ-H2AX and RAD51 have shown potential in being useful markers of DNA repair in response to chemotherapeutic drugs. However to further validate the work carried out here, my future work would involve

- Increasing the number of DNA repair normal cell lines
- Expanding the scope of DNA repair deficiencies
- Include cell lines that have been made resistant to other chemotherapeutic drugs such as Pt
- Examine other biomarkers representing the FA pathway

References

Abbaszadeh, F., P. H. Clingen, C. F. Arlett, P. N. Plowman, E. C. Bourton, M. Themis, E. M. Makarov, R. F. Newbold, M. H. Green and C. N. Parris (2010). "A novel splice variant of the DNA-PKcs gene is associated with clinical and cellular radiosensitivity in a patient with xeroderma pigmentosum." J Med Genet **47**(3): 176-181.

Abe, K. and N. Matsuki (2000). "Measurement of cellular 3-(4,5-dimethylthiazol-2-yl)-2,5-diphenyltetrazolium bromide (MTT) reduction activity and lactate dehydrogenase release using MTT." Neurosci Res **38**(4): 325-329.

Agarwal, R. and S. B. Kaye (2003). "Ovarian cancer: strategies for overcoming resistance to chemotherapy." Nat Rev Cancer **3**(7): 502-516.

Al-Minawi, A. Z., Y. F. Lee, D. Hakansson, F. Johansson, C. Lundin, N. Saleh-Gohari, N. Schultz, D. Jenssen, H. E. Bryant, M. Meuth, J. M. Hinz and T. Helleday (2009). "The ERCC1/XPF endonuclease is required for completion of homologous recombination at DNA replication forks stalled by inter-strand cross-links." Nucleic Acids Res **37**(19): 6400-6413.

Alison, M. (2002). The cancer handbook. London
New York, Nature Pub. Group ;
Distributed ... in the U.S. ... by Grove's Dictionaries.

Arlett, C. F., P. N. Plowman, P. B. Rogers, C. N. Parris, F. Abbaszadeh, M. H. Green, T. J. McMillan, C. Bush, N. Foray and A. R. Lehmann (2006). "Clinical and cellular ionizing radiation sensitivity in a patient with xeroderma pigmentosum." Br J Radiol **79**(942): 510-517.

Banath, J. P. and P. L. Olive (2003). "Expression of phosphorylated histone H2AX as a surrogate of cell killing by drugs that create DNA double-strand breaks." Cancer Res **63**(15): 4347-4350.

Beckman, R. A. and L. A. Loeb (2005). "Genetic instability in cancer: theory and experiment." Semin Cancer Biol **15**(6): 423-435.

Bhagwat N, Olsen A, Wang A, Hanada K, Stuckert P, Kanaar R, D'Andrea A, Niedernhofer L, McHugh P (2009) "XPF-ERCC1 Participates in the Fanconi Anaemia pathway of cross-link repair" Molecular and Cellular Biology **29 (4)** 6427 - 6437

Boehm, T., J. Folkman, T. Browder and M. S. O'Reilly (1997). "Antiangiogenic therapy of experimental cancer does not induce acquired drug resistance." Nature **390**(6658): 404-407.

Bohm, L. and C. Crane-Robinson (1984). "Proteases as structural probes for chromatin: the domain structure of histones." Biosci Rep **4**(5): 365-386.

Bourton, E. C., P. N. Plowman, D. Smith, C. F. Arlett and C. N. Parris (2011). "Prolonged expression of the gamma-H2AX DNA repair biomarker correlates with excess acute and chronic toxicity from radiotherapy treatment." Int J Cancer.

Bourton, E. C., P. N. Plowman, D. Smith, C. F. Arlett and C. N. Parris (2011). "Prolonged expression of the gamma-H2AX DNA repair biomarker correlates with excess acute and chronic toxicity from radiotherapy treatment." Int J Cancer **129**(12): 2928-2934.
Bourton, E. C., P. N. Plowman, S. A. Zahir, G. U. Senguloglu, H. Serrai, G. Bottley and C. N. Parris (2012). "Multispectral imaging flow cytometry reveals distinct frequencies of gamma-H2AX foci induction in DNA double strand break repair defective human cell lines." Cytometry A **81**(2): 130-137.

Britten, R. A., D. Liu, A. Tessier, M. J. Hutchison and D. Murray (2000). "ERCC1 expression as a molecular marker of cisplatin resistance in human cervical tumor cells." Int J Cancer **89**(5): 453-457.

Carreira, A., J. Hilario, I. Amitani, R. J. Baskin, M. K. Shivji, A. R. Venkitaraman and S. C. Kowalczykowski (2009). "The BRC repeats of BRCA2 modulate the DNA-binding selectivity of RAD51." Cell **136**(6): 1032-1043.

Carvalho, H., L. M. Garrido, R. L. Furlan, G. Padilla, M. Agnoletto, T. Guecheva, J. A. Henriques, J. Saffi and C. F. Menck (2010). "DNA damage induced by the anthracycline cosmomycin D in DNA repair-deficient cells." Cancer Chemother Pharmacol **65**(5): 989-994.
Clingen, P. H., C. F. Arlett, J. A. Hartley and C. N. Parris (2007). "Chemosensitivity of primary human fibroblasts with defective unhooking of DNA interstrand cross-links." Exp Cell Res **313**(4): 753-760.

Clingen, P. H., J. Y. Wu, J. Miller, N. Mistry, F. Chin, P. Wynne, K. M. Prise and J. A. Hartley (2008). "Histone H2AX phosphorylation as a molecular pharmacological marker for DNA interstrand crosslink cancer chemotherapy." Biochem Pharmacol **76**(1): 19-27.

Cole, R. S. (1973). "Repair of DNA containing interstrand crosslinks in Escherichia coli: sequential excision and recombination." Proc Natl Acad Sci U S A **70**(4): 1064-1068.

Coley, H. M. (2008). "Mechanisms and strategies to overcome chemotherapy resistance in metastatic breast cancer." Cancer Treat Rev **34**(4): 378-390.

Conklin, K. A. (2000). "Dietary antioxidants during cancer chemotherapy: impact on chemotherapeutic effectiveness and development of side effects." Nutr Cancer **37**(1): 1-18.

Crossan, G. P. and K. J. Patel (2012). "The Fanconi anaemia pathway orchestrates incisions at sites of crosslinked DNA." J Pathol **226**(2): 326-337.

Crul, M., R. C. A. M. van Waardenburg, S. Bocxe, M. A. J. van Eijndhoven, D. Pluim, J. H. Beijnen and J. H. M. Schellens (2003). "DNA repair mechanisms involved in gemcitabine cytotoxicity and in the interaction between gemcitabine and cisplatin." Biochemical Pharmacology **65**(2): 275-282.

Cui, Y., J. Konig, J. K. Buchholz, H. Spring, I. Leier and D. Keppler (1999). "Drug resistance and ATP-dependent conjugate transport mediated by the apical multidrug resistance protein, MRP2, permanently expressed in human and canine cells." Mol Pharmacol **55**(5): 929-937.

Dabholkar, M., F. Bostick-Bruton, C. Weber, V. A. Bohr, C. Egwuagu and E. Reed (1992). "ERCC1 and ERCC2 expression in malignant tissues from ovarian cancer patients." J Natl Cancer Inst **84**(19): 1512-1517.

Davies, A. A., J. Y. Masson, M. J. McIlwraith, A. Z. Stasiak, A. Stasiak, A. R. Venkitaraman and S. C. West (2001). "Role of BRCA2 in control of the RAD51 recombination and DNA repair protein." Mol Cell **7**(2): 273-282.
de Gruijl, F. R., H. J. van Kranen and L. H. Mullenders (2001). "UV-induced DNA damage, repair, mutations and oncogenic pathways in skin cancer." J Photochem Photobiol B **63**(1-3): 19-27.

de Jager, M., M. L. Dronkert, M. Modesti, C. E. Beerens, R. Kanaar and D. C. van Gent (2001). "DNA-binding and strand-annealing activities of human Mre11: implications for its roles in DNA double-strand break repair pathways." Nucleic Acids Res **29**(6): 1317-1325.

De Silva, I. U., P. J. McHugh, P. H. Clingen and J. A. Hartley (2002). "Defects in interstrand cross-link uncoupling do not account for the extreme sensitivity of ERCC1 and XPF cells to cisplatin." Nucleic Acids Res **30**(17): 3848-3856.

Deans, A. J. and S. C. West (2011). "DNA interstrand crosslink repair and cancer." Nat Rev Cancer **11**(7): 467-480.

Dickey, J. S., C. E. Redon, A. J. Nakamura, B. J. Baird, O. A. Sedelnikova and W. M. Bonner (2009). "H2AX: functional roles and potential applications." Chromosoma **118**(6): 683-692.

Diderich, K., M. Alanazi and J. H. Hoeijmakers (2011). "Premature aging and cancer in nucleotide excision repair-disorders." DNA Repair (Amst) **10**(7): 772-780.

Digweed, M. (2003). "Response to environmental carcinogens in DNA-repair-deficient disorders." Toxicology **193**(1-2): 111-124.

Dipple, A. (1995). "DNA adducts of chemical carcinogens." Carcinogenesis **16**(3): 437-441.

Dizdaroglu, M., P. Jaruga, M. Birincioglu and H. Rodriguez (2002). "Free radical-induced damage to DNA: mechanisms and measurement." Free Radic Biol Med **32**(11): 1102-1115.
Dronkert, M. L. and R. Kanaar (2001). "Repair of DNA interstrand cross-links." Mutat Res **486**(4): 217-247.

Faghri, S., D. Tamura, K. H. Kraemer and J. J. Digiovanna (2008). "Trichothiodystrophy: a systematic review of 112 published cases characterises a wide spectrum of clinical manifestations." J Med Genet **45**(10): 609-621.

Fernandez-Capetillo, O., A. Lee, M. Nussenzweig and A. Nussenzweig (2004). "H2AX: the histone guardian of the genome." DNA Repair (Amst) **3**(8-9): 959-967.
Ferry, K. V., T. C. Hamilton and S. W. Johnson (2000). "Increased nucleotide excision repair in cisplatin-resistant ovarian cancer cells: role of ERCC1-XPF." Biochem Pharmacol **60**(9): 1305-1313.

Fojo, T. and H. M. Coley (2007). "The role of efflux pumps in drug-resistant metastatic breast cancer: new insights and treatment strategies." Clin Breast Cancer **7**(10): 749-756.

Fousteri, M. and L. H. Mullenders (2008). "Transcription-coupled nucleotide excision repair in mammalian cells: molecular mechanisms and biological effects." Cell Res **18**(1): 73-84.

Franken, N. A., H. M. Rodermond, J. Stap, J. Haveman and C. van Bree (2006). "Clonogenic assay of cells in vitro." Nat Protoc **1**(5): 2315-2319.

Friesner, J. D., B. Liu, K. Culligan and A. B. Britt (2005). "Ionizing radiation-dependent gamma-H2AX focus formation requires ataxia telangiectasia mutated and ataxia telangiectasia mutated and Rad3-related." Molecular Biology of the Cell **16**(5): 2566-2576.

Furuta, T., T. Ueda, G. Aune, A. Sarasin, K. H. Kraemer and Y. Pommier (2002). "Transcription-coupled nucleotide excision repair as a determinant of cisplatin sensitivity of human cells." Cancer Res **62**(17): 4899-4902.

Garcia-Villa, A., P. Balasubramanian, B. L. Miller, M. B. Lustberg, B. Ramaswamy and J. J. Chalmers (2012). "Assessment of gamma-H2AX levels in circulating tumor cells from patients receiving chemotherapy." Front Oncol **2**: 128.

Gary, R., K. Kim, H. L. Cornelius, M. S. Park and Y. Matsumoto (1999). "Proliferating cell nuclear antigen facilitates excision in long-patch base excision repair." J Biol Chem **274**(7): 4354-4363.

Gewirtz, D. A. (1999). "A critical evaluation of the mechanisms of action proposed for the antitumor effects of the anthracycline antibiotics adriamycin and daunorubicin." Biochem Pharmacol **57**(7): 727-741.

Giudice, S., L. Benassi, G. Bertazzoni, M. P. Costi, A. Gelain, A. Venturelli, C. Bernardi, G. Gualdi, A. Coppi, T. Rossi, A. Giannetti and C. Magnoni (2007). "New thymidylate synthase inhibitors induce apoptosis in melanoma cell lines." Toxicol In Vitro **21**(2): 240-248.

Giuliani, I., A. Baeza-Squiban and F. Marano (1997). "Early cytotoxic effects of mechlorethamine, a nitrogen mustard, on mammalian airway epithelium." Toxicol In Vitro **11**(5): 695-702.

Godwin, A. K., A. Meister, P. J. O'Dwyer, C. S. Huang, T. C. Hamilton and M. E. Anderson (1992). "High resistance to cisplatin in human ovarian cancer cell lines is associated with marked increase of glutathione synthesis." Proc Natl Acad Sci U S A **89**(7): 3070-3074.

Goldie, J. H. and A. J. Coldman (1983). "Quantitative model for multiple levels of drug resistance in clinical tumors." Cancer Treat Rep **67**(10): 923-931.

Graeser, M., A. McCarthy, C. J. Lord, K. Savage, M. Hills, J. Salter, N. Orr, M. Parton, I. E. Smith, J. S. Reis-Filho, M. Dowsett, A. Ashworth and N. C. Turner (2010). "A marker of homologous recombination predicts pathologic complete response to neoadjuvant chemotherapy in primary breast cancer." Clin Cancer Res **16**(24): 6159-6168.

Haaf, T., E. I. Golub, G. Reddy, C. M. Radding and D. C. Ward (1995). "Nuclear foci of mammalian Rad51 recombination protein in somatic cells after DNA damage and its localization in synaptonemal complexes." Proc Natl Acad Sci U S A **92**(6): 2298-2302.

Hanahan, D. and R. A. Weinberg (2000). "The hallmarks of cancer." Cell **100**(1): 57-70.

Hannay, J. A., J. Liu, Q. S. Zhu, S. V. Bolshakov, L. Li, P. W. Pisters, A. J. Lazar, D. Yu, R. E. Pollock and D. Lev (2007). "Rad51 overexpression contributes to chemoresistance in human

soft tissue sarcoma cells: a role for p53/activator protein 2 transcriptional regulation." Mol Cancer Ther **6**(5): 1650-1660.

Harmers, F. P., W. H. Gispen and J. P. Neijt (1991). "Neurotoxic side-effects of cisplatin." Eur J Cancer **27**(3): 372-376.

Harper, J. W. and S. J. Elledge (2007). "The DNA damage response: ten years after." Mol Cell **28**(5): 739-745.

Hawtin, R. E., D. E. Stockett, O. K. Wong, C. Lundin, T. Helleday and J. A. Fox (2010). "Homologous recombination repair is essential for repair of vosaroxin-induced DNA double-strand breaks." Oncotarget **1**(7): 606-619.

Hefferin, M. L. and A. E. Tomkinson (2005). "Mechanism of DNA double-strand break repair by non-homologous end joining." DNA Repair (Amst) **4**(6): 639-648.

Henning, K. A., L. Li, N. Iyer, L. D. McDaniel, M. S. Reagan, R. Legerski, R. A. Schultz, M. Stefanini, A. R. Lehmann, L. V. Mayne and E. C. Friedberg (1995). "The Cockayne syndrome group A gene encodes a WD repeat protein that interacts with CSB protein and a subunit of RNA polymerase II TFIIH." Cell **82**(4): 555-564.

Hickson, I., Y. Zhao, C. J. Richardson, S. J. Green, N. M. Martin, A. I. Orr, P. M. Reaper, S. P. Jackson, N. J. Curtin and G. C. Smith (2004). "Identification and characterization of a novel and specific inhibitor of the ataxia-telangiectasia mutated kinase ATM." Cancer Res **64**(24): 9152-9159.

Hoeijmakers, J. H. (2001). "Genome maintenance mechanisms for preventing cancer." Nature **411**(6835): 366-374.

Hoffman, R. M. (1991). "In vitro sensitivity assays in cancer: a review, analysis, and prognosis." J Clin Lab Anal **5**(2): 133-143.

Huang, X., M. Okafuji, F. Traganos, E. Luther, E. Holden and Z. Darzynkiewicz (2004). "Assessment of histone H2AX phosphorylation induced by DNA topoisomerase I and II inhibitors topotecan and mitoxantrone and by the DNA cross-linking agent cisplatin." Cytometry A **58**(2): 99-110.

Ichihashi, M., M. Ueda, A. Budiyanto, T. Bito, M. Oka, M. Fukunaga, K. Tsuru and T. Horikawa (2003). "UV-induced skin damage." Toxicology **189**(1-2): 21-39.
Jackson, S. P. (2002). "Sensing and repairing DNA double-strand breaks." Carcinogenesis **23**(5): 687-696.

Jensen, R. B., A. Carreira and S. C. Kowalczykowski (2010). "Purified human BRCA2 stimulates RAD51-mediated recombination." Nature **467**(7316): 678-683.
Johnson, S. W., P. B. Laub, J. S. Beesley, R. F. Ozols and T. C. Hamilton (1997). "Increased platinum-DNA damage tolerance is associated with cisplatin resistance and cross-resistance to various chemotherapeutic agents in unrelated human ovarian cancer cell lines." Cancer Res **57**(5): 850-856.

Johnson, S. W., R. P. Perez, A. K. Godwin, A. T. Yeung, L. M. Handel, R. F. Ozols and T. C. Hamilton (1994). "Role of platinum-DNA adduct formation and removal in cisplatin resistance in human ovarian cancer cell lines." Biochem Pharmacol **47**(4): 689-697.

Katz, D., E. Ito, K. S. Lau, J. D. Mocanu, C. Bastianutto, A. D. Schimmer and F. F. Liu (2008). "Increased efficiency for performing colony formation assays in 96-well plates: novel applications to combination therapies and high-throughput screening." Biotechniques **44**(2): ix-xiv.

Klungland, A. and T. Lindahl (1997). "Second pathway for completion of human DNA base excision-repair: reconstitution with purified proteins and requirement for DNase IV (FEN1)." EMBO J **16**(11): 3341-3348.

Koberle, B., K. A. Grimaldi, A. Sunters, J. A. Hartley, L. R. Kelland and J. R. Masters (1997). "DNA repair capacity and cisplatin sensitivity of human testis tumour cells." Int J Cancer **70**(5): 551-555.

Komatsu, K., A. Antoccia, S. Sakamoto, J. Kobayashi, S. Matsuura and H. Tauchi (2007). "NBS1 and MRE11 associate for responses to DNA double-strand breaks." International Congress Series **1299**(0): 158-163.
Kow, Y. W. (2002). "Repair of deaminated bases in DNA." Free Radic Biol Med **33**(7): 886-893.

Krokan, H. E., R. Standal and G. Slupphaug (1997). "DNA glycosylases in the base excision repair of DNA." Biochem J **325 (Pt 1)**: 1-16.

Kuefner, M. A., S. Grudzenski, S. A. Schwab, S. Azoulay, M. Heckmann, M. C. Heinrich, M. Lobrich and M. Uder (2009). "[X-ray-induced DNA double-strand breaks after angiographic examinations of different anatomic regions]." Rofo **181**(4): 374-380.

Kuraoka, I., W. R. Kobertz, R. R. Ariza, M. Biggerstaff, J. M. Essigmann and R. D. Wood (2000). "Repair of an interstrand DNA cross-link initiated by ERCC1-XPF repair/recombination nuclease." J Biol Chem **275**(34): 26632-26636.

Lanzi, C., P. Perego, R. Supino, S. Romanelli, T. Pensa, N. Carenini, I. Viano, D. Colangelo, R. Leone, P. Apostoli, G. Cassinelli, R. A. Gambetta and F. Zunino (1998). "Decreased drug accumulation and increased tolerance to DNA damage in tumor cells with a low level of cisplatin resistance." Biochem Pharmacol **55**(8): 1247-1254.

Lees-Miller, S. P. and K. Meek (2003). "Repair of DNA double strand breaks by non-homologous end joining." Biochimie **85**(11): 1161-1173.

Lehmann, A. R. (2003). "DNA repair-deficient diseases, xeroderma pigmentosum, Cockayne syndrome and trichothiodystrophy." Biochimie **85**(11): 1101-1111.

Li, X. and W. D. Heyer (2008). "Homologous recombination in DNA repair and DNA damage tolerance." Cell Res **18**(1): 99-113.

Longley, D. B., D. P. Harkin and P. G. Johnston (2003). "5-fluorouracil: mechanisms of action and clinical strategies." Nat Rev Cancer **3**(5): 330-338.

Lorico, A., G. Rappa, R. A. Flavell and A. C. Sartorelli (1996). "Double knockout of the MRP gene leads to increased drug sensitivity in vitro." Cancer Res **56**(23): 5351-5355.
Malumbres, M. and M. Barbacid (2009). "Cell cycle, CDKs and cancer: a changing paradigm." Nat Rev Cancer **9**(3): 153-166.

Masters, J. R. and B. Koberle (2003). "Curing metastatic cancer: lessons from testicular germ-cell tumours." Nat Rev Cancer **3**(7): 517-525.

Masuda, H., R. F. Ozols, G. M. Lai, A. Fojo, M. Rothenberg and T. C. Hamilton (1988). "Increased DNA repair as a mechanism of acquired resistance to cis-diamminedichloroplatinum (II) in human ovarian cancer cell lines." Cancer Res **48**(20): 5713-5716.

McHugh, P. J., V. J. Spanswick and J. A. Hartley (2001). "Repair of DNA interstrand crosslinks: molecular mechanisms and clinical relevance." Lancet Oncol **2**(8): 483-490.
McKinnon, P. J. (2004). "ATM and ataxia telangiectasia." EMBO Rep **5**(8): 772-776.

Mueller, M. M. and N. E. Fusenig (2004). "Friends or foes - bipolar effects of the tumour stroma in cancer." Nat Rev Cancer **4**(11): 839-849.

Murnane, J. P., L. F. Fuller and R. B. Painter (1985). "Establishment and characterization of a permanent pSV ori--transformed ataxia-telangiectasia cell line." Exp Cell Res **158**(1): 119-126.

Niedernhofer, L. J., H. Odijk, M. Budzowska, E. van Drunen, A. Maas, A. F. Theil, J. de Wit, N. G. Jaspers, H. B. Beverloo, J. H. Hoeijmakers and R. Kanaar (2004). "The structure-specific endonuclease Ercc1-Xpf is required to resolve DNA interstrand cross-link-induced double-strand breaks." Mol Cell Biol **24**(13): 5776-5787.

Niles, J. C., J. S. Wishnok and S. R. Tannenbaum (2006). "Peroxynitrite-induced oxidation and nitration products of guanine and 8-oxoguanine: structures and mechanisms of product formation." Nitric Oxide **14**(2): 109-121.

Olive, P. L. and J. P. Banath (2009). "Kinetics of H2AX phosphorylation after exposure to cisplatin." Cytometry B Clin Cytom **76**(2): 79-90.

Osborn, A. J., S. J. Elledge and L. Zou (2002). "Checking on the fork: the DNA-replication stress-response pathway." Trends Cell Biol **12**(11): 509-516.
Pabla, N., S. Huang, Q. S. Mi, R. Daniel and Z. Dong (2008). "ATR-Chk2 signaling in p53 activation and DNA damage response during cisplatin-induced apoptosis." J Biol Chem **283**(10): 6572-6583.

Plo, I., C. Laulier, L. Gauthier, F. Lebrun, F. Calvo and B. S. Lopez (2008). "AKT1 inhibits homologous recombination by inducing cytoplasmic retention of BRCA1 and RAD51." Cancer Res **68**(22): 9404-9412.

Rabbani, A., R. M. Finn and J. Ausio (2005). "The anthracycline antibiotics: antitumor drugs that alter chromatin structure." Bioessays **27**(1): 50-56.

Raderschall, E., E. I. Golub and T. Haaf (1999). "Nuclear foci of mammalian recombination proteins are located at single-stranded DNA regions formed after DNA damage." Proc Natl Acad Sci U S A **96**(5): 1921-1926.

Rink, S. M. and P. B. Hopkins (1995). "A mechlorethamine-induced DNA interstrand cross-link bends duplex DNA." Biochemistry **34**(4): 1439-1445.

Rogakou, E. P., W. Nieves-Niera, C. Boon, Y. Pommier and W. M. Bonner (1998). "Histone H2AX serine-139 phosphorylation is induced by the introduction of the initial breaks into DNA as a result of the apoptotic endonuclease." Molecular Biology of the Cell **9**: 109a-109a.

Rudas, M., M. Filipits, S. Taucher, T. Stranzl, G. G. Steger, R. Jakesz, R. Pirker and G. Pohl (2003). "Expression of MRP1, LRP and Pgp in breast carcinoma patients treated with preoperative chemotherapy." Breast Cancer Res Treat **81**(2): 149-157.

Salles, B., P. Calsou, P. Frit and C. Muller (2006). "The DNA repair complex DNA-PK, a pharmacological target in cancer chemotherapy and radiotherapy." Pathol Biol (Paris) **54**(4): 185-193.

San Filippo, J., P. Sung and H. Klein (2008). "Mechanism of eukaryotic homologous recombination." Annu Rev Biochem **77**: 229-257.

Satoh, M., A. Naganuma and N. Imura (1988). "Metallothionein induction prevents toxic side effects of cisplatin and adriamycin used in combination." Cancer Chemother Pharmacol **21**(2): 176-178.

Schwaiger, M. and C. Peschel (2006). "Biological imaging for selecting and monitoring cancer therapy; a pathway to individualised therapy." Eur J Nucl Med Mol Imaging **33 Suppl 1**: 1-5.

Scott, S. P. and T. K. Pandita (2006). "The cellular control of DNA double-strand breaks." Journal of Cellular Biochemistry **99**(6): 1463-1475.

Sedelnikova, O. A., E. P. Rogakou, I. G. Panyutin and W. M. Bonner (2002). "Quantitative detection of (125)IdU-induced DNA double-strand breaks with gamma-H2AX antibody." Radiat Res **158**(4): 486-492.

Seeberg, E., L. Eide and M. Bjoras (1995). "The base excision repair pathway." Trends Biochem Sci **20**(10): 391-397.

Shiloh, Y. (2001). "ATM and ATR: networking cellular responses to DNA damage." Curr Opin Genet Dev **11**(1): 71-77.

Siddik, Z. H. (2003). "Cisplatin: mode of cytotoxic action and molecular basis of resistance." Oncogene **22**(47): 7265-7279.

Smith, K. J., C. G. Hurst, R. B. Moeller, H. G. Skelton and F. R. Sidell (1995). "Sulfur mustard: its continuing threat as a chemical warfare agent, the cutaneous lesions induced, progress in understanding its mechanism of action, its long-term health effects, and new developments for protection and therapy." J Am Acad Dermatol **32**(5 Pt 1): 765-776.

Takata, M., M. S. Sasaki, E. Sonoda, C. Morrison, M. Hashimoto, H. Utsumi, Y. Yamaguchi-Iwai, A. Shinohara and S. Takeda (1998). "Homologous recombination and non-homologous end-joining pathways of DNA double-strand break repair have overlapping roles in the maintenance of chromosomal integrity in vertebrate cells." EMBO J **17**(18): 5497-5508.

Takemura, G. and H. Fujiwara (2007). "Doxorubicin-induced cardiomyopathy from the cardiotoxic mechanisms to management." Prog Cardiovasc Dis **49**(5): 330-352.

Tamminga, R. Y., W. V. Dolsma, J. A. Leeuw and H. H. Kampinga (2002). "Chemo- and radiosensitivity testing in a patient with ataxia telangiectasia and Hodgkin disease." Pediatr Hematol Oncol **19**(3): 163-171.

Thiebaut, F., T. Tsuruo, H. Hamada, M. M. Gottesman, I. Pastan and M. C. Willingham (1987). "Cellular localization of the multidrug-resistance gene product P-glycoprotein in normal human tissues." Proc Natl Acad Sci U S A **84**(21): 7735-7738.

Tokarska-Schlattner, M., M. Zaugg, C. Zuppinger, T. Wallimann and U. Schlattner (2006). "New insights into doxorubicin-induced cardiotoxicity: the critical role of cellular energetics." J Mol Cell Cardiol **41**(3): 389-405.

Turner, N., A. Tutt and A. Ashworth (2005). "Targeting the DNA repair defect of BRCA tumours." Curr Opin Pharmacol **5**(4): 388-393.

Tysnes, B. B. and R. Bjerkvig (2007). "Cancer initiation and progression: involvement of stem cells and the microenvironment." Biochim Biophys Acta **1775**(2): 283-297.

Ulus-Senguloglu, G., C. F. Arlett, P. N. Plowman, J. Parnell, N. Patel, E. C. Bourton and C. N. Parris (2012). "Elevated expression of artemis in human fibroblast cells is associated with cellular radiosensitivity and increased apoptosis." Br J Cancer **107**(9): 1506-1513.
Valerie, K. and L. F. Povirk (2003). "Regulation and mechanisms of mammalian double-strand break repair." Oncogene **22**(37): 5792-5812.

Van Cutsem, E., M. Findlay, B. Osterwalder, W. Kocha, D. Dalley, R. Pazdur, J. Cassidy, L. Dirix, C. Twelves, D. Allman, J. F. Seitz, J. Scholmerich, H. U. Burger and J. Verweij (2000). "Capecitabine, an oral fluoropyrimidine carbamate with substantial activity in advanced colorectal cancer: results of a randomized phase II study." J Clin Oncol **18**(6): 1337-1345.

Vilmar, A. and J. B. Sorensen (2009). "Excision repair cross-complementation group 1 (ERCC1) in platinum-based treatment of non-small cell lung cancer with special emphasis on carboplatin: a review of current literature." Lung Cancer **64**(2): 131-139.

Walker, J. R., R. A. Corpina and J. Goldberg (2001). "Structure of the Ku heterodimer bound to DNA and its implications for double-strand break repair." Nature **412**(6847): 607-614.

Wang, A. T., B. Sengerova, E. Cattell, T. Inagawa, J. M. Hartley, K. Kiakos, N. A. Burgess-Brown, L. P. Swift, J. H. Enzlin, C. J. Schofield, O. Gileadi, J. A. Hartley and P. J. McHugh (2011). "Human SNM1A and XPF-ERCC1 collaborate to initiate DNA interstrand cross-link repair." Genes Dev **25**(17): 1859-1870.

Wang, Y., D. Cortez, P. Yazdi, N. Neff, S. J. Elledge and J. Qin (2000). "BASC, a super complex of BRCA1-associated proteins involved in the recognition and repair of aberrant DNA structures." Genes Dev **14**(8): 927-939.

Wang, Y. and J. A. Heddle (2004). "Spontaneous and induced chromosomal damage and mutations in Bloom Syndrome mice." Mutat Res **554**(1-2): 131-137.

Welsh, C., R. Day, C. McGurk, J. R. Masters, R. D. Wood and B. Koberle (2004). "Reduced levels of XPA, ERCC1 and XPF DNA repair proteins in testis tumor cell lines." Int J Cancer **110**(3): 352-361.

Weterings, E. and D. J. Chen (2008). "The endless tale of non-homologous end-joining." Cell Res **18**(1): 114-124.
Wilsker, D. and F. Bunz (2007). "Loss of ataxia telangiectasia mutated- and Rad3-related function potentiates the effects of chemotherapeutic drugs on cancer cell survival." Mol Cancer Ther **6**(4): 1406-1413.

Yuan, S. S., H. L. Chang and E. Y. Lee (2003). "Ionizing radiation-induced Rad51 nuclear focus formation is cell cycle-regulated and defective in both ATM(-/-) and c-Abl(-/-) cells." Mutat Res **525**(1-2): 85-92.